Influence of seawater ageing on the behaviour of adhesives : a rapid characterization of the evolution of mechanical properties of bonded joints

Alin Ilioni

université de bretagne occidentale

UNIVERSITE BRETAGNE LOIRE

THÈSE / UNIVERSITÉ DE BRETAGNE OCCIDENTALE
sous le sceau de l'Université Bretagne Loire

pour obtenir le titre de
DOCTEUR DE L'UNIVERSITÉ DE BRETAGNE OCCIDENTALE
Mention : Mécanique des solides, des matériaux, des structures et des surfaces
École Doctorale Sciences Pour l'Ingénieur

présentée par
Alin ILIONI
préparée à l'**Institut de Recherche Dupuy De Lôme (CNRS FRE 3744)** et en collaboration avec l'**IFREMER**

Influence of seawater ageing on the behaviour of adhesives

A rapid characterization of the evolution of mechanical properties of bonded joints

Soutenue le 27 novembre 2017 à 10h30
devant le jury composé de :

Jocelyne GALY
Directrice de Recherche CNRS, IMP, Lyon / *Rapporteur*

Jean-Claude GRANDIDIER
Professeur des Universités, Institut PPRIME, Poitiers / *Rapporteur*

Robert ADAMS
Professor Emeritus, University of Bristol, England / *Examinateur*

Frédéric JACQUEMIN
Professeur des Universités, GeM, Saint-Nazaire / *Examinateur*

Stéphanie MALLARINO
Maitre de conférences, LaSIE, La Rochelle / *Examinateur*

Claudiu BADULESCU
Maitre de conférences de l'ENSTA Bretagne, IRDL, Brest / *Co-encadrant*

Peter DAVIES
Ingénieur de recherche (HDR), IFREMER, Brest / *Co-directeur*

David THÉVENET
Professeur de l'ENSTA Bretagne, IRDL, Brest / *Directeur de thèse*

Nicolas CARRÈRE
Ingénieur (HDR), SAFRAN Tech - Composites, Itteville / *Invité*

COmportement, modélisation et **SI**mulation du **CO**llage structural

This work is part of the **ANR COSICO** project

I would like to thank all the people who supported me and those who were involved in this work.

Je tiens à remercier toutes les personnes qui m'ont soutenu et qui ont contribué, de près ou de loin, à ce travail.

Mulţumesc tutoror celor care m-au susţinut şi au contribuit la finalizarea acestei lucrări.

Contents

1 Structural bonding: state of the art **26**

1.1 A close look at the bonding process 28

1.1.1 Mechanisms of adhesion 28

1.1.2 Surface preparation techniques 31

1.2 Mechanical characterisation of structural adhesives 32

1.2.1 Introduction 32

1.2.2 Multi-scale approach 32

1.2.3 Tests using bulk specimens 33

1.2.4 Joint tests 35

1.2.5 Types of failure in a bonded joint 39

1.3 Modelling the mechanical behaviour of adhesives 40

1.3.1 Brief introduction 40

1.3.2 Analytical models 41

1.3.3 Long-time creep behaviour 45

1.3.4 Influence of the hydrostatic stress: 3D models 46

1.3.5 Fracture mechanics approach 51

1.4 Environmental conditions and the adhesives behaviour 52

1.4.1 Water diffusion in adhesives 53

1.4.2 Physico-chemical degradation of epoxy adhesives 57

1.4.3 Influence of water on mechanical properties 59

1.5 Predicting the mechanical behaviour of aged bonded joints 64

1.5.1 Cohesive failure approach 65

1.5.2 Adhesive failure approach 66

1.6 Aims of the present study 68

1.7 Presentation of the adopted approach 68

2 Characterization of the initial state of the studied adhesive 70

2.1 General informations on the adhesive studied 72

2.1.1 Technical specifications 72

2.1.2 Chemical formulation 72

2.1.3 Mixture preparation 72

2.2 Mechanical behaviour of the unaged bulk adhesive 73

2.2.1 Manufacturing of a sheet of bulk adhesive 74

2.2.2 Tensile behaviour 74

2.2.3 Shear behaviour 76

2.2.4 Tensile creep behaviour 77

2.2.5 Shear creep behaviour 78

2.2.6 Dynamic mechanical analysis 79

2.3 Mechanical behaviour of unaged bonded specimens 80

2.3.1 Arcan tests 80

2.3.2 Specimens 81

2.3.3 Equipment 82

2.3.4 Monotonic behaviour 82

2.3.5 Creep behaviour 86

2.4 Differential scanning calorimetry analysis (DSC) 88

2.5 Overview 88

3 Modelling the mechanical behaviour of the adhesive at initial state 90

3.1 Numerical modelling of the Arcan test 92

3.1.1 Approach 92

3.1.2 Finite element model 93

3.1.3 Inverse identification method 95

3.2 Constitutive law 97

3.2.1 Identification of elastic parameters 98

3.2.2 The modified viscoelastic spectral model 100

3.2.3 Identification of the viscoelastic parameters 102

3.2.4 Viscoelastic-viscoplastic model 106

3.2.5 Identification of viscoplastic parameters 107

3.3 Validation of the constitutive law . . . 110
3.3.1 Validation of the viscoelastic part . . . 111
3.3.2 Validation of the complete model . . . 111
3.3.3 Validation of the yield function . . . 113
3.3.4 Validation of the loading rate effect . . . 114
3.4 From Arcan tests to bulk behaviour . . . 114
3.4.1 Prediction of the tensile bulk behaviour . . . 115
3.4.2 Prediction of the shear bulk behaviour . . . 116
3.5 From bulk tests to the Arcan behaviour . . . 117
3.6 Conclusions . . . 119
3.6.1 Overview on the model . . . 119
3.6.2 Perspectives . . . 120
3.6.3 Proposal for a rapid characterisation of a water-aged bonded joints . . . 120

4 Influence of water content on the mechanical properties of the adhesive 122
4.1 Introduction and complementary bibliography . . . 124
4.2 Water diffusion in different environmental conditions . . . 125
4.2.1 Samples used for water uptake . . . 126
4.2.2 Water absorption . . . 126
4.2.3 Water absorption in completely immersed state . . . 127
4.2.4 Water absorption in controlled relative humidity environment . . . 130
4.3 Short-term study of water ageing: absorption/desorption . . . 132
4.3.1 Experimental measurements . . . 132
4.3.2 Analytical modelling of each cycle . . . 132
4.4 Transition glass temperature evolution with water content . . . 133
4.5 Tensile behaviour changes with water content . . . 134
4.6 Short-term study of water ageing . . . 136
4.7 Long-term study of seawater ageing . . . 136
4.7.1 Experimental approach . . . 136
4.7.2 Analysis of the mechanical properties . . . 137
4.8 Dynamic mechanical-thermal analysis (DMTA) . . . 137
4.9 Creep tests at different constant water content . . . 139

4.9.1 Tensile creep behaviour 139
4.9.2 Shear creep behaviour 140
4.10 Overview 141

5 Modelling the water diffusion and its consequences on the mechanical behaviour of the adhesive 142

5.1 Prediction of water diffusion in a bulk sample 144
5.2 Evolution of elastic parameters with water content 148
5.2.1 Description of elastic modulus changes with water content 148
5.2.2 Description of Poisson's ratio changes with water content 148
5.3 Viscoelastic parameters as a function of water content 150
5.3.1 Spectrum parameters with water content: n_0, n_c 150
5.3.2 Linear viscoelastic parameters versus water content: a_D, a_H 153
5.3.3 Non-linear viscoelastic parameters as a function of water content 155
5.4 Viscoplastic parameters as a function of water content 155
5.4.1 Yield stress evolution 155
5.4.2 Evolution of the yield function 157
5.4.3 Evolution of hardening parameters 158
5.5 Mechanical behaviour of an aged bulk specimen before saturation 159
5.5.1 Coupling the diffusion model with the constitutive law 159
5.5.2 Validation tensile tests during ageing in seawater 159
5.5.3 Validation of the approach 161
5.5.4 Limits of prediction 161
5.6 Modelling the water diffusion in a bonded joint 162
5.7 Aged bonded joints with a constant water profile 164
5.7.1 Prediction of the mechanical behaviour 164
5.7.2 Experimental tests used for validation 164
5.7.3 Discussion of the results 165
5.7.4 Comparison between model prediction and experimental results 167
5.8 Aged bonded joints with a profile of water in the adhesive layer 167
5.8.1 Modelling the mechanical behaviour 168
5.8.2 Comparison between model prediction and experimental results 168

5.8.3 Overview 169

6 General conclusions and perspectives **172**

List of Tables

1 Historical development of structural adhesives [1] 21

1.1 Theories of adhesion [2] 28
1.2 Strengths of chemical bonds 30
1.3 Hydrostatic pressure dependant yield criterion 51

2.1 Technical specifications [3] 72
2.2 Components properties [3] 72
2.3 Cure cycle performances [3] 73

3.1 Elastic parameters 100
3.2 Identified viscoelastic parameters 105
3.3 Identified viscoplastic parameters 111
3.4 Mechanical properties in tensile behaviour 115
3.5 Comparison between the model parameters identified using Arcan test and those identified from tests performed on bulk specimens 118

4.1 Diffusion coefficient for different water temperatures [*1mm thick*] 129
4.2 Water activity model parameters 131
4.3 Water uptake at saturation for different ageing conditions 138

5.1 Material characteristics used in simulation 144
5.2 Tests during ageing in seawater 160
5.3 Saturation times for an Arcan sample 163

List of Figures

1 Structure of a reactive epoxide group (a) DGEBA (b) 22
2 Characteristics of some structural adhesives [4] 22
3 Examples of structures for the marine renewable energy industry involving adhesive bonding 23

1.2 Mechanisms of adhesion 28
1.3 Surface energy 29
1.4 Water droplet on a super-hydrophilic a), highly wettable (b), non-wettable (c) and hydrophobic (d) surfaces [5] 29
1.5 Multi-scale approach 32
1.6 Manufacturing of bulk specimens 33
1.7 Tensile test on bulk specimen 34
1.8 Bulk torsion specimen [6] 34
1.9 Iosipescu and Arcan tests 35
1.10 Nano-indentation across the interface of an aluminium/adhesive joint [7] 36
1.11 Comparison between thin-film and bulk form behaviour 36
1.12 Single Lap Joint 36
1.13 Double lap shear 37
1.14 Thick adherend shear test (TAST) 37
1.15 Butt joint 37
1.16 Schematic representation of the testing device and the mounted specimen (a) Geometry of the specimens beaks (b) [8] 38
1.17 Modified Arcan test 38
1.18 Calculated stress distribution in a thick bonded joint [7] 39
1.19 Types of failure in a bonded joint 40
1.20 Common elements used to model the mechanical behaviour of materials: Spring (a), Linear dashpot (b), Non-linear dashpot (c), Frictional device (d) 41
1.21 Maxwell elementary model 42
1.22 Maxwell model response [9] 43
1.23 Kelvin-Voigt elementary model 43
1.24 Kelvin-Voigt model response [9] 44
1.25 Bingham-Norton elementary model 44
1.26 Bingham-Norton model response [9] 44
1.27 Creep tests of an epoxy adhesive at room temperature [10] 45
1.28 Cyclic creep-recovery data for a rate dependent adhesive [11] 46

1.29 Unified theory viscoplastic model fits to the constant strain rate data using the model from Chiu [11] . . . 47
1.30 Generalized Kelvin model . . . 47
1.31 Creep test of a laminate at different loadings [12] . . . 49
1.32 Experimental data versus experimental yield function in the Mises-Hydrostatic plane [13] . . . 52
1.33 Water diffusion in an adhesive layer . . . 54
1.34 Water uptake in epoxy adhesive immersed in seawater at different temperatures [14] . . . 55
1.35 Non-Fickian behaviour . . . 56
1.36 Evolution of the diffusion coefficient as a function of temperature and water activity 56
1.37 Evolution of T_g as a function of immersion time for different types of epoxy adhesives [15] . . . 58
1.38 Mass variation as a function of ageing time for a polyurethane elastomer immersed in artificial seawater at 60^oC [16] . . . 58
1.39 Changes in the elastic modulus and yield stress with water uptake . . . 60
1.40 Effect of absorbed moisture on the bulk mechanical properties of a modified epoxy adhesive at 22^oC [17] . . . 60
1.41 Example of modelling the water diffusion in a single lap joint [18] . . . 60
1.42 Water concentration as a function of position in a square bonded joint [19] . . . 61
1.43 Water diffusion in an epoxy adhesive . . . 62
1.44 Influence of water ageing in shear and tensile behaviour . . . 62
1.45 Water diffusion at interface . . . 63
1.46 Epoxy adhesive exposed to water at 50^oC [20] . . . 64
1.47 Predicting the apparition of plasticity in the adhesive layer of an aged Arcan sample subjected to shear stress [21] . . . 66
1.48 Spring elements along the interface adhesive/adherend in a finite element code [22] 66
1.49 Presentation of the adopted approach . . . 69

2.2 Preparation of the adhesive . . . 73
2.3 Manufacturing of a sheet of bulk adhesive . . . 74
2.4 Geometry of the tensile specimens [ISO 37] . . . 74
2.5 Digital image correlation used for bulk tensile tests . . . 75
2.6 Tensile test on bulk specimen . . . 75
2.7 Experimental set-up for shear tests on bulk specimens . . . 76
2.8 Deformation of the bulk specimen in shear test (not to scale) . . . 76
2.9 Shear behaviour on bulk specimen . . . 77
2.10 Tensile creep behaviour performed on bulk specimens . . . 78
2.11 Experimental result for tensile creep behaviour on bulk form . . . 78
2.12 Experimental result for tensile creep behaviour on bulk form . . . 79
2.13 Dynamic mechanical analysis at initial state . . . 80
2.14 Different types of Arcan device loading . . . 81
2.15 Main dimensions of the substrates (not to scale) [23] . . . 81

2.16 Modified Arcan specimen . . . 82
2.17 Measurement of substrate displacements . . . 82
2.18 Monotonic test: tensile (a) and shear (b) . . . 83
2.19 Monotonic tests . . . 83
2.20 Type of failure obtained in tensile (a) and in shear (b) tests . . . 84
2.21 Schematic representation of the applied load ($F_{applied}$) and projections of the tensile/compression load and tangential load . . . 84
2.22 Combined tensile/shear test ($\gamma = 45^o$) . . . 85
2.23 Combined compression/shear tests ($\gamma = 135^o$) . . . 85
2.24 Failure envelope determined using Arcan specimens . . . 86
2.25 Multi-level creep tests: tensile (a) and shear (b) . . . 87
2.26 Evolution of the viscous and elastic displacements at the end of each creep level: tensile (a) and shear (b) . . . 87
2.27 Differential scanning calorimetry (DSC) analysis at initial state . . . 88

3.2 Arcan device ready to be mounted on a tensile machine . . . 92
3.3 (a) Specimen ready to the be mounted in the Arcan device (b) Equivalent model for the Arcan specimen . . . 93
3.4 Complete 3D finite element model . . . 94
3.5 3D finite element model with symmetry/anti-symmetry conditions . . . 94
3.6 Mesh of the 3D FE model . . . 95
3.7 Mesh of the 2D FE model . . . 95
3.8 Inverse identification in an iterative procedure [23] . . . 96
3.9 Inverse identification in an optimisation procedure [23] . . . 97
3.10 Monotonic tests . . . 98
3.11 Calculated errors obtained for different couples of (E, ν) under (a) tensile and (b) shear loading. (c) Intersection of the best couples (E, ν) . . . 99
3.12 Validation of the elastic parameters . . . 99
3.13 Spectrum definition . . . 101
3.14 Multi-level creep tests: tension (a) and shear (b) . . . 102
3.15 (a) Multi-level creep test used to identify the deviatoric parameters of the viscoelastic model, (b) Isochronism principle . . . 103
3.16 (a) Normalized viscous displacement for different couples (n_0, n_c) (b) Error calculated for different couples (n_0, n_c) . . . 103
3.17 (a) First level of the shear creep test (b) Identification of the viscoelastic model . 104
3.18 (a) First level of the shear creep test (b) Identification of the viscoelastic model . 105
3.19 Viscoelastic model prediction in monotonic (a) tensile and (b) shear tests . . . 106
3.20 Identification of the elastic threshold R_0 . . . 107
3.21 Distribution of the (a) von Mises stress and (b) hydrostatic pressure in the middle plane of the adhesive layer corresponding to the elastic threshold in a monotonic shear test . . . 108
3.22 (a) Identification of the elastic limit in tension and (b) definition of the yield function . . . 109

3.23 Distribution of the (a) von Mises stress and (b) hydrostatic pressure in the middle plane of the adhesive layer corresponding to the elastic threshold in a monotonic tensile test . . . 109
3.24 Identification of the (a) hardening parameters and (b) the flow function . . . 110
3.25 Identification of the viscous parameters: K, n . . . 111
3.26 Model validation in multi-level creep/recovery (a) shear and (b) tensile tests . . . 112
3.27 Viscoelastic-viscoplastic model validation in combined tensile/shear test . . . 112
3.28 Distribution of the (a) von Mises stress and (b) hydrostatic pressure in the middle plane of the adhesive layer corresponding to the elastic threshold in a combined tensile/shear monotonic test . . . 113
3.29 Validation of the yield function . . . 113
3.30 Validation of the viscoelastic-viscoplastic model under tensile loading; effect of loading rate . . . 114
3.31 (a) Tensile test on bulk specimen (b) FE model for tensile test on bulk specimen 115
3.32 Comparison of the predicted tensile behaviour with the experimental data . . . 116
3.33 Identification of viscoelastic parameters that characterise the deviatoric part . . . 116
3.34 Comparison of the predicted tensile behaviour with the experimental data . . . 117
3.35 Prediction of the (a) shear and (b) tensile behaviour of an Arcan test using the model parameters identified on bulk specimens . . . 119

4.2 Experimental resources used for different ageing conditions . . . 125
4.3 Geometry of the squared samples used for water uptake (1mm thickness) . . . 126
4.4 Water diffusion in bulk specimens immersed in different seawater temperatures . 128
4.5 Evolution of saturated mass and diffusion coefficient with water temperature . . 129
4.6 Water absorption, at 40^{o}C, in adhesive for different water activities (symbols are experimental data and lines show Fickian behaviour model) . . . 130
4.7 Evolution of saturated mass and diffusion coefficient with water activity . . . 131
4.8 Cycles of absorption/desorption performed on the studied adhesive . . . 132
4.9 Absorption/Desorption cycles . . . 133
4.10 DSC analysis on samples saturated in different ageing conditions (a) Zoom on the zone of interest (b) . . . 133
4.11 Decrease in Tg as a function of water content at saturation in the epoxy adhesive 134
4.12 Tensile behaviour as a function of water content at saturation (*i.e.* without any water profile gradient through the thickness) . . . 135
4.13 Evolution of the mechanical properties as a function of water content at saturation 135
4.14 Evolution of the mechanical properties as a function of water content at saturation 135
4.15 Tensile behaviour for unaged samples, fully saturated samples and dried after 14 days of ageing in seawater at 40^{o}C . . . 136
4.16 Long term evolution of tensile behaviour . . . 137
4.17 Geometry and experimental device used for DMA analysis of samples saturated in different ageing conditions . . . 138
4.18 Comparison between the evolution of the Young's modulus of a dried sample and an immersed saturated sample . . . 138

4.19 DMA analysis on samples saturated with different quantities of water and constant profiles . . . 139
4.20 Tensile creep load levels for different ageing conditions . . . 140
4.21 Tensile creep results for different water contents . . . 140
4.22 Shear creep results for different water contents . . . 141

5.1 3D finite element model used for diffusion law validation . . . 144
5.2 3D finite element model used for diffusion law validation . . . 145
5.3 3D finite element model used for diffusion law validation . . . 146
5.4 Detailed cross-section of the water profile through the section of a sample . . . 146
5.5 Evolution of the water profile in the cross-section of a square sample exposed at different water ageing times . . . 146
5.6 Prediction of local water profiles through thickness for the adhesive immersed in seawater at 40^oC . . . 147
5.7 Evolution of Tg through the thickness of an aged sample . . . 147
5.8 (a) Water uptake at saturation for different environmental conditions, (b) Tensile test on sample saturated in different environments . . . 149
5.9 (a) Evolution of the elastic modulus with water content, (b) Evolution of Poisson ratio with water content . . . 149
5.10 Creep behaviour performed on dried samples . . . 150
5.11 Isochronism principle . . . 151
5.12 Comparison between normalised strain of the first bulk creep level and the *Master curve* . . . 152
5.13 Comparison between aged and unaged creep behaviour . . . 152
5.14 Normalised viscous strains in tensile creep behaviour . . . 153
5.15 First creep levels obtained in (a) shear and (b) tensile tests performed on bulk samples saturated with different water contents . . . 153
5.16 (a) Fixture used to characterise the tensile creep behaviour and (b) the FEM used in the inverse identification procedure . . . 154
5.17 Evolution of the linear viscosity parameters with water content . . . 155
5.18 Relationship between yield stress and Tg-T obtained from tensile tests with several water contents at 21^oC, and at several testing temperatures on dry specimens 156
5.19 Tensile behaviour as a function of testing temperature on dry sample . . . 156
5.20 Evolution of the mechanical properties as function of testing temperature . . . 157
5.21 Relationship between yield stress and Tg-T_{test} obtained from tensile tests with several water contents at 21^oC, and at several testing temperatures on dry specimens 157
5.22 (a) Evolution of the yield stress as a function of water uptake (b) Finite element model used for the identification procedure . . . 158
5.23 Changes in yield function for different water contents . . . 159
5.24 Water diffusion in a tensile sample . . . 160
5.25 Tensile curves obtained for samples immersed in seawater at 40^oC for several durations . . . 160
5.26 Evolution of the mechanical properties as a function of immersion time . . . 161

5.27 Evolution of the mechanical properties as a function of immersion time 161
5.28 Comparison of predicted tensile behaviour (continuous lines) with experimental data (symbols) for different immersion times in seawater 162
5.29 Water diffusion in an Arcan sample 163
5.30 Prediction of the mechanical behaviour with the moisture dependent model . . . 164
5.31 Prediction of the mechanical behaviour with the moisture dependent model . . . 165
5.32 Arcan samples saturated with different water contents - experimental results . . 165
5.33 Fracture surfaces for different water contents and loading conditions 167
5.34 Comparison between model prediction and the experimental results obtained on saturated samples with different water contents 168
5.35 Water diffusion in an Arcan sample 169
5.36 Comparison between model predictions and experimental results obtained on saturated samples with different water contents 169

6.1 From assembly behaviour to the mechanical behaviour of a bonded specimen . . 173
6.2 From bulk behaviour to Arcan behaviour and vice-versa 175
6.3 Ageing tanks with continuously renewed natural seawater - IFREMER 176
6.4 Aged Arcan specimen 177
6.5 Failure surface SEM analysis on saturated Arcan specimen 179

Introduction

A brief history of structural adhesives

The early times

Putting together different materials in order to make useful tools or objects is a technique that has contributed to human evolution. A good example of this kind of tool is the stone axe, built from a piece of a cutting stone (silex) and a stick usually made from a piece of wood or bone. The two materials were tied together and became a stand-alone object that could be used in different activities such as building or hunting.

Another technique of assembling two materials is bonding them using a "sticky" material. More commonly, these bonding materials are called glues or adhesives. Looking back in history, they have been made from various vegetal or animal substances.

R.D. Adams in one of his books about adhesive bonding techniques [24], provides an interesting introduction to early bonded objects. He cites *Koller et al.* [25] who found in the Harz Mountains in Germany, some Neanderthal tools that date from 80.000 years ago. These tools appear to have residues of ancient adhesive substances. Also from that period of time, *Cârciumaru et al.* [26] found in a cave in Rasnov, Romania, some artefacts belonging to the Upper and Middle Palaeolithic ages. Using different techniques, they identified traces of bitumen on lithic tools which demonstrate the use of adhesives in their manufacture.

Adhesive bonding is not limited to human activities. For example, in the animal world, the chameleon uses a special gland that produces a very sticky substance on its tongue. Capturing prey becomes easier by projecting the sticky tongue directly onto the target. Barnacles also use an adhesion technique in order to fix themselves to rocks. Other interesting examples can be found in an online article written by Barquins [27].

Records of using adhesives in daily life were given by ancient Egyptians. They used different kinds of substances to repair their broken jars [28]. By the beginning of the 11th century, the adhesion technique had been adopted by the clerics and used to decorate the churches [29]. Throughout the Middle Ages, this technique of assembling objects was adopted in a wide range of domains such as ship construction, furniture or more exclusive areas such as the arts. In the 18th century the industrialization of adhesives started, and the first manufacturers could be found in Europe.

Throughout the 20th Century

At the beginning of the 20th century, the adhesives used in almost all industrial applications were still made from natural substances. According to the work of Adams [24], who cites Judge [30], in the 1920s the aircraft and automobile manufacturers were using the following adhesives:

1. Animal glue (hide, bone or hoof)
2. Fish glue
3. Liquid glues (animal glues in liquid, ready-to-use state)
4. Marine glues (made from indiarubber, naphtha and shellac)
5. Casein glues
6. Waterproof glues (modified 'ordinary glue')
7. Vegetable glues
8. Flexible glue (modified animal glue)
9. Albumen glues

All these natural adhesives are polymers made from organic molecules. An important step in the development of structural adhesives was the discovery of synthetic polymers. Various definitions can be found in the literature concerning polymers, but all indicate a substance that is made from small units (molecules) that are linked together by different mechanisms. Among the first synthetic polymers that were developed can be listed: the phenol-formaldehydes, the polyvinyl acetates, the polyvinyl chlorides. They were at the origin of the first structural adhesives. A chronological history of the development of these adhesives is given in *Table1.*

Table 1: Historical development of structural adhesives [1]

Year of commercial availability	**Adhesives**
1910	Phenol-formaldehyde
1930	Urea-formaldehyde
1940	Vinyl-phenolic, acrylic, polyurethane (PUR)
1950	Epoxies, cyanoacrylate, anaerobics
1960	Polyamides, polybenzimidazole, polyquinoxaline
1970	Second-generation acrylic

In the mid 1950s, adhesives were increasingly used, the epoxies were favoured because of their versatility and mechanical properties. It should be mentioned that an adhesive is considered structural if the failure strength is superior to $10MPa$. The present work consists of a study of an epoxy structural adhesive, so this family will be examined in more detail.

Epoxy adhesives

The epoxy resins were first developed in the late 1930s, in France. All epoxy adhesives (the most widely used structural adhesives) are based on formulations of this type of resin, often mixed with other components to improve their characteristics. They can be divided in three classes: two-part room temperature-curable material, one part heat-curable material and film adhesives.

The one feature common to all epoxy resins is the three-membered, oxygen containing epoxy group (*Fig.*1a). Adhesives can be formulated using only a mono-functional epoxy resin but generally these types of formulation lead to poor performance at high temperatures or in creep loading. Therefore, multifunctional epoxy resins are preferred. The most commonly used multifunctional epoxy resin is based on the diglycidylether of bisphenol-A (DGEBA). Its chemical formulation is shown in *Fig.*1b.

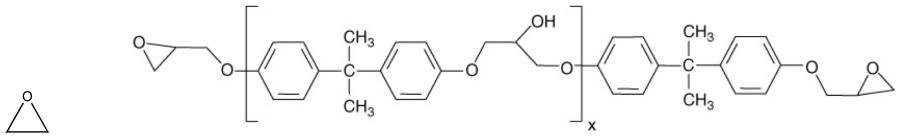

(a) (b)

Figure 1: Structure of a reactive epoxide group (a) DGEBA (b)

The two-part adhesives are generally composed of the epoxy resin and a hardener that could be an aromatic or aliphatic amine. They can be cured at room temperature, or the process can be accelerated by heating. In general, aliphatic amines need 12 hours or more to cure at room temperature. This time can be reduced to 3 hours when heating the adhesive at 80^oC. Regarding the aromatic amine hardeners, they need more elevated temperatures (typically 2 hours at 150^oC) [24].

The curing process involves a chemical reaction between the epoxy resin and the hardener. This can lead to shrinkage of the material which is common to polymerisation systems [1]. Therefore, some residual stress can develop in bonded joints. *Fig.*2 presents the properties of commonly used structural adhesives in terms of modulus, elongation and lap shear strength (LSS) [4].

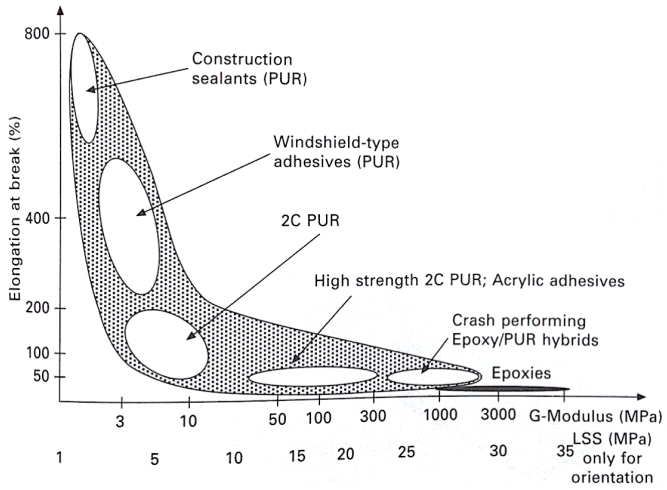

Figure 2: Characteristics of some structural adhesives [4]

Adhesive bonding in marine and renewable energy industries today

Lightweight design is increasingly sought in nearly all industrial sectors. Fibre reinforced composite materials have found many applications in marine and renewable energy industries over the past 50 years.

A key point for the development of renewable energy lies in the use of larger turbine blades in order to increase the performance. This is the reason why wind turbine blades or tidal blades are manufactured using composite materials in order to decrease the weight, but they are composed of several pieces (*Fig.*3) . The assembly of these composite parts (but also of composite and metal parts between blade and hub) is thus of critical importance, and will determine the in-service durability. Adhesive bonding is an attractive joining technique, especially when assembling dissimilar or composite materials. This joining technique, unlike riveted or bolted joints, does not require holes which can lead to large stress concentrations in composites.

Figure 3: Examples of structures for the marine renewable energy industry involving adhesive bonding

However, bonded assemblies can often contain large stress concentrations at the ends of the overlap length. Thus, the failure in adhesively bonded assemblies involving composites is often associated with crack initiation in the adhesive or delamination of the composite plies close to the adhesive joint caused by interlaminar or through-thickness stresses. This is the reason why a fine description of the adhesive behaviour up to final failure is of major importance. The development of accurate non-linear models for such assemblies (i.e. for the adhesive and the composite) requires a large data base of experimental results under various

compression/tensile-shear out-of-plane loads using for instance the modified Arcan test device. Moreover, in order to sturdy the effect of the wet aging on the behaviour of the adhesive, these tests must be performed at different degrees of aging. The use of the multi-model strategy proposed in this project will enable the number of "macroscopic" tests necessary to identify the 3D behaviour of the adhesive and its evolution as a function of the aging time to be significantly reduced.

COSICO project

This work is part of the COSICO project ("**CO**mportement, modélisation et **SI**milation du **CO**llage structural") which means "Behaviour, simulation and modelling of structural bonding". The project was funded by the French National Agency for Research (ANR) and was shared between four research institutes and two industrial partners:

Research Institute Dupuy de Lôme (IRDL): with an extensive experience on the behaviour, the damage and the failure of adhesives and bonded structures.

French Ocean Research Institute (IFREMER): has been working on the long term durability of polymers and composites for over 25 years. The main research activities are directed at developing lifetime prediction models for fibre reinforced composites, adhesives, polymer fibres and bio-polymers.

Processing and Engineering in Mechanics and Materials laboratory (PIMM): is internationally recognized in the field of ageing of polymers and organic matrix composites. Its field of expertise is the study of the long-term behavior and embrittlement of polymeric structures in their use conditions, the emphasis being focused on the effects of environment.

ICUBE Strabourg laboratory: specialized in the modelling of the deformation behaviour of polymers, microstructure-properties- relationships, numerical simulations as well as experimental characterization of the dynamic behaviour of polymers.

RESCOLL: an industrial partner of the project specialised in adhesives formulation.

Florian Madec Composite (FMC): specialised in the design and manufacturing of composite structures for marine and offshore industries.

The aim of the project is to propose a robust and efficient approach for the design of bonded structures for renewable energy and marine applications. It thus fits with the objective "Resource management and adaptation to climate change". The development of a 3D model able to predict the behaviour of a bonded assembly during the in-service life of a marine energy system is of major importance, and is the central theme of the project. Indeed, the cost of the maintenance of marine systems is very high compared to onshore structures. However, the identification of such models usually requires a large data base. The multi-model approach proposed in this project will reduce the cost and the time necessary to perform this identification. The use of tests, originally developed for polymers, on adhesives will facilitate the choice of an adhesive for a specific renewable marine energy system. Moreover, the polymer tests are simpler

to perform and require a smaller amount of material. This approach could also accelerate the development of new adhesives. The project aims to contribute to more efficient design for renewable marine energy systems and thus fits with the objective “Clean, safe and efficient energy”.

Chapter 1

Structural bonding: state of the art

"Bonding is the noble conquest of the irrational, the coupling of two realities, irreconcilable in appearance, upon a plane which apparently does not suit them."

Max Ernst, Écritures, "Au-delà de la peinture"

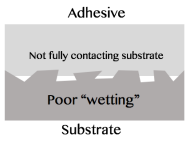

A close look at the bonding process

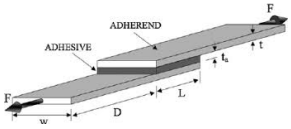

Experimental tests

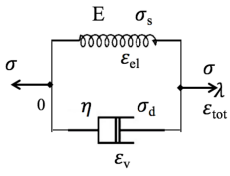

Models describing adhesives behaviour

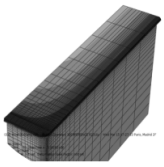
Water diffusion in bonded joints

The aim of this chapter is to give an overview of structural bonding and to introduce the challenges that have to be accomplished when characterising the mechanical behaviour of adhesively bonded joints. It starts with a presentation and some useful explanations regarding the mechanisms of adhesion. Furthermore, the most used experimental tests are presented and another important part is devoted to different approaches that can be adopted in order to model the adhesives mechanical behaviour. The influences of environmental conditions and their effects on adhesives mechanical properties are also introduced in this chapter. Finally, the objectives of this work are given together with the adopted approach.

Contents

1.1 A close look at the bonding process **28**
1.1.1 Mechanisms of adhesion 28
1.1.2 Surface preparation techniques 31
1.2 Mechanical characterisation of structural adhesives **32**
1.2.1 Introduction 32
1.2.2 Multi-scale approach 32
1.2.3 Tests using bulk specimens 33
1.2.4 Joint tests 35
1.2.5 Types of failure in a bonded joint 39
1.3 Modelling the mechanical behaviour of adhesives **40**
1.3.1 Brief introduction 40
1.3.2 Analytical models 41
1.3.3 Long-time creep behaviour 45
1.3.4 Influence of the hydrostatic stress: 3D models 46
1.3.5 Fracture mechanics approach 51
1.4 Environmental conditions and the adhesives behaviour **52**
1.4.1 Water diffusion in adhesives 53
1.4.2 Physico-chemical degradation of epoxy adhesives 57
1.4.3 Influence of water on mechanical properties 59
1.5 Predicting the mechanical behaviour of aged bonded joints **64**
1.5.1 Cohesive failure approach 65
1.5.2 Adhesive failure approach 66
1.6 Aims of the present study **68**
1.7 Presentation of the adopted approach **68**

1.1 A close look at the bonding process

1.1.1 Mechanisms of adhesion

The theory of adhesion is a much-discussed topic in the literature on adhesive bonding technology. Detailed information can be found in the referenced works of *Adams* [24], *Cognard* [31] or *Ebnesajjad* [2]. The bonding process is the result of a combination of several "mechanisms" that occur at different scales. Theories of mechanical interlocking, electrostatics, adhesive diffusion, wetting and chemical reaction have been developed in order to explain this process. It may be difficult to associate the adhesive bonding to an individual mechanism.

Table 1.1: Theories of adhesion [2]

Theory of adhesion	**Scale of action**
Mechanical interlocking	Microscopic
Wettability	Molecular
Electrostatic	Macroscopic
Diffusion	Molecular
Chemical bonding	Atomic
Weak boundary layer	Molecular

The *mechanical interlocking* theory assumes that the strength of a bonded joint depends on the roughness of the bonded surfaces. A high roughness coefficient increases the theoretical bonded area (*Fig.*1.2a) which may lead to better strength of the assembly. This has been shown by *McBain et al.*[32] in the early 1920s. But recent investigations [33] have shown that in some particular cases, for example, the bonding of two pieces of maple wood with a urea-formaldehyde resin, increasing the roughness of the surfaces leads to a reduction of the shear strength of the assembly.

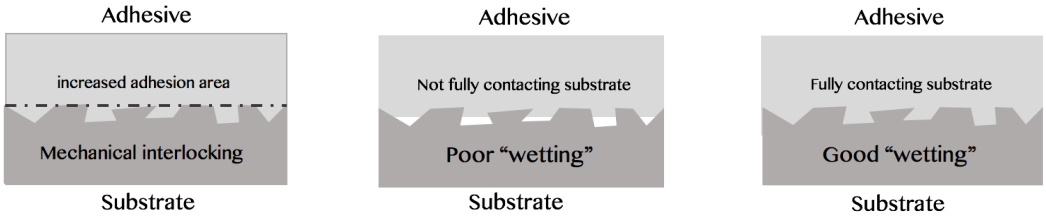

(a) Mechanical Interlocking (b) Poor wetting (c) Good wetting

Figure 1.2: Mechanisms of adhesion

Filling the gaps of a rough surface can be associated with a microscopic scale of action of the adhesive (*Fig.*1.2b). The physics of how an adhesive or viscous material wet a surface has been developed in another theory named *wettability*. The molecules of the studied viscous material are held together by attraction forces. The sum of all forces applied in any molecule is equal to zero. When the viscous material comes into contact with a surface, the resultant of these forces (*cohesion force*) becomes non-zero (*Fig.*1.3a). The energy needed to counteract the cohesion force is called *surface energy*. By introducing this new quantity, it is possible to define the

surface tension (γ) which is equal to the work (dW) required to increase the area of a surface by unit amount (dS) (*Eq.1.1*).

$$\gamma = \frac{dW}{dS} \tag{1.1}$$

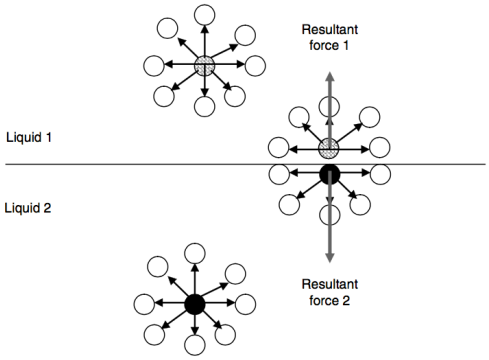

(a) Liquid-liquid interface and balance of forces on molecules of liquids [2]

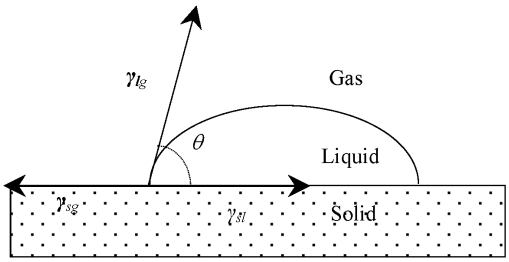

(b) Wetting of a solid surface with a viscous liquid, with gas as a surrounding medium [5]

Figure 1.3: Surface energy

A droplet on a smooth surface will wet it to a certain degree which can be defined by a *contact angle*(θ). *Fig.*1.3b illustrates the angle θ measured at equilibrium in an ideal system which contains a homogeneous, smooth, planar and rigid surface and a drop of a liquid surrounded by an ideal gas. The three environments are limited by interfacial tensions: γ_{sl} (solid-liquid), γ_{lg} (liquid-gas) and γ_{sg} (solid-gas). A relation between these quantities (Eq.1.2) and the contact angle was first developed by *Young* in 1805 [34] but without presenting a proof. More recent research has proved the theory [35][36].

$$\gamma_{lg} \cos\theta = \gamma_{sg} - \gamma_{sl} \tag{1.2}$$

Some interesting examples of the wettability phenomenon have been shown by *Wang et al.*[5] who studied the wetting of leaf surfaces. *Fig.*1.4 shows a droplet of water on different types of surface.

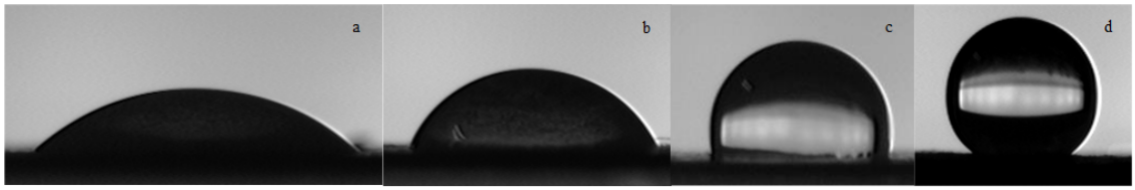

Figure 1.4: Water droplet on a super-hydrophilic a), highly wettable (b), non-wettable (c) and hydrophobic (d) surfaces [5]

An adhesive with a high contact angle will show poor wettability *Fig.*1.2b and will not be able to fill the gaps of a rough surface. An optimal contact angle is needed to obtain a full contact with the surface of a substrate (*Fig.*1.2c). In order to measure the contact angle, several methods can be found in the literature. One of the most common is the sessile drop method [37]

which consists of measuring the contact angle with a goniometer using an optical subsystem to capture the profile of the drop.

At a macroscopic scale, two materials could be bonded by the electrostatic force between them. Usually when two conducting materials are in contact, electrons are transferred from one to another creating a force of attraction. Since adhesives are in general polymers, they are insulators so this may not be pertinent. But *Adams* [24] cites an interesting study made by *Randow, Williams et al.* [38] on the"cling films" used for food packaging. They concluded that the most important factor influencing the adhesion of the films is their surface smoothness but the electrostatic charge also has an influence on the bonding process .

Diffusion is another mechanism of adhesion at a molecular scale. The pioneer of this theory was *Voyutskii* [39] in the early 1960s. He assumed that the strength of a bonded joint is due to the diffusion of the long molecular chains of the adhesive into the substrate and vice-versa. Obviously, this should happen at temperatures above the glass transition temperature (when the molecular chains become mobile) when the two materials are compatible and put in contact. In order for this mechanism to be possible, the two materials must have similar chemical structures. This theory is more suitable for assembling rubbery polymers (autohesion).

One of the strongest mechanisms of adhesion is chemical bonding. This occurs at an atomic scale and involves the formation of strong interactions between the atoms of the adhesive and those of the adherend. Ionic and covalent bonds form strong and durable interfaces while the much weaker forces like hydrogen bonds, Lewis acid-base and van der Waals forces also contribute to the strength of the joint. *Tab.*1.2 presents the range of bond energies for each type of chemical bond.

Table 1.2: Strengths of chemical bonds

Type of bond or interaction	**Energy** $[kJmol^{-1}]$
Ionic	700 - 6000
Covalent	200 - 1000
Hydrogen bond	10 - 100
Lewis acid-base	10 - 80
Van der Waals forces	0.05 - 50

Certainly, all these mechanisms of adhesion have an important role in making a strong bonded joint but, in some particular cases, even though the adhesive and the adherend are compatible, a premature failure of the assembly is obtained. This is possible due to a contamination of the contact surfaces with impurities. Thus external factors may be responsible for the failure. The weak boundary layer theory (WBL) is one example. *Bikerman* [40] was one of the pioneers of this theory in 1967. He showed that air trapped at the interface between the adhesive and the substrate can cause a weak boundary layer which may finally lead to an adhesive failure of the bond. Moreover, oxides present on the bonding surfaces can also develop a WBL. Contaminants like oils or greases may be dissolved by the adhesive but their presence on the bonded surface introduces an important risk of adhesive failure. The ability of certain acrylic structural adhesives to dissolve greases, may be an advantage compared to the epoxy adhesives, which are inferior from this point of view.

1.1.2 Surface preparation techniques

As shown in the last paragraph of section 1.2.1, the bonded surface of the substrates has an important role in order to avoid the appearance of weak boundary layers which may lead to premature failure of the assembly. This is why surface preparation techniques have been developed to ensure good conditions of adhesion. Since the present work is based on the results obtained on an aluminium-epoxy assembly, a close look at surface treatment techniques for aluminium is essential.

The aim of surface treatment is to ensure good adhesion conditions between the adhesive and the adherend which, in this case, will be the aluminium substrate. Depending on the bonding requirements and the service conditions, it is possible to identify different types of treatments; mechanical, chemical, and electrochemical.

Mechanical treatments include physical methods, usually abrasion, sanding and grit blasting, which are applied directly to the bonded surface in order to generate the properties needed for adhesion. By applying these methods all the friable layers will be removed and a good roughness will be obtained. Solvent degreasing with acetone or other non-chlorinated or chlorinated substances will clean the impurities left after these processes. Mechanical preparation of the surfaces is considered as the minimal required treatment for improving the adhesion properties.

Chemical treatments used for aluminium alloys are methods that involve coupling agents, etchants and conversion coatings. These treatments will chemically modify the surface of the substrate by introducing inorganic networks that will interact with the adhesive. Furthermore, as in the case of solvent degreasing, they can remove the remained friable layers or corrosion mechanisms. Aluminium surfaces can be cleaned with solutions that mainly consist of mixtures of sodium, hydroxide, sodium carbonate, tri-sodium phosphate, sodium pyrophosphate or sodium metasilicate with a pH range between 9 and 11 [41].

Electrochemical treatments are the most complex methods of surface preparation but also the most efficient. They can control the wettability or the surface roughness and can give the best level of initial adhesion and durability. Indeed, excellent performance can be obtained but with a high cost and these treatments are time consuming. The most widely used electro-chemical processes are the phosphoric acid anodising (PAA), chromic acid (CAA) and sulphuric acid anodising (SAA).

A detailed investigation of these processes and their application can be found in a paper published by *Critchlow et al.* in 2005 [41]

These treatments must be adapted to the required properties of the bonded joint and the environmental conditions. As specified earlier, at least a mechanical treatment is needed to obtain good mechanical properties of the joint. However, using bonded joints in marine or offshore industries also requires considering the moisture resistance of the bonded joint.

A lot of information can be found in the literature on this topic. *Critchlow et al.* in an article entitled "Surface Treatments for Moisture Resistance" published in 2013 [42] presents different studies and surface preparation techniques that show considerable improvements in the

moisture resistance of the designed bonded joints. Among those, chemical and electro-chemical treatments were considered to be the most efficient but there are some previous studies [43] that showed that in some cases, just a mechanical treatment, such as grit-blasting, has provided more durable joints in seawater conditions than some more complex chemical treatments.

1.2 Mechanical characterisation of structural adhesives

1.2.1 Introduction

Different techniques are used today for assembling parts of a structure. For the metallic parts, several solutions can be employed (bolts, fasteners or welding methods). These solutions are well mastered by mechanical designers and manufacturers. When an increase in performance of the structure (dimensions, weight, strength, etc) is required, advanced materials may be the solution. Fiber reinforced composites are an example of this kind of material.

Parts made from composite materials are more difficult to design and they need special techniques to assemble them. For example, a hole made in such a part may lead to stress concentrations that can be catastrophic, so bolts or other fasteners should be avoided. Bonding represents an interesting solution.

During the different stages of the development and manufacturing of a bonded structure, engineers and designers must certify their products. They need to perform tests to approve the requirements of their assemblies. These tests should be related to the real application including the applied loadings and the adherends of the real structure.

1.2.2 Multi-scale approach

The mechanical behaviour of a bonded joint is influenced by all the phenomena that take place at different scales (*Fig.*1.5). The best tests are those performed directly on a joint that is part of the real structure, but these tests could rapidly become expensive. An interesting solution that could lead to good results is the development of tests on a smaller scale that could still represent the real loading of the joint.

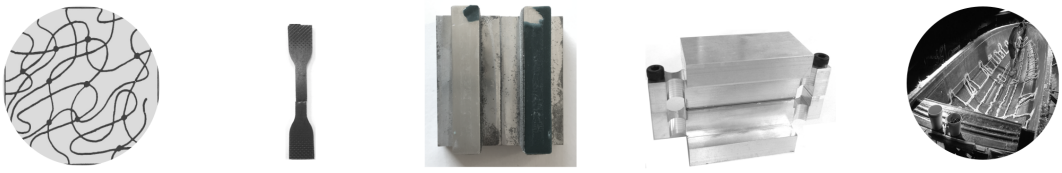

(a) Microstructure (b) Bulk (c) Interface (d) Bonded joint (e) Structure

Figure 1.5: Multi-scale approach

There are two main categories of tests used to characterise the mechanical behaviour of an adhesive up to failure: test on bulk specimens and tests of the adhesive in a joint or in situ. A short presentation of the main experimental tests is made hereafter.

1.2.3 Tests using bulk specimens

1. Tensile tests

   The basic mechanical properties of an adhesive such as Young's modulus, Poisson's ratio or the failure load, can easily be determined using tensile tests on bulk specimens. The identified properties will not be influenced by the nature of the adherends and will be considered as intrinsic properties of the studied adhesive.

   Tensile tests involve applying a uni-axial state of stress to a thin bulk specimen. A good characterisation of the mechanical behaviour of the adhesive will be obtained using specimens with clean edges and no voids. Adhesives that are liquid in the uncured state (generally one-part adhesives) can be injected or poured in a mould with the final shape of the specimen (Fig.1.6a) [44]. For more viscous adhesives, a different method has been developed in France (NF T 76-142 [45]). Using this method, it is possible to obtain a homogeneous plate of adhesive (*Fig.*1.6a). The final form of the specimen is cut out from this plate using a water jet cutter. The results obtained from specimens with voids inside cannot be considered valid (*Fig.*1.6c).

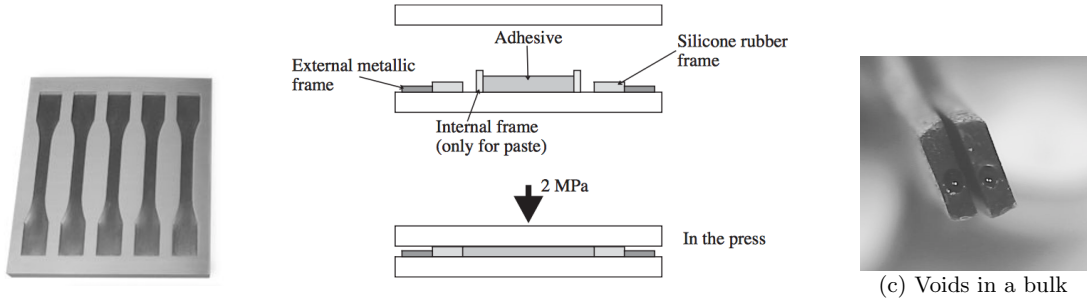

(a) Mould for pouring (b) French method NF T 76-142 [46] (c) Voids in a bulk specimen

Figure 1.6: Manufacturing of bulk specimens

   Dimensions of the dog-bone specimens are determined by the standard NF EN ISO 527 [47]. An example of this kind of geometry is given in *Fig.*1.7a. For more rigid adhesive, longer specimens can be used for the tests.

   The typical tensile mechanical response of a structural adhesive bulk specimen can be observed in *Fig.*1.7b. Using this strain-stress curve, it is possible to calculate a value for Young's modulus, failure strength and even the Poisson's ratio. These techniques will be described in the next section of this document.

   For adhesives with a mechanical behaviour depending on the hydrostatic pressure, compressive tests may be needed. The geometries for this kind of test can be found in the French standard NF T 51 101 [48].

2. Shear tests

   In order to be able to understand the entire mechanical behaviour of the adhesive, it is also necessary to characterise its shear behaviour. Experimental tests performed on bulk tubes of adhesive are a solution to this problem. The torque is applied as shown in *Fig.*1.8.

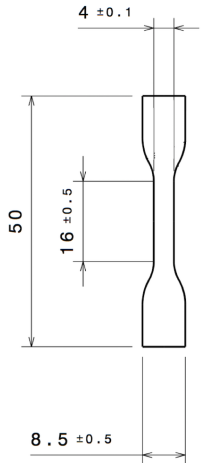

(a) Dimensions for a dog-bone specimen

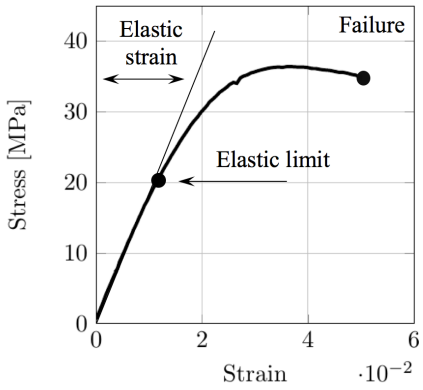

(b) Example of tensile behaviour of a structural adhesive

Figure 1.7: Tensile test on bulk specimen

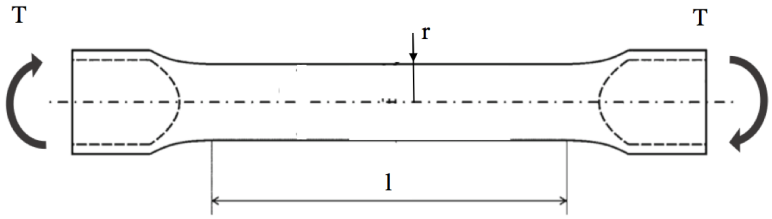

Figure 1.8: Bulk torsion specimen [6]

The shear stress and the shear strain can be calculated using *Eq.*1.3 and *Eq.*1.4 where T is the applied torque at the ends of the specimen, r is the radius, I_0 the polar moment of inertia and l is the gauge length. There are no standards to define the geometries of the specimens for this kind of test. Authors who have worked with this kind of geometry are *Chen et al.* [6] or *Gali et al.* [49].

$$\tau = \frac{T \times r}{I_0} \tag{1.3}$$

$$\gamma = r \times \frac{\phi}{l} \tag{1.4}$$

3. Other advanced tests

For more complex cases of loading, Iosipescu tests [50] (*Fig.*1.9a) or Arcan tests [51] (*Fig.*1.9b) allow tensile and shear loads to be combined. With these tests, it is possible to characterise the bulk or adhesive's behaviour in situ. These kinds of tests have a special importance because they allow a first comparison to be made between the mechanical behaviour of the adhesive in bulk specimens and the mechanical behaviour of the bonded joint.

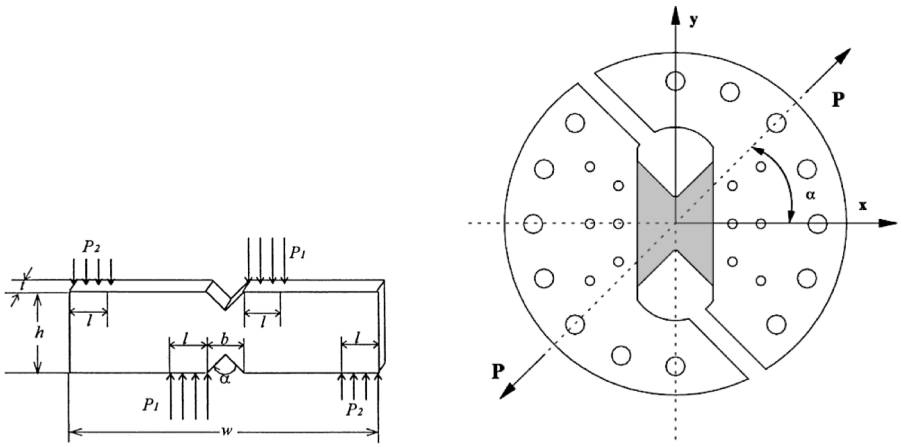

(a) Sample for Iosipescu test

(b) Modified Arcan fixture for bulk specimens [52]

Figure 1.9: Iosipescu and Arcan tests

4. Dynamic mechanical analysis tests

   The aim of the dynamic mechanical analysis (DMA) test is to measure the response of a material to a sinusoidal mechanical load as a function of time or temperature. Because epoxy adhesives are polymers with a viscous behaviour, this kind of test can be used to get information about the evolution of the mechanical properties such as Young's modulus under different conditions.

   The applied stress and the strain response are usually shifted in time with a factor called $tan\delta$ or *loss factor*. This is the ratio between the elastic modulus $E^{'}$ and the viscoelastic properties of the material $E^{''}$. The standard ISO 6721-1 [53] contains all the information required for performing these tests in good conditions.

1.2.4 Joint tests

The *in-situ* or joint experimental tests allow the characterisation of mechanical behaviour of the adhesive inside a bonded joint. Because the thickness of the joint is usually smaller (up to $100\mu m$) than that of the bulk specimens (1 to 2mm), the same adhesive (nominally) may have a different behaviour in the two cases. This is due to the fact that, depending on how they are manufactured, even though the same curing cycle is applied, the bulk specimens and the joint adhesive can reach different degrees of polymerisation. Also, the existence of the so-called interface, between the adhesive and the adherend, where the local properties of the adhesive may be altered, can influence the global behaviour of the adhesive in the bonded joint [7].

However, as has been shown by some authors [56][55][54] the mechanical behaviour of an adhesive in bulk specimens and in a bonded joint may be quite similar. For instance, *Da Silva and Adams* [54] presented results from TAST (see next section) tests which provided a good prediction of the modulus and the strength in tensile bulk tests *Fig.*1.11a. Certainly, these results are accurate only when a cohesive failure is obtained in the in-situ tests. Another example is the results obtained by *Lilleheden* [55], who showed that the elastic properties of an

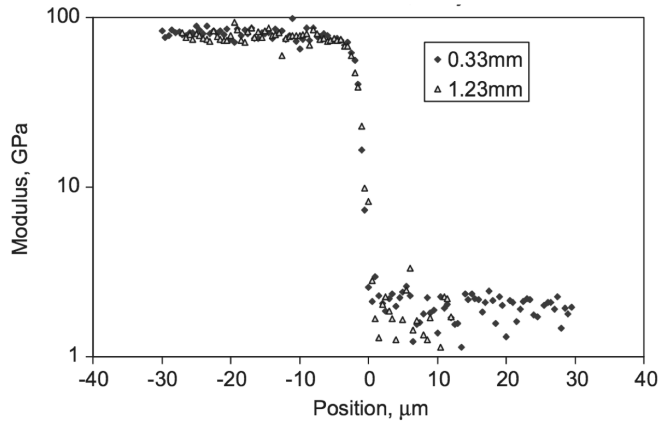

Figure 1.10: Nano-indentation across the interface of an aluminium/adhesive joint [7]

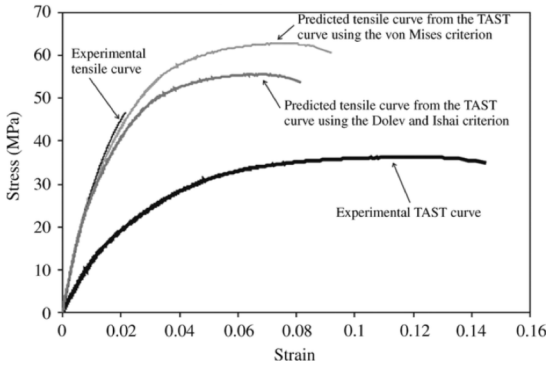

(a) Experimental *vs.* predicted tensile stress–strain curve from the experimental TAST curve for Supreme 10HT at $22^{o}C$ [54]

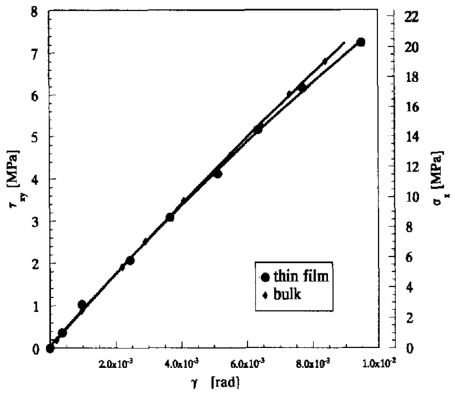

(b) Comparison of elastic properties of the adhesive in thin-film and bulk forms [55]

Figure 1.11: Comparison between thin-film and bulk form behaviour

adhesive in bulk and thin film are very close *Fig.*1.11b.

1. Lap joint test

   Generally, most of the experimental tests that allow the characterisation of the mechanical properties of adhesives in joints are lap shear tests. These tests are very easy to implement and they can be done without sophisticated equipment. One example is the single-lap joint test (SLJ)(*Fig*1.12). The preparation of the samples is very important in order to obtain a good characterisation of the adhesive's behaviour. The geometry for the samples can be found in the standard ISO 4586 [57].

Figure 1.12: Single Lap Joint

   In this kind of test, the stress distribution is non-uniform throughout the bonded surface and the edge effects are very important [58]. The peel stress can lead to premature

fracture of the sample near the interfaces. Even though these tests are cheap and simple to manufacture, it is difficult to use them to obtain good exploitable results for design.

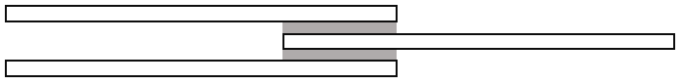

Figure 1.13: Double lap shear

An alternative to the single-lap joint is the double-lap joint test (*Fig.*1.13). Using three adherends, the specimens become more rigid and the deformation of the substrates is considerably reduced. This may lead to a peel stress at the bonded surface that is 2 times smaller than for the case of a single lap joint test.

2. Thick adherend shear test (TAST)

   This test was developed by *Krieger et al.* [59] in order to further decrease the peel stress in the adhesive. The same principle as the SLJ test is adopted the only difference being the thickness of the adherends (*Fig.*1.14). By changing this dimension, the peel stress is considerably reduced, and a more uniform shear stress distribution is obtained. Even so, the finite element simulations (FE) performed by *Créac'hcadec et al.* [60] show that high peel stress concentrations are still present at the edges, near the overlap. They can be the cause of premature failure during the test.

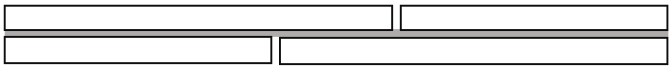

Figure 1.14: Thick adherend shear test (TAST)

3. Butt joint

   Several tests characterise the shear behaviour of an adhesive in a bonded joint have been presented in this section. But tensile behaviour of a joint is important, especially when the elastic modulus, compression modulus, or the Poisson's ratio need to be identified. The butt joint tests (*Fig.*1.15) allow access to these values, using circular specimens with dimensions that can be found in the standard *ISO 6922* [61]. The geometry of the specimens gives a uniform stress distribution in the bonded joint. Nevertheless, this test is difficult to perform due to the precise alignment of the adherends required.

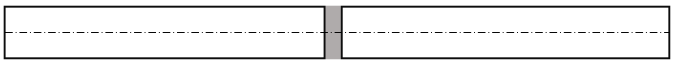

Figure 1.15: Butt joint

A more complex butt joint test that uses multi-axial loadings was developed and proposed by *Arnaud et al.* [8]. This uses a complex device (*Fig.*1.16a) that combines traction and torsion in order to obtain different ratios of tensile compression/shear. The substrates are machined with beaks that minimize the stress concentration near the edges. The geometry of the beaks was optimised using FE simulations and the dimensions that influence the

stress distribution near the edges can be observed in *Fig.*1.16b, where e represents the thickness of the bonded joint. However, while this test is better in terms of scatter than the simple butt-joint test, the machining of the substrates needs special tools and the bonding system remains quite complicated.

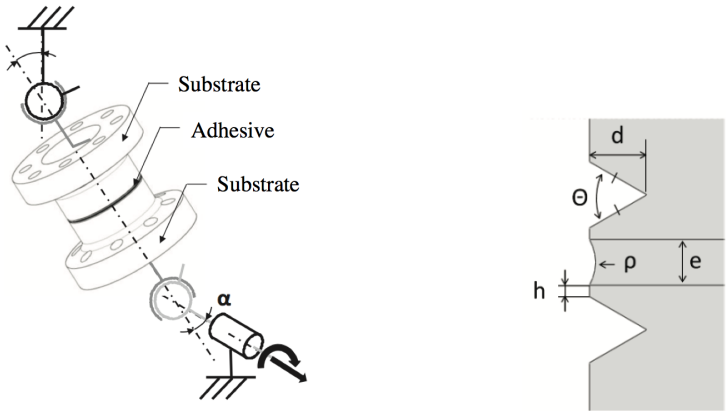

(a) (b)

Figure 1.16: Schematic representation of the testing device and the mounted specimen (a) Geometry of the specimens beaks (b) [8]

4. Modified Arcan test

The possibility of applying multi-axial loading conditions to a bonded joint is a characteristic of the most recently developed experimental tests for bonded joints. Inspired by the initial device created by *Arcan et al.* [51] to characterise the mechanical behaviour of epoxy resins for composites under mixed fracture modes, the modified Arcan test was developed by *Cognard et al.* [62] to analyse the behaviour of adhesives in bonded joints.

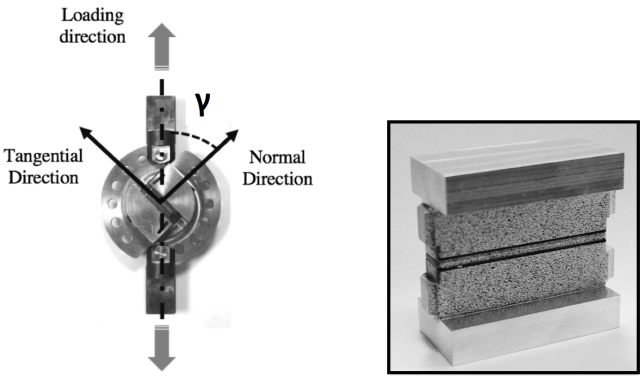

(a) Arcan device (b) Arcan specimen

Figure 1.17: Modified Arcan test

The special characteristic of this test is the loading device, which allows various ratios of combined proportional tensile compression / shear loadings to be applied. The positioning angle on the tensile machine defines the state of load that is applied to the bonded joint

(*Fig.*1.17a).

The bonded specimen (*Fig.*1.17b) is mounted between these two components using a special fixing system that was improved by *Cognard et al.* [63] in order to reduce the stress induced when the screws are tightened. The specimens are machined with beaks near the edges [64] which allow the reduction of stress concentrations.

Davies et al. [7] studied the influence of the thickness of the bonded joint using this device and the special geometry of the specimens. The results showed that the stress distribution of the hydrostatic pressure and the von Mises stress are dependent on the thickness of the bond line. However, in the middle of the joint a uniform stress is obtained, as can be observed in *Fig*1.18a and *Fig*1.18b, where the abscissa represents the length of the bond.

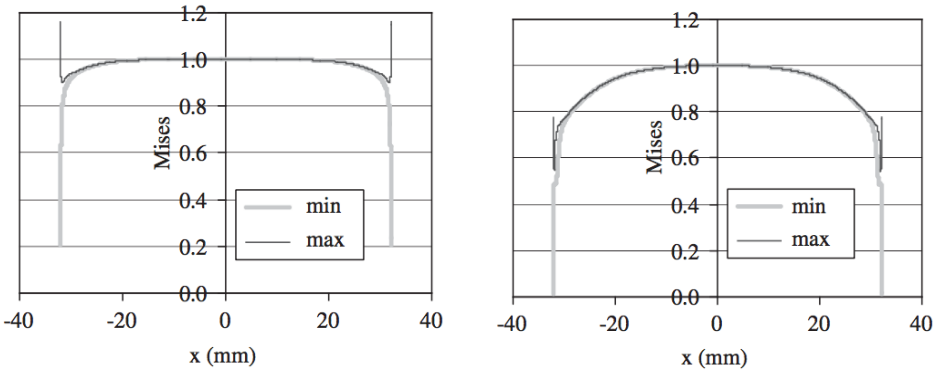

(a) Tensile (b) Shear

Figure 1.18: Calculated stress distribution in a thick bonded joint [7]

Thévenet et al. [65] and other authors [66], have also used this device to characterise the mechanical behaviour of adhesively bonded joints under cyclic loadings.

5. Scarf tests

   An alternative to the Arcan device that allows the characterisation of the mechanical behaviour of bonded joints under multi-axial loadings is the scarf joint test. This test is simple and could be an interesting industrial solution because no special devices are needed to perform it. The bonded specimens are mounted directly on the tensile machine. Several authors have used this test in their investigations [67][68][69].

1.2.5 Types of failure in a bonded joint

The failure mode of a bonded joint is very important in order to completely understand its mechanical behaviour. The results obtained in experimental tests, such as the maximum load value, depend on the initiation and propagation of cracks. Different scenarios can be imagined when the failure of a bonded joint occurs.

Adhesive failure involves crack initiation at the substrate-adhesive interface and then propagation along this separation line (*Fig.*1.19a). Generally, this type of behaviour leads to poor

(a) Adhesive (b) Mixed (c) Cohesive (d) Adherend

Figure 1.19: Types of failure in a bonded joint

results concerning the mechanical properties of the joint and, in many cases, is due to interface damage mechanisms. These could be linked to the surface preparation techniques, the chemical incompatibility of the bonded materials (the adhesive and the adherend) or to external factors such as diffused moisture.

Mixed failure is a more complex type of failure (*Fig.*1.19b). In some cases, the crack may initiate at one of the interfaces and propagate throughout the adhesive until it reaches the other interface and it may then alternate between the two.

Cohesive failure allows the best characterisation of a bonded joint, as the adhesive's mechanical properties will dictate the strength of the joint. In order to be able to characterise the mechanical behaviour of the adhesive in a bonded joint, this type of failure needs to be obtained. The crack is propagating in the adhesive (*Fig.*1.19c) and this means that sufficient adhesion strength was developed between the two materials.

Substrate failure may occur when the mechanical properties of the adhesive and the bonded joint are superior to those of the adherends (*Fig.*1.19d).

1.3 Modelling the mechanical behaviour of adhesives

1.3.1 Brief introduction

The experimental tests presented in the last section can be used to characterise the adhesive directly in the bonded joint as shown by [70]. Single or double lap joints are an interesting solution to this problem [71], but due to the geometries of the substrates, they may present high stress singularities near the edges that can cause a premature failure of the joint [72]. *Cognard et al.* [63] proposed the modified Arcan device in order to characterise the mechanical behaviour of adhesives in bonded joints up to failure. This can be achieved using substrates with special geometries [62] that reduce the stress concentrations near the edges.

Characterisation of the mechanical behaviour of the adhesive used in bonded joints is a very important step in order to be able to describe the failure of this kind of structure. Even though these adhesives are essentially polymers with a viscous behaviour, the load transfer between the components of the bonded joint is usually linked to their instantaneous elastic properties [73]. However, the viscous behaviour represents a major characteristic of polymeric adhesive materials. Therefore, the understanding of these phenomena is important in order to accurately predict the failure and the lifetime of bonded structures. The experimental tests performed on

bulk specimens show a non-linear behaviour of most adhesives that is very sensitive to the strain rate [74][11]. The viscous response of different structural adhesives has also been revealed under impact loadings in previous studies [75]. All these tests require homogeneous bulk specimens, without any defects, that may be difficult to obtain [76].

Different models have been proposed in the literature in order to predict the mechanical behaviour of epoxy adhesives. In some cases, viscoelastic models [77][78][10][79] can be perfectly adapted to characterise the time-dependent behaviour and to predict the influence of the strain rate. Other authors have proposed elastoplastic models [80][81] or viscoplastic models [82][83] which are characterised by a threshold and a permanent strain.

This section will briefly present an overview of the different approaches that can be adopted to model the mechanical behaviour of the adhesive as well as describing two models that inspired the present work; one viscoelastic and one viscoplastic.

1.3.2 Analytical models

The response of a material to a mechanical load can be modelled mathematically. Applying a stress, in a specific direction, to a bulk specimen will cause a deformation that depends on the nature of the material. Therefore, the applied stress can be written as a function of the strain (Eq.1.5) where σ is the stress in the system and ε is the strain.

$$\sigma = f(\varepsilon) \tag{1.5}$$

The form of this function allows materials to be classified in different categories. A linear function will define the group of elastic materials. The more complex responses will describe the mechanical behaviour of other types of materials such as the viscoelastic or the viscoplastic ones.

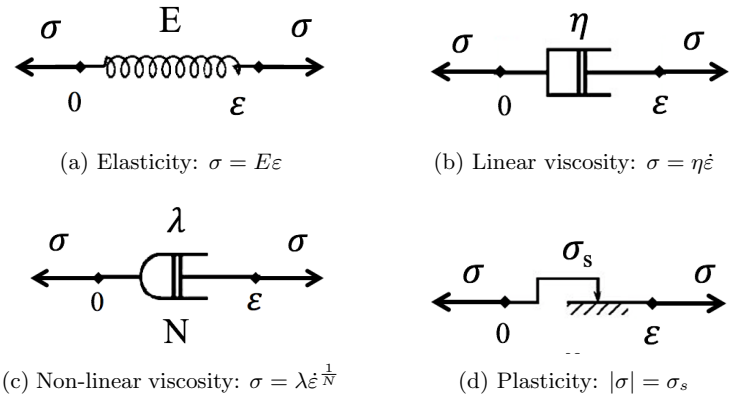

(a) Elasticity: $\sigma = E\varepsilon$ (b) Linear viscosity: $\sigma = \eta\dot{\varepsilon}$

(c) Non-linear viscosity: $\sigma = \lambda\dot{\varepsilon}^{\frac{1}{N}}$ (d) Plasticity: $|\sigma| = \sigma_s$

Figure 1.20: Common elements used to model the mechanical behaviour of materials: Spring (a), Linear dashpot (b), Non-linear dashpot (c), Frictional device (d)

Analogical models are based on mechanical elements that have a response similar to a real material. They are usually used to give an image of the functions used to model the mechanical behaviour and they don't represent any physical mechanisms in the materials. The

most common mechanical elements and their mathematical relations are represented in *Fig.*1.20, where σ is the applied stress, ε is the strain, E is the equivalent of the elastic modulus, η,λ,N are viscous parameters and σ_s is the yield stress threshold.

Adhesives are polymers that may have a complex mechanical behaviour. For example, they can behave like viscous fluids, viscoelastic or viscoplastic solids or a combination of these behaviours. In this case, the model is set up by assembling the basic elements in more complicated systems. The mathematical solution of these systems will give the response of the material.

1.3.2.1 Viscous behaviour

These materials have a mechanical behaviour which is strongly rate dependant. They can be modelled by putting together a spring that corresponds to the elasticity and a dashpot which describes the viscosity. Of course, the two elements can be assembled in two ways: in series or in parallel.

1. Maxwell model

   This model is obtained by arranging the spring and the dashpot in a serial combination (*Fig.*1.21) [84]. The total strain ε_{tot} is obtained by adding together the elastic ε_{el} and the viscous ε_v strains. The stress σ is supposed to be the same in the spring σ_s and in the dashpot σ_d (*Eq.*1.6).

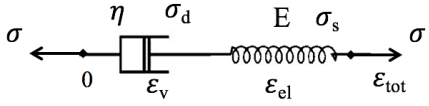

Figure 1.21: Maxwell elementary model

$$\varepsilon_{tot} = \varepsilon_{el} + \varepsilon_v \qquad \sigma = \sigma_s = \sigma_d \tag{1.6}$$

Using the *Eq.*1.6, it is possible to determine the constitutive equation for this model:

$$\dot{\varepsilon} = \frac{\dot{\sigma}}{E} + \frac{\sigma}{\eta} \qquad \sigma = E\varepsilon_0 exp(-\frac{E}{\eta}t) \tag{1.7}$$

Thus, the model can describe the mechanical behaviour of materials which behave as shown in *Fig.*1.22. Thermoplastic polymers can exhibit this behaviour near their transition glass temperature.

As it can be seen in *Fig.*1.22, the stress in the material is influenced by the strain rate (*Fig.*1.22a) and the creep behaviour is close to a fluid, allowing unlimited deformation under finite stress (*Fig.*1.22b).

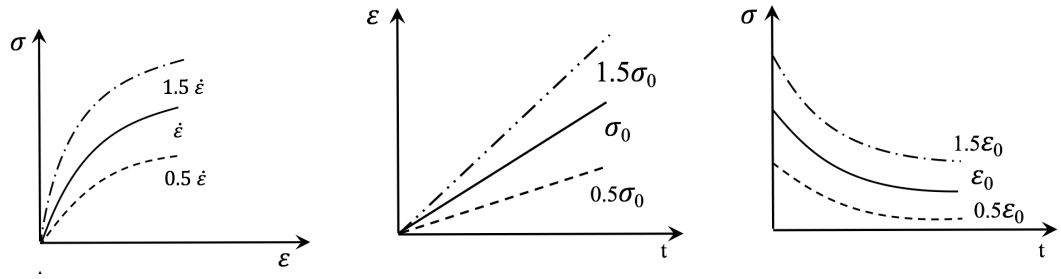

(a) Hardening (b) Creep (c) Relaxation

Figure 1.22: Maxwell model response [9]

2. Kelvin-Voigt model

In this model the two basic elements (spring and dashpot) are assembled in parallel (*Fig.*1.23) [9]. The applied stress is equally distributed in the two elements and the total strain is equal to the strain in each element (*Eq.*1.8).

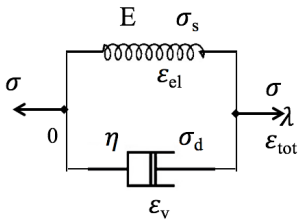

Figure 1.23: Kelvin-Voigt elementary model

$$\varepsilon_{tot} = \varepsilon_{el} = \varepsilon_v \qquad \sigma = \sigma_d + \sigma_s \tag{1.8}$$

Applying the same reasoning as for the Maxwell model, in this case, the obtained constitutive equation is equal to:

$$\varepsilon = \frac{\sigma}{E}\left[1 - exp\left(-\frac{E}{\eta}t\right)\right] \qquad \sigma = E\varepsilon + \eta\dot{\varepsilon} \tag{1.9}$$

The mechanical response of this system (*Fig.*1.24) is slightly different from the Maxwell model, even though the same elementary mechanical elements were used. This model is characterised by different creep behaviour. Because the dashpot is restricted by the spring, a delayed elasticity can be observed when the creep strain approaches the final value. Organic polymers or rubber may exhibit this kind of mechanical behaviour.

1.3.2.2 Viscoplastic behaviour

Some authors have modelled the adhesive behaviour using visco-plastic models [8][13]. The materials exhibiting this kind of behaviour present a permanent strain after a certain value of the

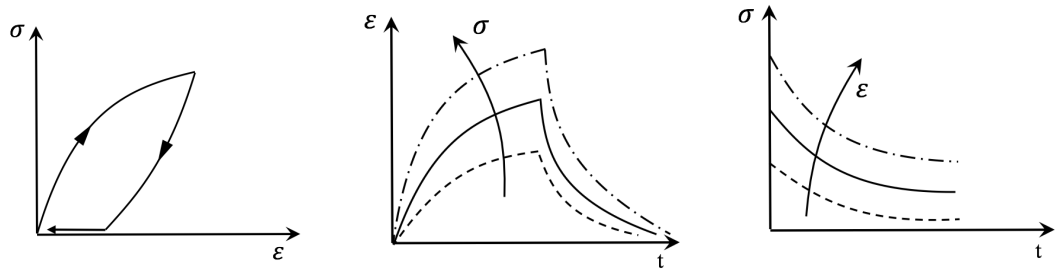

(a) Hardening (b) Creep (c) Relaxation

Figure 1.24: Kelvin-Voigt model response [9]

applied stress. This is called the yield stress (σ_0) and it can be considered by adding a frictional device in the analogical models. One of these systems was proposed by *Bingham-Norton* [85].

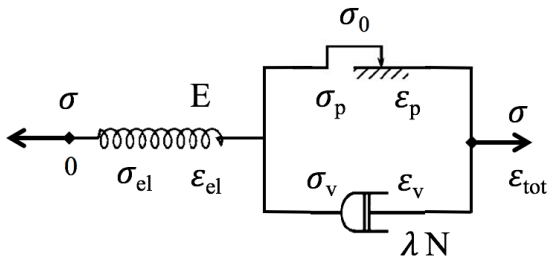

Figure 1.25: Bingham-Norton elementary model

The constitutive law for this model is becoming more complex but the same principle is adopted to find the solution σ_{el}, σ_v, σ_p represent the stress in the three mechanisms and ε_{el}, ε_v, ε_p the associated strains. The applied stress σ and the total strain ε_{tot} can be written as shown in the *Eq.*1.10:

$$\varepsilon_{tot} = \varepsilon_{el} + \varepsilon_v = \varepsilon_{el} + \varepsilon_p \qquad \sigma = \sigma_{el} = \sigma_v + \sigma_p \tag{1.10}$$

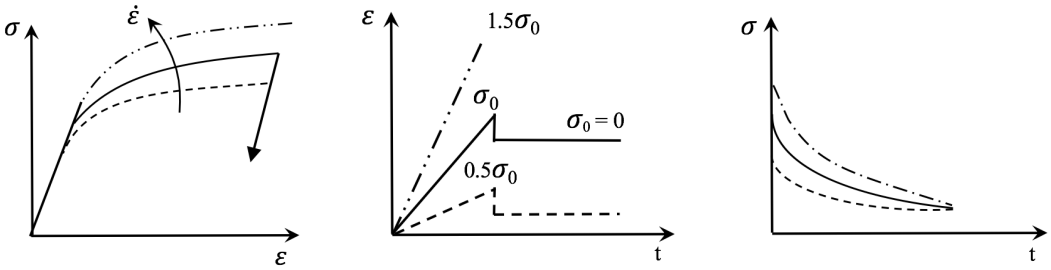

(a) Hardening (b) Creep (c) Relaxation

Figure 1.26: Bingham-Norton model response [9]

This model shows elastic behaviour if the applied stress is smaller than the yield stress *Fig.*1.26a. When the threshold is reached, the hardening occurs but it depends only on the strain rate *Eq.*1.11 and *Eq.*1.12. The creep behaviour is represented in *Fig.*1.26b and the

response in relaxation *Fig.*1.26c is given by a more complex equation (*Eq.*1.13).

$$\sigma < \sigma_0 \Rightarrow \qquad \varepsilon_{tot} = \varepsilon_e = \frac{\sigma}{E} \tag{1.11}$$

$$\sigma \geq \sigma_0 \Rightarrow \qquad \varepsilon_{tot} = \varepsilon_{el} + \varepsilon_p \qquad \dot{\varepsilon}_{tot} = \frac{\dot{\sigma}}{E} + f(\sigma) \tag{1.12}$$

$$\varepsilon_{tot} = \varepsilon_0 H(t) \rightarrow \sigma = \sigma_0 + \frac{E\varepsilon_0 - \sigma_0}{\left[1 + \frac{(N-1)E}{\lambda^N}\left(E\varepsilon_0 - \sigma_0\right)^{N-1} t\right]^{\frac{1}{N-1}}} \tag{1.13}$$

1.3.3 Long-time creep behaviour

Characterising the monotonic and short-time behaviour of adhesives is a first step in order to understand the mechanical behaviour of adhesives and bonded structures, but the prediction of long-time loading effects is an important issue that must also be analysed.

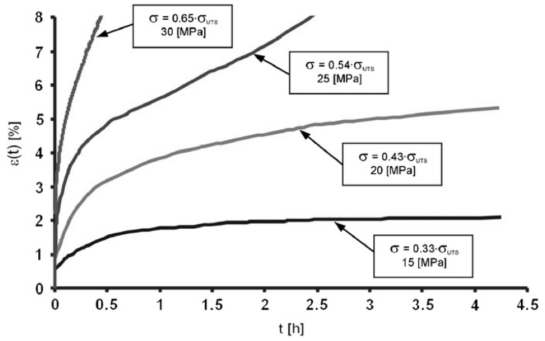

Figure 1.27: Creep tests of an epoxy adhesive at room temperature [10]

A typical response of an adhesive subjected to different long-time loadings can be seen in *Fig.*1.27 [10]. After the elastic strain, an inelastic evolution of the strains is observed as a function of decreasing speed. This stage is called the primary creep range and is followed by a stationary range in which the strain rate remains constant. The third creep range may occur after long periods of time or high stresses just before the failure.

The prediction of mechanical behaviour under long creep loads needs more complex mathematical models which can describe a non-linear dependency between the strain evolution and the time. *Weitsman et al.*[86] proposed a non-linear viscoelastic model in which the compliance C is modelled as a function of time, using three material parameters (C_0, C_1, t) that have to be identified. *Ha et al.*[87] adopted this model to describe the time dependent behaviour of laminated composite at elevated temperature and propose a reliable method for identifying the parameters.

$$C(t) = C_0 + C_1 t^n \tag{1.14}$$

These kinds of models are named "*power-law*" models because the compliance is an exponential or a logarithmic function of time. They can correctly describe the long-time creep behaviour but

the recovery is predicted to be linear, which is not the case for most of the viscous adhesives. An example can be seen in a paper written by *Yu et al.* [11] who tested a rate dependent adhesive under cyclic creep-recovery loadings.

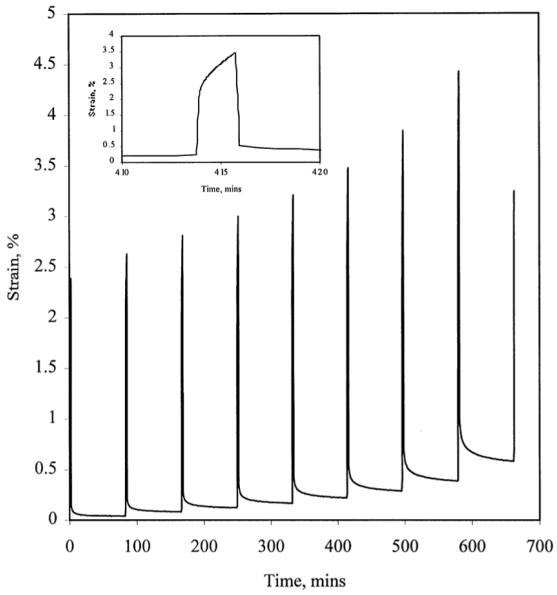

Figure 1.28: Cyclic creep-recovery data for a rate dependent adhesive [11]

In order to be able to describe the time-dependent recovery, some authors [88] have proposed the so-called unified theory models in which the total strain is divided into an elastic part (*Eq.*1.15) and an inelastic part which generates strains without using a yield function. E represents the elastic modulus and the function $g(\varepsilon)$ represents the so-called equilibrium or back-stress response of the material.

$$\dot{\varepsilon}^{in} = \frac{\sigma - g(\varepsilon)}{Ek(\sigma - g(\varepsilon))'} \tag{1.15}$$

Two other unified theory models can be found in the literature, those proposed by *Chiu et al.* [77] and *Bodner et al.* [89]. As can be shown in *Fig.*1.29 this kind of model allows a reasonable description of the non-linear behaviour, the viscous phenomena and the loading rate under monotonic tests.

1.3.4 Influence of the hydrostatic stress: 3D models

The analogical models presented in the previous section can predict the mechanical behaviour of an adhesive in a single direction. In bonded joints, recent studies have shown that the adhesives may present anisotropy due to the geometry of the joint. In these specific cases, 3D models may be more accurate, but they need to be implemented in 3D finite element software.

As shown by many authors [67][83][90][91], the models that take into account the hydrostatic pressure are more adapted to describe the mechanical behaviour of adhesives in bonded joints, especially when they are subjected to mixed loadings.

The viscoelastic-viscoplastic model that will be presented in this work is based on two

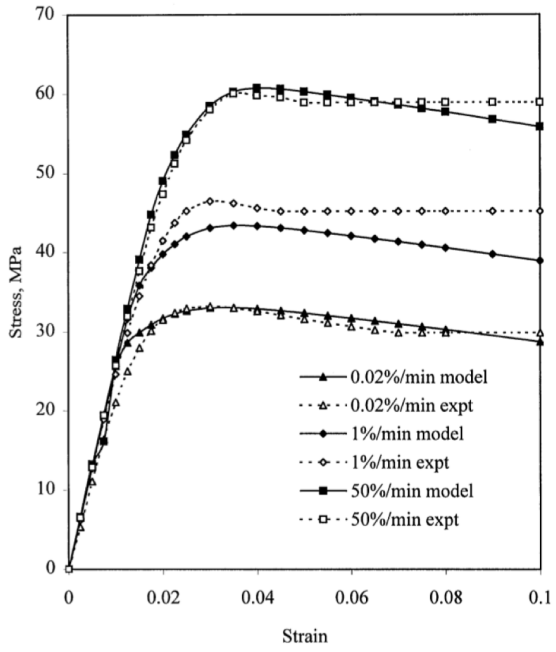

Figure 1.29: Unified theory viscoplastic model fits to the constant strain rate data using the model from Chiu [11]

separate models that allow the hydrostatic pressure to be taken into account: the viscoelastic spectral model and a viscoplastic model derived from the *Mahnken et al.* [80] elastoplastic model.

1.3.4.1 Viscoelastic spectral model

The viscoelastic spectral model was initially developed by *Maire* [92] to study the mechanical behaviour of polymer-matrix composites as a function of thermal ageing [12]. Before describing the characteristics of this model, a short introduction will be made by presenting an older analytical model which is based on the same principle, the so-called generalized Kelvin model, also known as generalized Kelvin-Voigt Standard Linear Solid model (SLS).

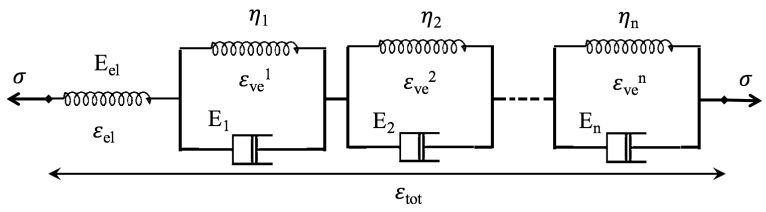

Figure 1.30: Generalized Kelvin model

$$\sigma = \sigma_{el} = \sigma_{ve}^{1} = \sigma_{ve}^{2} = ... = \sigma_{ve}^{n} \tag{1.16}$$

$$\varepsilon_{tot} = \varepsilon_{el} + \varepsilon_{ve} \quad where \qquad \varepsilon_{ve} = \sum_{i=1}^{n} \varepsilon_{ve}^{i} \tag{1.17}$$

In this phase this model is behaving like an analogical model so the constitutive law can be determined using the *Eq.*1.16 and *Eq.*1.17. The first equation means that the applied stress is equally distributed between the elastic spring and each viscous mechanism (Kelvin-Voigt basic mechanical element). The second equation describes the total strain as the sum of the elastic strain and the strains of each viscous mechanism.

The viscoelastic strain rate can be written as:

$$\dot{\varepsilon}_{ve} = \sum_{i=1}^{n} \left(\frac{\sigma}{\eta_i} - \frac{E_i}{\eta_i} \varepsilon_{ve}^{i} \right) \tag{1.18}$$

or,

$$\dot{\varepsilon}_{ve} = \sum_{i=1}^{n} \frac{1}{\tau_i} \left(\mu_i \sigma - \varepsilon_{ve}^{i} \right) \tag{1.19}$$

where

$$\mu_i = \frac{1}{E_i} \qquad \tau_i = \frac{\eta_i}{E_i} \tag{1.20}$$

The substitutions made in *Eq.*1.19 are called the compliance modulus or weight (μ_i) and the relaxation time (τ_i) (*Eq.*1.20). As can be observed, each viscous mechanism is defined by a relaxation time and a weight. The number of parameters of this generative model is proportional to the number of viscous mechanisms used to model the viscoelastic part. This may be problematic when using many mechanisms.

Schapery [93] developed a similar viscoelastic model based on an integral formulation and *Maire* [92] adapted it by adding a spectral formulation with a non-linear function and the thermal effect. His approach was developed using the thermodynamics laws and is based on the existence of two potentials:

1. The free energy potential:

$$2\rho\Psi = (\varepsilon - \varepsilon_a - \varepsilon_{th}) : C_0 : (\varepsilon - \varepsilon_a - \varepsilon_{th}) + \sum_{i=1}^{n} \frac{1}{\mu_i} (\xi_i : C_r : \xi_i) \tag{1.21}$$

   where ρ is the relative density, C_0 and C_R are rank 4 tensors which describe the elastic and the viscous anisotropy, ε_a and ε_{th} are the viscous and the thermal strains. The viscous mechanisms ξ_i describe a Gaussian continuous spectrum defined by τ_i and μ_i which are the relaxation time and the weight.

2. The dissipation potential:

$$2\rho^* = \sum_{i=1}^{n} \frac{\mu_i}{\tau_i} \left(\omega_i : C_R^{-1} : \omega_i \right) \tag{1.22}$$

where $\omega_i = g(\sigma_a) + \chi_i$ is a non linear function.

Finally the constitutive equations for this model are:

$$\sigma = C_0 : (\varepsilon - \varepsilon_a - \varepsilon_{th}) \tag{1.23}$$

$$\dot{\varepsilon_a} = g(\sigma) \sum_{i=1}^{n} \dot{\xi}_i \quad \text{with} \quad \dot{\xi}_i = \frac{1}{\tau_i} \left(\mu_i g(\sigma) C_R^{-1} : \sigma - \xi_i \right) \tag{1.24}$$

$$\varepsilon_{th} = \alpha(T - T_0) \tag{1.25}$$

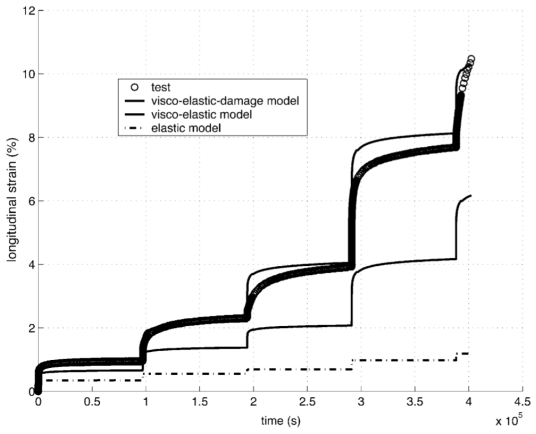

Figure 1.31: Creep test of a laminate at different loadings [12]

The viscoelastic damage is introduced in the viscous compliance (C_R) (*Eq.*1.24) as shown in *Eq.*1.26 where d is the damage variable, μ is the damage deactivation index [94]. S_R and H_r are $4th$ rank tensors that represent the initial viscous compliance and the damage effect tensor on the viscoelastic behaviour:

$$C_R = S_R^{-1} \quad with S_R = S_R + \mu d H_r \tag{1.26}$$

The validation of the model was made using complex laminate and long creep tests *Fig*1.31. *Badulescu et al.* [79] also used this model to predict the time-dependent mechanical behaviour of an epoxy adhesive using the Arcan device. *Medina* [95] has also used a modified version of this model to predict the mechanical behaviour of adhesives. His version will be discussed in a later section of this work.

1.3.4.2 Modelling the hydrostatic pressure in plasticity

Viscoelastic models that consider the hydrostatic pressure can describe in a correct manner the long term mechanical behaviour of adhesives when the applied loads are under a pseudo-elastic limit or yielding stress. As has been shown by many authors [80][13][21][96][97], the yield stress of polymeric adhesives is also strongly dependent on the hydrostatic stress component. Above this limit, adhesives may present plastic flow behaviour.

In order to be able to predict the mechanical behaviour up to failure, a plastic component may need to be added to the total strain. Thus, the total strain (ε_{tot}) will be the sum of an elastic strain (ε_{el}), a viscous strain (ε_{ve}) and a plastic strain (ε_p) (*Eq.*1.27). It should be noted that the plastic strain will induce a permanent deformation that will not be reversible.

$$\varepsilon_{tot} = \varepsilon_{el} + \varepsilon_{ve} + \varepsilon_p \tag{1.27}$$

Because the plastic deformation is dependent on the hydrostatic pressure, the yield limit will be given by a function that is defined using the components of the stress tensor. This function is called the *yield function* and it can be written as in *Eq*1.28, where σ_y represent the yield stress.

$$f(\underline{\sigma}) = g(\underline{\sigma}) - \sigma_y \leq 0 \tag{1.28}$$

The stress tensor being defined in a six-dimensional space, the yield function will be a convex surface of 5 dimensions defined in the stress space. In order to be able to visualize it, the yield function is usually defined using the stress invariants J_1, J_2, J_3:

$$f(\underline{\sigma}) = g(J_1, J_2, J_3) - \sigma_y \leq 0 \tag{1.29}$$

$$J_1 = Tr(\underline{\sigma}) = 3\sigma_H \tag{1.30}$$

$$J_2 = \frac{1}{2}Tr(\underline{\sigma}^2) = \sqrt{\frac{3}{2}\underline{\sigma}_D : \underline{\sigma}_D} = \sigma_{VM} \tag{1.31}$$

$$J_3 = \frac{1}{3}Tr(\underline{\sigma}^3) = det(\underline{\sigma}) \tag{1.32}$$

where, J_1, J_2, J_3 represent the 3 invariants, $\underline{\sigma}$ is the stress tensor, σ_H the hydrostatic pressure, σ_D deviatoric stress tensor and σ_{VM} the von Mises stress.

The mechanical behaviour of adhesives being dependent on the hydrostatic pressure, the yield function should be influenced by this component of the stress tensor. The most common yield criteria that are dependent on the hydrostatic pressure were resumed by *Arnaud* [21] and *Bidaud* [98] and are shown in *Tab.*1.3.

For each criterion, the parameters represent: σ_0 the shear yield stress, μ the sensitivity to hydrostatic pressure, p the tensile yield stress and a_0, a_1 material parameters.

When the yield criterion is achieved the flow rule will depend on the stress tensor $\underline{\sigma}$ and the slip rate $\partial\lambda$ (plastic multiplier) (*Eq.*3.22). The hardening is attributed to the thermodynamic forces A_i which are associated to the state variables V_i (*Eq.*3.23).

Flow rule

$$\dot{\varepsilon_p} = \partial\lambda\frac{\partial f}{\partial\underline{\sigma}} \tag{1.33}$$

Hardening rule

$$\partial V_i = -\partial\lambda\frac{\partial F}{\partial A_i} \tag{1.34}$$

Table 1.3: Hydrostatic pressure dependant yield criterion

Name	**Yield function**	**Parameters**
Modified von Mises [99]	$f = \sigma_{VM} - \sigma_0 - \mu p$	σ_0 μ
Modified Tresca [100]	$f = \max\lvert\sigma_i - \sigma_j)\rvert - \sigma_0 - \mu p$	σ_0 μ
Exponent Drucker Prager [101]	$f = a\sigma_{VM}^b + p - p_{t_0}$	a, b p
Rolfes [102]	$f = \sigma_{VM}^2 - a_1 p - a_0$	a_1 a_0
Mahnken Schlimmer [80]	$f = \sigma_{VM}^2 - \frac{1}{3}\left(\sigma_0^2 - a_1\sigma_0\sigma_H - a_2\sigma_0\sigma_H^2\right)$	a_0, a_1 σ_0

It is important to notice that if the flow rule and the yield function are defined using the same function the formulation is called *associated* otherwise the formulation will be *non-associated*:

associated formulation: $\dot{\varepsilon_p} = \partial\lambda\frac{\partial f}{\partial\underline{\sigma}} \qquad \partial V_i = -\partial\lambda\frac{\partial F}{\partial A_i}$

non-associated formulation: $\dot{\varepsilon_p} = \partial\lambda\frac{\partial g}{\partial\underline{\sigma}} \qquad \partial V_i = -\partial\lambda\frac{\partial F}{\partial A_i}$ with $f \neq g$

Mahnken and Schlimmer [80] proposed a *non-associated* formulation using the following two functions:

yield function: $f = \sigma_{VM}^2 - \frac{1}{3}\left(\sigma_0^2 - a_1\sigma_0\sigma_H - a_2\sigma_0\sigma_H^2\right)$ yield function

flow function: $g = \sigma_{VM}^2 - \frac{1}{3}\left(\sigma_0^2 - a_1^*\sigma_0\sigma_H - a_2^*\sigma_0\sigma_H^2\right)$ flow function

The yield function and the function that defines the flow rule differ from each other because of the material parameters: a_1, a_2, a_1^*, a_2^*. Moreover, the hardening function has been defined as in *Eq.*1.35, where H, q, b are three parameters that must be identified.

$$Y = Y_0 + He_v + q(1 - e^{-be_v}) \tag{1.35}$$

This model was used by *Maurice* [13][103] and *Arnaud* [21] to characterise the influence of the hydrostatic pressure on the behaviour of adhesively bonded joints under monotonic tensile/compression-shear loads. As can be observed (*Fig.*1.32), a quadratic function was needed to model the yield surface. The experimental tests were made using the Arcan device which allowed the studied adhesive to be tested in shear (the hydrostatic pressure is almost zero), tensile or to combine the tensile/shear (45^0) and compression/shear (135^0) loadings.

1.3.5 Fracture mechanics approach

All the models presented in the last section were developed using the strength of materials theory (SoM) which involves tracking the stress and the strain in a structure (material or joint) when a load is applied. This enables engineers to conceive efficient designs of bonded structures and to take into account the overlap length, the bond line thickness or the geometry of the joint. Coupled with Finite Element method, the SoM theory is an indispensable approach to

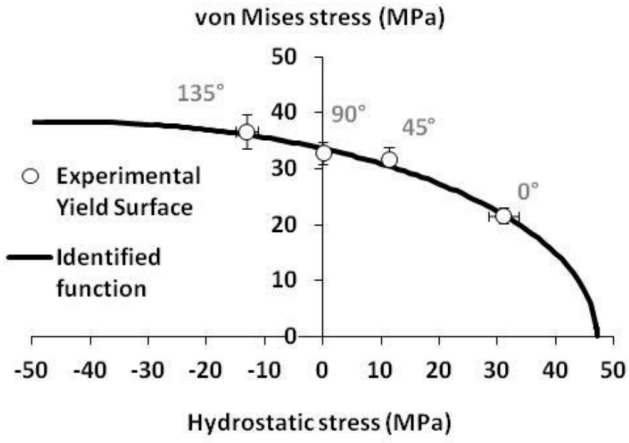

Figure 1.32: Experimental data versus experimental yield function in the Mises-Hydrostatic plane [13]

predict the mechanical behaviour of adhesives and it assumes that the failure is produced when the stress achieves a given value.

Fracture Mechanics (FM) is a different approach, which can also provide a prediction of the failure of bonded joints. The theory was initially developed by *Griffith* [104] to predict the failure of brittle materials containing a crack. It was adopted by other authors to model more ductile materials using the hypothesis that the plastic zone near the crack tip is insignificant compared to the crack length. Because it is based on the idea that a crack exists already in the material, this approach is very useful for estimating the service life of a damaged structure. It is completely complementary to the SoM approach which doesn't take into account the cracks or other defects.

Two models derived from FM are generally used today to predict the failure loads of bonded joints: the cohesive zone model (CZM) and the coupled criterion. The CZM developed by *Dugdale* [105] to predict the crack propagation in steel sheets was adopted by *Stigh* [106] to analyse the damage and the crack of the double cantilever beam bonded specimens. Nowadays, this method is implemented in almost all FE software. The coupled criterion is a more recent theory based on two main issues: calculation of the stress distribution within the adhesive layer and the definition of a failure criterion derived from a stress, strain or energetic criterion [107][108]. More information concerning these subjects can be found in the cited references.

1.4 Environmental conditions and the adhesives behaviour

In the previous sections, a part of the tools that currently exist and can be used to design adhesively bonded joints were presented. In addition, using various experimental tests, it is possible to determine the mechanical behaviour of the joint and the adhesive itself. Moreover, Finite Element software allows complicated models to predict how an external load may influence the strength of bonded structures to be developed. But it should not be forgotten that these

structures may be facing extreme operating conditions and the external factors (temperature or water activity) may completely change the mechanical behaviour. Therefore, the influence of environmental conditions should be considered when designing bonded structures.

Because the main topic of the present work is the effects of water ageing on the behaviour of adhesives, the following section will give an in-depth examination of the influence of water on the mechanical properties of bonded joints.

1.4.1 Water diffusion in adhesives

Structural adhesives are polymers. It is well known that all the polymers are permeable to water because of their structure. This means that the water molecules can move throughout the polymer chains. *Comyn* [109] " *diffusion in polymers is to put a billiard ball into a bucket of spaghetti with sauce. As the ball descends, the strands move out of the way to let it pass, and then reform behind it. Motion of the strands is essential for the ball to pass. The sauce assists motion as does a plasticiser*".

More technically, this can be described using diffusion laws. As can be observed in the published literature [14][110][111], the most common law used to model the water diffusion in adhesives is Fick's law [112][113]. It assumes that there is no interaction between the molecules of the two entities.

1.4.1.1 Fick's law

Fick defined two hypotheses to describe the water diffusion. In the first one, he assumed that the flux of water in the x-direction F_x is proportional to the concentration gradient $\partial c/\partial x$ (*Eq.*1.36).

$$F_x = -D\frac{\partial c}{\partial x} \tag{1.36}$$

where F_x is the amount crossing area and D is the diffusion coefficient.

The second hypothesis has several forms and it depends on the geometry of the sample. Assuming a bulk sample of adhesive like a rectangular box completely immersed in water, there will be six fluxes across the six faces. The concentration will evolve with time following the equation:

$$\frac{\partial c}{\partial t} = D\left(\frac{\partial^2 c}{\partial^2 x} + \frac{\partial^2 c}{\partial^2 y} + \frac{\partial^2 c}{\partial^2 z}\right) \tag{1.37}$$

where x, y, z are the Cartesian coordinates of a system attributed to the box and t is time. Of course, if the sample is cylindrical or spherical, this equation (*Eq.*1.37), can be written in polar coordinates. Usually the experiments are arranged so that the diffusion is limited to one direction (one of the sample dimensions is insignificant compared to the others) so the second law is written as:

$$\frac{\partial c}{\partial t} = D\left(\frac{\partial^2 c}{\partial^2 x}\right) \tag{1.38}$$

Considering a thin layer of adhesive, wide and narrow with its width equal to $2L$, which is immersed in a constant temperature bath of water or exposed to wet air on the wide side, with a concentration equal to C_1, it is possible to predict the water concentration across the adhesive layer using the (Eq1.39):

$$\frac{C}{C_1} = 1 - \frac{4}{\pi}\sum_{n=0}^{\infty}\frac{(-1)^n}{(2n+1)}exp\left[-D(2n+1)^2\frac{\pi t}{4L^2}\right]\cos\frac{(2n+1)\pi x}{2L} \tag{1.39}$$

where x represents the distance between the middle of the layer and the side in contact with the water activity (*Fig.*1.33a1.33b), L is half of the specimen thickness and t is the immersion time.

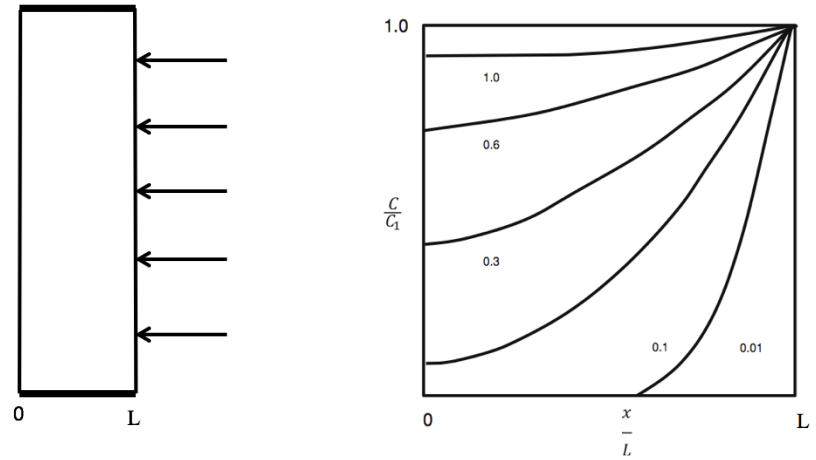

(a) 1D Diffusion in a half of an adhesive layer

(b) Plots of water concentration across adhesive thickness for different values of t [109]

Figure 1.33: Water diffusion in an adhesive layer

Generally, the samples are dried before the experiments are performed, meaning that the initial water concentration tends toward zero. Assuming that M_t is the mass absorbed at time t and M_∞ is the mass at equilibrium, the solution of (Eq.1.39) is given by the (Eq.1.40). For short periods of time, when $\frac{M_t}{M_\infty} < 0.6$ the solution is given by the Eq.1.41.

$$\frac{M_t}{M_\infty} = 1 - \frac{8}{\pi^2}\sum_{n=0}^{\infty}\frac{1}{(2n+1)^2}exp\left[-D\pi^2 t\frac{(2n+1)^2}{4L^2}\right] \tag{1.40}$$

$$\frac{M_t}{M_e} = \frac{4}{L}\sqrt{\frac{Dt}{\pi}} \tag{1.41}$$

According to *Fujita* [114], the principal features of the Fickian diffusion are listed below:

1. Both absorption and desorption curves are linear in the region of small values of the abscissa. For absorption the linear region is obtained below 60% of the M_∞;

2. Above the linear portions both absorption and desorption curves are always concave against the abscissa axis;

3. When the initial and final concentrations are fixed, the reduced absorption curves for films of different thicknesses all coincide with each other, yielding a single curve. This applies for the corresponding family of reduced desorption curves;

4. The single absorption curve so obtained is always above the corresponding desorption curve when D is an increasing function of C_1. Both coincide over the entire range of the abscissa when and only when D is constant.

Bordes et al. [14] studied the water uptake of an epoxy adhesive immersed in sea water at different temperatures (*Fig.*1.34). $M_t(\%)$ is calculated using the *Eq.*1.42, where M_t is the mass of the immersed sample at a given moment and M_0 is the initial mass.

$$M_t(\%) = \frac{M_t - M_0}{M_t} \times 100 \tag{1.42}$$

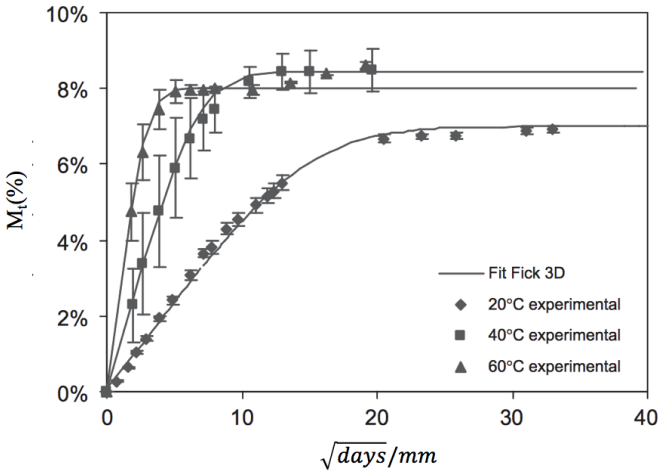

Figure 1.34: Water uptake in epoxy adhesive immersed in seawater at different temperatures [14]

1.4.1.2 Non-Fickian behaviour

Fick's model is the simple model that can predict the water diffusion polymer materials and it is sufficient in most of the cases. This model is strongly dependent on the equilibrium mass but there are several materials which do not present a stabilized plateau at equilibrium.

The dual-stage Fickian model assumes that two Fickian diffusion occur simultaneously each of them with its own diffusion coefficient and its equilibrium mass [115]. The prediction depends on four parameters $D_1, D_2, M_\infty^1, M_\infty^2$. As can be observed in *Fig.*1.35a, this model is able to predict a continuously increasing water uptake in contrast to the normal Fick model.

Carter and Kibler [118] proposed the so-called Langmuir-type diffusion model, another approach that can be used to predict the non-Fickian water uptake. It is based on the assumption that the diffusion depends on the amount of free molecules that are able to migrate in the material. Three parameters have to be identified to fit the model and it is important to

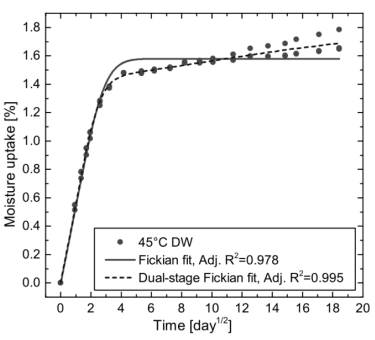

(a) Experimental moisture-uptake data and theoretical diffusion fitting curves for a polymer[116]

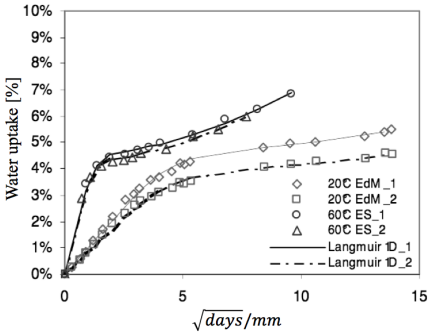

(b) Experimental water uptake data and Langmuir model prediction for a methacrylate adhesive [117]

Figure 1.35: Non-Fickian behaviour

note that the prediction of this model depends on the thickness of the sample. *Bordes* [117] used this model to fit the experimental water uptake data for a methacrylate adhesive (*Fig.*1.35b). Water diffusion in epoxy adhesives may also present this kind of behaviour as shown by *Popineau et al.* [119].

1.4.1.3 Diffusion coefficient

Being a thermally-activated process (dependant on the water temperature), the diffusion coefficient visually obeys an Arrhenius law (*Eq.*4.7) where T is the absolute temperature, R is the universal gas constant and E_D is the activation energy for diffusion. *Brettle et al.*[120] obtained these kinds of results. More recent studies on epoxy adhesives [121], show similar results *Fig.*1.36a.

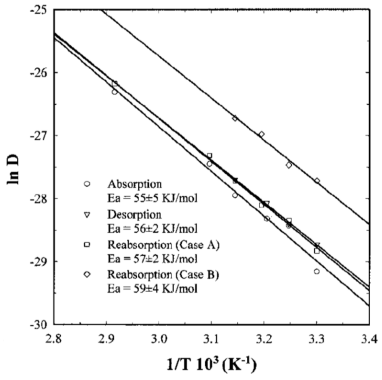

(a) Evolution of diffusion coefficient as a function of ageing temperature for an epoxy adhesive [121]

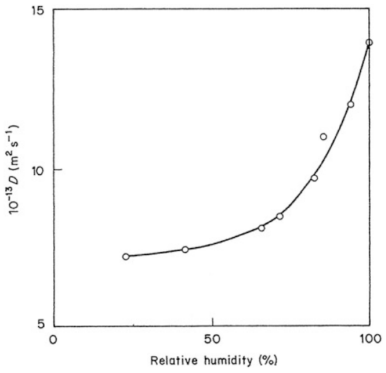

(b) Variation of diffusion coefficient of an epoxide adheisve as a function of relative humidity [122]

Figure 1.36: Evolution of the diffusion coefficient as a function of temperature and water activity

For samples saturated in controlled relative humidity chambers at the same temperature, the diffusion coefficient could be independent of the $\%RH$ specially for epoxy materials with an amine hardener [122] or can evolve in an exponential way [123] (*Fig.*1.36b). It should be noted

that the $\%RH$ is related to the saturated vapour pressure of water p_0 by the relation:

$$\%RH = \frac{p_0}{p} \times 100 \tag{1.43}$$

where p is the actual vapour pressure. The rapport p_0/p is also noted as a and it is called *water activity*.

1.4.2 Physico-chemical degradation of epoxy adhesives

The interaction between water molecules and the polymer structure causes structural changes. The nature of these changes can be a physical or a chemical phenomenon. It has been shown by many authors that physical changes are generally reversible (plasticization or swelling) but a chemical reaction will induce structural changes that are irreversible (hydrolysis, oxidation).

1.4.2.1 Plasticization

Water molecules that diffuse into the polymer damage the weak chemical forces (Van der Waals force) that tie together the neighbouring chains. This phenomenon can break the mechanical cohesion of the network and lead to a softening of the polymer [124]. In other terms, this process is called plasticization and it induces an increase in macromolecular chain mobility and so, a decrease of the glass transition temperature (T_g) which is directly proportional to the amount of diffused water. Moreover, it depends on the immersion time, as can be observed on the results obtained by *Savvilotidou et al.* [15] on different types of structural epoxy adhesives (*Fig.*1.37).

In some cases, the evolution of T_g can be predicted using the theory of free volume, which assumes that the diffused water molecules are causing an increase of the initial volume of the polymer. Hence, the evolution of the polymer T_g can be predicted using the Kelly and Bueche equation [125] simplified by the Simha-Boyer rule [126] which will be detailed in the *Chapter* 4 of this work.

For many polymers, this process is completely reversible [127] meaning that if the sample is dried, its T_g will return to the initial value.

1.4.2.2 Swelling

During the diffusion process, the water occupies the position between the polymer molecules forcing these macromolecules to separate from each other [128]. The strains induced by swelling can vary between 1% and 10% for epoxy adhesives [129][130] and this may lead to a decrease of the mechanical properties of the bonded joint.

Even though the swelling is due to the water presence in the sample, it is not possible to conclude if it depends on the quantity of water. *Toscano et al.* [123] showed a low sensitivity of the swelling with the amount of absorbed water. However, *Loh et al.* [128] found a linear dependency with the fractional mass uptake, for a rubber toughened epoxy adhesive.

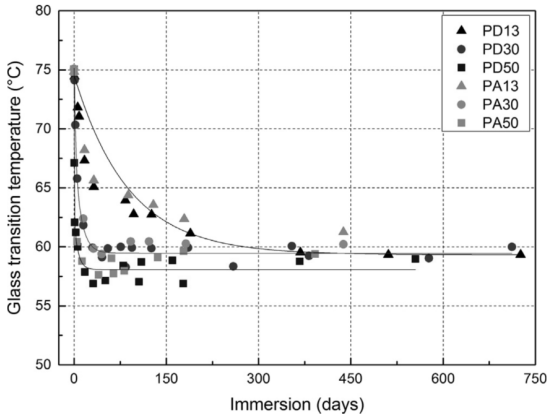

Figure 1.37: Evolution of T_g as a function of immersion time for different types of epoxy adhesives [15]

1.4.2.3 Hydrolysis

Hydrolysis is a chemical reaction between the water and the polymer. The water molecules will react with the polar groups of the polymers breaking the chains (*Eq.*1.44). This is an irreversible process which may lead to a gain in mass after a complete desorption if the sample is immersed for a short period.

$$R - X - Y - R' + H_2O \longrightarrow R - X - OH + HY - R' \tag{1.44}$$

Due to the hydrolysis, samples immersed for long periods of time will have a saturation mass that will decrease in time. This is caused by the leaching process. Small polymer chains that were broken up by the hydrolysis will migrate inside the polymer structure until they finally reach the edges and pass into the surrounding environment.

De Olivera et al. [16] studied the evolution of the saturated mass of a polyurethane elastomer. He observed a continuous mass drop over a large period of time which could be attributed to the loss of the inorganic additives contained by the material.

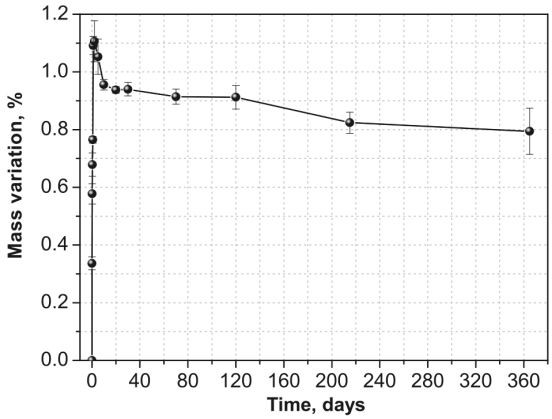

Figure 1.38: Mass variation as a function of ageing time for a polyurethane elastomer immersed in artificial seawater at 60^{o}C [16]

1.4.3 Influence of water on mechanical properties

It has been shown that the presence of water in a polymer induces physical and chemical changes. These modifications have an important impact on the mechanical behaviour and the properties of a bonded joint. In order to be able to quantify the evolution of mechanical properties of an aged bonded joint, several scales should be analysed.

Because of the boundary conditions, water diffusion in bulk samples subjected to hydrothermal conditions occurs in small amounts of time compared to bonded joints. This allows quick and easy access to the evolution of mechanical properties, such as elastic modulus or yield stress, for constant water profiles.

Water diffusion in an immersed bonded joint is usually considered in one or two directions because of the adherends that are generally impermeable. The result is a gradient of water concentration before complete saturation. Hence, the mechanical properties of the bonded joint will change progressively. The experimental tests should be performed concomitantly with the water diffusion in order to understand the consequences of the water ageing.

The interface between the adhesive and the adherend is also a factor that is influenced by the presence of water. This should also be another point of interest when analysing the behaviour of an aged bonded joint.

1.4.3.1 Bulk samples

Testing bulk specimens that have been subjected to hydrothermal conditions is not simple. The specimens are usually tested using tensile machines that do not have humidity-controlled chambers. If they are not tested quickly, the evaporation of water during the test may influence the results. Moreover *Sato* [131] suggested the use of other measurement techniques (*e.g.* digital image correlation) rather than more usual strain gauges because of the difficulty in bonding to wet surfaces.

The geometries of the samples used to characterise the water influence on bulk specimens are the same as those used to perform the tests on unaged samples.

As expected, the mechanical properties of the aged bulk specimens change during the water uptake. Besides the drop of the Tg, there are three important mechanical characteristics that are considerably affected: the Young's modulus, the failure strength and the strain at break.

The change in Young's modulus can be highlighted using *DMA* tests. *Savvilotidou et al.* [132] used this approach to characterise the evolution of elastic properties of an epoxy adhesive as a function of immersion time (*Fig.*1.39a). A drop of 1000MPa can be observed between an unaged specimen and a completely saturated one. Plasticization due to the water uptake also changed the material tensile behaviour from almost linear in the dry condition to highly non-linear at full saturation [132].

Bordes et al. [117] have also studied the influence of water uptake on the tensile yield stress for another epoxy adhesive (*Fig.*1.39b). The drop is obvious even for the small amounts of water uptake. Moreover, *Sugiman et al.* [133] observed that an epoxy adhesive become softer and more ductile as a function of the water uptake.

Another interesting study was made by *Comyn and Ashcroft* [17] who saturated epoxy bulk specimens with different water quantities and constant profiles (*Fig.*1.40). The results obtained

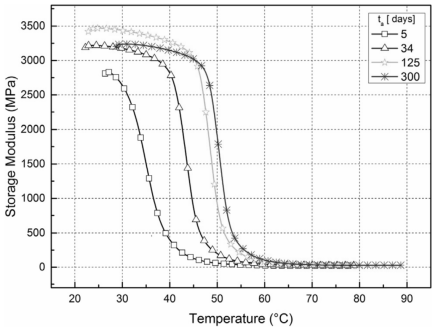

(a) DMA storage modulus curves at increasing ageing times for an epoxy adhesive [132]

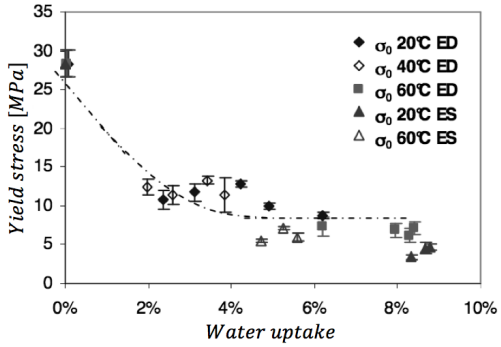

(b) Evolution of the yield stress as a function of water uptake for an epoxy adhesive [117]

Figure 1.39: Changes in the elastic modulus and yield stress with water uptake

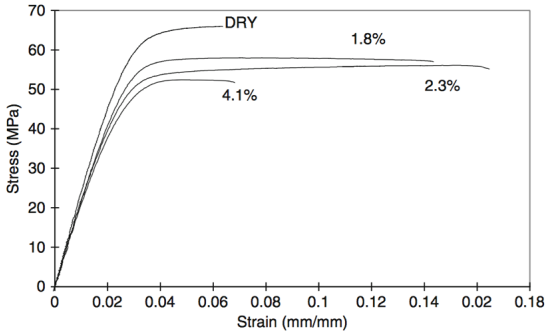

Figure 1.40: Effect of absorbed moisture on the bulk mechanical properties of a modified epoxy adhesive at 22^{o}C [17]

showed that the water quantity in the material reduces the yield stress and increases the strain at break.

1.4.3.2 Joint strength

Water diffusion has an important impact on the mechanical properties of epoxy adhesives as bulk samples. It is also well known that it affects the strength of the bonded joints. Using different experimental tests, several authors have tried to understand the mechanisms that produce the loss in the mechanical properties.

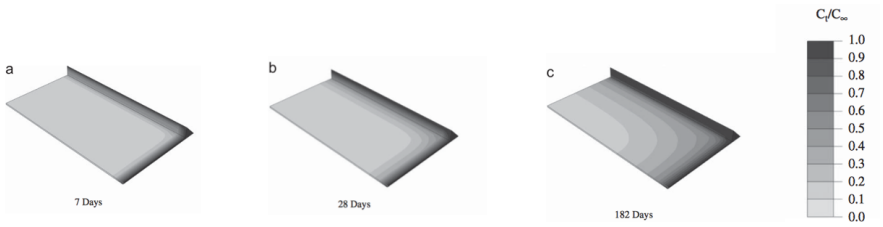

Figure 1.41: Example of modelling the water diffusion in a single lap joint [18]

In order to be able to predict the mechanical behaviour of an aged bonded joint it is

important to model the water diffusion in the adhesive joint using the boundary conditions of the tested specimen. This is usually done using Finite Element software. Various authors like *Mubashar et al.* [18] or *Léger et al.* [134] modelled the water diffusion in single lap joint tests, others have studied TAST (Thick Adherent Shear Test) specimens [22] or the diffusion in Arcan samples [21][117]. All these studies have been performed using the hypothesis that the water diffuses only in the adhesive layer (*Fig.*1.41).

Weylde and Spelt [19] have also managed to give a 3D representation of the water concentration in a sandwich bonded joint (*Fig.*1.42). They used this information to characterise the influence of water on the failure strength of the joint.

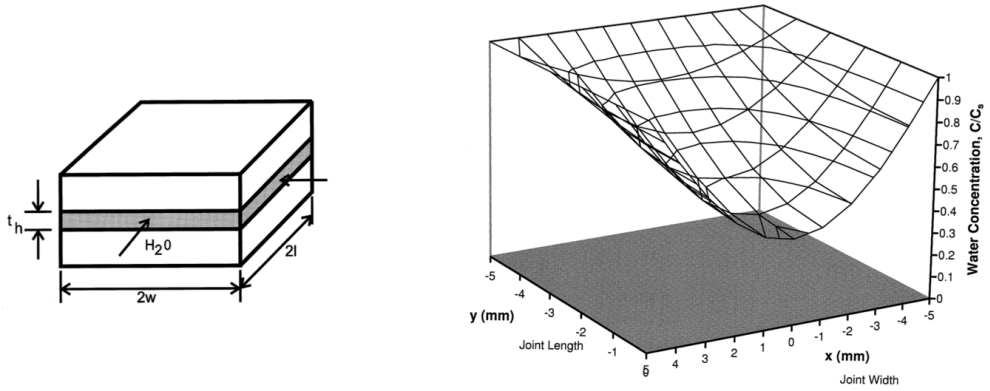

Figure 1.42: Water concentration as a function of position in a square bonded joint [19]

Among the factors that influence the rate of water diffusion in a bonded joint, the most important are:

1. **Water temperature (rapid ageing)**

   Because the diffusion coefficient depends on the water temperature, the times needed to saturate a bonded specimen, completely immersed, can be considerably reduced by increasing the water temperature (rapid ageing). This is very useful for accelerated studies that need saturated samples in short periods of times. *Arnaud et al.* [21] calculated that for an Arcan specimen (using a structural epoxy adhesive), the saturation time can change from several years to a few months by increasing the water temperature from 25^oC to 40^oC. But it is particularly important to note that these studies should be performed below the glass transition temperature of the adhesive. *Ashcroft et al.* [135] have also analysed the equivalence between rapid ageing and normal ageing in terms of evolution of the mechanical properties and concluded that this approach has its limits.

2. **Mechanical loading**

   The mechanical load is another factor that can influence the water diffusion in a bonded joint. Some studies [136][137] showed that applying a constant stress to a bonded joint located in a humid environment could facilitate the water diffusion and the degradation, but the applied stress should reach a certain limit in order to show an effect. *Bowditch et al.* [138] showed using a steel/epoxy joint that for a load below 20% of the failure static

stress, the bonded joint did not fail after 3 years (*Fig.*1.43a). This may be explained by the fact that the applied load is opening the voids and the cavities in the polymer which facilitates the water diffusion.

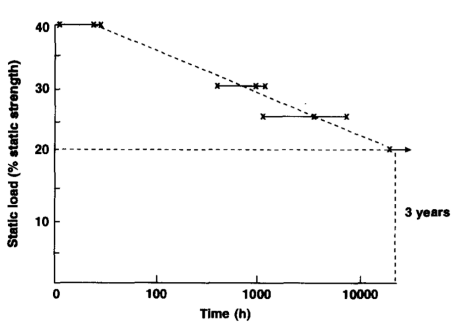

(a) Durability of an epoxy/steel joint immersed in seawater subjected to different stress levels [138]

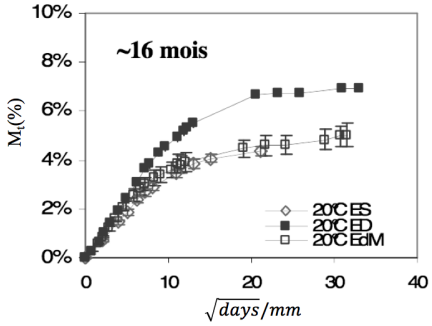

(b) Diffusion in an epoxy adhesive for: deionised water (ED), water + 3.5%$NaCl$ and seawater [117]

Figure 1.43: Water diffusion in an epoxy adhesive

3. **Purity of water**

It is important to mention that the purity of water can also play an important role in water diffusion. *Bordes et al.* [117] showed that an epoxy adhesive immersed in deionised water will saturate faster than in seawater and the quantity of water at saturation can be 50% more important (*Fig.*1.43b).

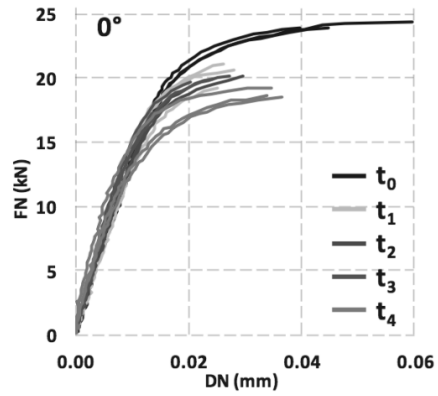

(a) Water influence in tensile behaviour for an Arcan sample (epoxy/aluminium)[21]

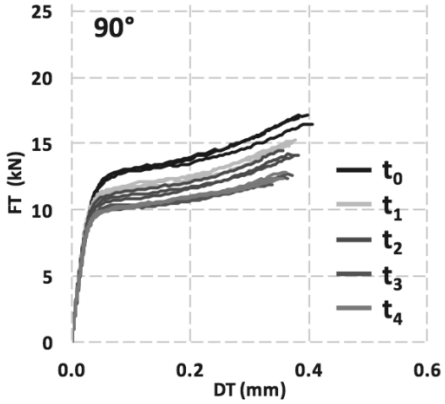

(b) Water influence in shear behaviour for an Arcan sample (epoxy/aluminium) [21]

Figure 1.44: Influence of water ageing in shear and tensile behaviour

As in the case of bulk specimens, the mechanical properties of a bonded joint tend to decrease in the presence of water. Some interesting results were presented by *Arnaud et al.* [21] who studied the influence of water on the strength of an epoxy/aluminium joint using the *Arcan* device. He tested different types of samples from dry (t_0) to completely saturated (t_5). It can easily be observed that under tensile loading (*Fig.*1.44a) the failure strength decreases

by $20-25\%$ between the two extreme states (dry and saturated). Moreover, a change in the elastic modulus and substrate break can also be noted. The shear modulus is not affected by the water (*Fig.*1.44b) but the shear failure stress decreases by the same amount, $20-25\%$ of the initial failure stress.

1.4.3.3 Interface

Some non-destructive studies using ultrasonic scans on adhesive-joint specimens exposed to water at 50^oC for periods of up to 18 months [139] have shown that water exposure may influence the interface toughness. This can lead to premature failure of the joint (usually adhesive failure) which is not caused by the loss of the adhesive's mechanical properties. Moreover, the water exposure can change the mechanics of fracture from cohesive failure in the dry state to adhesive failure for saturated samples.

Wahab et al. [140] compared the water diffusion between a bulk adhesive sample and a laminated disc consisting of cast adhesive and perforated aluminium foil with the same exposed area (*Fig.*1.45a). They concluded that the presence of the interface between the adhesive and the adherends may accelerate the water flux (diffusion) by up to 50% (*Fig.*1.45b) which can be catastrophic for the bonded joint. In other terms, the water front can be more advanced at the interface than in the middle of the adhesive layer as has been shown by *Bruneaux* [141].

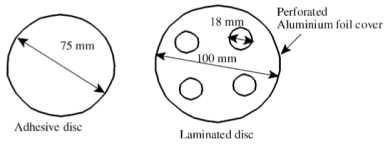

(a) Diffusion discs [140]

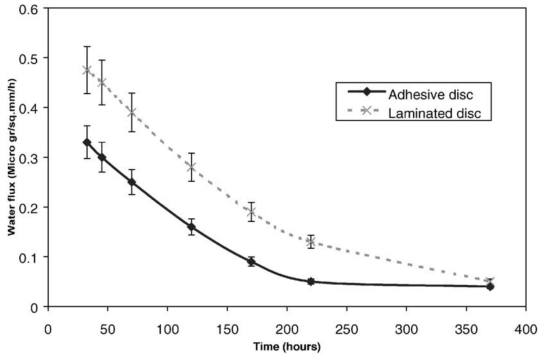

(b) Effect of interface on water diffusion [140]

Figure 1.45: Water diffusion at interface

The degradation at the interface has been analysed by *Kinloch and Gledhill* [142] who defined the work of adhesion as the energy required to separate a unit area of two phases forming an interface. In the presence of a liquid, in this case water, the work of adhesion will be defined as in (*Eq.*1.45):

$$W = \gamma_{AL} + \gamma_{SL} - \gamma_{AS} \tag{1.45}$$

where γ_{AL}, γ_{AS} and γ_{SL} are the surface free energies of the adhesive-liquid, adhesive-substrate and substrate-liquid.

Another scenario was proposed by *Cognard* [31] to explain the degradation of the interface by the appearance and development of voids due to the osmotic pressure created by the water

in contact with the metal. Authors like *Popineau et al.* [143] concluded that in order for these degradations to take place, a minimum of around 1% of water must be present at the interface.

The performance of interfaces in the presence of water can be improved by applying an adapted surface pretreatment to the adherend. Chemical treatments are the most adapted in this respect. According to *Baldan* [20], for bonded aluminium joints, pretreatments like *phosphoric acid anodizing*, *chromic acid anodizing* or *pickle-etching* are well adapted for long-term durability applications (*Fig.*1.46):

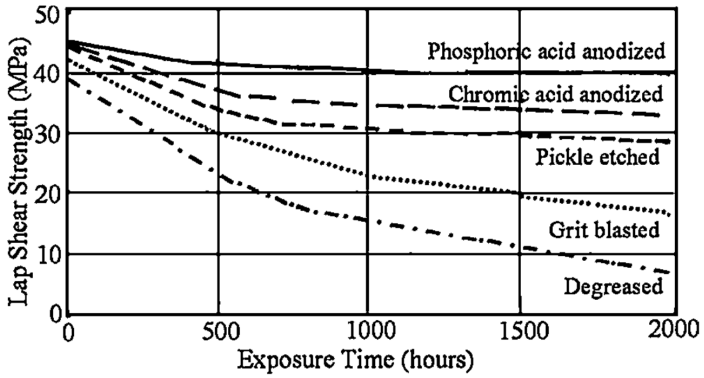

Figure 1.46: Epoxy adhesive exposed to water at 50^oC [20]

1.5 Predicting the mechanical behaviour of aged bonded joints

It has been shown in *Section 1.4* that there are many numerical models able to predict the mechanical behaviour of adhesives in their initial state, without taking into account the influence of water ageing or temperature. These models are very interesting but in order to be completely useful for engineers who design structures with bonded joints, they should be able to predict the changes in the mechanical behaviour induced by the external factors.

On the other hand, with regard to this work, the diffusion of water in bonded joints can be predicted using the approaches presented in *Section 1.5.* Without doubt, there is a link between the quantity of water present in the adhesive and its mechanical properties. This fact can be analysed from a microscopic point of view considering the physico-chemical mechanisms of degradation or by characterising the macroscopic response of the assembly (phenomenological approach).

One of the first attempts to develop a phenomenological concept that can be adopted to predict the mechanical behaviour of an aged bonded joint was made by *Crocombe* [144]. Using the Finite Element method, he proposed coupling the diffusion phenomenon and the evolution of mechanical properties by using both diffusion and behaviour models. He assumed that the global mechanical response of an aged bonded joint is influenced by the changes induced by the water, in the adhesive and at the interface.

Depending on their experimental results (cohesive or adhesive failure), researchers can simplify the prediction of the mechanical behaviour of an aged bonded joint in two ways. First, by taking account only of the changes induced by water in the adhesive, they can assume that

the strength of the aged joint will be governed by the adhesive properties (cohesive approach). Otherwise, they can consider that an adhesive failure is induced in the sample, so they model the influence of water on the interface (adhesive approach). The two approaches will be discussed in the latter part of this chapter.

1.5.1 Cohesive failure approach

As mentioned earlier, in this case the failure of the aged joint is supposed to be due to the influence of the water on the mechanical properties of the adhesive. The role of the interface is not taken into account.

The model used to predict the water diffusion in the adhesive can be identified directly on bulk samples. Using the determined diffusion coefficient, a finite element code and the right boundary conditions, it is possible to predict the gradient of water in the joint after a given period of time. In parallel, using saturated bulk samples, the mechanical properties of the adhesive such as yield stress or elastic modulus can be evaluated. This information can be coupled in order to predict the macroscopic response of the aged joint.

Arnaud [21] used this approach to predict the mechanical behaviour of an aged Arcan sample. After the identification of the diffusion coefficient, he could predict the profile of water in the adhesive layer.

Separately, he identified the initial mechanical behaviour of the adhesive using an elasto-plastic model developed by *Mahnken and Schlimer* [80] and the Arcan device. The yield stress at saturation was identified using a tensile bulk specimen. Furthermore, the yield stress was described as a function of the water concentration in the adhesive layer as in *Eq.*1.46 :

$$Y_O(C) = \begin{cases} Y_0 e^{-\alpha_1 C}, & \text{if } C < \gamma_1 \\ Y_0 e^{-\alpha_1 \gamma_1} e, & \text{if } C \geq \gamma_1 \end{cases} \tag{1.46}$$

where Y_0 is the yield stress, α_1 is a parameter that has to be identified, C is the water concentration in the adhesive layer ($C \in [0, 1]$) and γ_1 is a value of water concentration at which the adhesive is considered yielded (criterion).

Using this approach, he managed to predict the zones in the adhesive layer that were yielded by the presence of water. *Fig.*1.47 shows the elements that are yielded in the adhesive layer of an aged Arcan sample subjected to shear stress by associating the points on a *force-displacement* diagram. These results show that the adhesive begins to yield at the edge of the sample and progresses toward the interior.

This technique has shown good results compared to the experimental results but because of the use of the γ_1 criterion for the yielded zone, it is not possible to model and predict a progressive damage in the adhesive layer, which is what actually happens because of the water diffusion.

Hua et al. [145] have also used a cohesive failure approach and a coupled diffusion-mechanical model to predict the evolution of the failure load of an epoxy/aluminium bonded joint.

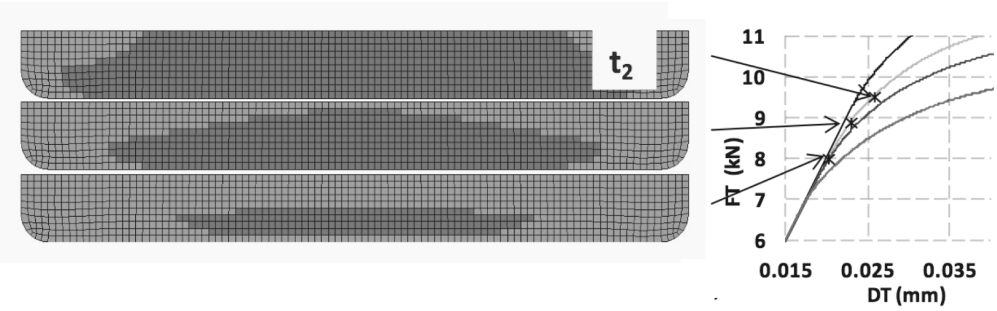

Figure 1.47: Predicting the apparition of plasticity in the adhesive layer of an aged Arcan sample subjected to shear stress [21]

1.5.2 Adhesive failure approach

This approach assumes that the strength of the bonded joint is given by the interface. The water diffusion at the interface adhesive-adherend will produce a loss of mechanical properties of the joint. Authors like *Crocombe et al.* [22] and *Creach'cadec et al.* [146] used this technique to predict the mechanical behaviour of bonded joints with a thin layer of adhesive.

Modelling the interfacial failure using finite element software is done by supposing that the elements representing the adhesive and those representing the adherend are linked together with spring elements that need a certain amount of energy to be deformed (Fig.1.48). The distance between two springs (Δa) is called the crack extension. By applying a force F on the joint, the springs start to deform until they reach a critical point and they separate. Thus, the spring element is effectively broken and is removed, and the crack propagates.

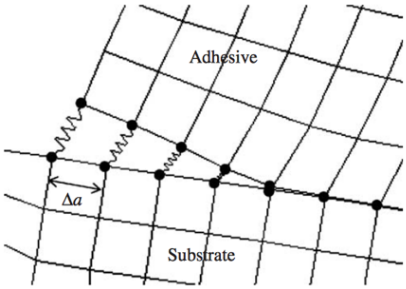

Figure 1.48: Spring elements along the interface adhesive/adherend in a finite element code [22]

The model used by *Crocombe* to predict the joint's mechanical behaviour is governed by the work E needed to separate the spring and the force F distributed in each element as shown in equations below:

$$E = G\Delta \text{aw} \tag{1.47}$$

$$F = G\Delta \text{aw} \tag{1.48}$$

$$U = 2E/F \tag{1.49}$$

where G is the fracture energy of the interface, T is the applied force in each element, U the maximum displacement between two springs, w the width of the interface and Δa the crack length.

Using this method, he managed to predict the failure load of the aged bond by defining the evolution of T and G as a function of ageing time.

1.6 Aims of the present study

In this chapter, the reader was able to discover important aspects concerning the evolution of structural adhesives and how researchers developed advanced tools in order to understand their behaviour and made of them useful materials for different kinds of industries.

No matter the field of activity, engineers should be able to predict the mechanical behaviour of the structures they are designing and to take into account different factors that may influence their integrity. When they are using structural bonding in their designs, it is important for them to have access to constitutive laws for the adhesives they use.

A first objective of this work was **to develop a reliable model** that would be able to accurately describe **the mechanical behaviour** of an epoxy adhesive in a **bonded joint** at initial state (no water ageing effects). Moreover, in order to reduce the time and other costs, the second objective was to **decrease the number of experimental tests** needed for the identification procedure.

Once these two objectives were accomplished, the aim of the present study was **to develop a rapid method to characterise the effects of water ageing on the mechanical behaviour of aged bonded joints**. As shown in previous sections of this chapter, water affects the long-term behaviour of adhesives. The effect of water can be observed on the adhesively bonded structures, once the water has diffused in the adhesive structure. Because the kinetics of diffusion depends on the geometry of the joint, these phenomena are very slow which makes the study of aged bonded joints very expensive in terms of time.

1.7 Presentation of the adopted approach

In order to be able to develop a reliable model, able to accurately describe the mechanical behaviour of a bonded joint at initial state, the Arcan test was used in this study.

In *Chapter* 2, the studied adhesive is analysed at the initial state (no water ageing) together with its main characteristics. To completely understand its mechanical behaviour, mechanical tests are performed on bulk specimens and on bonded joints using the Arcan device.

Chapter 3 describes the constitutive law used to model the adhesive behaviour in the initial state. It is important to note that its behaviour is identified using the Arcan test and the inverse identification method. A series of validation tests is also made in this chapter. Moreover, a correlation is made between the adhesive behaviour in a bonded joint and its bulk behaviour.

This opened the way for *Chapter* 4. In this section, the kinetics of water diffusion are studied using bulk specimens. Also in this chapter, a series of mechanical tests are performed on water aged bulk specimens saturated in different environmental conditions. This makes possible to determine the mechanical behaviour of the adhesive for different water contents and constant profiles.

In the last *Chapter* of this work, a method is presented for identifying the parameters of the model developed previously, as a function of water content. In parallel a diffusion model is developed and both models are coupled in order to predict the water effect on the mechanical behaviour of the studied adhesive. In a first step, this calculated for bulk samples

aged in seawater for different times before complete saturation. Finally, the prediction of the presented approach will be compared with the experimental results obtained on aged bulk samples immersed in seawater.

A schematic representation of the adopted approach is presented in *Fig.*1.49.

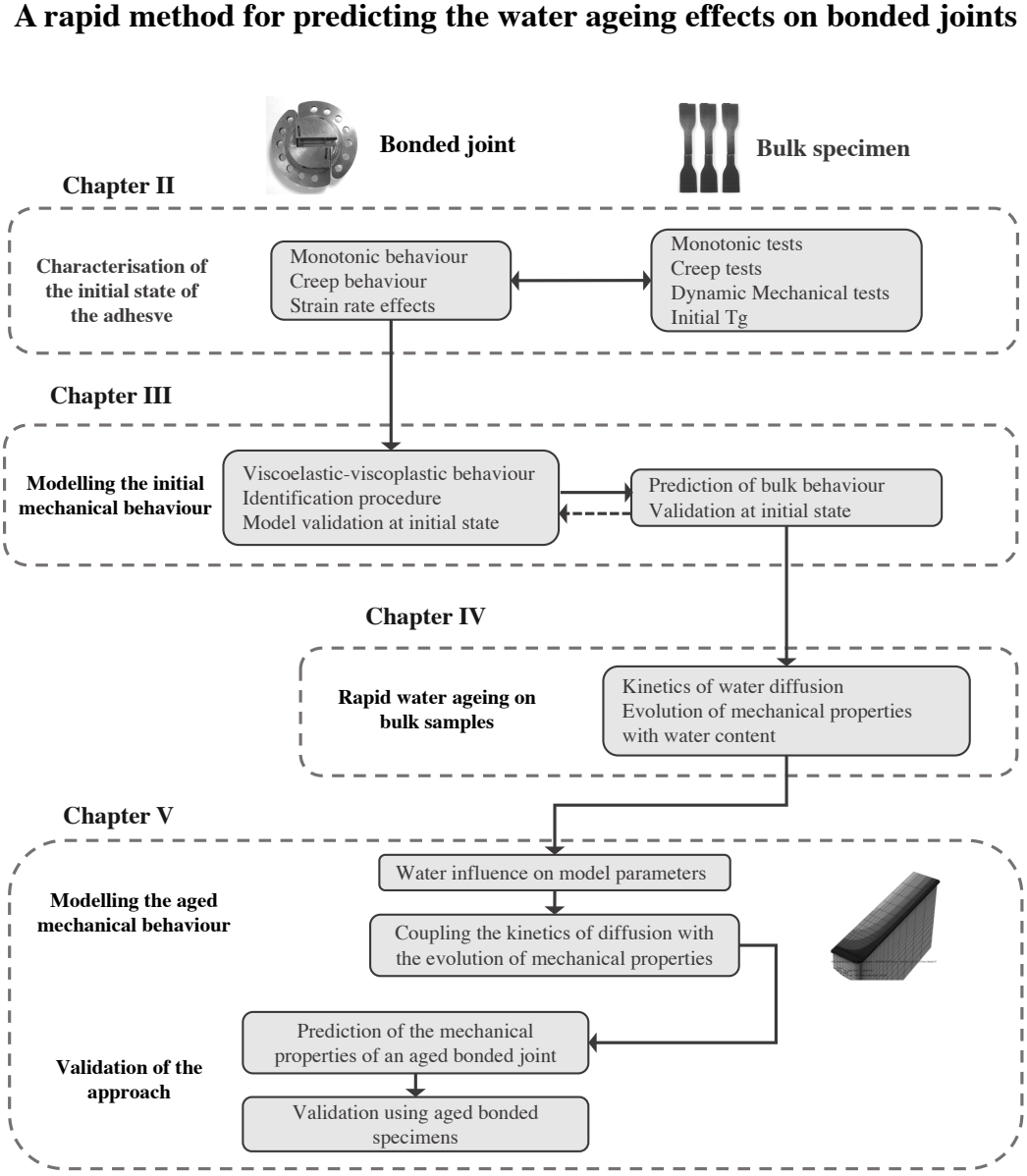

Figure 1.49: Presentation of the adopted approach

Chapter 2

Characterization of the initial state of the studied adhesive

The modern invention of materials science and structural analysis is assimilated to a return to pythaghorism

Matila C. Ghyka, The Golden Number "Pythagorean Rites and Rhythms in the Development of Western Civilization."

General information about the adhesive

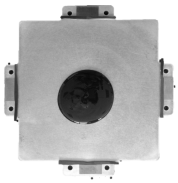

Manufacturing of bulk samples

Mechanical behaviour as a bulk sample

Mechanical behaviour in a bonded joint

This chapter presents the main characteristics of the selected adhesive. Because one of the objectives of this study is the development of a rapid method for predicting the effects of water ageing on the evolution of mechanical behaviour of a bonded joint, it is important to completely understand the properties of the adhesive in its initial state. The different experimental tests presented here allowed to be developed the model able to predict the mechanical behaviour of the adhesive in a bonded joint.

Contents

2.1 General informations on the adhesive studied **72**
2.1.1 Technical specifications 72
2.1.2 Chemical formulation 72
2.1.3 Mixture preparation 72
2.2 Mechanical behaviour of the unaged bulk adhesive **73**
2.2.1 Manufacturing of a sheet of bulk adhesive 74
2.2.2 Tensile behaviour 74
2.2.3 Shear behaviour 76
2.2.4 Tensile creep behaviour 77
2.2.5 Shear creep behaviour 78
2.2.6 Dynamic mechanical analysis 79
2.3 Mechanical behaviour of unaged bonded specimens **80**
2.3.1 Arcan tests 80
2.3.2 Specimens 81
2.3.3 Equipment 82
2.3.4 Monotonic behaviour 82
2.3.5 Creep behaviour 86
2.4 Differential scanning calorimetry analysis (DSC) **88**
2.5 Overview **88**

2.1 General informations on the adhesive studied

The use of structural bonding in humid environments such as those encountered in the marine industry or more recently, in the renewable energy domain is no longer a challenge for engineers. Companies like *3M, Henkel, Huntsman or Sika* offer a large range of structural adhesives resistant to water ageing. This was one of the selection criteria. The adhesive chosen for this study should also provide good adhesion properties with adherents made from aluminium alloy.

Araldite 420 A/B is a structural two-component epoxy adhesive produced by *Huntsman*^{TM}, an important supplier in the domain. According to the producer, it offers excellent adhesion on metals, high performance composites and thermoplastic substrates. Regarding the mechanical properties it is "*extremely tough and resilient with good combination of high shear and peel strength*" [3]. This adhesive has been used for marine application for many years.

2.1.1 Technical specifications

The main specifications given by the supplier are listed in *Tab*2.1:

Table 2.1: Technical specifications [3]

Property	Value	Unit
Viscosity	40	$Pa \times s$
Gel time 23^oC	60	min
Elastic modulus	1500	MPa
Strain at break	5	%
Lap Shear Strength test (aluminium)	24	MPa
Mix ratio (by weight)	100 : 40	-
Mix ratio (by volume)	100 : 50	-
Color	Dark Green	-

2.1.2 Chemical formulation

Araldite 420 A/B is an epoxy based adhesive with a Bisphenol A diglycidyl ether prepolymer and a diamine hardener mixed in stoichiometric conditions.

Table 2.2: Components properties [3]

Property	Araldite 420 A	Araldite 420 B	Mixed Adhesive	Test method
Colour	Yellow	Blue	Dark green	visual
Specific gravity	1.2	1.0	1.1	ASTM-D-792
Viscosity	100-300 $Pa \times s$	0.6 - 1.4 $Pa \times s$	40 $Pa \times s$	ASTM-D-2196

2.1.3 Mixture preparation

The resin and the hardener are provided separately into two different containers ($1kg$ of resin and $400g$ of hardener). For multiple uses, they are stored at 4^oC in a dry environment.

The adhesive is prepared in plastic pots ($50g$ or $100g$) as in *Fig.*2.2a and the weight ratio is measured using a balance *Precisa XT22A* which has a precision of $0.1mg$ (*Fig.*2.2b).

(a) Plastic pot (b) Precision balance (c) Speedmixer^{TM}

Figure 2.2: Preparation of the adhesive

Using a Speedmixer^{TM} (FlackTek Inc., Landrum, USA), the two components are mixed at $2500rev/min$ for 5 minutes (*Fig.*2.2c). This technique provides an homogeneous mixture, free of air bubbles, that can accurately be repeated for each batch of samples.

According to the supplier, this adhesive can achieve 90% its full strength if cured at room temperature for 4 to 5 days. Curing can be accelerated by heating. The maximum strength can be obtained after 1 hour at 120^oC. This was calculated using lap shear strength (LSS) tests. Other cure cycle performances can be seen in *Tab.*2.3.

Table 2.3: Cure cycle performances [3]

Cure cycle	**LSS test at** 22^oC	**Test method**
22^oC for 7 days	34 MPa	A.E.C.M.A EN2243-1
50^oC for 4 hours	36 MPa	A.E.C.M.A EN2243-1
70^oC for 1 hour	37 MPa	A.E.C.M.A EN2243-1
120^oC for 1 hour	43 MPa	A.E.C.M.A EN2243-1

All the samples used for this study (bulk and bonded joints) were manufactured using the framework presented above. The curing cycle was set to 115^oC for *1h10*.

2.2 Mechanical behaviour of the unaged bulk adhesive

This section will present an experimental characterization of the mechanical behaviour of the adhesive in the bulk state. The analysis of the monotonic and creep behaviour have been performed on bulk specimens that were completely dry before each test. No influence of water will be considered for the results obtained in this section.

2.2.1 Manufacturing of a sheet of bulk adhesive

All the bulk samples used for this study were obtained from sheets of adhesive which were obtained using two aluminium plates (*Fig.*2.3a) and a mould release agent. The adhesive is first applied in the middle of the first plate (*Fig.*2.3b). The second plate is then used to apply a constant pressure which will spread the adhesive between the two plates. They are put in contact with four spacers (one on each side of the aluminium plates – *Fig.*2.3b) using eight screws and a torque screwdriver. Because the bulk samples will also be used for water ageing tests, the thickness of the adhesive plates was set to 1mm. This thickness will allow reasonable times for sample saturation.

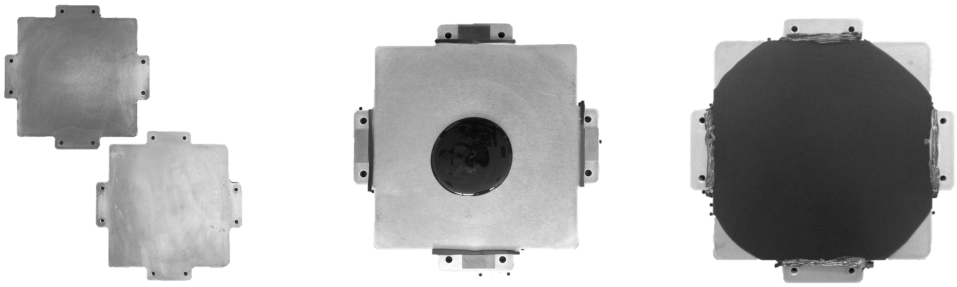

(a) Aluminium plates (b) Before curing cycle (c) After curing cycle

Figure 2.3: Manufacturing of a sheet of bulk adhesive

After the curing process ($1h10$ at 115^oC) the adhesive sheet is obtained as shown in *Fig.*2.3c. The geometries for the different types of bulk samples used in this study are cut out from the adhesive sheet using a water jet cutting system. This cutting procedure minimises the edge defects which can be important, especially for the tensile tests.

2.2.2 Tensile behaviour

The mechanical behaviour of the adhesive was characterised in a first stage using tensile tests on bulk specimens. These tests provide access to important mechanical characteristics of the adhesive such as elastic modulus, Poisson's ratio and yield stress.

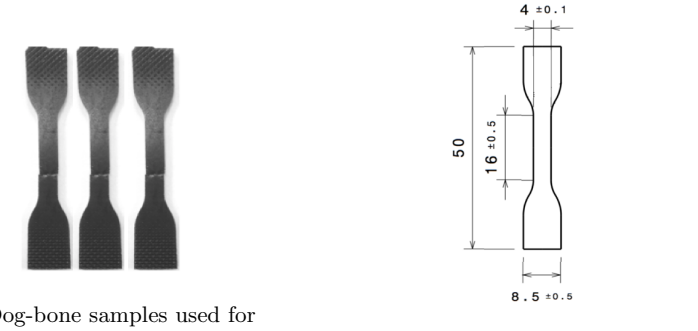

(a) Dog-bone samples used for tensile test (b) Sample dimensions (ISO 37)

Figure 2.4: Geometry of the tensile specimens [ISO 37]

The tests were performed in a controlled room temperature of 21^oC using at least three dog-bone samples per condition (*Fig.*2.4a) and a geometry *type H3* from the standard ISO 37 [47]. The main dimensions can be observed in *Fig.*2.4b. It is important to note that before tests, the samples were kept in a dry environment (less than 1%RH), as the aim here was not to study water influence on the mechanical behaviour.

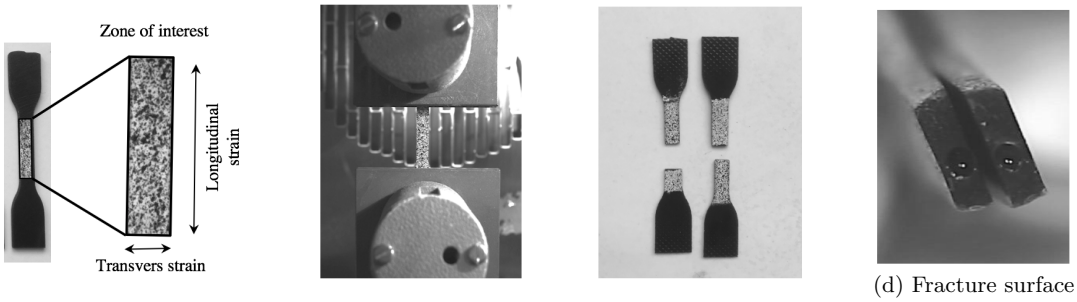

(a) DIC technique (b) Pneumatic jaws (c) Valid samples (d) Fracture surface defect

Figure 2.5: Digital image correlation used for bulk tensile tests

The longitudinal and transverse strains were measured using a Digital Image Correlation (DIC) system. The average strains in the two directions were determined using post-treatment software which calculates the strain of each pixel of the zone of interest (*Fig.*2.5a). Each sample is fixed in the tensile machine using pneumatic jaws. Only the specimens broken in the zone of interest were considered as valid(*Fig.*2.5c). Moreover, the fracture surfaces have been analysed and those with defects were eliminated (*Fig.*2.5d). All the tests were performed using an $Instron^{TM}$ machine and the load was measured using a *500N* load cell. The stress is defined as the measured loading force divided by the section of the sample in the zone of interest (around $4mm^2$).

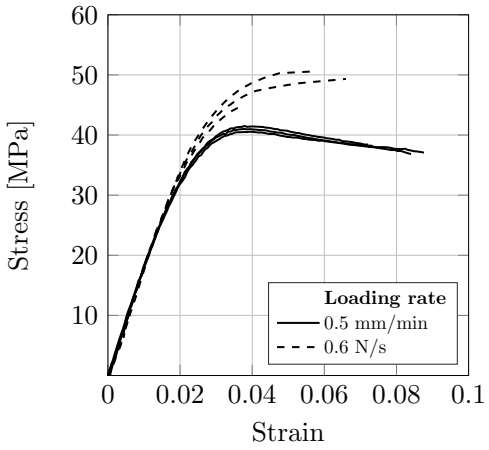

Figure 2.6: Tensile test on bulk specimen

The tests were performed in two conditions: by applying a crosshead speed of $0.5mm/min$ and a loading rate of $0.6N/s$. In both cases, the strain rate in the zone of interest was calculated at $5 \times 10^{-4}s^{-1}$, therefore the two responses are represented in the same figure (*Fig.*2.6). by superposing three valid curves for each. Very low scattering can be observed in terms of elastic

modulus and yield stress. The strain at break appears to be more scattered.

2.2.3 Shear behaviour

For further investigations, experimental tests have been performed to characterise the monotonic shear behaviour of the bulk adhesive up to failure. These tests were performed at 21^oC using a fixing device available on a *Metravib*^{TM} dynamic mechanical analyser (DMA) (*Fig.*2.7a).

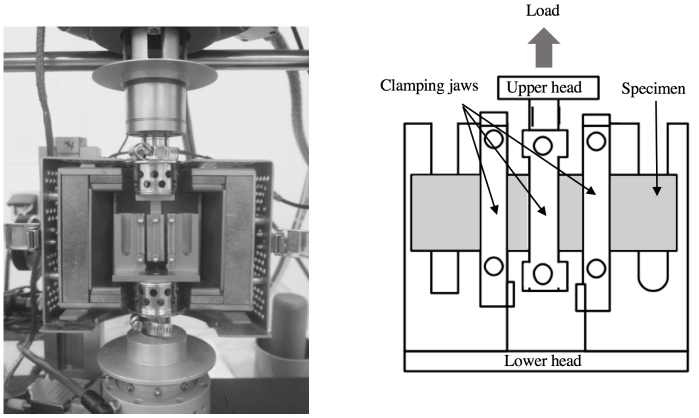

(a) Shear fixture mounted on the DMA machine

(b) Representation of the shear fixture

Figure 2.7: Experimental set-up for shear tests on bulk specimens

The system is composed of a fixed lower head connected to the load sensor and a mobile upper head which allows a controlled displacement or load to be applied. The sample is fixed between the two parts using three clamping jaws (one on the upper head and two on the lower head) as shown in *Fig.*2.7b. The two areas of the sample situated between the clamping jaws are subjected to a pure shear stress.

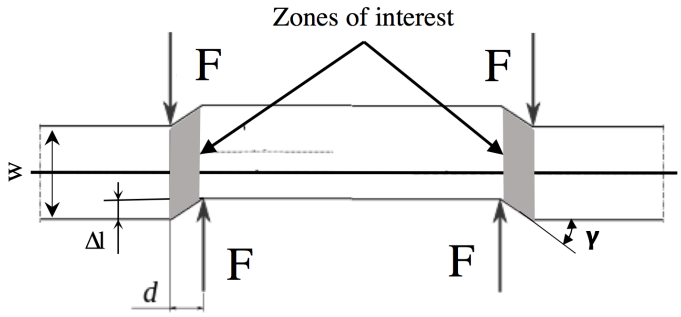

Figure 2.8: Deformation of the bulk specimen in shear test (not to scale)

Specimens have a rectangular shape (30mm × 4.2mm) with a thickness of $1mm$ and were cut out from an adhesive plate. According to international standard ISO 6721 [147], the width of the sample should be at least two times bigger than the gap between the clamping jaws which in this case is equal to $2mm$.

Five samples have been tested, and a constant loading rate of $1N/s$ has been applied during

each test. *Fig.*2.8 illustrates the two zones of interest subjected to pure shear stress, where F represents the applied load, Δl is the displacement measured by the machine, d the gap between the clamping jaws ($1.8mm$) and w the width of the sample ($4.2mm$).

The shear stress was calculated using the relation (*Eq.*2.1):

$$\tau = \frac{F}{S} \qquad \text{with} \qquad S = \mathrm{w} \times e \tag{2.1}$$

where F is the applied load and S the cross-section area of the material (parallel of the applied vector) and e the thickness of the sample.

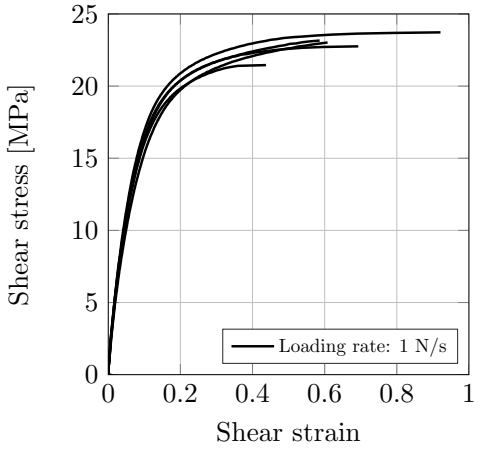

Figure 2.9: Shear behaviour on bulk specimen

The shear strain ε_{12} is calculated using the *Eq.*2.2, where Δl is the displacement of the upper header and d the distance between the clamping jaws.

$$\gamma = \frac{\Delta L}{d} \tag{2.2}$$

The result can be observed in *Fig.*2.9. It is important to note that all the samples were completely dried before the test and no water influence is being considered here.

2.2.4 Tensile creep behaviour

Testing the monotonic behaviour of the adhesive allows access to the most important characteristics of the material such as Young's modulus and the elastic threshold. Moreover it gives an idea of the maximal stress in different loading conditions. However, in order to complete this characterization the viscous behaviour of an adhesive can be investigated by creep tests.

In this study, the tensile creep behaviour of the bulk adhesive has been analysed using the $Metravib^{TM}$ DMA machine with a tensile loading device mounted on it (*Fig.*2.10a). The specimens used in these tests were cut from the adhesive sheet using a water jet cutting system and they have a rectangular shape (*Fig.*2.10b) with a thickness of $1mm$.

The strain was calculated using the *Eq.*2.3, where Δl represents the displacement of the upper load point measured by the machine and l_0 the initial length of the specimen (*Fig.*2.10c).

(a) Tensile fixture mounted on the DMA machine

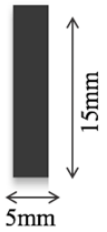

(b) Specimen for tensile creep behaviour

(c) Calculation of the tensile strain

Figure 2.10: Tensile creep behaviour performed on bulk specimens

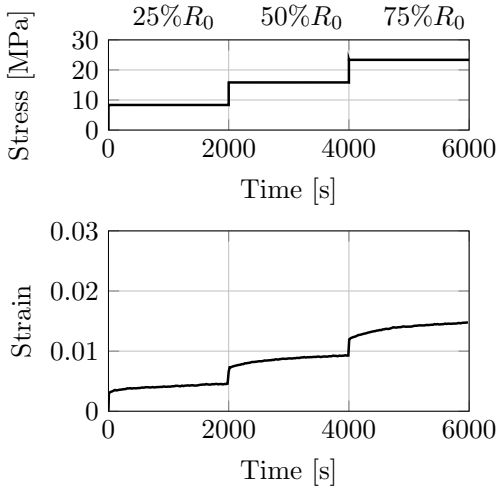

(a) Tensile creep behaviour

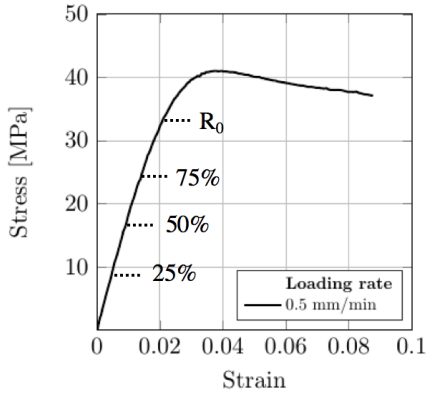

(b) Monotonic tensile behaviour

Figure 2.11: Experimental result for tensile creep behaviour on bulk form

$$\varepsilon = \frac{\Delta l}{l_0} \tag{2.3}$$

In order to highlight the tensile creep behaviour and to avoid plastic strains during the tests, the applied load levels represent 25%, 50% and 75% of the yield stress R_0, calculated using the monotonic tensile tests (*Fig.*2.11b). Moreover, the loading times have been set to 2000 *seconds* per level (*Fig.*2.11a).

The results can be observed in *Fig.*2.11a. As expected, for each applied load level, the adhesive presents a viscous behaviour dependent on the load level.

2.2.5 Shear creep behaviour

The shear creep behaviour has been analysed using the same approach. The experimental device used for these tests and the geometry of the samples are the same as those used to

characterise the monotonic shear behaviour (*Fig.*2.7a) and(*Fig.*2.7b). Also, the shear stress and the shear strain were determined using the (*Eq.*2.1) and (*Eq.*2.2).

Four load levels have been applied, representing 20%, 40%, 60%, 80% of the shear yield stress R_{0_s} (*Fig.*2.12b). The duration of each level was also set to 2000 *seconds*.

As can be observed in *Fig.*2.12a, like in the case of tensile creep behaviour, the shear creep strain is increasing with the applied load. Moreover, it is important to notice that the creep behaviour depends on the loading conditions.

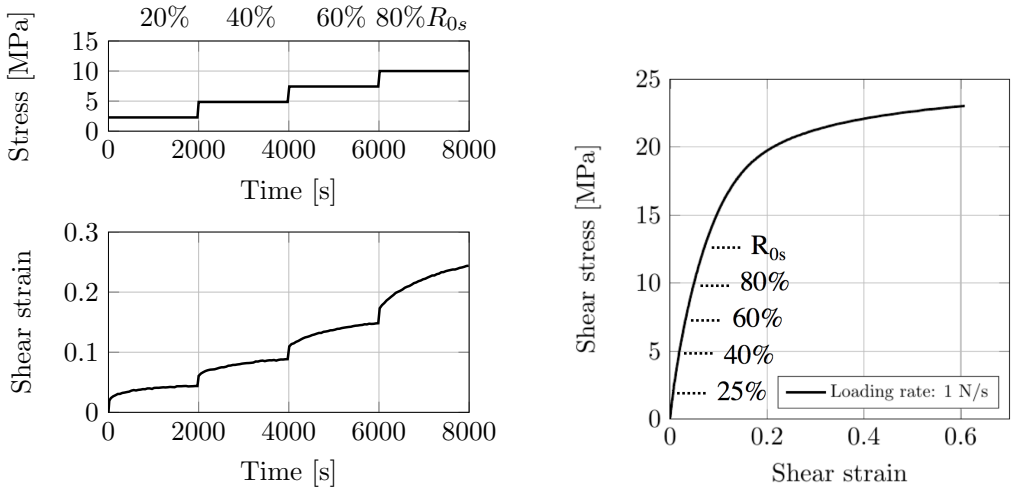

(a) Shear creep behaviour

(b) Monotonic shear behaviour

Figure 2.12: Experimental result for tensile creep behaviour on bulk form

2.2.6 Dynamic mechanical analysis

Another important aspect of the mechanical behaviour of adhesives, and polymers in general, is that their behaviour is highly influenced by the temperature. The aim of this analysis is to determine the evolution of Young's modulus as a function of temperature. As for the previous tests, this analysis was performed on dried samples.

The equipment used for these tests is identical with the one used to characterise the tensile creep behaviour. The fixture device (*Fig.*2.13a) is mounted on the $Metravib^{TM}$ DMA testing machine and the rectangular samples with a thickness of $1mm$ are cut from an adhesive sheet (*Fig.*2.3c) using a water jet cutting system. The test was performed under tensile-tensile loading condition. A strain of $\Delta\varepsilon = 10^{-3}$ was imposed with a frequency of $1Hz$. The response of the material was studied in a range of temperature starting from 0^oC to 100^oC with a rate of $10^oC/min$.

In *Fig.*2.13b the evolution of the elastic modulus E (defined as the sum of the storage modulus E' and the loss modulus E'') with temperature can be observed. The loss factor $tan\delta$ is a non-dimensional characteristic of the material. A high value is indicative of a material that is more viscous, while a low value indicates one that is more elastic.

(a) Tensile fixture used for DMA analysis

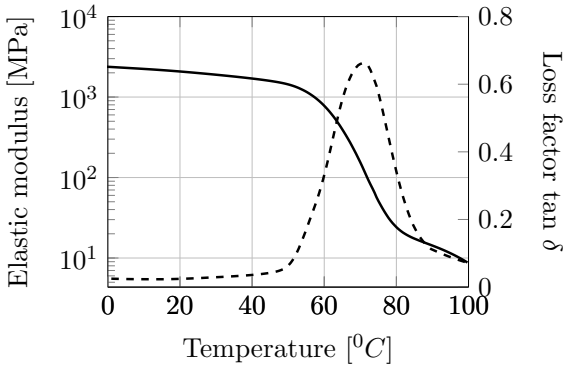

(b) Evolution of the elastic modulus as a function of temperature

Figure 2.13: Dynamic mechanical analysis at initial state

At room temperature, the measured elastic modulus is equal to $1980MPa$ which is in accordance with the elastic modulus calculated using the monotonic tensile tests. The change of the elastic properties with the temperature is related to a change in the polymer network which provides to another important characteristic of the adhesive, *the glass transition temperature.*

There are several methods to determine the value of the glass transition temperature T_g that can be found in literature. According to standard [148] the T_g can be considered as the point where the loss factor is maximal. This is the method that gives the highest value and in this case is equal to 69^oC. Using the method based on the standardized DSC method (ISO 11357-1) that involves ascertaining the onset, end, and midpoint temperatures of the transition zone, the calculated T_g value is around 61^oC.

2.3 Mechanical behaviour of unaged bonded specimens

The previous sections presented the main characteristics of the studied adhesive as a bulk material (Young's modulus E, elastic threshold R_0, transition glass temperature T_g). But in order to be able to completely understand its mechanical behaviour it is important to characterise its behaviour in a bonded joint.

As presented previously in the first chapter of this work, there are several types of experimental tests that can be used to test the mechanical behaviour of an adhesive. For this study, the modified *Arcan* test has been used.

2.3.1 Arcan tests

The principal characteristic of the modified *Arcan* device [62] is the possibility of combining proportional compression-tensile/shear loadings on a bonded specimen. A detailed description of this test was presented in *Chapter* 1 of this work.

Using a uniaxial tensile machine, it is possible to apply shear (*Fig.*2.14a) or tensile (*Fig.*2.14b) loads to a bonded joint. The combined loads are obtained by modifying the angle of the device

(a) Shear $\gamma = 90°$ (b) Tensile $\gamma = 0°$ (c) Tensile/shear $\gamma = 45°$ (d) Compression/shear $\gamma = 135°$

Figure 2.14: Different types of Arcan device loading

as can be seen in (*Fig.*2.14c,2.14d). Two "half-moons" are made of high stiffness steel and they are connected to the tensile machine using special clevis pins.

2.3.2 Specimens

The substrates (*Fig.*2.16a) used in the tests are made from aluminium alloy, $AW2017$. Their geometry was developed and optimized previously as described in the literature [149], and the main dimensions are shown in *Fig.*2.15.

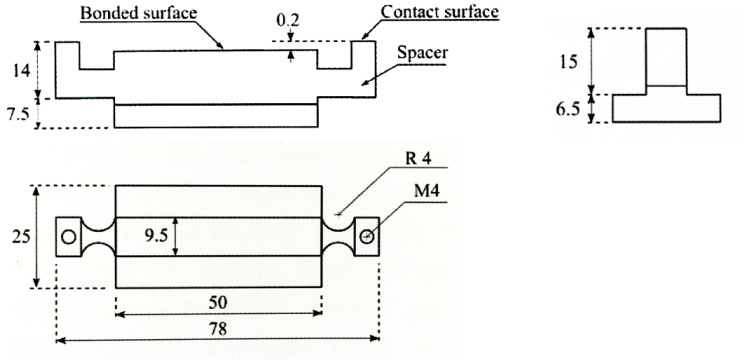

Figure 2.15: Main dimensions of the substrates (not to scale) [23]

The substrates are provided with spacers (*Fig.*2.16a) that are directly machined from a single block of aluminium alloy. These have an important role in order to obtain a correct alignment and keep a constant thickness when bonding a specimen. The results presented in this paper are obtained using a thickness of the bonded joint that is equal to $400 \pm 10\mu m$. During the curing cycle the substrates are kept in the final position by screws (*Fig.*2.16b). A constant torque of $2.5Nm$ is applied to the screws.

Before starting the process of bonding, the bonded surfaces of the specimen ($50\text{x}9.5mm^2$) are subjected to a mechanical treatment that involves a sanding process with different grades of emery cloth ($220 - 180$ grit cloth) in order to ensure a clean surface. The next step is to degrease it using acetone. To ensure a homogeneous joint, the adhesive is applied on the surface of each substrate that will form the specimen. The excess adhesive after the bonding process is cleaned with a spatula.

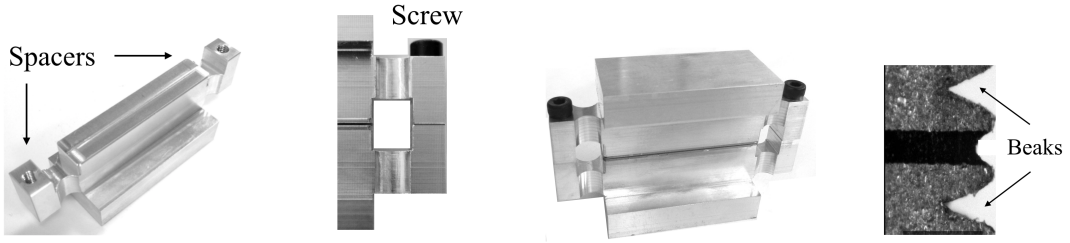

(a) Substrate (b) Screw (c) Specimen (d) Beaks

Figure 2.16: Modified Arcan specimen

The final bonded specimen can be seen in *Fig.*2.16c. After the curing process, the spacers are removed. An important characteristic of the specimens is the beaks (*Fig.*2.16d). They allow the edge effects to be reduced, as shown by *Cognard et al.* [150] and encourage a cohesive failure of the assembly.

2.3.3 Equipment

To perform the experimental tests, the Arcan device was inserted in a hydraulic tensile testing machine (*Instron 1342*). The temperature in the testing room is controlled at about 23^0C. The load cell can measure a maximum load of $100kN$.

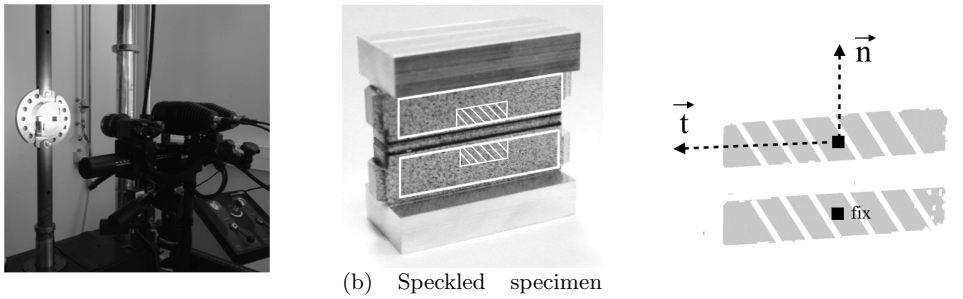

(a) GOM System (b) Speckled specimen ready for test (c) Digital Image Correlation

Figure 2.17: Measurement of substrate displacements

The relative displacement of the substrates is measured using a DIC system (*Fig.*2.17a). The specimen is speckled on one face before installing it in the Arcan device (*Fig.*2.17b) and the shaded zone represents the area of interest for calculating the displacements. This relative displacement is correlated with the load measured by the tensile machine load cell.

The relative displacement between the two substrates during a test is decomposed into a *normal displacement* (ND) and a *tangential displacement* (TD), (*Fig.*2.17c).

2.3.4 Monotonic behaviour

Using the Arcan device, it was possible to characterise the monotonic behaviour of this adhesive in a pure tensile ($\gamma = 0^o$) and a shear load ($\gamma = 90^o$). For each condition, two loading rates have been used: $0.2kN/s$ and $2kN/s$. It is clear for the two cases (tensile and shear), that

this adhesive has a mechanical behaviour influenced by the loading rate (*Fig.*2.18). In tensile tests (*Fig.*2.18a), the apparent elastic threshold is increased by about 12% from $13kN$ to $16kN$ when the applied loading rate is multiplied by ten. The failure load is also influenced by the loading rate. The same phenomenon is observed in the shear test. This time, it can be seen that the apparent elastic threshold is increased from 8kN to 10.2kN when the loading rate is increased ten times.

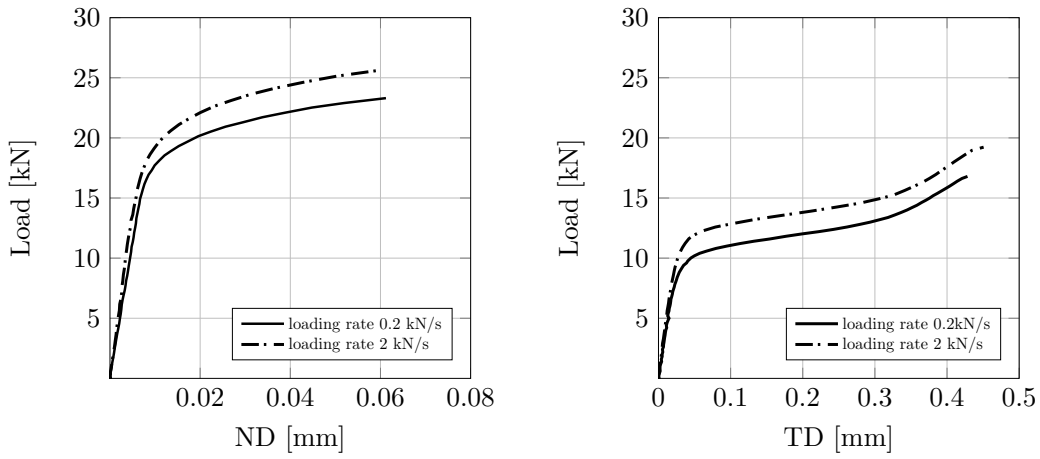

(a) (b)

Figure 2.18: Monotonic test: tensile (a) and shear (b)

For each loading condition, between two and three samples were tested. *Fig.*2.19a represents the scatter between the three samples tested in the same condition ($0.2kN/s$) in tensile loading. As can be observed, the modulus values and the maximal stresses are very close from one sample to another. In shear loading (*Fig.*2.19b) the scattering is also very low. For all other tested conditions a small dispersion of results could be noted therefore, for the readability of the figure, only one curve will be represented by condition.

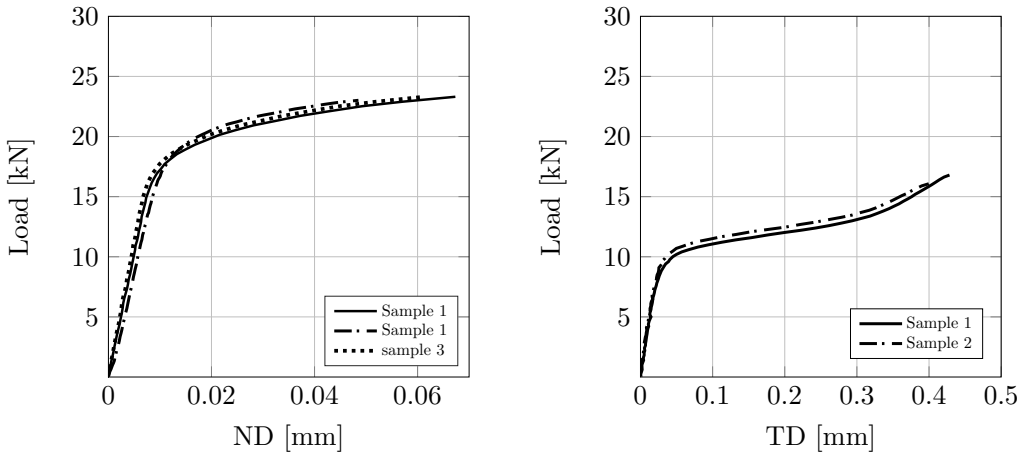

(a) Scattering in tensile tests (0.2 kN/s) (b) Scattering in shear tests (0.2 kN/s)

Figure 2.19: Monotonic tests

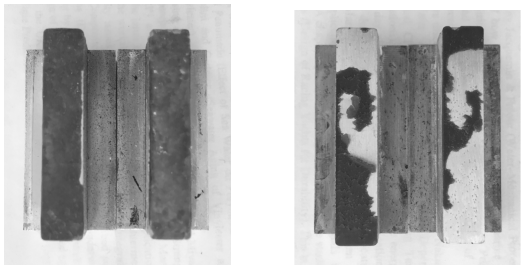

(a) Tensile failure (b) Shear failure

Figure 2.20: Type of failure obtained in tensile (a) and in shear (b) tests

Another important aspect of this analysis is the type of failure that was obtained in tensile and in pure shear loading conditions. It is important to notice that in tensile load a cohesive failure is obtained for all the tested samples (*Fig.*2.20a). In pure shear the adhesive has a more complex type of failure. The failure is considered as mixed (*Fig.*2.20b), with regions of cohesive and regions of adhesive failure.

The differences in fracture mode observed for the two conditions can be explained by the fact that when subjected to a tensile loading, the distribution of the normal stress in the adhesive layer leads to local stress concentrations that allow the formation of voids. These voids will finally coalesce and will lead to a macro-crack that will propagate in the adhesive layer. On the contrary, when the samples are subjected to pure shear loadings, the stress distribution is completely different. The voids are elongated in a manner such that they create micro-cracks between the two adherents which will lead to a different propagation of the macro-crack.

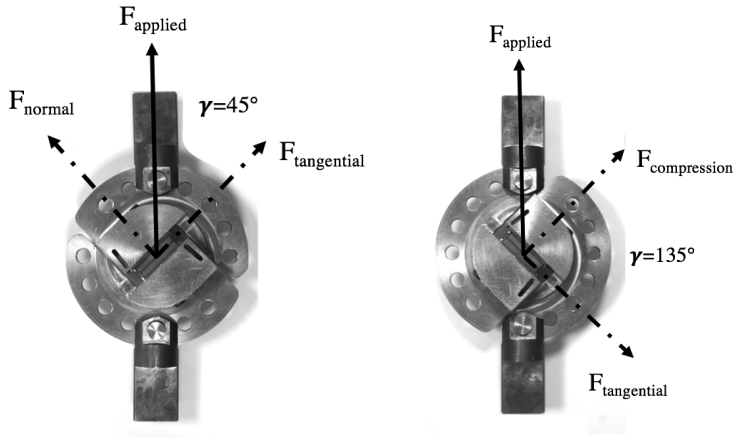

(a) Tensile/Shear test (b) Compression/Shear test

Figure 2.21: Schematic representation of the applied load ($F_{applied}$) and projections of the tensile/compression load and tangential load

In order to be able to have a better understanding of the mechanical behaviour of the adhesive in a bonded joint, proportional mixed load tests were also been performed at $0.2kN/s$. In this type of test, the applied load can be divided into a tensile/compression load and a tangential load as can be seen in *Fig.*2.21a and *Fig.*2.21b. Moreover, the measured displacements

were also divided into two components: a tangential one (TD) and a normal one (ND).

The combined tensile/shear test is represented in *Fig.*2.22. As can be observed the strength of the adhesive has decreased compared to the cases of tensile or pure shear loading. A more important scattering can be observed beyond the elastic limit. In contrast, the combined compression/shear loading case (*Fig.*2.23) presents an increased failure load and a behaviour that is completely different especially in the non-linear part. This may be explained by the fact that the compression component inhibits the damage initiation in the adhesive layer.

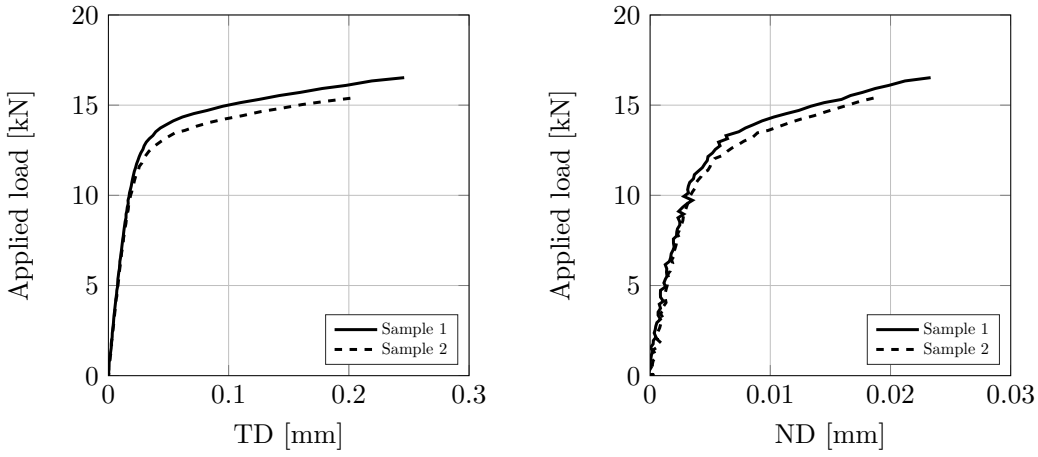

(a) Load - Tangential displacement

(b) Load - Normal displacement

Figure 2.22: Combined tensile/shear test ($\gamma = 45^o$)

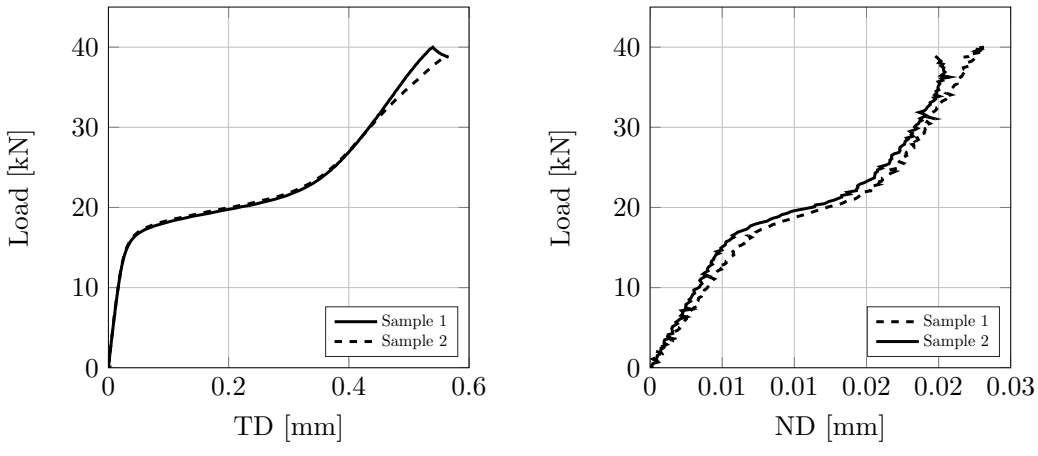

(a) Scattering in tensile tests

(b) Scattering in shear tests

Figure 2.23: Combined compression/shear tests ($\gamma = 135^o$)

The different experimental tests performed in monotonic loading conditions allow to determine the failure envelope for this adhesive to be determined (*Fig.*2.24). For tensile and pure shear loading conditions, the ultimate stress was calculated by dividing the maximal load by the bonded area (9.5mm × 50mm). For the combined loading conditions, the ultimate strength for tensile/compression and shear was calculated using the *Eq.*2.4 and *Eq.*2.5 where $\sigma_{T/C}$ and

σ_S are the ultimate strength in tensile/compression and shear loading, $F_{T/C}$ and F_S are the calculated loads in tensile/compression and shear loading, S is the area of the bonded surface, F_{max} is the maximal load measured by the machine and γ the positioning angle of the Arcan device ($\gamma = 45^o$ for tensile/shear and $\gamma = 135^o$ for compression shear)

$$\sigma_{T/C} = \frac{F_{T/C}}{S} \quad \text{where} \quad F_{T/C} = F_{max} \times \cos\gamma \tag{2.4}$$

$$\sigma_S = \frac{F_S}{S} \quad \text{where} \quad F_S = F_{max} \times \sin\gamma \tag{2.5}$$

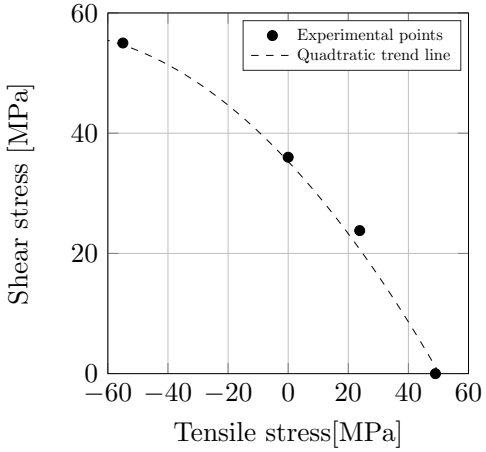

Figure 2.24: Failure envelope determined using Arcan specimens

2.3.5 Creep behaviour

In order to be able to characterise the viscous behaviour of this adhesive, multi-level creep tests have been performed. The aim was also to highlight any differences between the viscous behaviour under tensile and shear loading conditions.

In tension (*Fig.*2.25a), three load levels have been applied for a period of 2000 seconds. These values correspond to 25%, 50%, and 80% of the apparent elastic limit at $0.2kN/s$ loading rate. This loading rate was used to make the passage from one level to another.

Under shear load (*Fig.*2.25b), four load levels have been applied. These levels represent 20%, 40%, 60%, 80% of the apparent elastic threshold observed in monotonic shear tests for a loading rate of $0.2kN/s$. Four levels of loads have been applied (and not three as in tensile loading) due to the fact that under shear loading condition, a more significant creep response was observed.

Based on the work of *Badulescu et al.* [79] the observed displacements at the end of each creep level were divided into two parts, as in *Eq.*2.6 and *Eq.*2.7, where $ND^i_{elastic}$, $TD^j_{elastic}$ represent the displacements generated by the applied load at the beginning of each creep level and $ND^i_{viscous}$, $TD^j_{viscous}$ are the displacements measured at the end of the creep levels.

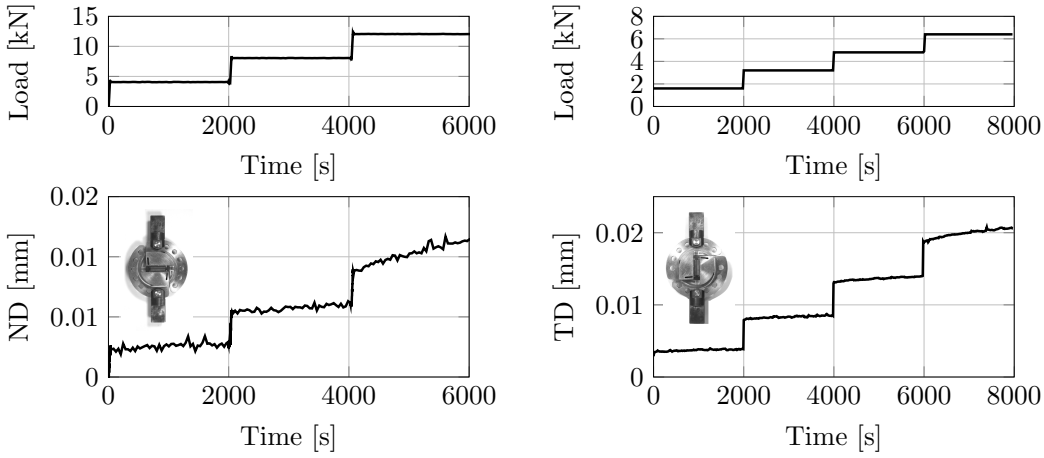

Figure 2.25: Multi-level creep tests: tensile (a) and shear (b)

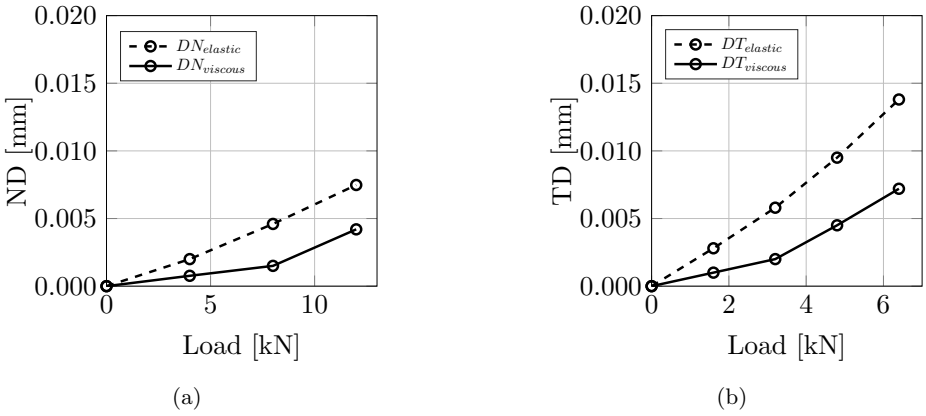

Figure 2.26: Evolution of the viscous and elastic displacements at the end of each creep level: tensile (a) and shear (b)

$$ND^i_{total} = ND^i_{elastic} + ND^i_{viscous} \quad i = 1:3 \tag{2.6}$$

$$TD^j_{total} = TD^j_{elastic} + TD^j_{viscous} \quad j = 1:4 \tag{2.7}$$

Analysing the results obtained in *Fig.*2.26a and *Fig.*2.26b it is possible to note that even though the applied load is below the apparent elastic threshold, viscous displacements are taking place in both cases: tensile and shear. Another important aspect is that the viscous behaviour is not linear and it depends on the applied load. Moreover, viscous behaviour is more important in shear than in tensile loading.

2.4 Differential scanning calorimetry analysis (DSC)

Differential scanning calorimetry (DSC) allows the thermal phenomena which derive from a physical change in the material to be characterised. Among the information that can be extracted by using this technique, it is possible to enumerate: the melting temperature, the heat of fusion, the latent heat of melting, the reaction energy and temperature, the glass transition temperature, the crystalline phase transition temperature and energy, the precipitation energy and temperature, the denaturization temperatures, the oxidation induction times, and the specific heat or heat capacity.

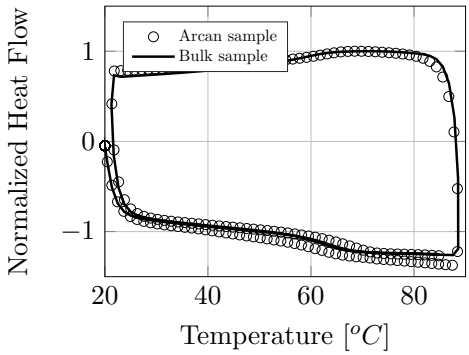

Figure 2.27: Differential scanning calorimetry (DSC) analysis at initial state

The DSC measurements were performed on a standard $Q10$ machine from *TA Instruments*. The aim of this test was to measure the initial transition glass temperature (Tg) of a dried bulk sample of the studied adhesive and compare it to a sample from a tested Arcan specimen. This allows to verify if the adhesive has the same polymerisation state in both cases for the same curing time. The analysis was made over the temperature range from 20^{o}C to 90^{o}C with a speed of 10^{o}C/min. At least 3 samples were tested with a weight around *10 mg*.

The obtained results can be observed in *Fig*2.27. Using the standardized DSC method (ISO 11357 [151]) it was possible to determine the Tg as equal to $66^oC \pm 2^oC$. This is in reasonable agreement with the Tg measured using the DMA analysis and the method that considers the point of the maximal loss factor as the point of Tg. It should be emphasized, however, that these two methods (DSC and DMA) do not measure the same property, and results often differ slightly.

2.5 Overview

The first objective of this chapter was to present the main characteristics of the studied adhesive in the initial state. It is important to note that all the experimental tests have been performed on unaged specimens and no water effects were considered here.

Bulk specimens were manufactured using two aluminium plates and a moulding release agent. They were dried in a desiccator at 0%RH before the tests. The monotonic tensile and shear experimental tests will be used to determine important mechanical characteristics such as Young's modulus, Poisson's ratio, yield stress and the strain at break (*Chapter* 3). Using

the creep tests, it was possible to reveal the viscous behaviour of the adhesive and the dynamic mechanical analysis allowed to have access to the glass transition temperature.

The second objective of this chapter was to create a base of experimental data that will be used to develop a model able to predict the mechanical behaviour of the adhesive in a bonded joint. This will be the subject of the next chapter of this work.

Chapter 3

Modelling the mechanical behaviour of the adhesive at initial state

"Developing a model consists in building an easy to use concept who explains the apparent complexity"

Claude Allègre, "La Défaite de Platon"

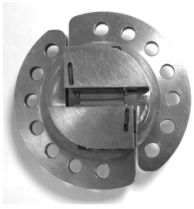

Model identification using Arcan tests

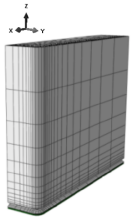

Inverse identification method

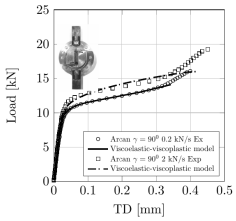

Constitutive law

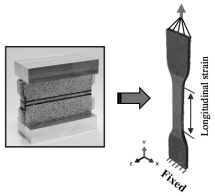

Towards the bulk behaviour

The previous chapter presented the main characteristics of the studied adhesive at initial state. The aim of this chapter is to develop a constitutive law able to predict the mechanical behaviour of the adhesive in the bonded joint. All the tests used in this chapter were performed just after the curing process. Thus, the model identification will characterize the initial state of the adhesive. No water ageing effects will be considered for this stage of the work. After the identification of the proposed constitutive law, a correlation between the adhesive's behaviour in a bonded joint and in bulk form will be analysed.

Contents

3.1 Numerical modelling of the Arcan test **92**
3.1.1 Approach 92
3.1.2 Finite element model 93
3.1.3 Inverse identification method 95
3.2 Constitutive law **97**
3.2.1 Identification of elastic parameters 98
3.2.2 The modified viscoelastic spectral model 100
3.2.3 Identification of the viscoelastic parameters 102
3.2.4 Viscoelastic-viscoplastic model 106
3.2.5 Identification of viscoplastic parameters 107
3.3 Validation of the constitutive law **110**
3.3.1 Validation of the viscoelastic part 111
3.3.2 Validation of the complete model 111
3.3.3 Validation of the yield function 113
3.3.4 Validation of the loading rate effect 114
3.4 From Arcan tests to bulk behaviour **114**
3.4.1 Prediction of the tensile bulk behaviour 115
3.4.2 Prediction of the shear bulk behaviour 116
3.5 From bulk tests to the Arcan behaviour **117**
3.6 Conclusions **119**
3.6.1 Overview on the model 119
3.6.2 Perspectives 120
3.6.3 Proposal for a rapid characterisation of a water-aged bonded joints . . 120

3.1 Numerical modelling of the Arcan test

3.1.1 Approach

As has been shown in previous studies *Cognard et al.* [149], the stress state in the adhesive joint of the specimens used in Arcan tests, is not uniform. Therefore, in order to be able to describe and to model the mechanical behaviour of the adhesive in the bonded joint, it is necessary to develop a realistic finite element model (FE model).

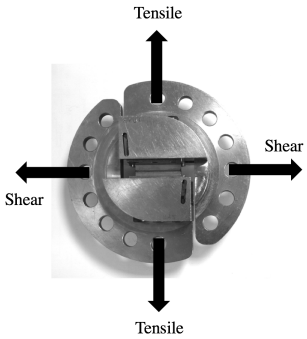

Figure 3.2: Arcan device ready to be mounted on a tensile machine

Because of the complex mechanical behaviour of the studied adhesive, a viscoelastic viscoplastic model will be used to model the observed behaviour. Generally, these models have an important number of parameters and they are expensive in terms of computation time. Moreover, the identification of the parameters is made using the inverse identification method (presented in the next section) and optimisation algorithms, which involve a great number of simulations. Thus, a model of the Arcan test should be considered first and some assumptions have then to be made in order to reduce the complexity of the FE model.

Performing an Arcan test involves the use of different components and interface elements between the specimen and the tensile machine. In the case of a tensile or shear test (*Fig.*3.2) the specimen is mounted in the Arcan device which is connected to the machine using a pin. In order to take into account the deformation of all these components, it would be necessary to include them in the FE model which may lead to important computation time (contacts, large number of elements, stress concentrations). By supposing that the applied load is perfectly transmitted to the specimen, it was possible to develop a model using only the geometry of the bonded specimen.

This first hypothesis permitted to consider that the applied load for different loading cases in concentrated in the middle of the specimen (*Fig.*3.3a). Thus, the FE model can be developed from a simplified version of the specimen by fixing one of the substrates and choosing a loading point that is kinematic coupled with the other substrate.

(a) (b)

Figure 3.3: (a) Specimen ready to the be mounted in the Arcan device (b) Equivalent model for the Arcan specimen

3.1.2 Finite element model

3.1.2.1 Complete 3D model

In a first step, a complete 3D finite element model was developed (*Fig.*3.4) based on the assumptions made in the previous section. This will be the reference model that will be used to validate the identified mechanical behaviour. Regarding the boundary conditions, one of the substrates is fixed using a reference point and a kinematic coupling. The load is computed on the loading point as follows: for tensile loading ($\gamma = 0^o$) in $\vec{x}$ direction, for shear loading ($\gamma = 90^o$) in $\vec{z}$ direction and for combined loadings ($\gamma = 45^o$) for instance at 45^o compared to $\vec{x}$ the axis. The relative displacement is calculated at the point located in the same zone as the one used for the experimental characterization ($3mm$ above the middle plane of the adhesive layer).

The mechanical behaviour of the substrates is assumed to be linear elastic with a Young's modulus equal to $70GPa$ and a Poisson's ratio of 0.34. These define the mechanical elastic behaviour of the aluminium alloy (Al2017) used for the substrates. The mechanical behaviour of the adhesives is described using the constitutive law presented in the next section of this chapter.

3.1.2.2 3D model with symmetry conditions

The geometry of the specimen allows simplifying the model by adding symmetry conditions. *Fig.*3.5 presents the boundary conditions applied to a model that represents an eighth part of a specimen. This approach permitted to decrease the number of elements used in the simulation.

The mesh used for this study is presented in *Fig.*3.6. Because of the important difference between the substrate stiffness and the adhesive one, stress concentrations will appear near the edges at the adhesive/substrate interface. In order to reduce their effect on the global mechanical response, the size of the elements was considerably reduced near the free edges. It is important to note that the complete 3D model was meshed in the same manner.

The type of elements used to model the substrate and the adhesive layer is 8-node linear

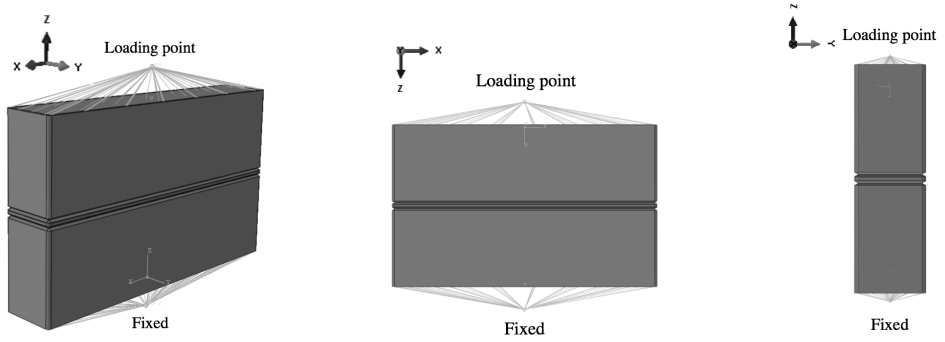

(a) Isometric view (b) Front view (c) Side view

Figure 3.4: Complete 3D finite element model

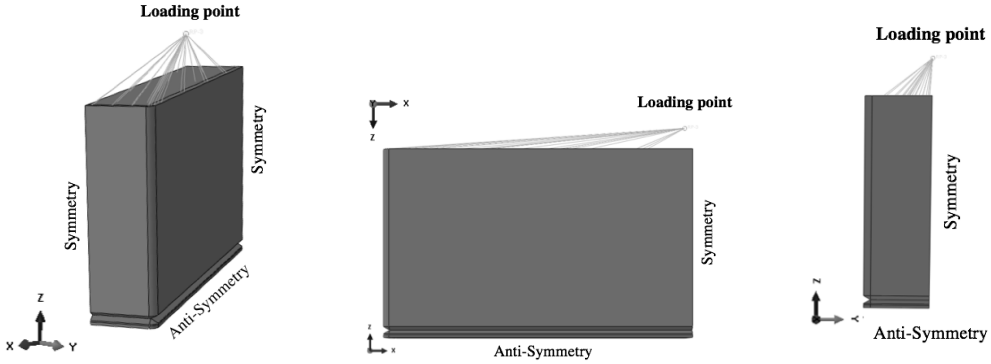

(a) Isometric view (b) Front view (c) Side view

Figure 3.5: 3D finite element model with symmetry/anti-symmetry conditions

brick elements with reduced integration and hourglass control ($C3D8R$).

The bonded joint has a thickness of $0.4mm$. three elements have been used to model half of the joint thickness because of the symmetry of the sample. A parametric study performed by *Badulescu et al.* [79] has shown that this number of elements, in the thickness of the adhesive, is enough to obtain a convergent macroscopic response, when, using a viscoelastic spectral model, for the adhesive behaviour.

3.1.2.3 Reduced 3D model with plane strain assumption

The 3D model presented in *Section* 3.1.2.2 has been used to identify the elastic parameters of the model (*Section*3.2.1) and to model the water diffusion in the adhesive layer (*Chapter*5). For the identification of the viscoelastic and viscoplastic parameters (*Section* $3.2.2 - 3.2.5$) a more simplified 3D model, with only one element in the thickness and a plane strain assumption, was used. This type of model allows an important reduction in terms of computation time due to the small number of elements.

The boundary conditions for this geometry are shown in *Fig*.3.7. The applied load was adapted to the actual area of the bonded surface and computed on the loading point which

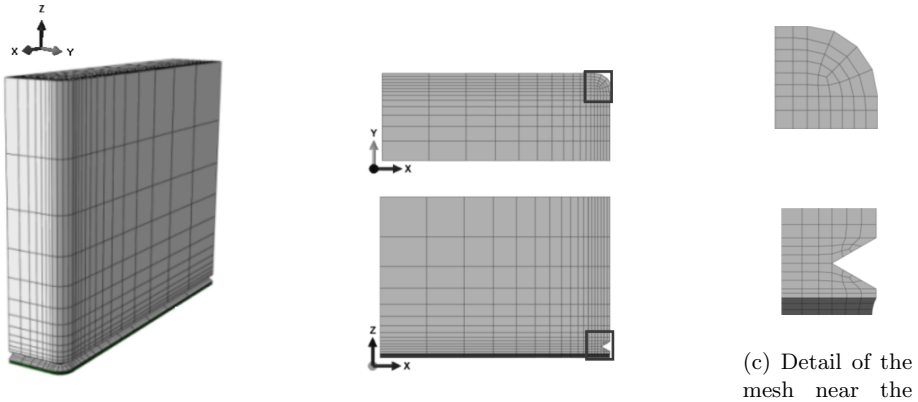

(a) Isometric view

(b) Front and top view

(c) Detail of the mesh near the edges

Figure 3.6: Mesh of the 3D FE model

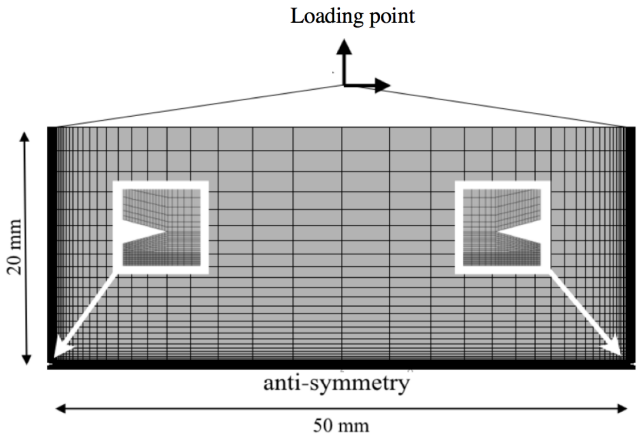

Figure 3.7: Mesh of the 2D FE model

is linked to the superior part of the substrate by a kinematic coupling. As shown in previous studies [23], the mechanical response predicted by the reduced model is almost identical to the one of the complete 3D model but it allows an 80% reduction in the computing time.

3.1.3 Inverse identification method

A classic method used in material science to identify the elastic parameters is based on the observed stress-strain curve of a given material. In the case of the Arcan test, the non-uniform stress distribution along the adhesive overlap makes it impossible to apply this approach. Therefore, the inverse identification method is used to identify the parameters of the model developed in the next section.

The principle of this method is to compare the results observed in an experimental test with the prediction of an equivalent FE model and a given set of parameters. This method has already been used in previous studies to identify the mechanical behaviour of an adhesive using Arcan tests [21][98][23]. As suggested by *Medina* [23] the results obtained using this method are strongly dependent on the accuracy of the FE model.

Once the FE model is validated as representative for the experimental test, the inverse identification method can be applied. The user has to define several sets of model parameters that will be used to predict the desired mechanical response. A schematic representation of the method is presented in *Fig.*3.8.

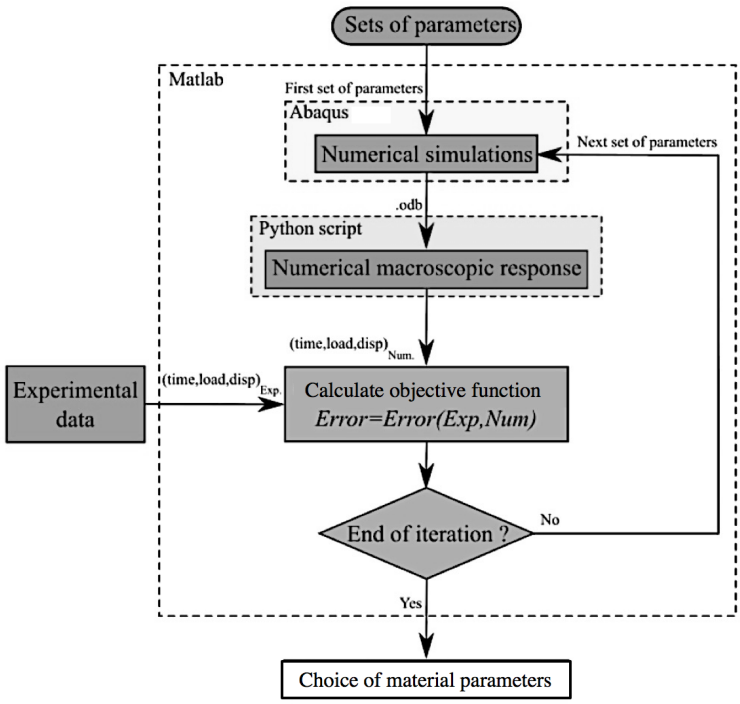

Figure 3.8: Inverse identification in an iterative procedure [23]

For a given set of parameters, a *Matlab iterative* function is used to launch the numerical simulations. The response of the FE model is recovered using a *Python* script and compared with the experimental results. By defining an objective function, it is possible to calculate an error between the experimental and numerical curves as in *Eq.*:

$$Error(k) = \sum_{i=1}^{n} \left(D_{num}(i) - D_{exp}(i)\right)^2 \tag{3.1}$$

where k is representing the current iteration, n the number of experimental and numerical points, and D_{num} and D_{exp} the numerical and experimental displacements.

The iterative function is ending when all the sets of parameters have been tested. At the end of the loop, the set of parameters that gives the minimal error is recovered and the values are stored.

If the value of the desired parameters is hard to estimate, an *optimisation* technique can be used to find the best set of model parameters. In this case the same approach is applied with the difference that the values of the parameters are not given by the user, they are generated by a matlab function "*fminsearch*" which minimises the objective function [152] at the end of each iteration (*Fig.*3.9).

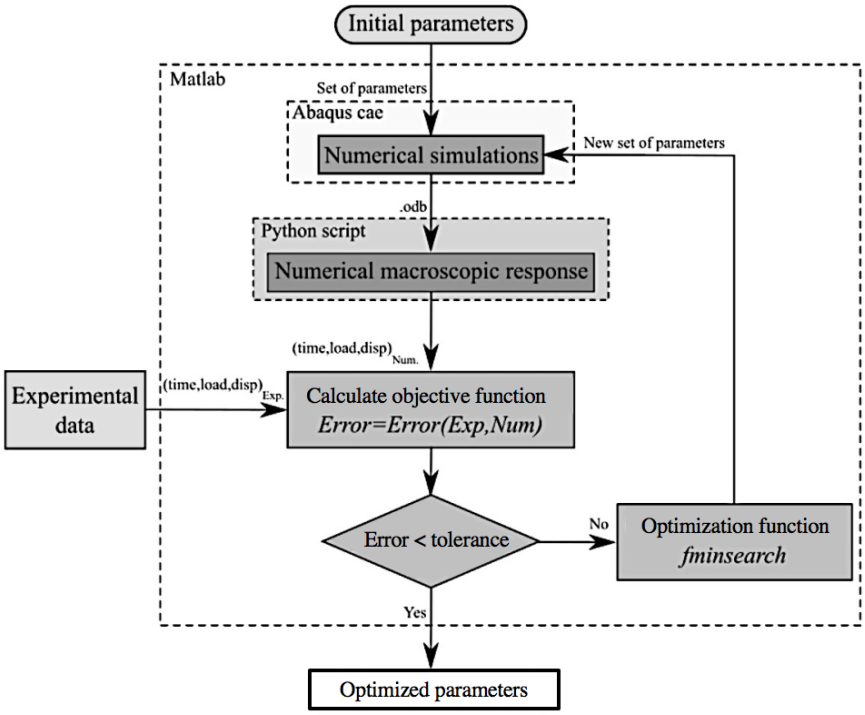

Figure 3.9: Inverse identification in an optimisation procedure [23]

3.2 Constitutive law

The constitutive law used to describe the mechanical behaviour of the adhesive in the bonded joint is based on a viscoelastic-viscoplastic model. As will be shown in the next subsections, the viscoelastic part of the model was not sufficient to describe accurately the mechanical behaviour of the adhesive.

The development of the behaviour law will be presented step by step, for different groups of parameters. First, a method for the identification of the elastic parameters is presented. The viscoelastic part is then described, and all its parameters. Finally, the viscoplastic part is added to the model in order to obtain the constitutive law.

It is important to note that in each case, the total strain $\underline{\varepsilon}$ is written as the sum of the different strains: elastic strain $\underline{\varepsilon_{el}}$, viscoelastic strain $\underline{\varepsilon_{ve}}$ and viscoplastic strain $\underline{\varepsilon_{vp}}$ (*Eq.*3.2). The stress tensor $\underline{\sigma}$ will then be written as in *Eq.*3.3, where $\underline{\underline{C}}$ represents the elastic stiffness (*Eq.*3.4).

$$\underline{\varepsilon} = \underline{\varepsilon_{el}} + \underline{\varepsilon_{ve}} + \underline{\varepsilon_{vp}} \tag{3.2}$$

$$\underline{\sigma} = \underline{\underline{C}} : \left(\underline{\varepsilon} - \underline{\varepsilon_{ve}} - \underline{\varepsilon_{vp}}\right) \tag{3.3}$$

$$\underline{\underline{C}} = \frac{E}{(1+\nu)(1-2\nu)} \begin{bmatrix} 1-\nu & \nu & \nu & 0 & 0 & 0 \\ \nu & 1-\nu & \nu & 0 & 0 & 0 \\ \nu & \nu & 1-\nu & 0 & 0 & 0 \\ 0 & 0 & 0 & \frac{1-2\nu}{2} & 0 & 0 \\ 0 & 0 & 0 & 0 & \frac{1-2\nu}{2} & 0 \\ 0 & 0 & 0 & 0 & 0 & \frac{1-2\nu}{2} \end{bmatrix} \tag{3.4}$$

3.2.1 Identification of elastic parameters

The elastic parameters of the model (*Young's modulus* E and *Poisson's ratio* ν) are the first parameters that have to be identified. It is important to note that in this step the viscoelasticity and the viscoplasticity have no influence on the mechanical response of the model. The experimental curves (load vs displacement), obtained in monotonic tensile and shear Arcan tests (*Fig.*3.10), are used to determine an experimental elastic stiffness (*Eq.*3.5,3.6) using the measured load (F), the normal (ND) and tangential (TD) displacements.

$$K_N = \frac{F}{ND} \tag{3.5}$$

$$K_T = \frac{F}{TD} \tag{3.6}$$

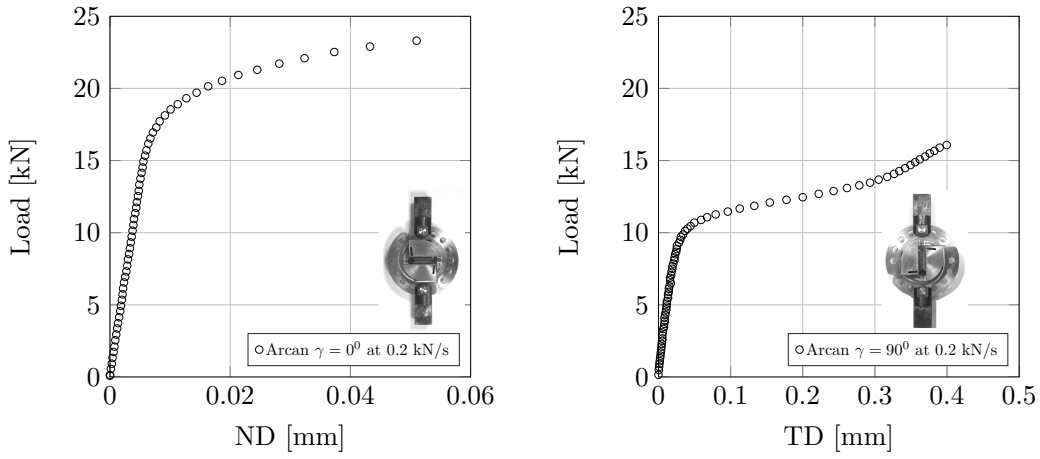

(a) Tensile behaviour

(b) Shear behaviour

Figure 3.10: Monotonic tests

In parallel, using the complete 3D FE model (*Fig.*3.4a) and the inverse identification method in an iterative procedure, a series of simulations is made using different couples of (E, ν). The range of *Young's Modulus* is chosen between $500MPa$ and $6000MPa$ (with a step of $100MPa$), and the Poisson's ratio between 0.2 and 0.45 (with a step of 0.01). These are classical values that can be found in the literature for this kind of adhesive. The numerical stiffness obtained for each couple in both cases (tension and shear) is compared with the experimental ones.

At the end of each simulation the objective function is computed and an error is calculated

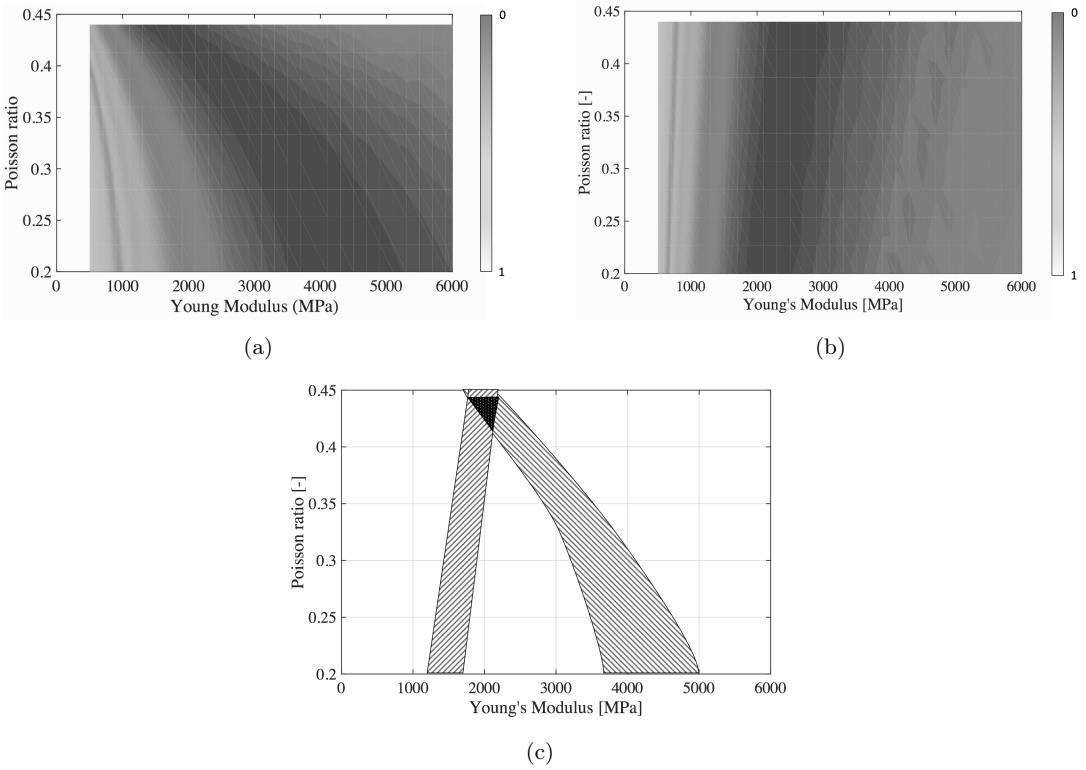

Figure 3.11: Calculated errors obtained for different couples of (E, ν) under (a) tensile and (b) shear loading. (c) Intersection of the best couples (E, ν)

(*Eq.*3.1) between the numerical and the experimental results. This error is represented in *Fig.*3.11a for the tensile loading and in *Fig.*3.11b for the shear loading case. The shadowed zone in those figures represents the couples (E, ν) for which the objective function was minimal. In *Fig.*3.11c the couples with the lowest values of the objective function are superposed in order to find the best couples that fit in both cases (tensile and shear loading).

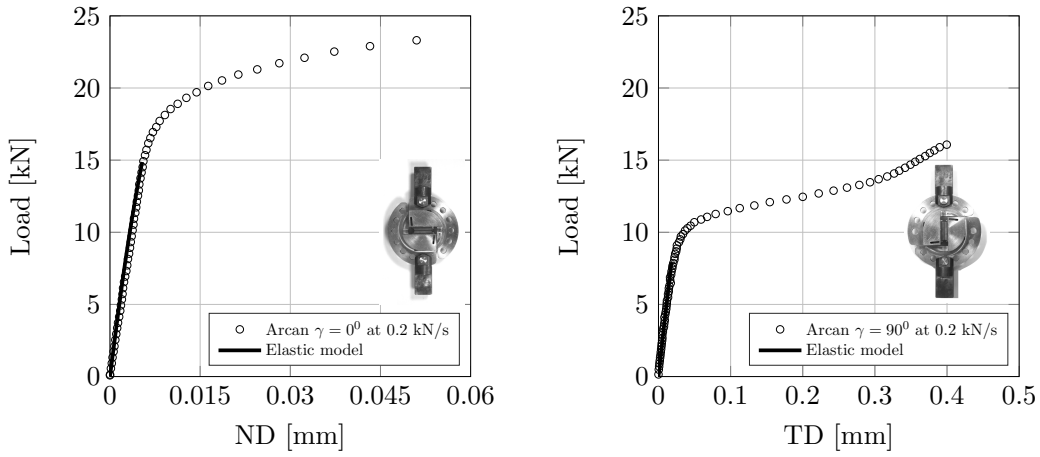

Figure 3.12: Validation of the elastic parameters

Once the values of the elastic parameters have been found, for both tensile and shear monotonic test, a simulation is made in order to validate these parameters. As can be observed in *Fig.*3.12 the numerical stiffness fits the experimental one accurately. In *Tab.*3.1 can be found the obtained values for the elastic parameters.

Table 3.1: Elastic parameters

Parameters	E	ν
Unit	MPa	[-]
Value	1850 ± 50	0.41 ± 0.01

3.2.2 The modified viscoelastic spectral model

In a first step, the viscoelastic spectral model has been chosen to model the viscous behaviour of the adhesive. In this model, the total strain $\underline{\varepsilon}$ is equal to the sum of the elastic strain $\underline{\varepsilon_{el}}$ and the viscous strain $\underline{\varepsilon_{ve}}$ (*Eq.*3.7). The mechanical behaviour of the adhesive written in the referential of the bonded joint is the following the *Eq.*3.8:

$$\underline{\varepsilon} = \underline{\varepsilon_{el}} + \underline{\varepsilon_{ve}} \tag{3.7}$$

$$\underline{\sigma} = \underline{\underline{C}} : \left(\underline{\varepsilon} - \underline{\varepsilon_{ve}}\right) \tag{3.8}$$

where $\underline{\sigma}$ is the stress tensor, $\underline{\underline{C}}$ is the elastic stiffness.

The spectral viscoelastic model describes the viscoelastic strain $\underline{\varepsilon_{ve}}$ as the sum of the strains of a fixed number n_t of viscous mechanisms $\underline{\xi_i}$. The presented results are obtained with a number of $n_t = 20$ mechanisms [92]. Each of these mechanisms is defined by a relaxation time τ_i, a weight μ_i in the total viscous strain and the viscoelastic compliance $\underline{\underline{S_R}}$ (*Eq.*3.9).

$$\underline{\dot{\varepsilon}_{ve}} = \sum_{i=1}^{n_t} \underline{\dot{\xi}_i} \quad with \quad \underline{\dot{\xi}_i} = \frac{1}{\tau_i}\left(\mu_i \underline{\underline{S}}_R : \underline{\sigma} - \underline{\xi}_i\right) \tag{3.9}$$

The relaxation times are defined as in *Eq.*3.10 where $n_i \in [n_1, n_2]$ is a value situated between two limits that depend on the material. In the case of an epoxy material, $n_1 = -20$ and $n_2 = 30$ as was shown by *Maire et al.* [92]. The mechanisms with high relaxation times have low weight in this case and they are not activated. By decreasing the upper limit and keeping the same number of viscous mechanism, it would be possible to increase the accuracy of the model but it would not be possible to predict the creep behaviour for very long periods of time.

$$\tau_i = exp\left(n_i\right) \tag{3.10}$$

$$\bar{\mu}_i = \frac{1}{n_0\sqrt{\pi}} exp\left(-\left(\frac{n_i - n_c}{n_0}\right)^2\right) \quad with \quad \mu_i = \frac{\bar{\mu}_i}{\sum_{i=1}^{n_t} \bar{\mu}_i} \tag{3.11}$$

The weight of each elementary viscous strain depends on two parameters, n_0 and n_c which are introduced in *Eq.*3.11. They have to be identified using the creep tests.

These two quantities, the relaxation time and the weight, define the so-called spectrum of the model. The form of this spectrum is defined by two parameters n_0 and n_c. Each of the points in *Fig.*3.13 represents the relaxation time and the weight of a viscous elementary mechanism.

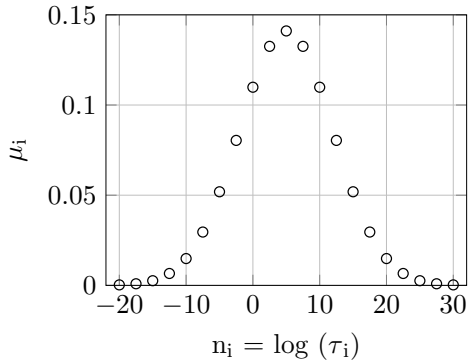

Figure 3.13: Spectrum definition

The term $\underline{\underline{S_R}}$ in *Eq.*3.9 represents the viscoelastic compliance. This is a fourth order tensor that has been modified from the previous version of the viscoelastic spectral model[79]. As presented in the second chapter, the adhesive mechanical behaviour depends on the loading conditions. In shear loading, the viscous displacements are more important than in tensile loading. Moreover, a non-linear evolution of the viscous behaviour can be seen in the two cases. These observations lead to the next equation representing the viscoelastic compliance (*Eq.*3.12).

$$\underline{\underline{S}}_R = \frac{1}{(1-d_H)\,a_H}\underline{\underline{H}}_H + \frac{1}{(1-d_D)\,a_D}\underline{\underline{H}}_D \tag{3.12}$$

The $\underline{\underline{S_R}}$ tensor is divided into two parts by the tensors $\underline{\underline{H_H}}$ and $\underline{\underline{H_D}}$ which allow the hydrostatic and the deviatoric mechanical behaviour to be defined (Eq.3.13). The $\underline{I}$ and $\underline{\underline{I}}$ are respectively $2nd$ and $4th$ degree tensors. This is the originality of the present model: the viscoelastic response is decomposed in two separate parts, hydrostatic and deviatoric, allowing different viscoelastic behaviour to be attributed to shear and tensile loading components.

$$\underline{\underline{H}}_H = \frac{1}{3}\underline{I}\otimes\underline{I} \qquad\qquad \underline{\underline{H}}_D = \underline{\underline{I}} - \underline{\underline{H}}_H \tag{3.13}$$

‘

Also, the parameters a_H and a_D (*Eq.*3.12) define the viscosity in the hydrostatic and deviatoric directions. These two parameters need to be identified. The non-linearity is introduced using the parameters d_H and d_D (*Eq.*3.14) which depend, each of them, on three parameters that need to be identified. The parameters y_D^0 and y_H^0 are the threshold of the non-linear behaviour of the viscosity and y_D^c and y_H^c define the kinetics.

$$d_H = {d_H}^{max}\left(1 - exp\left(\frac{-\langle y_H - y_H^0\rangle}{y_H^C}\right)\right) \quad d_D = {d_D}^{max}\left(1 - exp\left(\frac{-\langle y_D - y_D^0\rangle}{y_D^C}\right)\right) \tag{3.14}$$

The internal forces of the model are y_H and y_D, *Eq.*3.15. These depend on the hydrostatic and deviatoric stress tensors.

$$y_H = \frac{1}{2a_H}\left(\underline{\sigma} : \underline{\underline{H_H}} : \underline{\sigma}\right) \quad y_D = \frac{1}{2a_D}\left(\underline{\sigma} : \underline{\underline{H_D}} : \underline{\sigma}\right) \tag{3.15}$$

This modified viscoelastic spectral model has a total of 10 parameters that need to be identified (*Tab.*3.2).

3.2.3 Identification of the viscoelastic parameters

The viscoelastic parameters of the model only need two experimental multi-level creep tests in order to identify them (in two loading directions: tensile and shear). The hydrostatic parameters are identified using the tensile multi-level creep test shown in *Fig.*3.14a. In the case of the deviatoric parameters, the results obtained in *Fig.*3.14b will be used for identification. Because the method of identification is the same in both cases, in the next section, it will be applied only for the deviatoric parameters (shear loading).

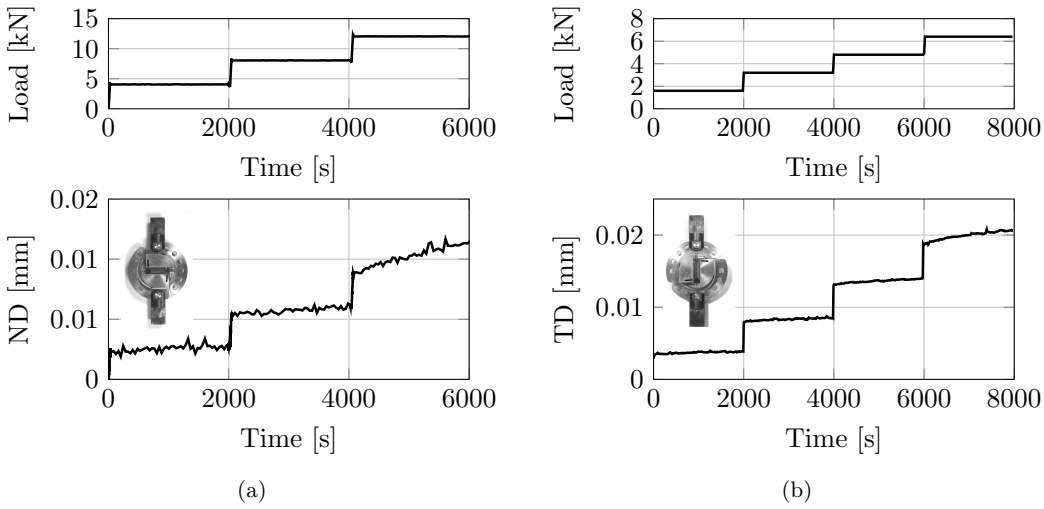

Figure 3.14: Multi-level creep tests: tension (a) and shear (b)

3.2.3.1 Identification of the spectrum parameters: n_0, n_c

The two parameters that define the spectrum are identified using the viscous displacements measured for each creep level. For this, the isochronism principle of the spectral viscoelastic model is used. In order to apply this principle, each creep level should have the same duration. The viscous displacements are normalized using *Eq.*3.16, where j represents the number of the creep level, $j \in \{1, 2, 3, 4\}$ because of the four shear creep levels (*Fig.*3.14b). In the same equation, t^j_{begin} is the time at the beginning of the j^{th} level and t^j_{end} is the time at the end of the same level.

$$TD^j_{viscous_{normalized}} = \frac{DT^j_{viscous}(t) - DT^j_{viscous}(t^j_{begin})}{DT^j_{viscous}(t^j_{end}) - DT^j_{viscous}(t^j_{begin})} \tag{3.16}$$

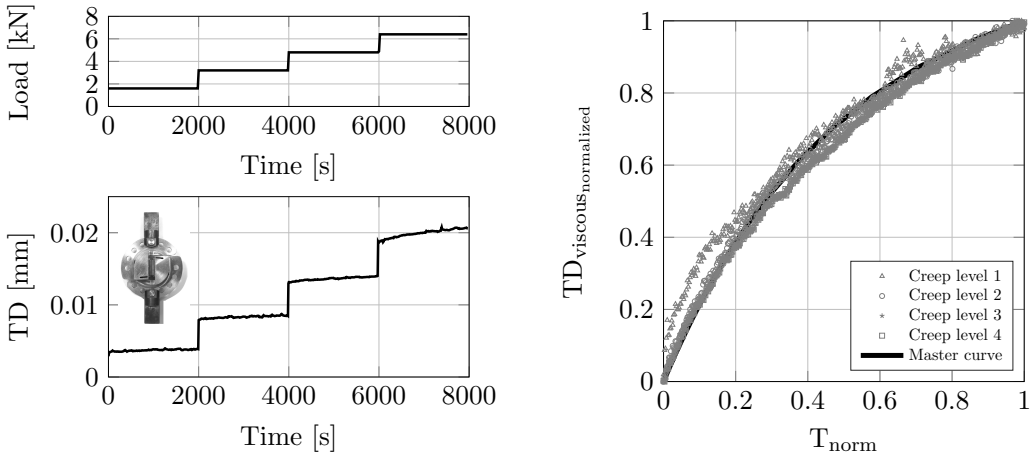

(a) (b)

Figure 3.15: (a) Multi-level creep test used to identify the deviatoric parameters of the viscoelastic model, (b) Isochronism principle

In *Fig.*3.15b, the normalized viscous displacement can be observed for the first four creep levels in *Fig.*3.15a. The normalized time for each creep level has been calculated using *Eq.*3.17.

$$T^j_{norm} = \frac{t - t^j_{begin}}{t^j_{end} - t^j_{begin}} \tag{3.17}$$

It can be observed in *Fig.*3.15b that the isochronism principle is respected for the four creep levels. These curves can be superposed to a master curve that will be defined by the two parameters that need to be identified: n_0 and n_c.

Using the finite element model presented in Section 3.1, it is possible to apply an inverse identification method to fit the obtained master curve. For this, a numerical simulation of the first creep level is made. The elastic parameters applied to the model are those identified using the monotonic tests.

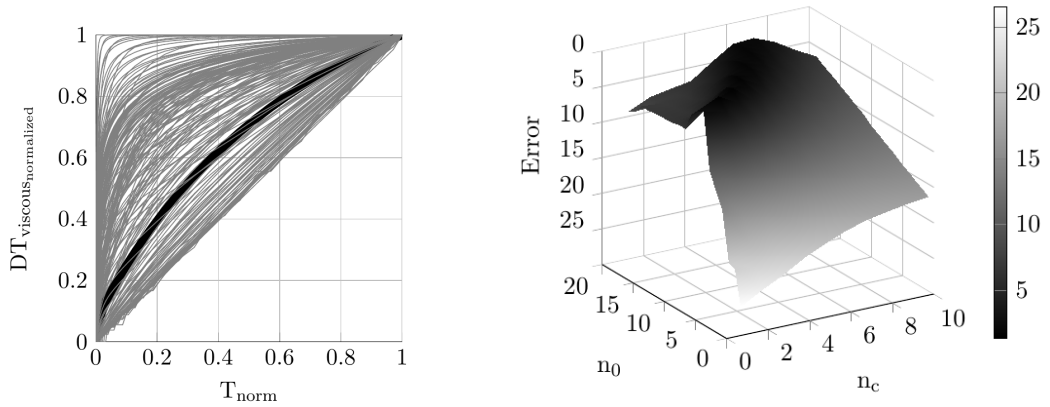

(a) (b)

Figure 3.16: (a) Normalized viscous displacement for different couples (n_0, n_c) (b) Error calculated for different couples (n_0, n_c)

Couples of parameters (n_0,n_c) have been generated using *Matlab* software: $n_c \in [1:10]$ and $n_0 \in [1:20]$ - a total number of 200 combinations. For each couple, a numerical simulation is made. After normalizing the time and the viscous displacements obtained, the results are compared with the master curve created from the experimental curves (*Fig.*3.16a). This process is made automatically using a Python routine.

For each couple an error is calculated using *Eq.*3.18. The couple with the closest error to zero is then used. The results can be represented in an error map, as in *Fig.*3.16b. The best couples are those that minimize this error and they have a low influence on the final results.

$$Error = \sum \left(DT^{FE}_{viscous_{normalized}} - DT^{EXP}_{viscous_{normalized}} \right)^2 \tag{3.18}$$

3.2.3.2 Identification of the linear viscoelastic parameters: a_H, a_D

Once the spectrum is defined, it is now possible to identify the parameters that correspond to the linear viscosity: a_H, a_D. These parameters are identified on the first creep level of the experimental tests performed in tensile (a_H) and in shear (a_D), using the inverse identification method and the numerical model. It is important to note that in the case of this procedure, the threshold of the non-linear viscosity is not defined. The identified value of this parameter is used to simulate all the creep levels. The results are shown in *Fig.*3.17a.

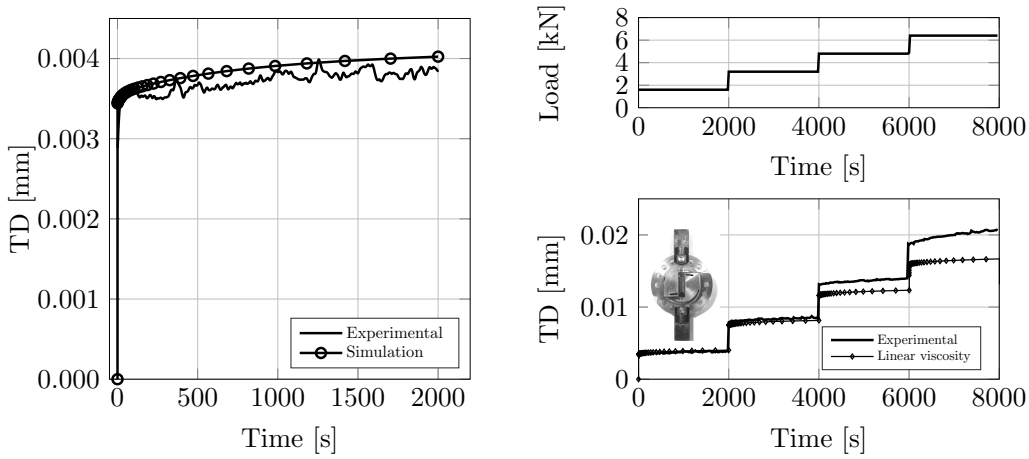

Figure 3.17: (a) First level of the shear creep test (b) Identification of the viscoelastic model

The identification has been made for the two cases of loading (tensile and shear) using the experimental results obtained in the multi-level creep tests.

3.2.3.3 Identification of the non-linear viscoelastic parameters: d_D^{max}, y_D^0, y_D^c, y_H^0, y_H^c, d_H^{max}

Examining *Fig.*3.17b, it can be noted that a linear viscoelastic model is not appropriate to describe correctly the behaviour of the adhesive in the multi-level creep tests. This is why the variables d_H and d_D were introduced in the definition of the compliance tensor.

The threshold between the linear and non-linear viscosity is determined as explained in *Section*2.4.5. Thus, analysing the *Fig.*3.18a it can be observed that at the end of the second creep level the viscous displacement becomes $DT_{viscous}$ non-linear. Using the FE model, it is possible to find the value of the internal force y_D at the end of that creep level. This value will correspond to the threshold y_D^0. The same approach is applied to find this variable in the case of a tensile creep test.

The last parameters of the model y_D^c and $d_D^{max}$are identified using the last creep levels. These influence the kinetics of the displacements for the last creep levels. It can be seen in *Fig.*3.18b that using the non-linear viscosity it is possible to have a good fit between the experimental curve and the numerical results.

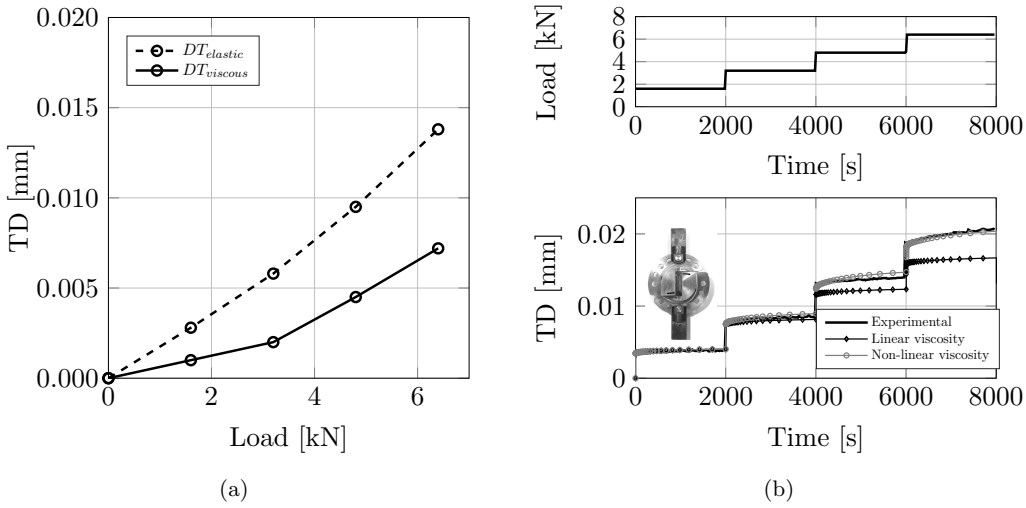

Figure 3.18: (a) First level of the shear creep test (b) Identification of the viscoelastic model

Once the model is validated using the creep tests, it is now possible to evaluate if the model is able to predict the monotonic behaviour.

*Fig.*3.19 represents the response of the identified viscoelastic model when simulating a monotonic shear or tensile test. These results are showing that even though the model is describing accurately the creep behaviour, it is not appropriate to predict the mechanical behaviour under monotonic loading. This justifies the need for the viscoplastic part in the constitutive law.

The identified parameters are shown in *Tab*3.2.

Table 3.2: Identified viscoelastic parameters

	Spectrum		Hydrostatic				Deviatoric			
Parameters	n_0	n_c	a_H	d_H^{max}	y_H^0	y_H^c	a_D	d_D^{max}	y_d^0	y_d^c
Unit	-	-	MPa^{-1}	-	-	-	MPa^{-1}	-	-	-
Value	5	10	1800	0.9	0.8	0.2	1500	0.6	0.6	0.015

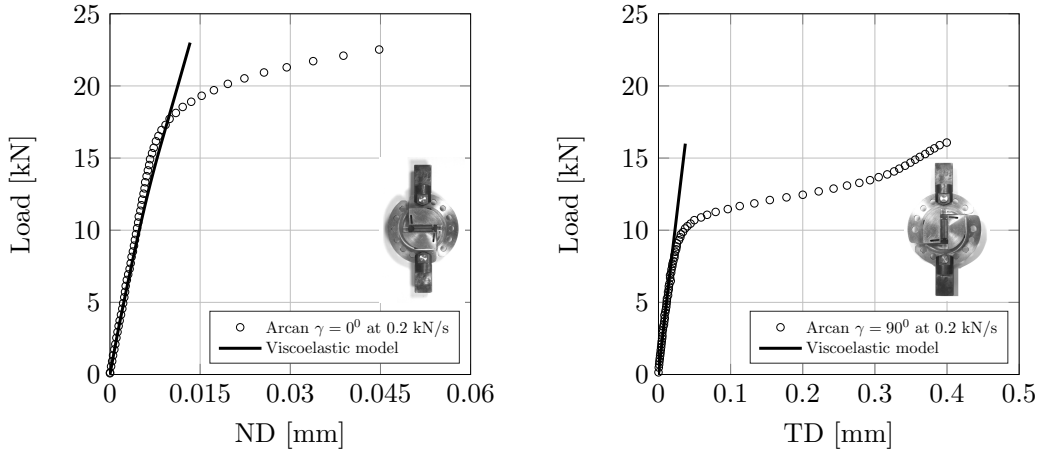

Figure 3.19: Viscoelastic model prediction in monotonic (a) tensile and (b) shear tests

3.2.4 Viscoelastic-viscoplastic model

It has been shown in *Section* 3.2.3 that the viscoelastic model is not sufficient to describe correctly the mechanical behaviour of this adhesive. In order to be able to predict the monotonic behaviour, a viscoplastic part has been added to the model. In this case, the total strain $\underline{\varepsilon}$ will be composed of the elastic strain $\underline{\varepsilon_{el}}$, the viscoelastic strain $\underline{\varepsilon_{ve}}$ and the viscoplastic strain $\underline{\varepsilon_{vp}}$, as shown in *Eq.*3.2.

The viscoplastic part of the model is inspired by the model proposed by *Mahnken-Schlimmer et al* [80]. In this case, the yield surface is described using a simplified relation (*Eq.*3.22), between *von Mises* stress and *hydrostatic pressure*. Other forms of this model could be found in literature [96][103]. This is a simple model that has few parameters to be identified as it will be shown in the next section.

The stress tensor $\underline{\sigma}$ is decomposed into a hydrostatic part $\sigma_H \underline{I}$ (*Eq.*3.19) and a deviatoric part $\underline{\sigma}_D$ (*Eq.*3.20). The *von Mises* stress σ_{VM} is then calculated using the *Eq.*3.21.

$$\sigma_H = \frac{1}{3} trace(\underline{\sigma}) \tag{3.19}$$

$$\underline{\sigma}_D = \underline{\sigma} - \sigma_H \underline{I} \tag{3.20}$$

$$\sigma_{VM} = \sqrt{\frac{3}{2} \underline{\sigma}_D : \underline{\sigma}_D} \tag{3.21}$$

The yield surface of the viscoplastic behaviour is determined using the *Eq.*3.22, where σ_{VM} represents the *von Mises* stress tensor, σ_H is the hydrostatic pressure and R is the hardening parameter. a_1 is a parameter that defines the shape of the yield function (the slope) in the *von Mises - hydrostatic pressure plane*.

$$f(\sigma_H, \sigma_{VM}) = \sigma_{VM} + a_1 {\sigma_H}^2 - R \tag{3.22}$$

The *Eq.*3.23 represents the evolution of the hardening parameter R. The parameters H, Q, b influence the monotonic non-linear behaviour of the adhesive and are identified from a pure shear test using the inverse identification method. It is important to note that when those parameters are identified, the viscoelastic part of the model is activated. R_0 is the elastic threshold.

$$R = R_0 + He_{vcum} + Q\left(1 - exp\left(-be_{vcum}\right)\right) \tag{3.23}$$

The hardening is driven by the internal strain variable e_{vcum} defined in *Eq.*3.24. The parameters K and n are identified after all the other parameters of the model are fixed. Because they depend on the strain rate, their identification needs a shear test at a different strain rate.

$$\dot{e}_{vcum} = \frac{3}{2}\left(\frac{\langle f \rangle}{K}\right)^n \tag{3.24}$$

The viscoplastic strain rate can finally be written as in *Eq.*3.25, where g represents the flow rule (*Eq.*3.26). In this particular case, a non-associative model has been developed, which means that the flow rule is described using a function that is different from yield surface [80].

$$\dot{\varepsilon}_{vp} = \dot{e}_{vcum}\frac{\partial g}{\partial \sigma} \tag{3.25}$$

$$g(\sigma_H, \sigma_{VM}) = \sigma_{VM} + a_1^* {\sigma_H}^2 - R \tag{3.26}$$

3.2.5 Identification of viscoplastic parameters

3.2.5.1 Identification of the elastic threshold: R_0

The elastic threshold of the model R_0, is identified using the monotonic shear test ($\gamma = 90^o$). It is important to note that the viscoelastic part is enabled during this operation. By comparing the model prediction and the experimental results (*Fig.*3.20), the load level corresponding to the point where the two curves diverge is chosen as the point where the hardening begins.

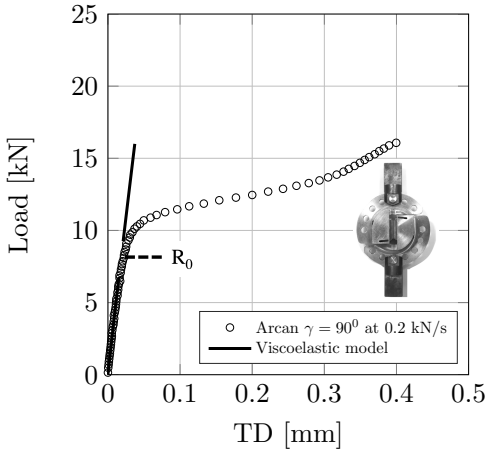

Figure 3.20: Identification of the elastic threshold R_0

Using the FE model it is possible to access the distribution of the von Mises stress and hydrostatic pressure in the middle plane of the adhesive layer for the load level corresponding to R_0 (*Fig.*3.21).

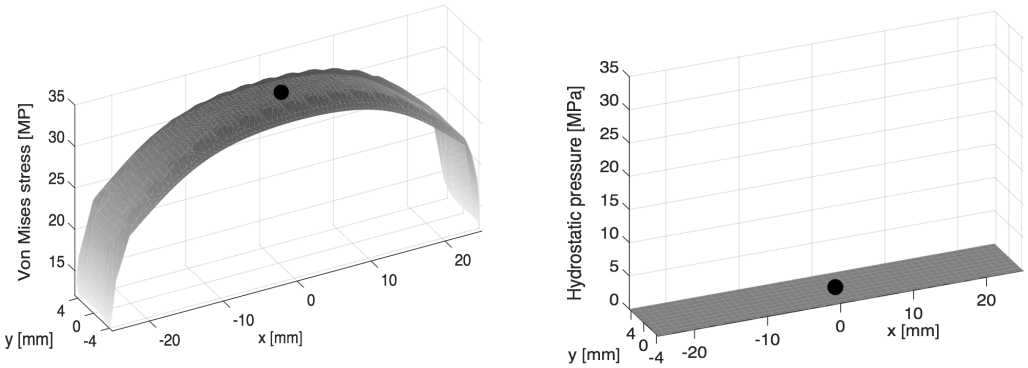

(a) (b)

Figure 3.21: Distribution of the (a) von Mises stress and (b) hydrostatic pressure in the middle plane of the adhesive layer corresponding to the elastic threshold in a monotonic shear test

It is important to notice that the referential system was placed in the center of the model, the *x axis* represents the length of the specimen ($50mm$) and *y axis* the width (9.5mm). Moreover, no hydrostatic pressure is applied in the adhesive layer during the monotonic shear test (*Fig.*3.21b).

The value of the elastic threshold is considered as the *von Mises* stress at the point with the coordinates $x = 0$ and $y = 0$. In this case R_0 was determined as equal to $32MPa$.

3.2.5.2 Identification of the yield function: a_1

The yield function *Eq.*3.22 is defined in the *von Mises stress* σ_{VM} and *hydrostatic pressure* σ_H (*Eq.*3.21) plane, by the equation of a parabola which is always perpendicular to the abscissa axis.

Because of its definition, only two points are needed to define this function. The first point is determined by the couple (σ_H, σ_{VM}) calculated previously using the monotonic shear test ($\sigma_H = 0MPa$ and $\sigma_{VM} = 32MPa$).

The second point that defines the yield function is determined using a tensile monotonic test at the same loading rate (0.2 kN/s). As in the previous case (monotonic shear test), using the FE model and the viscoelastic part activated the results of the numerical prediction are compared with the curve obtained in the monotonic tensile test (*Fig.*3.22a). The point where the two curves diverge is defined as the elastic threshold in tension. For this load level, the von Mises stress and the hydrostatic pressure in the middle of the adhesive layer are plotted (*Fig.*3.23). This time, for the point situated in the middle of the adhesive layer ($x = 0$ and $y = 0$), the hydrostatic pressure is non-zero as was expected. Hence, the coordinates of the second point (σ_H, σ_{VM}) were determined as: $\sigma_H = 13.8MPa$ and $\sigma_{VM} = 30MPa$)

Thus, the a_1 coefficient is determined and the equation of the yield function is written as

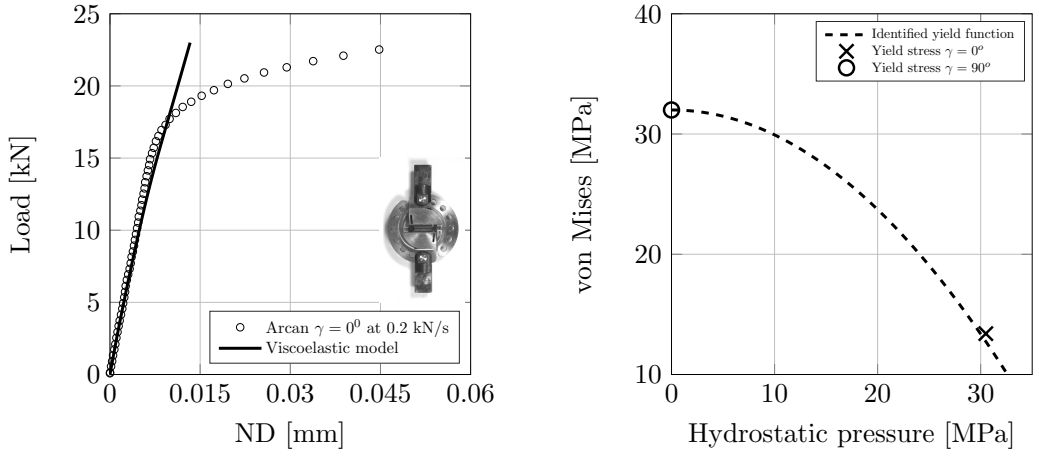

(a) (b)

Figure 3.22: (a) Identification of the elastic limit in tension and (b) definition of the yield function

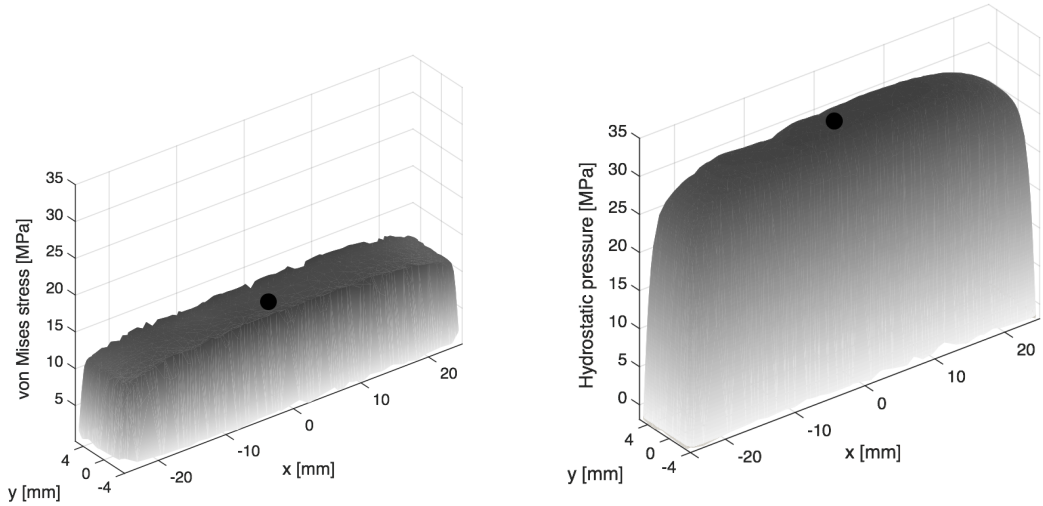

(a) (b)

Figure 3.23: Distribution of the (a) von Mises stress and (b) hydrostatic pressure in the middle plane of the adhesive layer corresponding to the elastic threshold in a monotonic tensile test

(*Eq.*3.27):

$$\sigma_{VM} = 32 - 0.0023 \times {\sigma_H}^2 \quad \text{[MPa]} \tag{3.27}$$

3.2.5.3 Identification of the hardening parameters: H, Q, b

The hardening parameters are also identified using the inverse identification method and the FE model. The $0.2kN/s$ monotonic shear test (*Fig.*3.24a) is used for the parameters identification. Since the hydrostatic pressure is negligible within the bonded layer in a shear configuration (*Fig.*3.21) and considering the definition of the flow rule that is symmetric with

respect to the Mises axis, the identification of the hardening function can be done in shear without knowing the value of a_1^*. An optimisation between the experimental curve and the numerical response of the finite element model has been performed in order to minimize the error between the two behaviours.

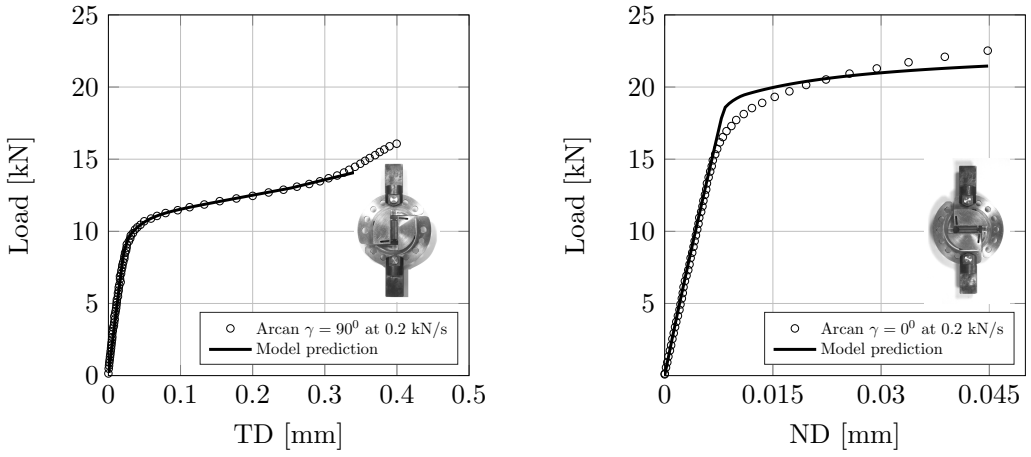

Figure 3.24: Identification of the (a) hardening parameters and (b) the flow function

3.2.5.4 Identification of the flow function: a_1^*

Once the hardening parameters have been identified, the flow function (*Eq.*3.26) is also determined by using the inverse identification method and the non-linear part of the monotonic tensile test. An optimisation has been performed in order to find the value of a_1^* that fits the most accurately the experimental results. As can be observed in *Fig.*3.24b, the compromise made by keeping the flow function simple (dependent to only one parameter) is influencing the hardening prediction in tension. For more accurate results, it would be interesting to define the flow function using a second-degree equation [80] but this would lead to a more expensive cost in terms of identification time.

3.2.5.5 Identification of the viscous parameters: K, n

The last parameters of the viscoelastic-viscoplastic model, that have to be identified are the couple (K, n). Because they depend on the strain rate, a second monotonic shear test ($2kN/s$) is used for the identification method. (*Fig.*3.24a). At this moment of the identification procedure, all the other parameters are fixed.

It is important to note that in order to identify the viscoplastic behaviour, one tensile and two monotonic shear tests have been used. The identified parameters can be found in *Tab*3.3.

3.3 Validation of the constitutive law

The model validation process is based on the comparison between experimental results and numerical predictions. In order to do this, experimental data that have not been used in the

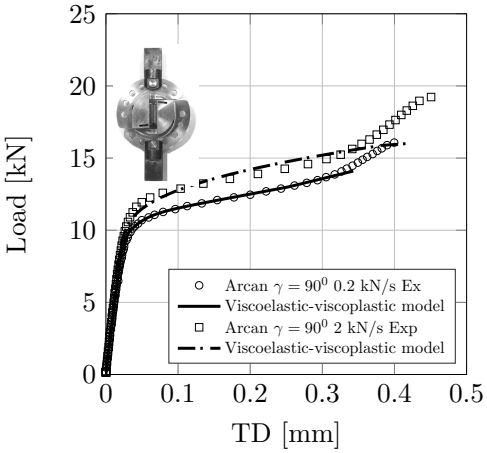

Figure 3.25: Identification of the viscous parameters: K, n

Table 3.3: Identified viscoplastic parameters

Parameters	R_0	a_1	H	Q	b	a_1^*	n	K
Unit	MPa	MPa^{-1}	MPa	MPa	-	MPa^{-1}	-	-
Value	32	0.0023	24.28	5.6	37.8	0.00262	3	10

identification procedure are analysed: tensile and shear recovery tests and a monotonic tensile test at a different loading rate ($2kN/s$). In addition, a combined tensile-shear test ($\gamma = 45^o$) is also used to validate the yield function and the prediction of the non-linear behaviour. The ability of the model to predict the loading rate effect is evaluated in a tensile test performed with a different strain rate. Finally, the identified model is used to predict the tensile mechanical behaviour of a bulk specimen and the results will be compared with the experimental curve.

3.3.1 Validation of the viscoelastic part

For both tensile and shear creep behaviour, multi-level recovery tests were used to validate the model. As can be observed in *Fig.*3.26, in the two cases, even though the model has been identified on the creep levels it can predict the behaviour of the recovery levels. An interesting point that should be mentioned is that looking at the last recovery level in shear (*Fig.*3.26a) the viscoelastic strain is not totally recovered when completely unloading the bonded joint. The prediction of this recovery level is still very accurate. Regarding the tensile recovery levels (*Fig.*3.26b), the model is slightly less accurate but this can be explained by the very small displacements that are measured.

3.3.2 Validation of the complete model

The prediction of the identified viscoelastic-viscoplastic model was also compared against the experimental results observed in a combined tesile/shear monotonic test ($\gamma = 45^o$) in *Fig.*3.27. It is important to notice that this test was not used in the identification procedure. For better understanding of the results, the applied load has been plotted as a function of tangential displacement (*Fig.*3.27a) and normal displacement (*Fig.*3.27b).

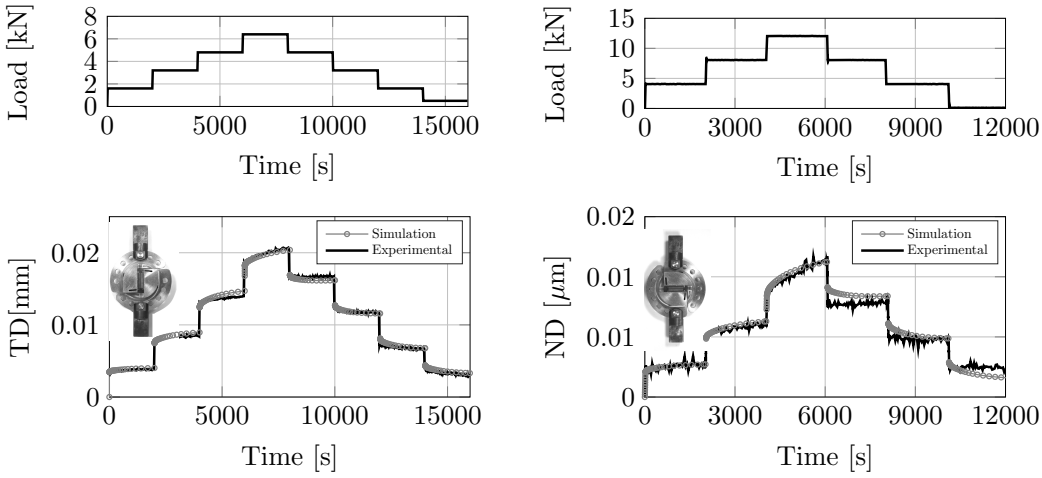

(a) (b)

Figure 3.26: Model validation in multi-level creep/recovery (a) shear and (b) tensile tests

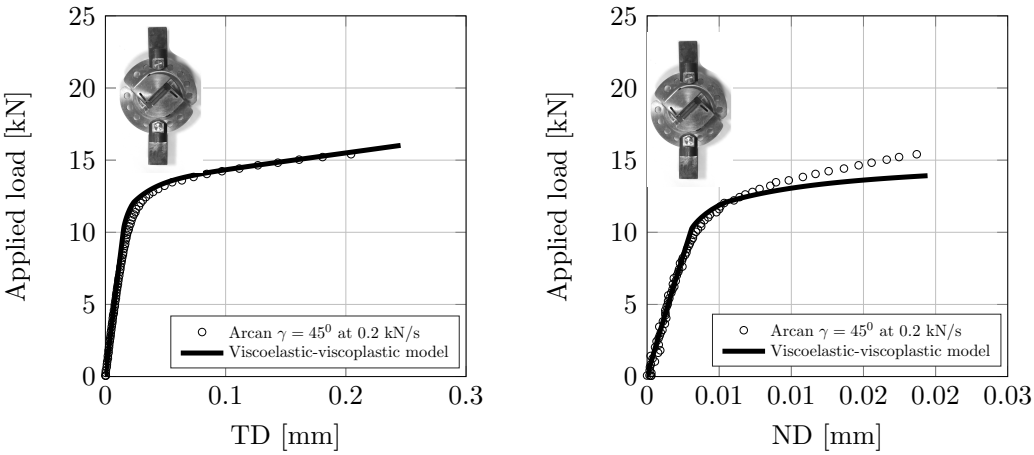

(a) Tangential displacement (b) Normal displacement

Figure 3.27: Viscoelastic-viscoplastic model validation in combined tensile/shear test

As might be seen, the tangential component of the measured displacement is accurately predicted by the model (*Fig.*3.27a). This behaviour is linked to the deviatoric part of the model. Hence, it is possible to conclude that the parameters describing the deviatoric behaviour are well identified. The normal component of the displacement plotted against the applied load in *Fig.*3.27b is less accurately predicted, especially at the end of the curve. This can be explained by the choice that has been made in the definition of the flow function (*Eq.*3.26). Moreover, since the optimal value of the a_1^* parameter was not able to accurately predict the monotonic tensile behaviour (*Fig.*3.24b), this behaviour was to be expected.

3.3.3 Validation of the yield function

Another interesting aspect is the prediction of the yield point under combined loading. For the monotonic tensile/shear test, the elastic threshold was determined as presented in the identification section. For this load level, the *von Mises* stress and *hydrostatic pressure* are presented in *Fig.*3.28. It may be useful to remember that the same FE model was used in this simulation and, as for the previous calculation, the reference system was located in the middle of the adhesive layer.

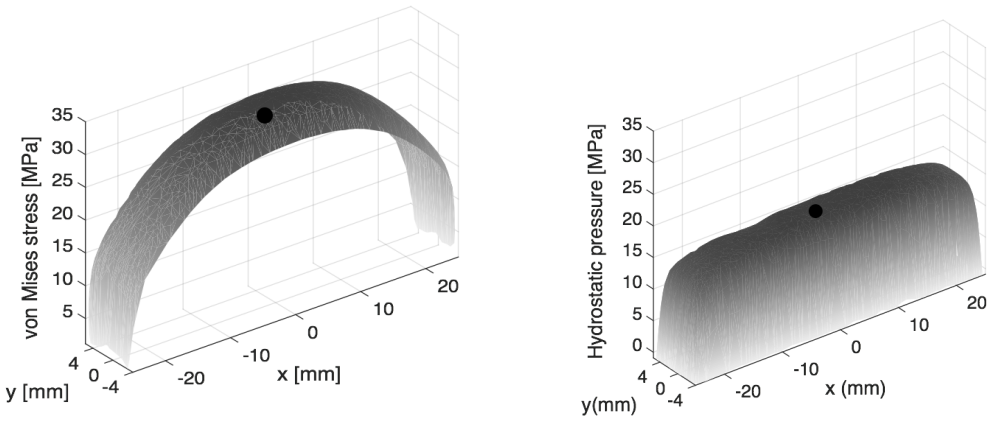

(a) (b)

Figure 3.28: Distribution of the (a) von Mises stress and (b) hydrostatic pressure in the middle plane of the adhesive layer corresponding to the elastic threshold in a combined tensile/shear monotonic test

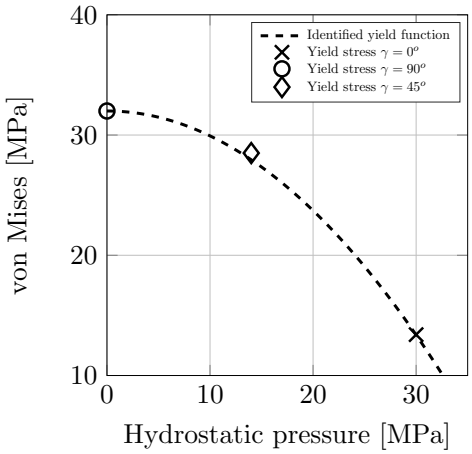

Figure 3.29: Validation of the yield function

The point located in the middle of the adhesive layer ($x = 0$ and $y = 0$) is defined by a *von Mises* stress equal to $\sigma_{VM} = 28.5MPa$ and a hydrostatic pressure equal to $\sigma_H = 14MPa$. By plotting this point in the *von Mises* vs *hydrostatic pressure* plane, it can be observed that it is placed perfectly on the predicted yield surface.

3.3.4 Validation of the loading rate effect

The prediction of the model was also compared with the experimental tensile tests at $2kN/s$ (*Fig.*3.30). The elastic modulus does not depend on the loading rate for this type of adhesive, instead, the failure load is increasing. It can be observed that by multiplying the loading rate by ten, the failure load is increased by about ten percent. This change in the mechanical behaviour of the adhesive can be predicted by the model.

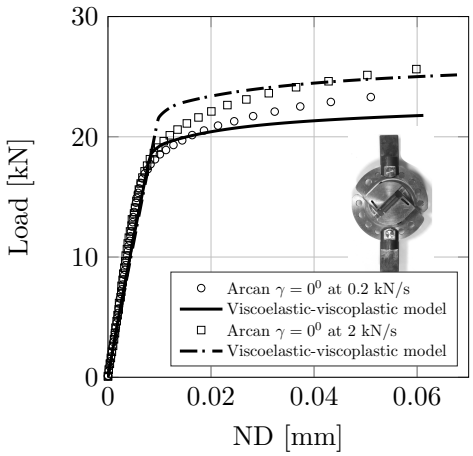

Figure 3.30: Validation of the viscoelastic-viscoplastic model under tensile loading; effect of loading rate

3.4 From Arcan tests to bulk behaviour

The prediction of the constitutive model was compared with the experimental results obtained in tensile and shear tests performed on bulk specimens. It is important to remember that in this section the model was identified using the mechanical behaviour observed in Arcan tests which is equivalent to the adhesive behaviour in a bonded joint. The inverse identification method allowed taking into account all the boundary conditions involved in a confined environment such as the bonded joint.

Two strong assumptions were made in this step of model validation:

Cohesive failure : The Arcan specimens presented a cohesive failure in tensile tests ($\gamma = 0^o$) but when tested in shear ($\gamma = 90^o$), the observed results presented a mixed failure. For both cases (tensile and shear behaviour), the obtained results were considered as being representative for the adhesive behaviour.

Interface : The role of interface was not taken into account in the present study.

Because all the experimental Arcan tests used in the identification procedure were performed just after the bonding process, no water influence on the mechanical behaviour was considered. Therefore, using this set of identified parameters, the model was supposed to be able to predict the mechanical behaviour of the adhesive in the initial state (dry specimen).

3.4.1 Prediction of the tensile bulk behaviour

The first validation step was realised using the experimental tensile tests performed on dried bulk specimens. As presented in *Chapter* 2, the tensile specimens have a dog-bone geometry and the strain in the zone of interest (ZOI) was measured using a DIC system (*Fig.*3.31a). An equivalent 3D model was designated for the simulation with a refined mesh and 8-node elements type C3D8R with reduced integration and hourglass control. By realising a mesh convergence study, only to elements were defined in the thickness of the sample (1 mm). The boundary conditions are represented in *Fig*3.31b

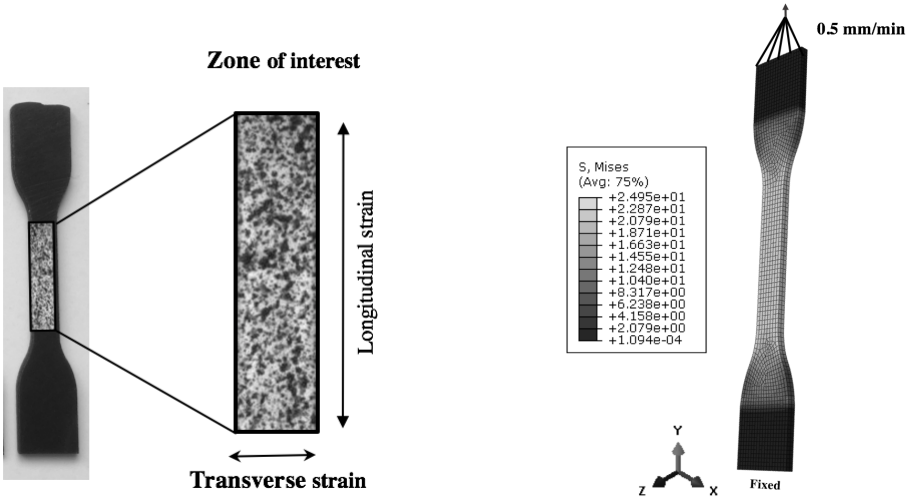

(a) (b) FE model for tensile test on bulk specimen

Figure 3.31: (a) Tensile test on bulk specimen (b) FE model for tensile test on bulk specimen

The experimental longitudinal strain was determine using the initial length of the ZOI (16mm) and the relative displacement between two lines located at the top and at the bottom of this area (Fig.3.31b). The stress is defined as the applied load divided by the initial cross-section area of the ZOI.

Table 3.4: Mechanical properties in tensile behaviour

Property	Value	Unit
Young's modulus	1840 ± 80	MPa
Poisson's ratio	0.39 ± 0.001	
Yield stress	36 ± 1	MPa

Young's modulus is defined as the slope between 0 and 2% strain. An average and a standard deviation is then calculated using all the tested samples for each condition. The yield stress is considered to be the point where the first derivative of the stress-strain curve changes by more than 5% of the initial value. Poisson's coefficient is defined as the ratio between the average transverse and longitudinal strains measured by DIC. These identified mechanical properties are represented in *Tab.*3.4.

*Fig.*3.32 presents the results obtained using the model prediction. A good agreement is

observed between the predicted tensile behaviour and experimental data. The Young's modulus identified using the method presented in *Section* 1.2.1 (1850 ± 50 MPa) is equivalent with the Young's modulus determined experimentally on bulk specimens. Hence, the model prediction of the modulus is correct, and also the yield surface.

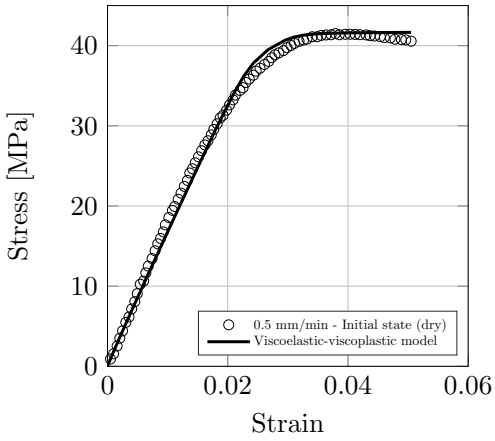

Figure 3.32: Comparison of the predicted tensile behaviour with the experimental data

3.4.2 Prediction of the shear bulk behaviour

The model prediction for shear bulk behaviour was also been compared against the experimental results. For this, a representative finite elements model was developed here.

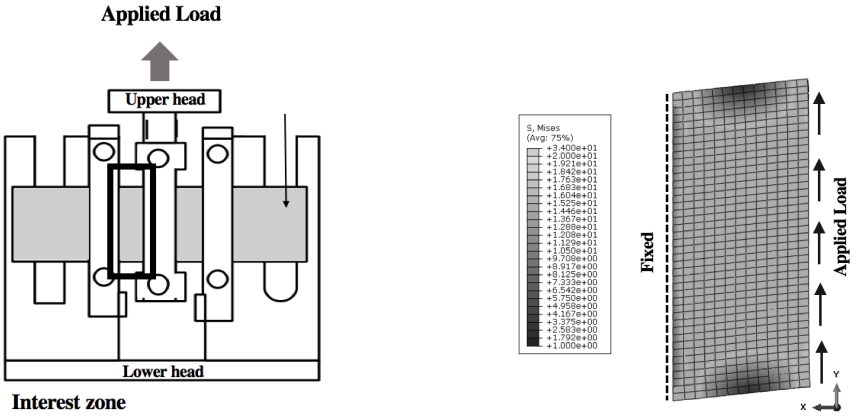

(a) Fixture used to characterise the shear bulk behaviour

(b) Finit element model used in inverse identification method

Figure 3.33: Identification of viscoelastic parameters that characterise the deviatoric part

The fixture used to perform the monotonic shear tests, on bulk specimens, is shown in *Fig.*3.33a. As can be observed, the rectangular bulk specimen is fixed in the lower head of the fixture and the load is applied using the upper head. Two zones of interest can be distinguished because of the symmetry of the system. Only one of them have been modelled using the finite element software and the boundary conditions have been applied as shown in *Fig.*3.33b.

The 3D model have one $C3D8R$ element in the thickness and a mesh convergence have been realised before simulations. For both cases (experimental and numerical), the shear stress was calculated as the applied stress divided by the initial section and the shear strain as the measured displacement over the distance between the clamping jaws (Chapter 2.2.3).

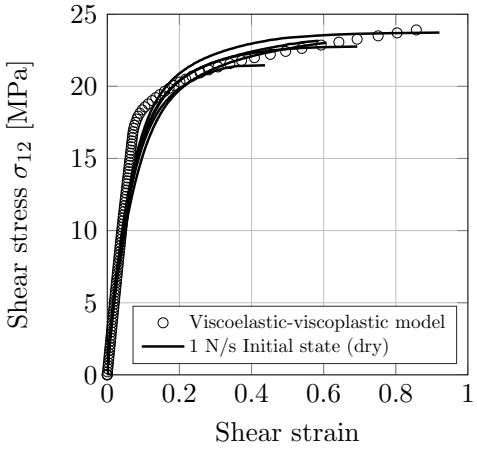

Figure 3.34: Comparison of the predicted tensile behaviour with the experimental data

The comparison between the model prediction and the experimental shear behaviour performed on bulk samples is represented in *Fig.*3.34. As can be observed the elastic part is accurately predicted by the model.

Moreover the elastic threshold (R_0) determined using the pure shear Arcan tests (Section 3.2.5.1) is equivalent to a *von Mises* stress σ_{VM} equal to 32MPa. Furthermore, if the shear stress σ_{12} is defined as in (*Eq.*3.28), its value will be equal to 18.49MPa which seems to correspond to the threshold observed experimentally (*Fig.*)3.34.

$$\sigma_{12} = \frac{\sigma_{VM}}{\sqrt{3}} \tag{3.28}$$

The non-linear behaviour is slightly under-estimated but the prediction of the model is considered in agreement with the experimental results. This permitted to validate once again the identification of the adhesive behaviour using the Arcan test.

3.5 From bulk tests to the Arcan behaviour

The method proposed in this chapter was also used to identify the developed model using the experimental tests performed on bulk specimens in order to test the capability of the model to predict the adhesive's behaviour in a bonded assembly (Arcan test). In a first step, the elastic parameters (Young's modulus and Poisson's ratio), determined using the monotonic tests performed on bulk specimens (*Section* 3.4.1), were directly introduced in the constitutive law. Secondly, using the same inverse identification method and associated FE models, the viscoelastic parameters were determined from the tensile and shear creep tests (also performed on bulk specimens). Finally, the viscoplastic parameters were determined using the non-linear behaviour observed in the monotonic tensile and shear tests.

A comparison between the values obtained in both cases is made in *Tab.*3.5. Some interesting observations can be made for each class of parameters as follows:

Elastic parameters: The elastic parameters can be determined directly using a tensile test performed on bulk specimens and there is no need to identify them using the more complicated method (*Section* 3.2.1) required for the Arcan tests.

Spectrum: In the present study, no differences have been observed in the values observed in the two cases (bulk and Arcan). This results are detailed in *Chapter* 5 of this document.

Viscoelasticity: The parameters that characterise the linear viscosity, a_H and a_D, were also determined as being close to the previous values (Arcan values). Some slightly differences have been observed for the thresholds of the non-linear viscosity (y_h^o, y_D^0) and the kinetics (y_H^c, y_D^c).

Viscoplasticity: By considering the shear yield stress as the point where the first derivative changes for 5%, the value of R_0 was determined as being slightly higher. The hardening parameters are not the same but the yield surface could been defined using the same parameter a_1.

Table 3.5: Comparison between the model parameters identified using Arcan test and those identified from tests performed on bulk specimens

Class	Parameter	Arcan Identification	Bulk Identification
Elastic	E	1850 MPa	1840 MPa
	ν	0.4	0.39
Spectrum	n_0	5	5
	n_c	10	10
Viscoelasticity	a_H	1800 MPa^{-1}	1700 MPa^{-1}
	d_H^{max}	0.9	0.9
	y_H^0	0.8	0.1
	y_H^c	0.7	0.13
	a_D	1500 MPa^{-1}	1420 MPa^{-1}
	d_D^{max}	0.6	0.6
	y_D^0	0.6	0.2
	y_D^c	0.015	0.3
Viscoplasticity	R0	32 MPa	33 MPa
	a_1	0.023 MPa^{-1}	0.023 MPa^{-1}
	H	24 MPa	30 MPa
	Q	56 MPa	60 MPa
	b	37	42
	a_1^*	0.0026 MPa^{-1}	0.0026 MPa^{-1}

Using the model parameters identified on bulk specimens, the prediction of the monotonic tensile and shear tests was made. It can be seen in *Fig.*3.35 that the elastic threshold is overestimated and some changes can be observed in the non-linear parameters due to the hardening. However, a good prediction can be made for the tensile and shear monotonic behaviour observed using the Arcan device.

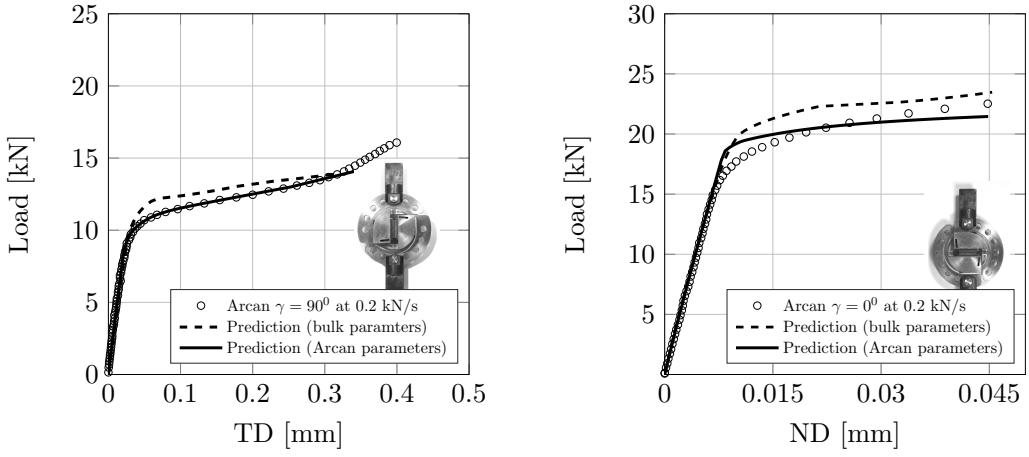

Figure 3.35: Prediction of the (a) shear and (b) tensile behaviour of an Arcan test using the model parameters identified on bulk specimens

3.6 Conclusions

3.6.1 Overview on the model

This chapter presents the development of a viscoelastic-viscoplastic model which describes the mechanical behaviour of an adhesive in a bonded joint. As can be seen in the literature, the mechanical behaviour of some types of adhesives can be modelled by only using a viscoelastic constitutive law [23]. In the case studied here, viscoelasticity was not sufficient to describe the important non-linearity in the behaviour of the studied adhesive. Moreover, the viscoelastic spectral model, initially developed to describe the composite matrix mechanical behaviour and then adapted by *Badulescu et al.* [79] for adhesives, has been modified in order to take into account the effect of the von Mises and the hydrostatic stress as proposed by *Carrere et al.* [153].

For identification and validation of the viscoelastic part of the model, only one multi-level creep/recovery test is needed in two directions (tension and shear). The loading of each level should be below the elastic threshold. For a better understanding of the time-dependent behaviour, long creep tests are recommended. The creep levels are only used for identification of the model parameters. The validation of the model is made afterwards using the recovery levels of the same sample.

Once the viscoelastic part of the model is defined, the viscoplastic part of the model can be identified. The yield surface is determined using monotonic tests in two directions ($\gamma = 0^0$, $\gamma = 90^0$). For the identification of the loading rate dependent parameters K and n, a second monotonic shear test ($\gamma = 90^0$), performed at another loading rate is needed.

Even though the proposed model has an important number of parameters (10 for the viscoelastic part and 7 for viscoplasticity), only two creep tests and three monotonic tests are needed to identify all these parameters. It is also important to highlight the method of identification which is quite easy to implement. Each parameter is determined step by step

using the inverse identification method.

3.6.2 Perspectives

For further investigations, the sensitivity of each parameter of the model can be studied. To quantify this, the relevant tests should be defined for each type of parameter (viscoelastic or viscoplastic). In a second phase, an approach should be developed to calculate an error with respect to the global mechanical response after changing a specific parameter with a certain ratio.

As from a qualitative point of view, it can be confirmed that the viscoelastic parameters (a_i, d_i^{max},y_i^0, y_i^C where $i = \{H, D\}$) have a great influence on the creep behaviour but they do not seem to influence that much the global mechanical response in monotonic tests. The spectrum parameters (n_0, n_c) characterize the form of the creep behaviour but they will not impact the predicted strains. Viscoplastic parameters have a great influence in both shear and tensile monotonic behaviour but they will not influence the creep behaviour as long as the applied load is below the elastic limit.

To test its capability, it would be interesting to validate the prediction of the model using adhesively bonded structures such as single lap joints. In further investigations, the model can be used to predict the cyclic mechanical behaviour, which is very important when considering fatigue lifetime prediction. Another aspect is to identify the evolution of the model parameters as a function of water ageing of the material, in order to predict the influence of water on the mechanical behaviour. This will be the subject of the next chapter of this work.

3.6.3 Proposal for a rapid characterisation of a water-aged bonded joints

In order to predict the influence of water on the mechanical behaviour of the adhesive in a bonded joint, the identification method, presented above, would need Arcan tests performed on aged specimens. However, it has been shown in the bibliographic study (Chapter 1) that water diffusion in bonded joints depends on the geometry of the sample and the boundary conditions. *Arnaud et al.*[21] calculated that Arcan specimens used in this study need almost two years to be saturated in water at 40^{o}C.

In order to accelerate the ageing process, the effects of water on the mechanical behaviour of the adhesive were studied on bulk specimens (1mm thickness), which will allow to decrease considerably the saturation time of the samples. Furthermore, the experimental results obtained using the water aged bulk samples were used to identify the evolution of the model parameters as a function of water content. By coupling these information with a diffusion model, a prediction of the mechanical behaviour of an aged bonded joint will be proposed.

Chapter 4

Influence of water content on the mechanical properties of the adhesive

"Explaining a phenomenon is like considering it the visible effect of a hidden cause linked to the invisible forces who are meant to rule the world"

Emilio Segrè

Water agieng in different environmental conditions

The aim of the present chapter is to focus on how water enter into the two-part epoxy adhesive and how it affects its mechanical behaviour, in order to provide a physically based relationship for subsequent predictive modelling of the adhesive in an aged bonded joint. The results obtained here will be used to identify the evolution of the proposed model parameters as a function of water content (*Chapter* 5).

Contents

4.1 Introduction and complementary bibliography **124**
4.2 Water diffusion in different environmental conditions **125**
4.2.1 Samples used for water uptake 126
4.2.2 Water absorption 126
4.2.3 Water absorption in completely immersed state 127
4.2.4 Water absorption in controlled relative humidity environment 130
4.3 Short-term study of water ageing: absorption/desorption **132**
4.3.1 Experimental measurements 132
4.3.2 Analytical modelling of each cycle 132
4.4 Transition glass temperature evolution with water content **133**
4.5 Tensile behaviour changes with water content **134**
4.6 Short-term study of water ageing **136**
4.7 Long-term study of seawater ageing **136**
4.7.1 Experimental approach 136
4.7.2 Analysis of the mechanical properties 137
4.8 Dynamic mechanical-thermal analysis (DMTA) **137**
4.9 Creep tests at different constant water content **139**
4.9.1 Tensile creep behaviour 139
4.9.2 Shear creep behaviour 140
4.10 Overview **141**

4.1 Introduction and complementary bibliography

Structural adhesives have a long history in marine applications, playing a key role in the assembly of pleasure boats and racing craft [154]. The interactions between water and polymers have been studied by many authors, and effects are usually classified as either reversible (plasticization [155], swelling [123]) or irreversible (hydrolysis [16], oxidation). The influence of water on epoxy resins has received particular attention. Zhou and Lucas described how water bonds with epoxy resins [156], and how this reduces the glass transition temperature [157]. Various studies have shown that significant amounts of water can enter epoxies. For those with amine hardener water content is usually less than 5%. Much higher water content can be observed when the polarity of the polymer increases or when fillers are used. Epoxy based adhesive formulations are more complex, often containing small amounts of fillers and other additives to assist bonding operations. For some epoxy adhesives and exposure conditions the weight gain plots show Fickian behaviour, *e.g.* [120], in others more complex behaviour is observed. For example, De Nève and Shanahan showed an initial Fickian response followed by a second increase in weight for an epoxy adhesive [158], while Mubashar *et al.* [18] proposed a dual Fickian model for water ingress into a rubber toughened 120^{o}C cure one-part epoxy system. This water can be quite detrimental to both adhesive properties and their assembled joints, and environmental effects are often cited as one of the main reasons for not using adhesive assembly more extensively [159]. For example, Bordes *et al.* [160] showed drops in adhesive tensile modulus and strength after saturation of up to 50% of initial unaged values. In many cases complete restoration of property losses has been noted after drying e.g. [161], suggesting that adhesive plasticization is the dominant mechanism.

In assembled joints the adhesive/substrate interfaces must also be considered. For example, Zanni-Deffarges and Shanahan described diffusion of water in adhesives and bonded joints [162]. They found considerably higher diffusion coefficients for the bonded joint, and suggested that capillary diffusion exacerbates water ingress but when focusing on water diffusion in bulk specimens, these considerations can be neglected. Brewis *et al.* [161] found a linear relationship between joint strength and the water content of metal/epoxy joints but a strong dependency on the aluminium surface preparation, with strength either decreasing or increasing as water content increased. This is not the subject here but it is interesting to note that some authors have suggested that the presence of a critical amount of water at the interface leads to interface failure [163]. A reliable diffusion model is essential to predict the local water concentration. Finally, it should be noted that residual stresses may also have a significant influence on the environmental degradation of adhesive assemblies [164].

There are a number of useful reviews available concerning moisture effects on adhesive joints; Bowditch presented an overview of the influence of water on durability [138] and Comyn and colleagues have provided detailed reviews of environmental effects [17][24][165].

This brief overview shows that there are a number of relevant test results in the published literature, and there is also considerable practical experience of the long-term reliability of adhesives in water. However, it is also clear that there is a range of behaviours which depend on adhesive formulation and environmental conditions, and there are few predictive tools available

to the designer looking to develop bonded assemblies in new marine applications, such as renewable marine energy structures. There are some exceptions, in particular, the work of Crocombe *et al.* [144][140][22], who have developed an overall methodology and also specific approaches based on both damage mechanics [145] and cohesive zone models [166] to account for the influence of moisture in a coupled approach.

Bordes et al. [160] also describe a partially coupled approach to predict long-term behaviour during immersion, while other recent work includes that of Arnaud *et al.* [21], who applied a Mahnken–Schlimmer model [167] with parameters identified on unaged and aged Arcan specimens. Leger *et al.* [134] have also studied coupling effects; they examined temperature/humidity equivalence in a highly filled adhesive and modelled the influence on mechanical behaviour. Moreover, Viana *et al* presented a review on the temperature and moisture degradation of adhesive joints [168] and correlated the glass transition temperature of a bulk epoxy adhesive with the water uptake to determine the evolution of its properties as a function of environmental temperature and moisture [169].

4.2 Water diffusion in different environmental conditions

The study of water ingress in the adhesive has been conducted using two kinds of ageing tests. In the first one, the bulk samples were immersed in continuously renewed natural sea water taken directly from the Brest estuary, more details about Ifremer ageing tanks (*Fig.*4.2a) being available in [170]. Five temperatures have been studied (4^oC, 15^oC, 25^oC, 40^oC, 60^oC) in order to completely understand the evolution of the diffusion coefficient as a function of water temperature.

(a) Ageing tanks with continously renewed natural seawater - IFREMER

(b) Conditioning chamber for humid ageing at IFREMER

Figure 4.2: Experimental resources used for different ageing conditions

The second study was conducted in controlled humidity chambers. The humid ageing was carried out at three humidity levels (33%, 50% and 75%), in $Memmert^{TM}$ conditioning

chambers (*Fig.*4.2b), type *HP110*. This analysis provided the amount of absorbed water, at saturation, as a function of the water activity.

4.2.1 Samples used for water uptake

The samples used for this study were taken from a sheet of adhesive as specified in *Section*2.1.3. The mixture was compressed between two aluminium plates, and the final thickness was controlled using 1mm calibrated thick spacers. The assembly was cured for $1h10$ at 115^oC. After curing, the adhesive sheets were removed from the mould and thermally post treated for one hour at 80^oC (*i.e.* above Tg) in order to release any residual stresses. Samples were then cut from the sheets using a water jet cutting system.

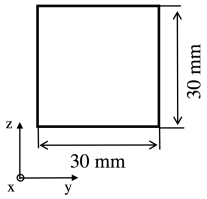

Figure 4.3: Geometry of the squared samples used for water uptake (1mm thickness)

In order to simplify the identification of the diffusion law in the bulk adhesive, the geometry of the samples used to characterise the water diffusion has been adapted so that two dimensions are much higher than the third one. This enabled the assumption to be made that the water diffuses in one direction, which is easier to model when determining the diffusion coefficient. A square shape with 30×30 mm^2 has been chosen for this study (*Fig.*4.3). All samples were dried prior to ageing in a desiccator until mass stabilization.

4.2.2 Water absorption

After being placed in different ageing conditions (immersion or relative humidity), the water diffusion was determined from the weight change of the square samples. Mass gain was followed by periodic weighing on a $Sartorius^{TM}$ LA 310 S balance (precision *0.1mg*). Samples were removed from the ageing containers and wiped with paper towels before weighing to dry the surfaces, three samples were tested per condition. The change in water content in each sample (M_t), with time, is defined with respect to the initial mass of the sample (m_0), using *Eq.*4.1:

$$M_t = \frac{m(t) - m_0}{m_0} \times 100 \tag{4.1}$$

where $m(t)$ is the mass of a sample at time t and m_0 the initial mass.

As mentioned above, given the dimensions of the samples, the water diffusion was considered unidirectional. The diffusion coefficient was determined on the initial linear part of the sorption curve , $\frac{M_t}{M_\infty} \leq 0.5$, M_∞ being the mass at complete saturation. Its value is calculated using Fick's 1D law (*Eq.*4.2):

$$D = \frac{\pi}{16}\frac{e^2}{t}\left(\frac{M_t}{M_\infty}\right)^2 \tag{4.2}$$

where, e represents half of the sample thickness in m and t is the immersion time in seconds.

4.2.3 Water absorption in completely immersed state

4.2.3.1 Experimental results

The curves representing the water uptake in a completely immersed state for the epoxy adhesive (*Araldite 420A/B*) are shown in *Fig.*4.4. Different seawater ageing temperatures have been studied, starting from 4^oC until 60^oC. The curves for each ageing temperature are represented in a separate figure.

The water uptake behaviour is similar for each ageing temperature. It starts with a linear evolution of the absorbed mass with the square root of time followed by a slowdown. For each ageing temperature, the saturated mass is stabilised around 4% of the initial mass. This is a normal value for epoxy materials with low quantities of fillers. In the presence of fillers, that are often used in adhesives, water absorption can be much higher due to osmotic cracking or poor polymer/filler interactions.

4.2.3.2 Analytical modelling of water diffusion

In the first chapter a series of models was presented which can describe the water diffusion in polymers. Among those models, one of the most used is Fick's model [124][113]. It defines the absorption/desorption of water in the polymer. This model was used to model analytically the water diffusion. As mentioned earlier, because of the geometry of the samples used in this study, (the $1mm$ thickness is much smaller than the other dimensions 30×30mm), the 1D approach was implemented.

Considering a unidirectional diffusion through the thickness of the sample (x - direction, see *Fig.*4.3), and a diffusion coefficient which is independent of water concentration it was possible to deduce the (*Eq.*4.3):

$$\frac{\partial C}{\partial t} = D\frac{\partial^2 D}{\partial x^2} \tag{4.3}$$

For samples immersed in an environment with a concentration of C_1, and if C_0 is the initial concentration of diffused material, the temporal and spatial evolution of C can be written as in *Eq.*4.4:

$$\frac{C - C_0}{C_1 - C_0} = 1 - \frac{4}{\pi}\sum_{n=0}^{\infty}\frac{(-1)^1}{(2n+1)^2}exp\left(-D\frac{(2n+1)^2}{4e^2}\pi^2 t\right)\cos\frac{(2n+1)\pi x}{2e} \tag{4.4}$$

x: distance from the middle plane of the sample in the thickness direction $[m]$

e: half of the sample thickness $[m]$

t: immersion time $[s]$

Knowing that the samples were dried before exposure, $C_0 = 0$ and that M_∞ is the saturated mass, the instant mass M_t, at time t, is obtained by integrating the *Eq.*4.4.

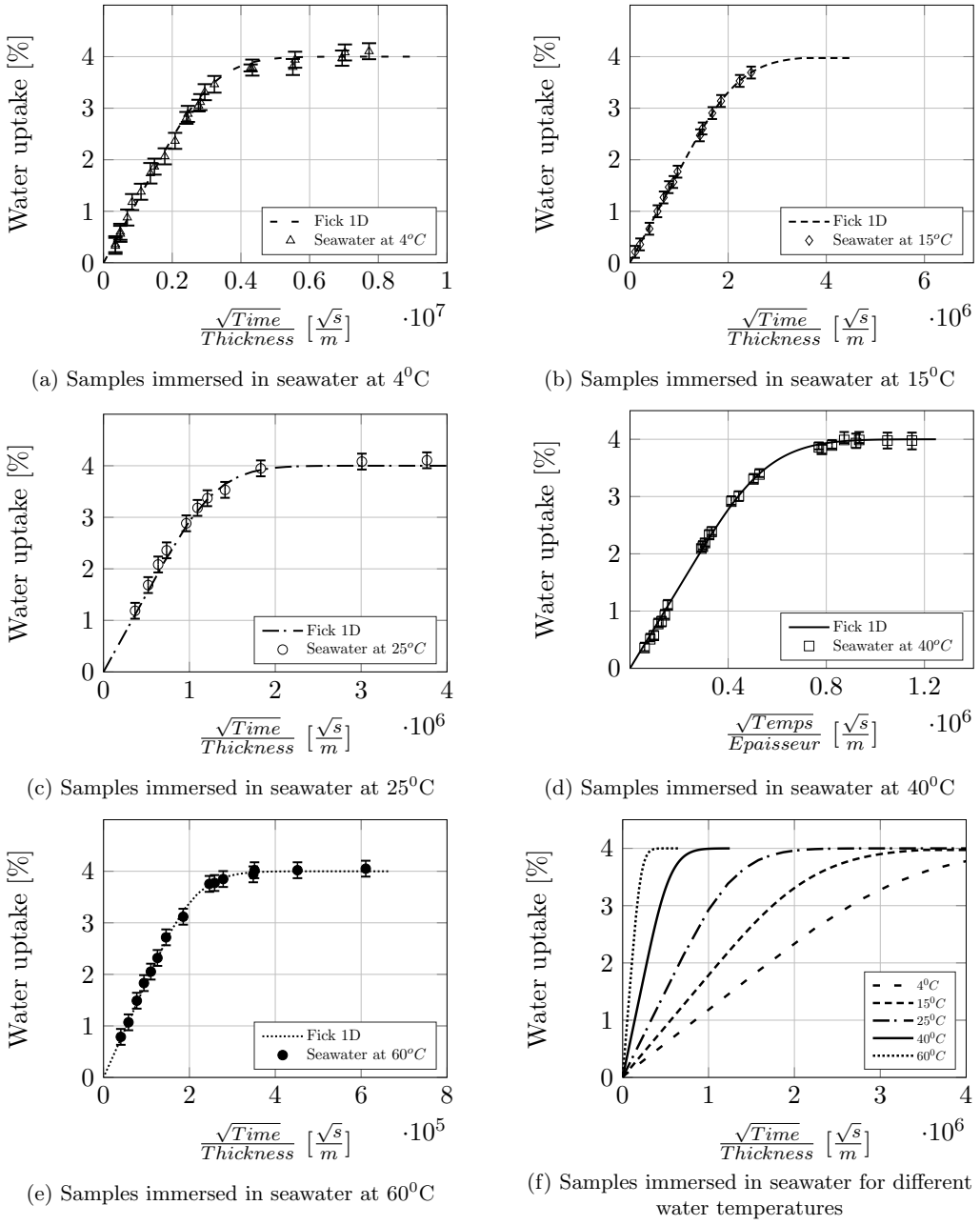

(a) Samples immersed in seawater at 4^0C

(b) Samples immersed in seawater at 15^0C

(c) Samples immersed in seawater at 25^0C

(d) Samples immersed in seawater at 40^0C

(e) Samples immersed in seawater at 60^0C

(f) Samples immersed in seawater for different water temperatures

Figure 4.4: Water diffusion in bulk specimens immersed in different seawater temperatures

$$\frac{M_t}{M_\infty} = 1 - \frac{8}{\pi^2} \sum_{n=0}^{\infty} \frac{1}{(2n+1)^2} exp\left(-D\frac{(2n+1)^2}{4e^2}\pi^2 t\right) \tag{4.5}$$

This equation has been implemented in *Matlab* software and the solution was compared with the experimental points. As can be observed in *Fig.*4.5a, the saturated mass is around 4% for each ageing temperature (*Fig.*4.4).

For low water uptakes, $\frac{M_t}{M_\infty} < 0.5$, the *Eq.*4.5 can be approximated by the equation *Eq.*4.6. This allows the diffusion coefficient to be determined for a given water temperature.

$$\frac{M_t}{M_\infty} = \frac{4}{e}\sqrt{\frac{Dt}{\pi}} \tag{4.6}$$

4.2.3.3 Diffusion coefficient D as a function of water temperature

The diffusion coefficients are obtained using the *Eq.*4.6 for each water ageing temperature that has been studied. The mean values obtained are presented in Table 4.1. Moreover, the times needed to saturate a sample of $1mm$ thickness are given in the third column.

Table 4.1: Diffusion coefficient for different water temperatures [*1mm thick*]

Water temperature	**Diffusion coefficient**	**Saturation time**
4^0C	1.2e-14 $[m^2s^{-1}]$	413 days
15^0C	7.1e-14 $[m^2s^{-1}]$	184 days
25^0C	2.1e-13 $[m^2s^{-1}]$	55 days
40^0C	1.1e-12 $[m^2s^{-1}]$	14 days
60^0C	5.1e-12 $[m^2s^{-1}]$	47 hours

Generally, water diffusion in polymers is a thermally activated phenomenon, the diffusion coefficient being dependent of the water temperature through an Arrhenius law (*Eq.*4.7):

$$D = D_0 exp\left(\frac{E_a}{RT}\right) \tag{4.7}$$

E_a: diffusion activation energy $[J]$

D_0: diffusion constant $[m^2s^{-1}]$

T: temperature of water $[K]$

R: perfect gas constant 8.3145 $Jmol^{-1}K^{-1}$

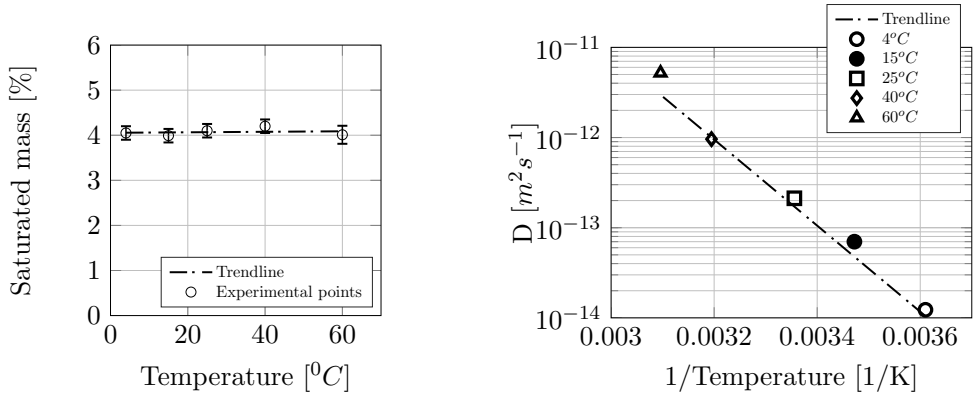

(a) Saturated mass value with water temperature

(b) Diffusion coefficient (Arrhenius law) with water temperature

Figure 4.5: Evolution of saturated mass and diffusion coefficient with water temperature

Based on *Eq.*4.7, if the diffusion coefficient D follows an Arrhenius law, its logarithm (lnD) should depend linearly on the inverse of temperature. Using the experimental results presented in *Fig.*4.5b, the evolution of D can be expressed as in *Eq.*4.8.

$$lnD = -1.1 \times \frac{10^4}{T} + 7.5 \tag{4.8}$$

In order to reduce the time needed for sample saturation, the water temperature of 40^oC was chosen as the reference for the water ageing study. As can be observed in *Table.*4.1, only 14 days are needed to saturate a sample of $1mm$ of thickness which is a reasonable time for the next studies. Moreover, because the initial glass transition temperature of the adhesive was determined at $66^oC \pm 2^oC$, studying the water diffusion at 60^oC would be too aggressive and it would involve a change in the material properties. This is also confirmed in *Fig.*4.5b, where the point corresponding to 60^oC does not seem to follow the Arrhenius law represented by the trendline.

4.2.4 Water absorption in controlled relative humidity environment

In this stage of the study, it was possible to predict the time needed to saturate a bulk sample of $1mm$ thickness in seawater for different water temperatures. It was also been observed that at 40^oC, 14 days are sufficient for saturation. Thus, the same ageing temperature was chosen for determining the kinetics of water absorption in controlled relative humidity environment.

4.2.4.1 Experimental results

The mass variation measured during exposure of the adhesive to a wet environment at 40^oC is plotted in *Fig.*4.6. For each of the conditions considered herein, i.e. a relative humidity of 32%, 50% and 75% and immersion in sea water, Fickian behaviour was observed, with increasing weight gain during the first stage of ageing and then the appearance of a saturation plateau. Based on these results it is possible to consider two main characteristics for water diffusion: the water diffusivity and the amount of absorbed water.

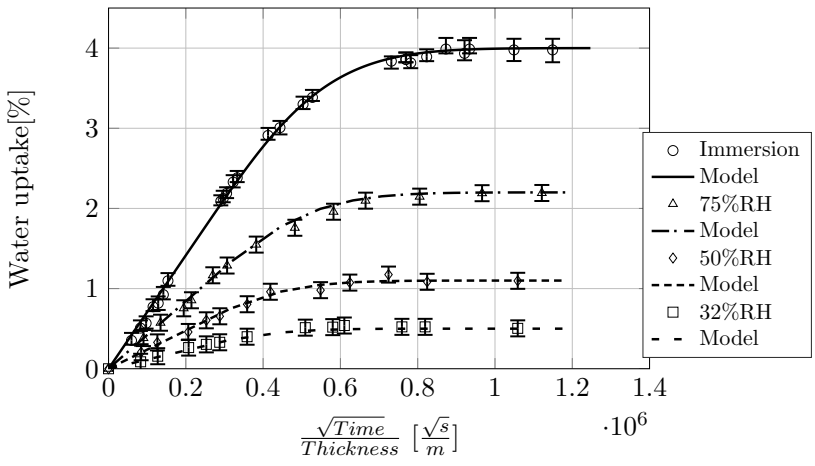

Figure 4.6: Water absorption, at 40^oC, in adhesive for different water activities (symbols are experimental data and lines show Fickian behaviour model)

4.2.4.2 Diffusion coefficient as a function of water activity

The water diffusion coefficient is equal to $1.1 \times 10^{-12}\ m^2 s^{-1}$ at 40^oC and independent of the relative humidity as shown in *Fig.*4.7b. This value is in accordance with existing results in the literature for epoxy material with an amine hardener [123][113].

The water uptake in the epoxy adhesive at saturation when immersed in sea water at 40^oC is 4%. Moreover, as expected, the amount of absorbed water at saturation depends on the water activity in the surrounding environment. The higher the water activity the higher the water content at saturation in the polymer as shown in *Fig.*4.7a. However, it also appears that water content at saturation is not directly proportional to the partial pressure of water indicating that Henry's law is not verified here.

The water content in the epoxy adhesive has been described based on an existing relationship (*Eq.*4.9) developed elsewhere [171][172]:

$$W_{H_2O} = H \times a + N \times a^m \tag{4.9}$$

where W_{H_2O} is the relative volume ratio of water in the polymer in %, a is the water activity in the surrounding environment and H, N and m are parameters identified experimentally.

The value of the three parameters (H, N, m), used to predict the evolution of the water content at saturation as a function of water activity, are represented in *Tab*4.2.

Table 4.2: Water activity model parameters

Parameter	Value
H	1.1
N	2.9
m	2.3

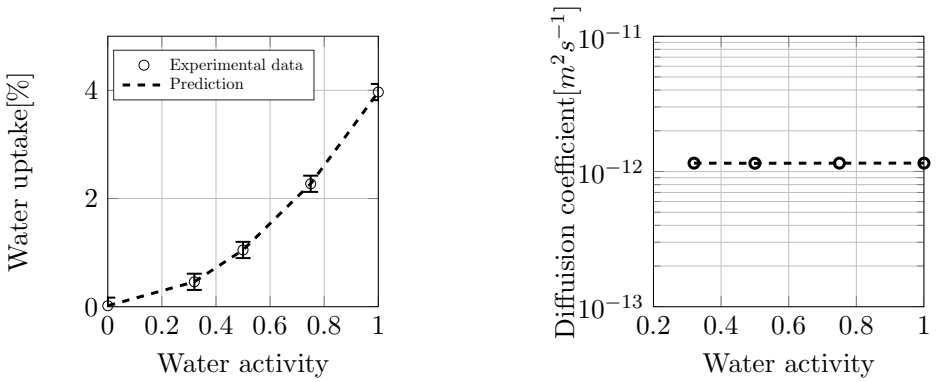

(a) Saturated mass value as a fonction of water activity

(b) Diffusion coeffficient as a fonction of water activity

Figure 4.7: Evolution of saturated mass and diffusion coefficient with water activity

This behaviour is usually explained by a clustering phenomenon where the water can form microscopic droplets of water [173][174] but this will not be considered in detail in this study.

4.3 Short-term study of water ageing: absorption/desorption

4.3.1 Experimental measurements

Another study of water absorption has been performed in seawater at 40^oC in order to determine the behaviour of water diffusion after several cycles of absorption/desorption. The Fig.4.8 shows the evolution of the kinetics of water diffusion during three absorptions and two desorptions performed on the same samples with a geometry as presented in *Section 4.2.1.* The desorption cycles have been made in desiccators at at 40^oC and with a controlled relative humidity kept at 0%. By analysing the curves, it is possible to note that after each cycle of absorption the same amount of water (4%) is observed at saturation.

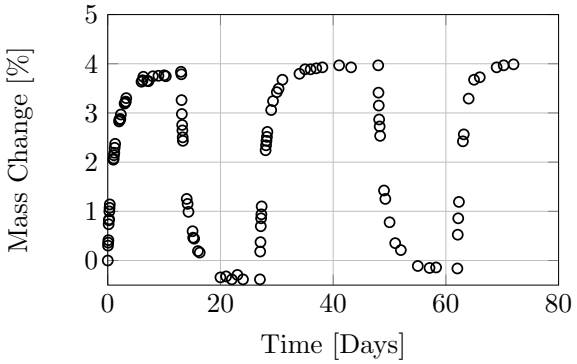

Figure 4.8: Cycles of absorption/desorption performed on the studied adhesive

After the first desorption cycle, each sample showed a final mass which was 0.5% below its initial mass. This could be due to the fact that the samples used in this study were not fully dried before the experiment. No other physical or chemical phenomenon was believed to occur. Moreover after the second desorption cycle, the weight of the samples was equivalent to their initial mass, which can confirm this theory.

4.3.2 Analytical modelling of each cycle

Some interesting results were obtained after modelling the three absorption cycles using the *Fick 1D* model, and superposing them on the same figure (*Fig.*4.9a). As can be observed, after the first absorption cycle, the diffusion coefficient is slightly increasing. However, the kinetics of diffusion seem to remain unchanged.

In *Fig.*4.9b, the first cycle of absorption and the first desorption cycle were compared. The desorption cycle was inverted and superposed on the absorption one in order to facilitate the comparison. As shown, the absorption diffusion coefficient is equivalent to the desorption rate, meaning that the same amount of time is needed to completely saturate a sample starting from the dried state as that needed to completely dry the same sample after being saturated in seawater.

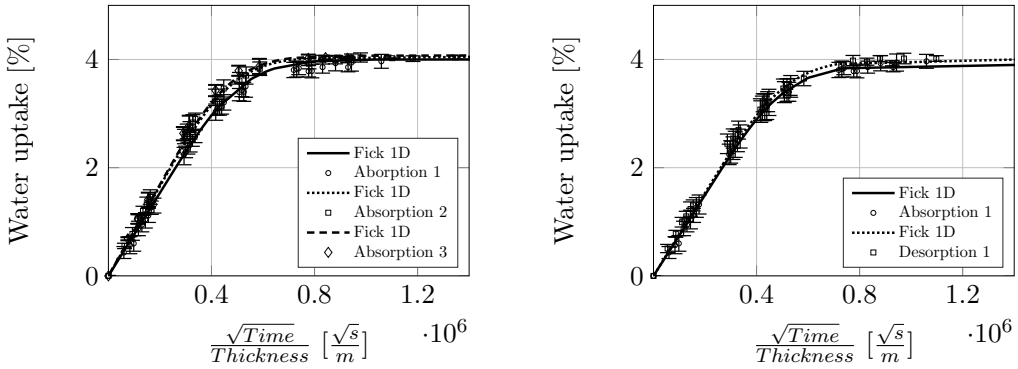

(a) Comparison of different absorption cycles

(b) Comparison of the firsts soprtion and a desoprtion cycles

Figure 4.9: Absorption/Desorption cycles

4.4 Transition glass temperature evolution with water content

It is well known that presence of water in the structure of an epoxy decreases its glass transition temperature. In a first step, the evolution of Tg was measured using DSC analysis. The experimental device used for this measurement is a Q200 machine from TA Instruments^{TM}, with a temperature scan between 20^oC and 90^oC at a heating rate of 10^oC/min. Two runs have been made for each condition in order to highlight any changes in the material (evolution of Tg) after a post-curing process.

The samples used in this study were saturated using the same ageing conditions (immersion in seawater and 32%RH, 50%RH, 75%RH) , which provided a constant water profile and different water quantities at saturation. *Fig.*4.10a shows the results obtained for these conditions. The Tg was calculated using the method that involves ascertaining the onset, midpoint and end point temperatures observed when a change of slope is noticed in the heat flow [151].

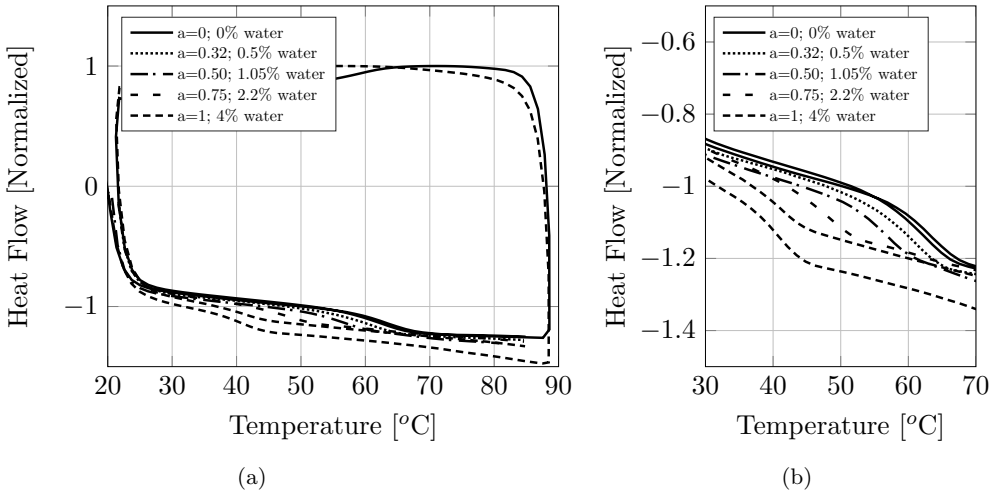

(a)

(b)

Figure 4.10: DSC analysis on samples saturated in different ageing conditions (a) Zoom on the zone of interest (b)

Fig.4.11 shows the Tg values as a function of water content. A large decrease from 66^oC in the dry state to 41^oC after saturation in sea water (*i.e.* with 4% of water) is observed. The water solubility in polymer is not related to the state of the material meaning that the amount of absorbed water by a polymer (with no fillers) is not greatly affected when the polymer goes from the glassy to the rubbery state. This behaviour can be explained by the fact that the presence of water in the polymer leads to an increase of the macromolecular chains mobility and so a decrease in Tg. This decrease in Tg with water content can be described by the Simha-Boyer equation [38]:

$$\frac{1}{Tg} = \frac{1}{Tg_{polymer}} + A \times W_{H_2O} \qquad \text{with} \qquad A = \frac{1}{Tg_{water}} - \frac{1}{Tg_{polymer}} \tag{4.10}$$

where Tg is the predicted glass transition temperature, $Tg_{polymer}$ is the glass transition temperature of the polymer in the initial state, Tg_{water} is the Tg of the solvent (here water), taken equal to 100K (a value between the range of accepted values since the real Tg of water is difficult to measure [175]), and W_{H_2O} is the volume fraction of water in the sample.

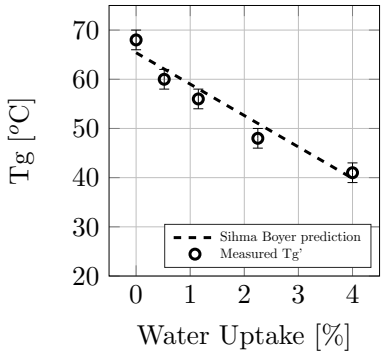

Figure 4.11: Decrease in Tg as a function of water content at saturation in the epoxy adhesive

4.5 Tensile behaviour changes with water content

This section is focused on the effect of water on the mechanical properties of the studied adhesive as a bulk form. It should be noted that all the results presented in this section were obtained on fully saturated samples but with different amounts of water, meaning that there is no water profile through the specimen thickness.

The tensile behaviour for several water contents is plotted in *Fig.*4.12. The presence of water leads to large changes in the mechanical behaviour of this epoxy with a large decrease in yield stress and modulus, and an increase in strain at break. All these changes in properties are plotted in *Fig.*4.13 together with the Poisson's ratio and the strain at break (4.14).

When exposed to humid environment, water diffuses into the polymer through a Fickian mechanism and the material absorbs up to 4% when immersed in sea water. The presence of water leads to an increase in mobility of the macromolecular chains and a decrease in Tg from 66°C to 41°C, this phenomenon is well known as plasticization. Large changes in mechanical behaviour are induced by the plasticization: a decrease of the adhesive's stiffness as well as the

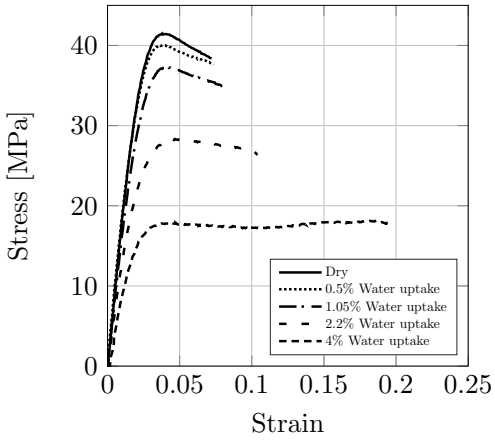

Figure 4.12: Tensile behaviour as a function of water content at saturation (*i.e.* without any water profile gradient through the thickness)

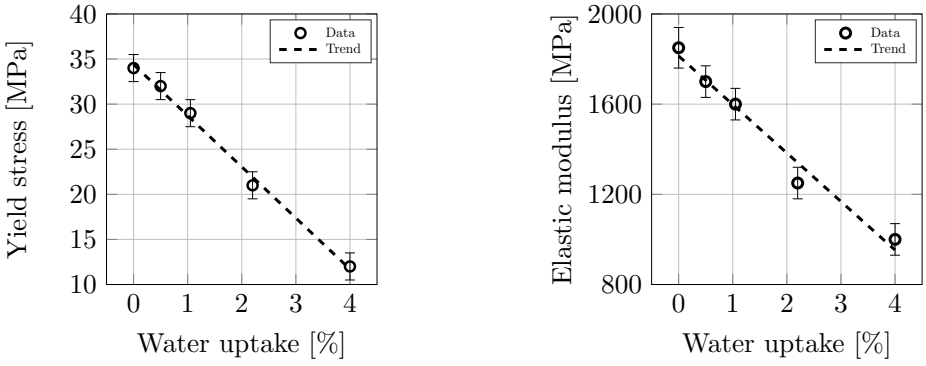

(a) Changes in Yield stress

(b) Changes in elastic modulus

Figure 4.13: Evolution of the mechanical properties as a function of water content at saturation

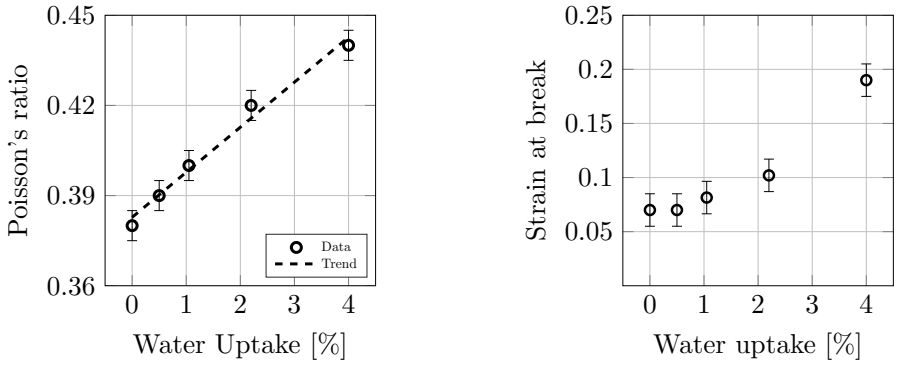

(a) Changes in Poisson ratio

(b) Changes of the strain at break

Figure 4.14: Evolution of the mechanical properties as a function of water content at saturation

yield stress and an increase in strain at break and Poisson's ratio. The increase in the Poisson's ratio can be explained by the fact that the polymer tends toward its rubbery behaviour when

Tg decreases.

4.6 Short-term study of water ageing

Furthermore, samples aged at 40^{o}C for 14 days in sea water have then been dried in a desiccator at 40^{o}C at 0%RH to remove all the absorbed water. Tensile results before and after drying are plotted in *Fig.*4.15 and compared to those for unaged samples. A similar behaviour is observed, with the same modulus, yield stress and strain at break after drying, compared to unaged samples. It is interesting to note that there is a small strain softening effect after yield for unaged specimens; the reasons for this are not clear and further work is underway to examine the parameters which affect post-yield behaviour.

Another important aspect is that the degradation observed here is fully reversible (*Fig.*4.14a) meaning that plasticization is the only mechanism involved (for the ageing conditions used in this study).

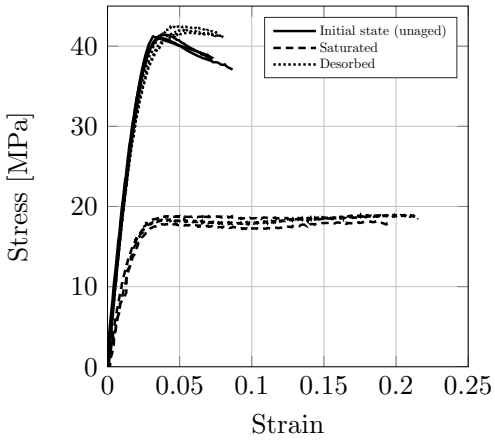

Figure 4.15: Tensile behaviour for unaged samples, fully saturated samples and dried after 14 days of ageing in seawater at 40^{o}C

4.7 Long-term study of seawater ageing

4.7.1 Experimental approach

Another set of tests was conducted in order to characterise the evolution of mechanical behaviour after immersion beyond saturation. For this, tensile dog-bone specimens with a thickness of $1mm$ were saturated in sea water at 40^oC (14 *days*) and then they were kept immersed in order to test them after different periods of time. A first series of samples was tested after three months and a second one after seven months. The results can be observed in *Fig.*4.16.

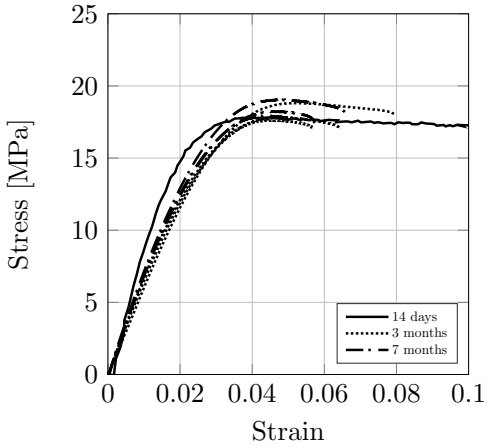

Figure 4.16: Long term evolution of tensile behaviour

4.7.2 Analysis of the mechanical properties

The Young's modulus is slightly decreasing after complete saturation and long-term ageing, and seems to stabilise after seven months. In addition, the yield stress does not change with the long-term immersion which is a positive result for industrial applications. However, the strain at break is drastically decreased after immersion for a long period of time suggesting the onset of degradation, and this requires further study in order to define the operating limits.

4.8 Dynamic mechanical-thermal analysis (DMTA)

Another study of water effects on the evolution of mechanical properties of aged bulk specimens has been performed using a dynamic thermal-mechanical analysis (DMTA) after they were saturated in different environmental conditions (immersion in seawater and 32%RH, 50%RH, 75%RH). The samples used for this study were cut out from an adhesive plate as presented in *Section* 2.2.1.

The same device (*Fig.*4.17a) as that used to characterise the initial state of the material (Section 2.2.6) has been used for these tests. The samples have a rectangular geometry with the dimensions presented in *Fig.*4.17b. Their thickness is equal to $1mm$ which is equivalent to the thickness of the squared samples (Fig.4.3) used to characterise the water diffusion in the bulk adhesive. Therefore, the time needed to saturate them is equal to 14 days at 40^oC for each environmental condition.

The results presented were obtained by imposing a dynamic strain of $\varepsilon = 10^{-3}$ with a frequency of $1Hz$. This corresponds to the strain rate applied for monotonic tensile tests performed using dog-bones bulk specimens. The mechanical properties were been analysed between 0^oC and 100^oC with a heating rate of $2^oC/min$. In order to avoid the evaporation of water during the test, the saturated samples were tested using a conditioning chamber mounted on the DMTA machine, which provided a relative humidity equivalent to the ageing conditions. For samples saturated in immersion, the conditioning chamber was set to 90%RH.

The evolution of the Young's modulus of a dried sample (0% water) and an immersed

(a) Tensile fixture mounted on the DMA machine

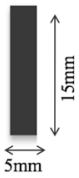

(b) Specimen for tensile creep behaviour

(c) Measurement of the tensile elongation

Figure 4.17: Geometry and experimental device used for DMA analysis of samples saturated in different ageing conditions

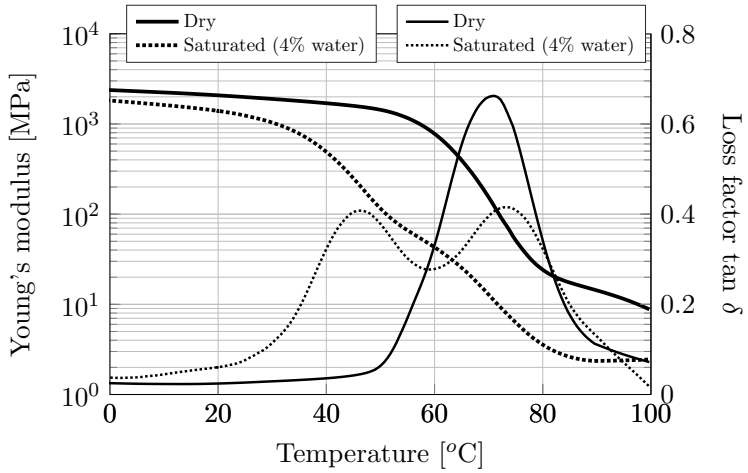

Figure 4.18: Comparison between the evolution of the Young's modulus of a dried sample and an immersed saturated sample

saturated sample (4% water) can be observed in *Fig.*4.18. Moreover, the right ordinate axis corresponds to the loss factor $tan\delta$ for each condition.

It is important to notice that the measured value of the Young's modulus at 21^oC, for a dried sample, is equivalent to the value obtained using a monotonic tensile test. This result shows a good correlation between the DMTA analysis and monotonic tests.

For the dried sample, the value of Tg calculated on the highest point of the loss factor $tan\delta$ is equal to 69^oC. This value seems to be slightly higher than the Tg measured with DSC (60^oC). In the case of an immersed saturated sample (4% water), the Tg (determined on the highest point of the loss factor) is calculated around 45^oC which is also slightly higher than the one measured by DSC (41^oC). This can be explained by the fact that, using a temperature rate of $2^oC/min$, some water has been evaporated during the test.

Table 4.3: Water uptake at saturation for different ageing conditions

Saturated condition	**0**	**32%RH**	**50%RH**	**75%RH**	**Immersion**
Water uptake	0%	0.45%	1.46%	2.05%	4%

A DMTA analysis was also performed on samples saturated at different relative humidities (32%RH, 50%RH and 75%RH). For the readability of the results they are presented separately

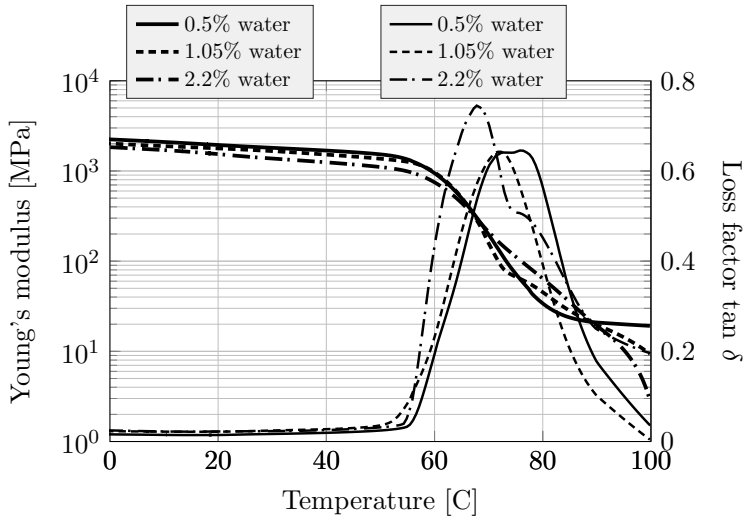

Figure 4.19: DMA analysis on samples saturated with different quantities of water and constant profiles

in *Fig.*4.19. For ease of understanding and to make the results more relevant, it should be remembered that these results correspond to samples saturated with different quantities of water (*Tab.*4.3) and a constant profile of water.

The Young's modulus at 21^oC can also be related to the one measured in tensile tests on samples saturated with the same quantities of water but the evolution of the Tg is different from the one observed in DSC. This may be related to the fact that even though the tests were performed in a conditioning chamber, the water evaporates during the test.

4.9 Creep tests at different constant water content

As presented in *Chapter* 3 the viscoelastic part of the proposed model need to be identified on creep tests. In order to give a dependency of each viscoelastic parameter as a function of water content, creep tests have also been performed on bulk samples saturated in different ageing conditions.

4.9.1 Tensile creep behaviour

The samples used for this study have exactly the same geometry as those used to characterise the creep behaviour in the dry state (*Fig.*2.9) and they were obtained in the same manner. Knowing the thickness of of the samples (1mm) it was possible to estimate the times needed until saturation for each ageing condition. They were then tested using the same device as the one presented in Chapter 2.2.4.

In order to be consistent with the tests performed on dry samples, three load levels, below the elastic threshold, were applied. These loads represent 25%, 50% and 75% of the elastic threshold determined in monotonic tensile tests calculated for each ageing condition.

Knowing that the presence of water results in a decrease of the elastic threshold from 34MPa to 12MPa (*Fig.*4.13a), the load levels were updated for each condition. In *Fig.*4.20a the three

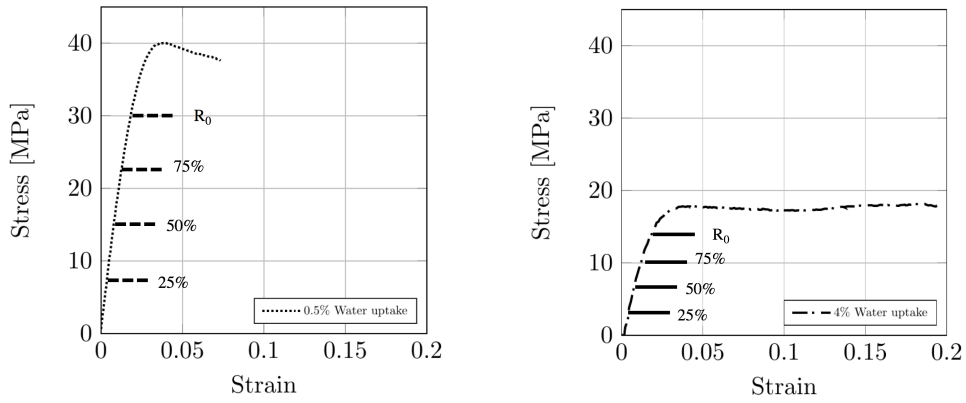

(a) Saturated at 32%RH - constant water profile

(b) Saturated in immersion - constant water profile

Figure 4.20: Tensile creep load levels for different ageing conditions

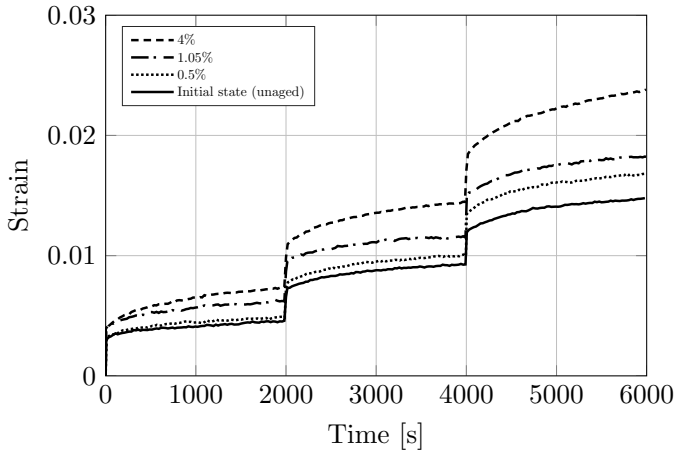

Figure 4.21: Tensile creep results for different water contents

load levels are shown, corresponding to samples with a constant profile of water and 0.5% water content (saturated at 32%RH) in comparison with the load level calculated for the samples saturated in immersion (4% water content and constant profile)

It is important to notice the results observed in *Fig.*4.21. Even though for each condition, the three load levels correspond to the same percentage of the elastic threshold, the corresponding strain for each level increases with the amount of water. This is consistent with the results observed in monotonic tensile tests. The presence of water increases the strain at break (*Fig.*4.13a).

4.9.2 Shear creep behaviour

The shear creep behaviour was studied using the same experimental approach as it was used to characterise the initial state of the adhesive. The samples have a thickness of 1mm and their geometry is equivalent to that presented in Section 2.2.3.

For these tests, four levels of load have been applied. They represent 20%,40%,60% and

80% of the elastic limit in monotonic shear stress. Each load level was applied for a period of 2000s.

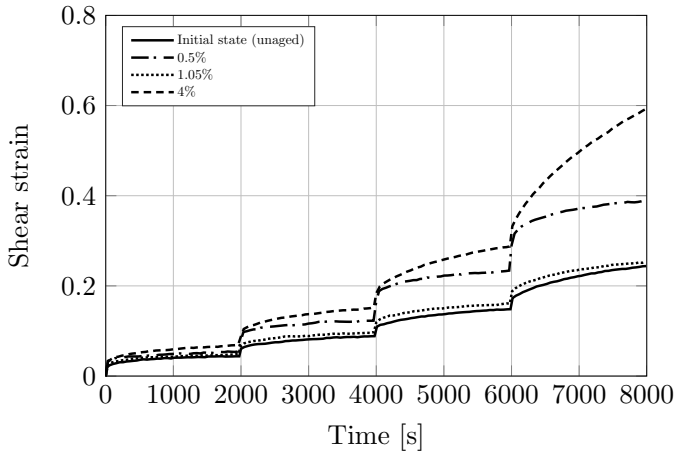

Figure 4.22: Shear creep results for different water contents

In the case of the shear creep behaviour, the observed shear strains are more important than in tensile creep behaviour. The water increases the mobility of the adhesive which leads to important shear strain for specimens with 4% water content.

4.10 Overview

In the first part of this chapter, it has been shown that water diffuses into the adhesive through a Fickian mechanism and the material absorbs up to 4% when immersed in sea water. The presence of water leads to an increase in mobility of the macromolecular chains and a decrease in Tg from 66^oC to 41^oC, this phenomenon is well known as plasticization.

Large changes in mechanical behaviour are induced by the plasticization: a decrease in stiffness as well as yield stress and an increase in strain at break and Poisson's ratio.

The increase in the Poisson's ratio can be explained by the fact that the polymer tends towards its rubbery behaviour when Tg decreases. It is worth noting that the degradation observed here is fully reversible (*Fig.*4.15) meaning that plasticization is the only mechanism involved (for the ageing conditions used in this study)

The experimental tests involved in this chapter will be used to determine the evolution of each of the parameters of the developed previously as a function of water content. The identification method will be presented in the next chapter.

Chapter 5

Modelling the water diffusion and its consequences on the mechanical behaviour of the adhesive

"Theory consists of putting in a coherent order a group of ideas who are or will be compared with experimental results."

Anatole Abgragam

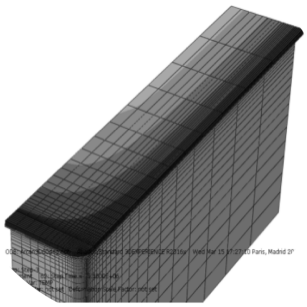

Water diffusion in Arcan specimen

The first objective of the present chapter is the development of a diffusion model capable of predicting the kinetics of water diffusion in the adhesive. In a second step, using the inverse identification procedure and the experimental tests performed on aged bulk samples, each model parameter will be described as a function of water content.

Contents

5.1 Prediction of water diffusion in a bulk sample **144**
5.2 Evolution of elastic parameters with water content **148**
5.2.1 Description of elastic modulus changes with water content 148
5.2.2 Description of Poisson's ratio changes with water content 148
5.3 Viscoelastic parameters as a function of water content **150**
5.3.1 Spectrum parameters with water content: n_0, n_c 150
5.3.2 Linear viscoelastic parameters versus water content: a_D, a_H 153
5.3.2.1 Finite element models used in the identification procedure . 154
5.3.2.2 Evolution of linear parameters with water content 154
5.3.3 Non-linear viscoelastic parameters as a function of water content . . . 155
5.4 Viscoplastic parameters as a function of water content **155**
5.4.1 Yield stress evolution 155
5.4.1.1 Physical considerations 155
5.4.1.2 Validation using tensile tests at different temperatures . . . 156
5.4.2 Evolution of the yield function 157
5.4.3 Evolution of hardening parameters 158
5.5 Mechanical behaviour of an aged bulk specimen before saturation **159**
5.5.1 Coupling the diffusion model with the constitutive law 159
5.5.2 Validation tensile tests during ageing in seawater 159
5.5.3 Validation of the approach 161
5.5.4 Limits of prediction 161
5.6 Modelling the water diffusion in a bonded joint **162**
5.7 Aged bonded joints with a constant water profile **164**
5.7.1 Prediction of the mechanical behaviour 164
5.7.2 Experimental tests used for validation 164
5.7.3 Discussion of the results 165
5.7.3.1 Residual stress in the specimens 165
5.7.3.2 Swelling 166
5.7.3.3 Physical ageing 166
5.7.3.4 The interface role 166
5.7.4 Comparison between model prediction and experimental results 167
5.8 Aged bonded joints with a profile of water in the adhesive layer **167**
5.8.1 Modelling the mechanical behaviour 168
5.8.2 Comparison between model prediction and experimental results 168
5.8.3 Overview 169

5.1 Prediction of water diffusion in a bulk sample

The prediction of water uptake through the thickness of a sample represents a first step in the development of a rapid method to predict the water effects on the mechanical behaviour of bonded joints. It can be done using a typical Fickian behaviour coupled with a FE model.

The development of the numerical diffusion model was based on the equivalence of water diffusion and heat transfer. The analogy between Fick's law and heat diffusivity is made using *Eq.*5.1 which connects the diffusion coefficient D to the heat conductivity λ, specific heat c, and density ρ, of the material. This approach was adopted by many authors, especially to describe the water diffusion in polymer composite materials [176][111].

$$D = \frac{\lambda}{\rho c} \tag{5.1}$$

The model was implemented in $Abaqus^{TM}$ software. This approach was validated by modelling the water diffusion in a square sample with the same geometry as that used to identify the water diffusion experimentally. The results obtained for an immersed sample in seawater at 40^oC were used as reference. For this particular case, the diffusion coefficient of the water was analytically calculated as equal to $1.1 \times 10^{-12} m^2/s$ (*Tab.*4.1).

For the simulation, the value of the specific heat c was taken from the literature (a standard value for epoxy adhesives) and the density ρ was determined using a pycnometer. The heat conductivity is given by *Eq.*4.2. Each parameter used in these calculations is represented in *Tab.*5.1 (consistent units for *Abaqus* software).

Table 5.1: Material characteristics used in simulation

Parameter	Symbol	Value	Unit
Diffusion coefficient	D	1.1e-7	$mm^2 s^{-1}$
Heat conductivity	λ	2.25e8	$mW mm^{-1} K{-}1$
Specific heat	c	1.8e9	$mJ tonne^{-1} K^{-1}$
Young's modulus	E	1850	MPa
Poisson ratio	ν	0.39	-
Density	ρ	1.075e-6	$tonne\ mm^{-3}$

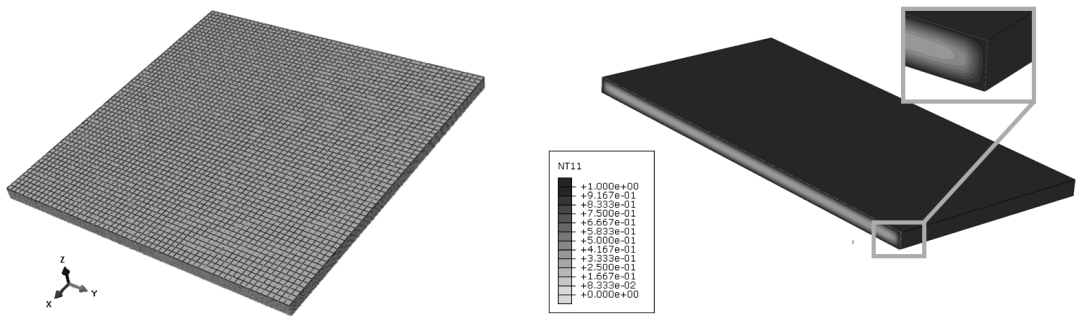

(a) Isometric view of a meshed square sample of adhesive

(b) Cut through half of a square sample during water diffusion

Figure 5.1: 3D finite element model used for diffusion law validation

The finite element model, meshed with 8 node convection/diffusion type elements DCC3D8, used for these calculations is shown in *Fig.*5.1a. A uniform temperature with a magnitude of 1 is applied as boundary condition on all the faces of the sample, a capture during the diffusion being represented in *Fig.*5.1b. The legend of the figure (variable NT11) represents the normalized relative concentration of water at a specific moment. The relative concentration of water through the sample C_r was calculated using a *UVARM* routine which allowed a sum to be made for each element, the product of the concentration c_i and its volume v_i and divided by the volume of the sample (*Eq.*5.2).

$$C_r = \frac{\sum_{i=1}^{n} c_i v_i}{\sum_{i=1}^{n} v_i} \tag{5.2}$$

where n represents the number of elements in the model.

Finally, water uptake of the sample M_t, in percentage, can be determined by multiplying the relative concentration C_r by the saturated mass M_∞ observed experimentally (in this case equal to 4%). (*Eq.*5.3). This approach was also applied with good results by *Arnaud* [21] and *Tual* [176] in their studies.

$$M_t = C_r \times M_\infty \tag{5.3}$$

Before comparing the water uptake prediction with the experimental results, a mesh convergence study has been performed. For short periods of water exposure, the prediction is very sensitive to the number of elements used in the simulation, especially through the thickness of the sample. *Fig.*5.2 presents three different meshes used for comparison.

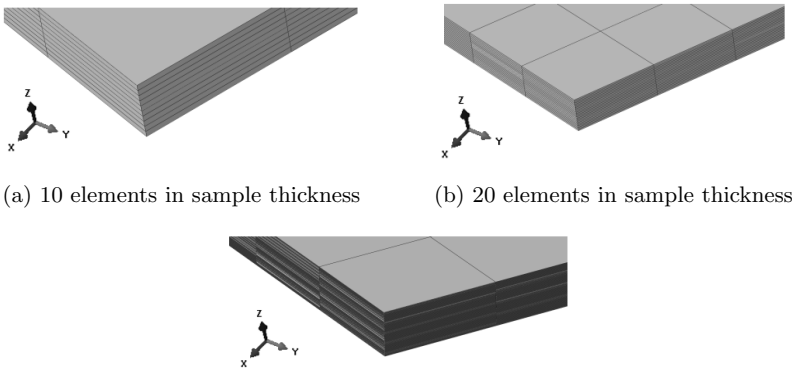

(a) 10 elements in sample thickness (b) 20 elements in sample thickness

(c) 100 elements in sample thickness

Figure 5.2: 3D finite element model used for diffusion law validation

As can be observed in *Fig.*5.3a the model prediction of water uptake fits accurately the experimental data obtained by weighing. Moreover, the results for the three types of meshes used in the study are superposed above 1% of water uptake.

The influence of the number of elements in the sample thickness becomes important when modelling the water diffusion for short immersion times (below 1%). The element discretization will cause a gap, just at the beginning of the prediction (*Fig.*5.3b). Increasing the number of elements will improve the model prediction. For the next studies, 100 elements were used.

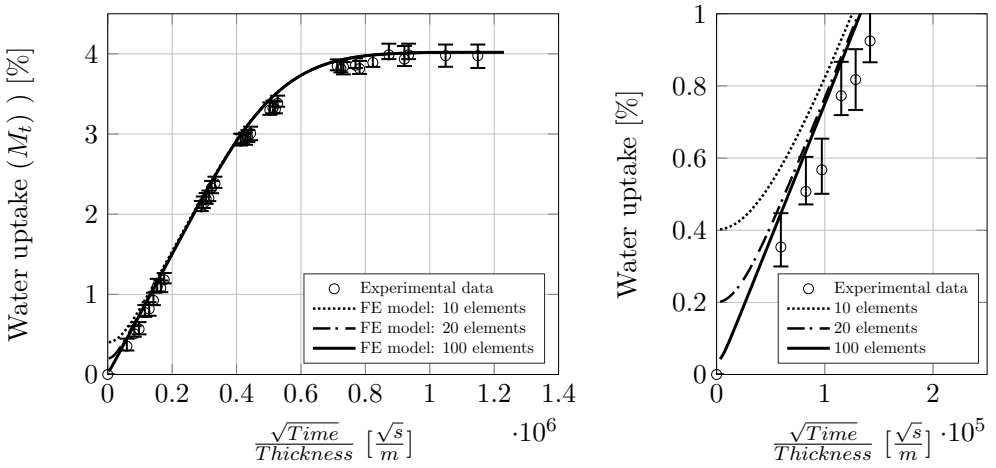

(a) FE model prediction against the experimental results for a sample immersed in water at 40^oC

(b) Convergence study for water uptake prediction

Figure 5.3: 3D finite element model used for diffusion law validation

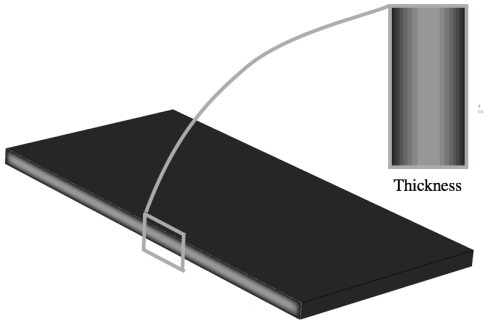

Figure 5.4: Detailed cross-section of the water profile through the section of a sample

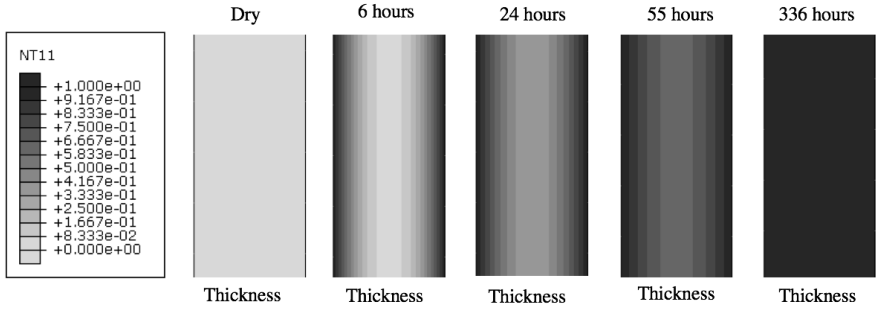

Figure 5.5: Evolution of the water profile in the cross-section of a square sample exposed at different water ageing times

Once the diffusion law was validated using the comparison between the prediction of total water uptake in samples with the experimental results, it was possible to plot the water profiles through the thickness during different immersion times. Three intermediate times were chosen between the dry state and completely saturated. These times correspond to 6 24, 55 hours of

exposure in seawater at 40^oC. *Fig.*5.4 and *Fig.*5.5 present a detailed cross-section of the water profile in a sample together with the profiles for the studied exposure times.

Moreover, the local water profiles for the three immersion durations can also be represented in the same figure as shown in *Fig.*5.6. Using this method, it is possible to predict the quantity of water in the adhesive as a function of thickness and external environment (for different water temperatures by changing the diffusion coefficient and relaunching the simulation).

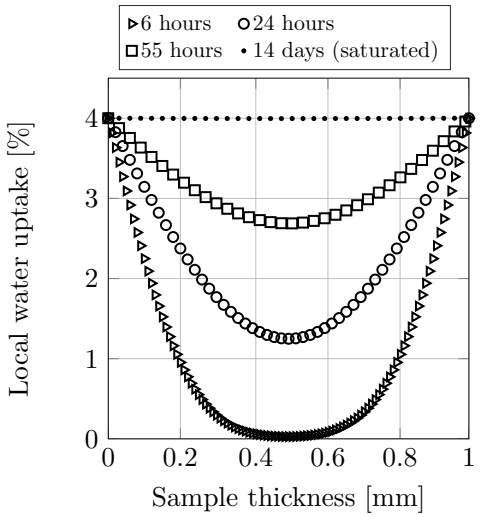

Figure 5.6: Prediction of local water profiles through thickness for the adhesive immersed in seawater at 40^oC

The diffusion model is now validated and it can be used to model the water diffusion in different geometries without being dependent on the thickness of the material. Furthermore, the local water profiles can be characterised.

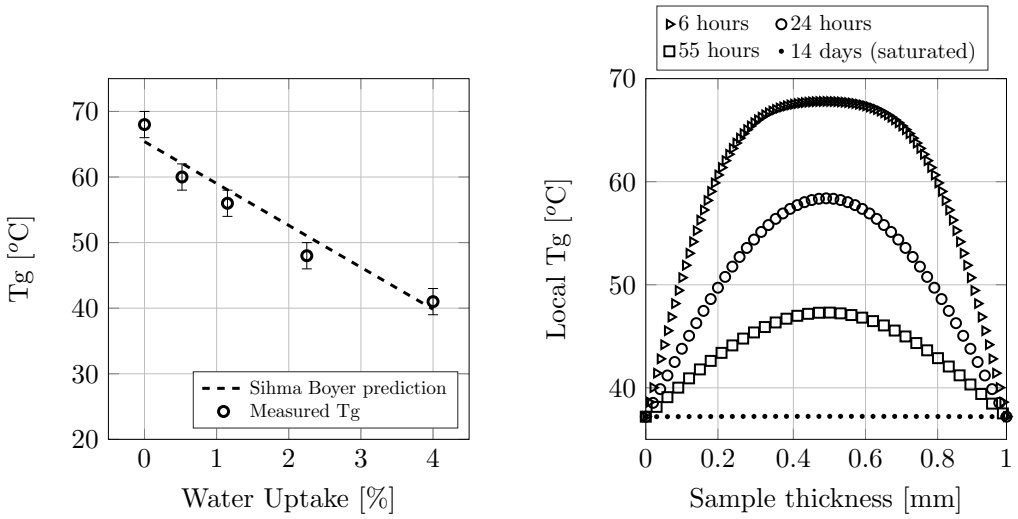

(a) FE model prediction against the experimental results for a sample immersed in water at 40^oC

(b) Local Tg through the thickness of a sample for different immersion durations

Figure 5.7: Evolution of Tg through the thickness of an aged sample

Moreover, the evolution of the Tg as a function of water content can be predicted using a Sihma-Boyer law (*Fig.*5.7a). This has been coupled with the diffusion model and allows a prediction of the local evolution of the Tg, through the thickness of a sample, as a function of water content. For different immersion times, the local Tg is plotted in *Fig.*5.7b. This important result can be used to link the evolution of some mechanical properties, such as the yield stress, to physical considerations.

In the next section, the study will be focused on the evolution of each model parameter developed in *Chapter* 3, as a function of water content. This will allow the diffusion approach to be coupled with the mechanical one in order to finally be able to predict the mechanical behaviour of a bonded joint. For this, the experimental tests performed on samples with constant water profiles aged in different environmental conditions (32%RH, 50%RH, 75%RH and immersion) will be used for identification.

5.2 Evolution of elastic parameters with water content

5.2.1 Description of elastic modulus changes with water content

As discussed previously, the changes in the elastic modulus with respect to the water uptake are identified using the tensile tests performed on samples saturated at 40^oC in different environmental conditions (32%RH, 50%RH, 75%RH and immersion). For each condition, the amount of water absorbed is different but the samples, being saturated, present a constant water profile.

*Fig.*5.8a presents the evolution of the water uptake as a function of ageing condition, defined here as the water activity (*e.g.* 0.5 water activity is equivalent to a relative humidity of 50%). The elastic modulus was calculated using the slope of the obtained stress-strain curves presented in *Fig.*5.8b.

The presence of water leads to a decrease in Young's modulus that can be explained by two main phenomena; the decrease in Tg and a decrease of the secondary transition as was observed in the previous chapter. Unfortunately, due to the presence of these two mechanisms this behaviour cannot be described easily using physical considerations, thus an empirical relationship (*Eq.*5.4) was used to relate water content and the Young's' modulus value:

$$E = 1850 - 220 \times W_{H_20} \qquad [MPa] \tag{5.4}$$

where E is the Young's modulus in MPa and W_{H_20} is the water content in the adhesive, in %.

This basic relationship is plotted in *Fig.*5.9a and compared to experimental results. It appears that despite its simplicity, it is useful to describe the Young's modulus loss. However, it is important to note that this relationship is only valid for a given test temperature, here 21^oC. It cannot be used to predict the evolution of properties at any other temperature.

5.2.2 Description of Poisson's ratio changes with water content

With the presence of water that leads to a decrease of Tg, the adhesive tends to move from glassy to rubbery behaviour. This leads to an increase of the Poisson's ratio that becomes

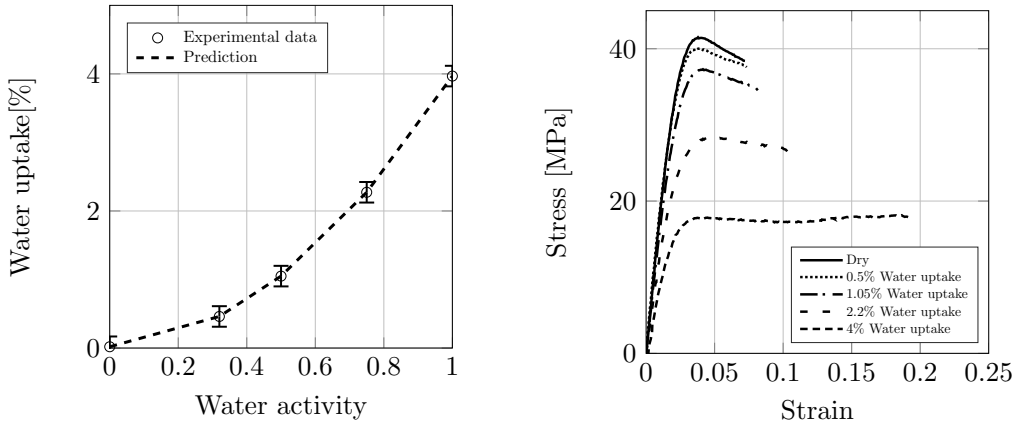

(a) (b)

Figure 5.8: (a) Water uptake at saturation for different environmental conditions, (b) Tensile test on sample saturated in different environments

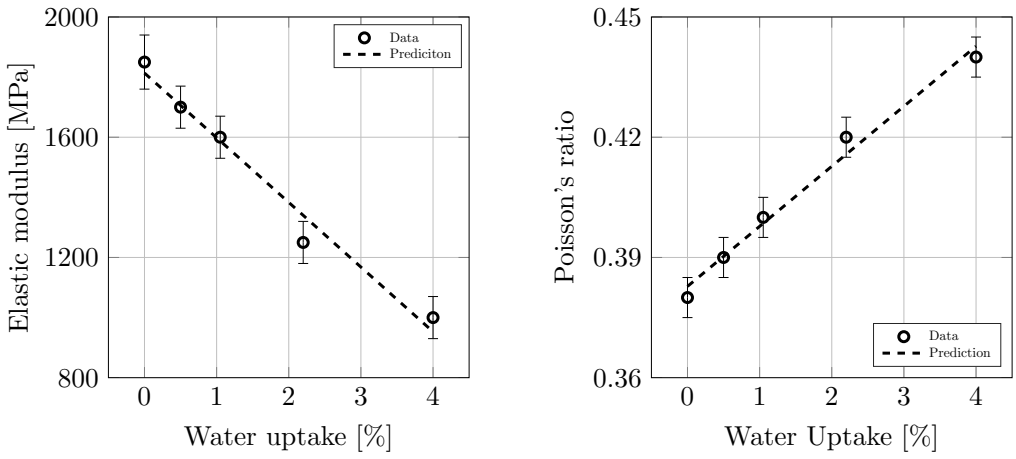

(a) (b)

Figure 5.9: (a) Evolution of the elastic modulus with water content, (b) Evolution of Poisson ratio with water content

closer to 0.45, the value for a rubber. Here again this increase has been described using a linear empirical relationship:

$$\nu = 0.395 + 0.015 \times W_{H_2O} \tag{5.5}$$

where ν is the Poisson's ratio and W_{H20} is the water content in the polymer in %.

*Fig.*5.9b shows that (*Eq.*5.5) can describe the increase in Poisson's ratio with water content at 21^oC, but again only for this temperature.

5.3 Viscoelastic parameters as a function of water content

In order to be able to predict the mechanical behaviour of a bonded joint using the model presented in *Chapter* 3 it is also important to characterise the evolution of the viscoelastic parameters of the model. The influence of water content will be analysed separately for each of three groups (*spectrum, linear and non-linear*) of viscoelastic parameters.

5.3.1 Spectrum parameters with water content: n_0, n_c

As presented in *Section* 3.2.3 the spectrum parameters were identified using the experimental creep tests performed using the Arcan device on the bonded specimens. It was also shown in *Fig.*3.14*b* that the *isochronism* principle could be respected for the four shear creep levels. This means that the normalised viscous displacements of each creep level (*Eq.*3.15) and the corresponding normalised time (*Eq.*3.16) are superposed and they are defined by the same *Master curve* (*Fig.*3.14*b*).

In this approach, the spectrum is described using the creep tests performed on bulk samples. First, a comparison between the spectrum identified using the Arcan device (on unaged samples) and the spectrum defined by tensile and shear creep tests realised on unaged bulk samples (dried) is made. This allows the adhesive creep behaviour in a bonded joint and as a bulk specimen to be compared.

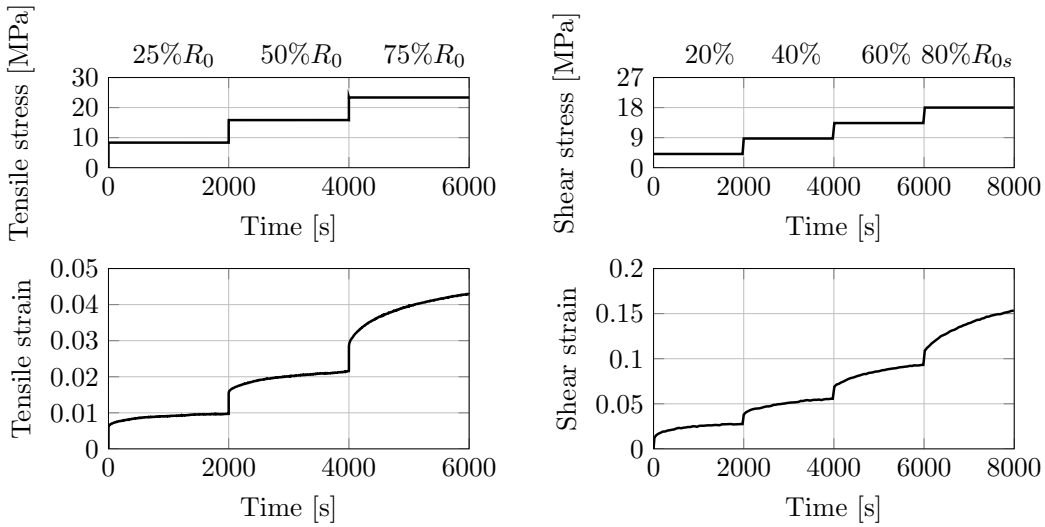

(a) Tensile creep behaviour performed on unaged bulk specimen

(b) Shear creep behaviour performed on unaged bulk specimen

Figure 5.10: Creep behaviour performed on dried samples

The application of the *isochronism* principle was tested for the creep behaviour of the bulk samples. For this study, the tensile and shear creep tests performed previously on dried samples were used (*Fig.*5.10). The viscous strain $\varepsilon^i_{viscous}$ and the duration t^i for each creep level ($i = 1:3$ for multiple tensile creep and $i = 1:4$ for multiple shear creep tests) were normalised using the *Eq.*5.6 and *Eq.*5.7.

$$\varepsilon^i_{viscous_{norm}} = \frac{\varepsilon^i_{viscous}(t) - \varepsilon^i_{viscous}(t^i_{begin})}{\varepsilon^i_{viscous}(t^i_{end}) - \varepsilon^i_{viscous}(t^i_{begin})} \tag{5.6}$$

$$T^i_{norm} = \frac{t - t^i_{begin}}{t^i_{end} - t^i_{begin}} \tag{5.7}$$

where t^i_{begin} is the time at the beginning of i^{th} creep level, t^i_{end} the time at the end of the same creep level.

The results obtained were plotted in the same figures (*Fig.*5.11). As shown in *Fig.*5.11a for tensile and in *Fig.*5.11b for shear behaviour, the curves corresponding to each level are superposed meaning that the *isochronism* principle is respected. However, it should be remembered that those creep tests were performed below the elastic threshold, which is an important condition to be fulfilled in order to obtain those results.

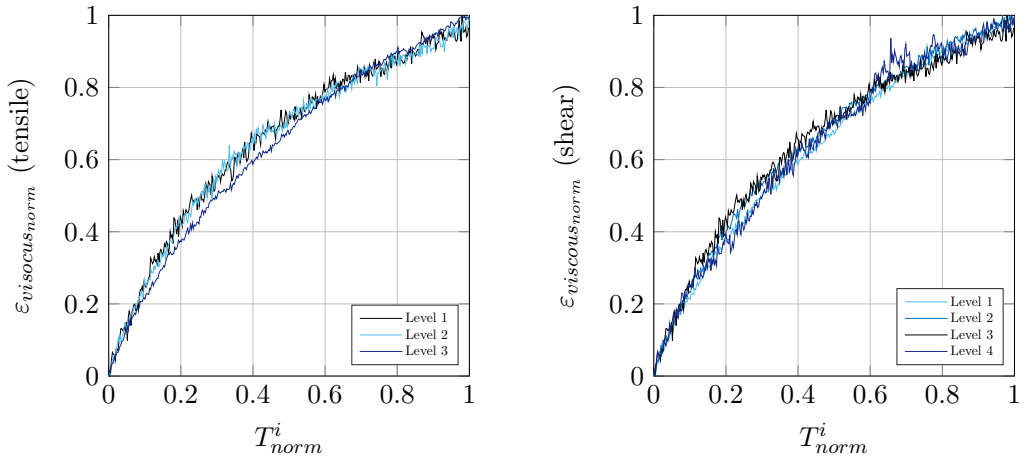

(a) Normalised viscous strains in unaged tensile creep behaviour

(b) Normalised viscous strains in unaged shear creep behaviour

Figure 5.11: Isochronism principle

The *isochronism* principle being validated on bulk samples, the normalised curves of the first creep level in tensile and shear behaviour were compared with the *Master Curve* obtained from the creep tests performed using the *Arcan* device (*Fig.*3.14*b*). Because the curves were normalized, the *Master curve* obtained using the viscous displacement (*Fig.*3.14*b*) can be compared directly with the curves obtained from normalising the viscous strains calculated using the bulk creep tests and it does not depend on the geometry of the sample since it is normalised.

Moreover, it should be noted that this *Master Curve* is defined by the spectrum parameters (n_0,n_c) identified previously in *Chapter* 3.2.3. As shown in *Fig.*5.12, the normalised strains in the two cases (tensile and shear) are superposed with the *Master curve* meaning that the spectrum parameters don't change between the bonded joint and bulk behaviour at unaged state.

The influence of water on the spectrum parameters was characterised by applying the same approach on the observed creep behaviour of saturated samples in immersion (4% water content). For comparison, the results are plotted in *Fig.*5.13 together with the unaged behaviour.

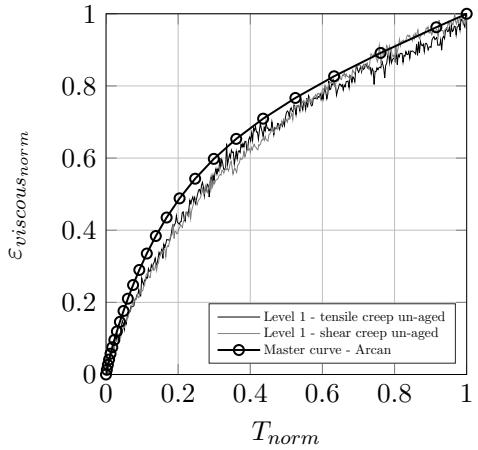

Figure 5.12: Comparison between normalised strain of the first bulk creep level and the *Master curve*

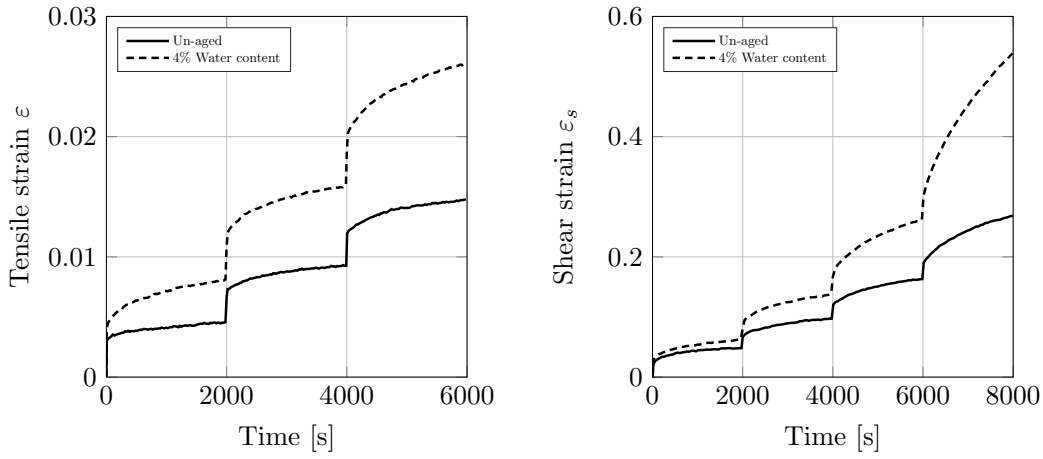

(a) Tensile creep behaviour of bulk samples

(b) Shear creep behaviour of bulk samples

Figure 5.13: Comparison between aged and unaged creep behaviour

Using the approach described previously, the *isochronism* principle is also respected for the aged specimens. These results permitted the comparison of the normalised viscous displacements of the aged specimens with the unaged ones.

Once again, the normalized curves obtained from the creep tests performed on aged and unaged sample are superposed. Thus, a first conclusion can be made: the spectrum parameters are not influenced by the quantity of water in the material and so, by the ageing conditions. Since the samples saturated in immersion were used in this analysis (those with 4% of water content at saturation), the next assumption has been made: a lower quantity of water in the adhesive will not affect the spectrum parameters. Thus, for the prediction of mechanical behaviour of water aged bonded joints, the spectrum parameters will not be modelled as a function of water content.

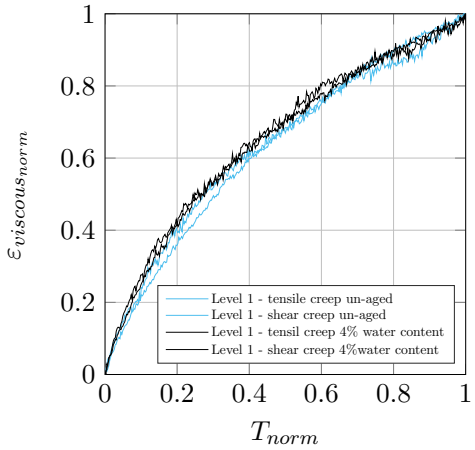

Figure 5.14: Normalised viscous strains in tensile creep behaviour

5.3.2 Linear viscoelastic parameters versus water content: a_D, a_H

Because the boundary conditions of the experimental device used for these tests allowed it, the deviatoric parameter a_D is identified first using the first creep level of each ageing condition (*Fig.*5.15a). Second, the hydrostatic parameter a_H was identified using the same approach on the tensile creep tests (*Fig.*5.15b).

For each case, the results obtained using saturated samples in four ageing conditions (initial state, 32%RH, 50%RH and completely immersed samples) (*Fig.*5.15a) were used. These conditions correspond to different water quantities in the sample, respectively: 0%, 0.5%, 1.05% and 4%.

It should be noted that the Young's modulus and the Poisson's ratio have been adopted for each ageing condition as they have been identified previously.

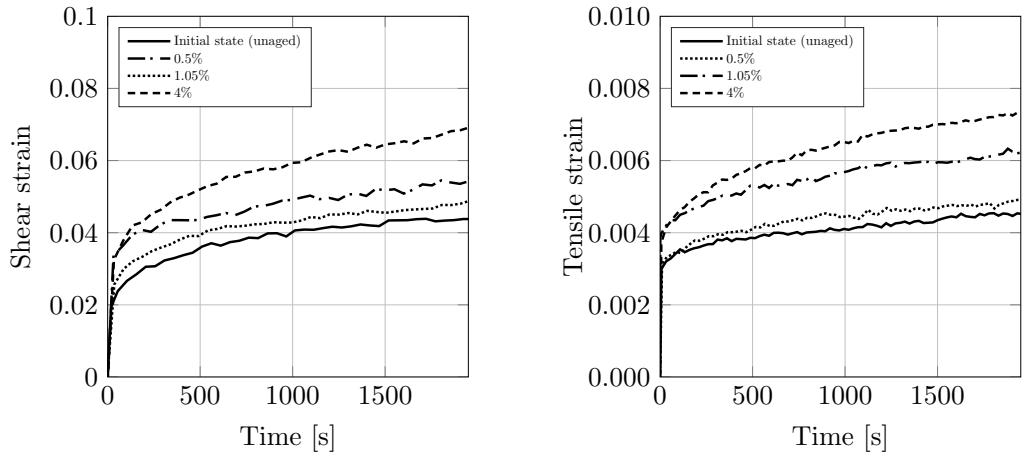

(a) (b)

Figure 5.15: First creep levels obtained in (a) shear and (b) tensile tests performed on bulk samples saturated with different water contents

5.3.2.1 Finite element models used in the identification procedure

These two parameters were identified using the inverse identification procedure as it was presented in *Section* 3.2.3.2. Two finite elements models were used in this step.

Since the shear creep tests were performed using exactly the same samples and experimental device as the monotonic shear tests, the FE model presented in *Section* 3.4.2 was utilised in the inverse identification procedure of the deviatoric parameter a_D. However, the boundary conditions were updated for this type of tests.

For the identification of the hydrostatic parameter a_H, a FE model equivalent to the experimental conditions has been developed. As specified in *Chapter* 2, the fixture used to perform the creep tensile tests is composed of the fixed lower head and the upper head which is mobile (*Fig.*5.16a). The specimens have a rectangular shape, a thickness of 1mm and the boundary conditions were applied as shown in *Fig.*5.16b. C3D8R elements with hourglass control and reduced integration were used in these calculations and only one element in the thickness of the model (z direction, *Fig*5.16b).

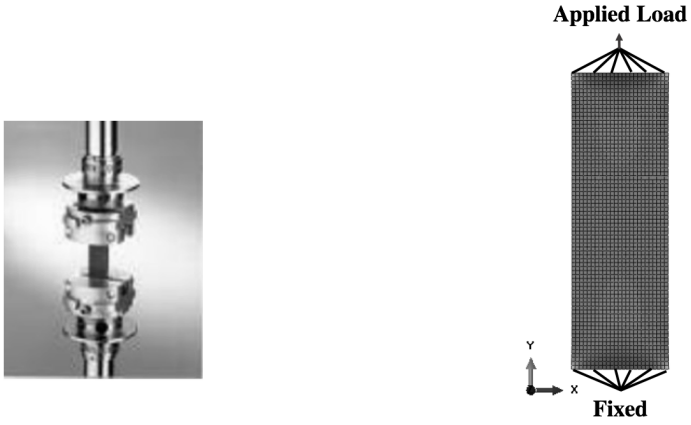

(a) (b)

Figure 5.16: (a) Fixture used to characterise the tensile creep behaviour and (b) the FEM used in the inverse identification procedure

5.3.2.2 Evolution of linear parameters with water content

The evolution of the parameters that define the linear viscosity in both cases (hydrostatic a_H and deviatoric a_D) is represented in *Fig.*5.17a and *Fig.*5.17b as a function of water content.

For both parameters, a linear function has been used to model their evolution with water content (*Eq.*5.8 and *Eq.*5.9).

$$a_D = 1500 - 200 \times W_{H_2O} \qquad [MPa^{-1}] \tag{5.8}$$

$$a_H = 1800 - 250 \times W_{H_2O} \qquad [MPa^{-1}] \tag{5.9}$$

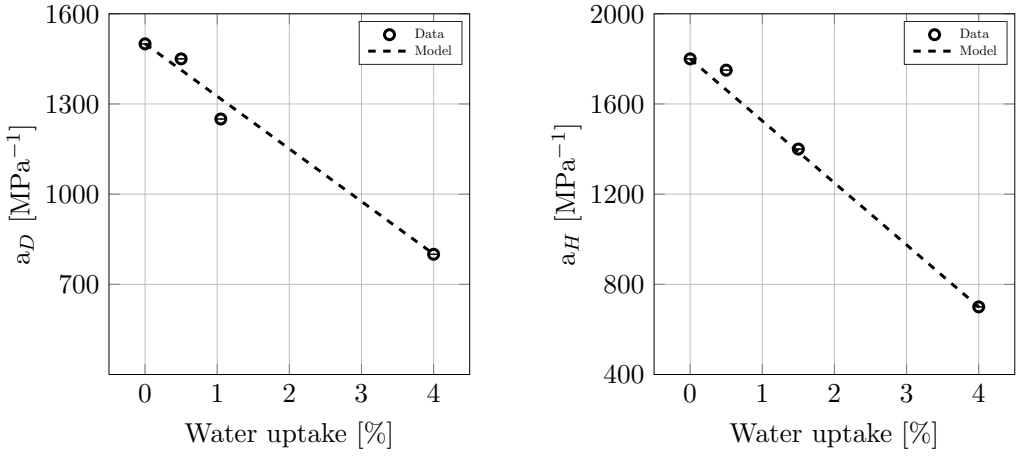

(a) Deviatoric linear viscosity

(b) Hydrostatic linear viscosity

Figure 5.17: Evolution of the linear viscosity parameters with water content

5.3.3 Non-linear viscoelastic parameters as a function of water content

The last set of parameters of the viscoelastic part of the model were also identified using the inverse identification method. The limits y_D^0 and y_H^0 were determined by applying the approach presented in *Chapter* 3.2.3.3. It should be noted that the parameters Y_D^c and y_H^c that defined the kinetics of the last tested shear and tensile creep test were not considered to be dependant on water content.

5.4 Viscoplastic parameters as a function of water content

5.4.1 Yield stress evolution

5.4.1.1 Physical considerations

Prediction of the yield stress was possible based on physical considerations. In fact, it has been shown that the yield stress is strongly affected by the mobility in polymer molecules and, moreover, is directly proportional to the difference between the polymer Tg and the testing temperature.

Because it is possible to model the water diffusion in the epoxy through the thickness (*Fig.*5.6), and the Tg can be related to water content through the Simha-Boyer equation (*Fig.*5.7a), it was possible to predict the local value of Tg (*Fig.*5.7). Moreover, once the Tg was known it was possible to calculate the local value of yield stress using the Eyring relationship that has been checked experimentally for several polymers [39][40][41]:

$$\sigma_y = A \times (Tg - T_{test}) + B \tag{5.10}$$

where Tg is the transition glass temperature of the adhesive and T_{test} is the testing temperature.

Using the tensile results obtained on dry samples and samples saturated at several levels of water content (*Fig.*5.8b), tested at room temperature, it is possible to show that the Eyring

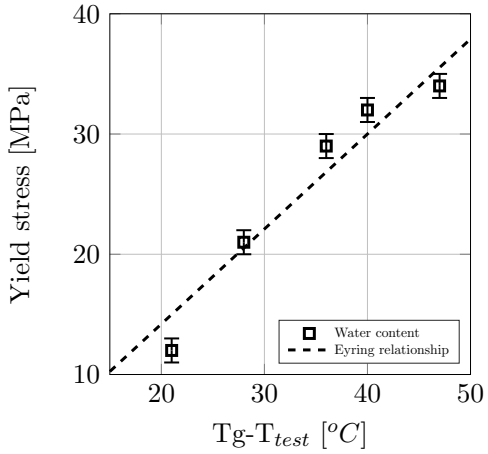

Figure 5.18: Relationship between yield stress and Tg-T obtained from tensile tests with several water contents at 21^{o}C, and at several testing temperatures on dry specimens

relationship is verified here (*Fig.*5.18) with A equal to 0.77 and B equal to 0.2. The correlation factorR^2 is equal to 0.97 based on experimental results.

5.4.1.2 Validation using tensile tests at different temperatures

Since the presence of water increases the mobility of the polymer chains, it leads to large changes in mechanical behaviour. An alternative way to increase the mobility was then investigated, by increasing the testing temperature with dried samples.

When samples were tested at higher temperature the samples were held for 20 minutes in the thermal chamber, at the testing temperature, to homogenise the temperature in the thickness of the sample before testing. Moreover, by increasing the testing temperature T_{test}, the value of $Tg - T_{test}$ was also modified. Thus, these tests could also be used to validate the prediction of the yield stress using the Eyring relationship.

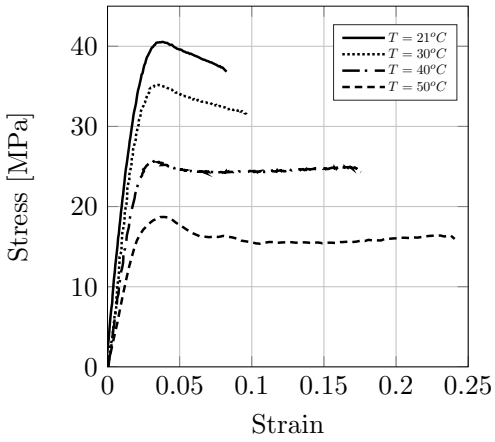

Figure 5.19: Tensile behaviour as a function of testing temperature on dry sample

Tensile results are plotted in *Fig.*5.19. Large changes in the tensile behaviour are induced by an increase of the testing temperature up to 50^{o}C (*i.e.* still in the glassy state). In fact, here

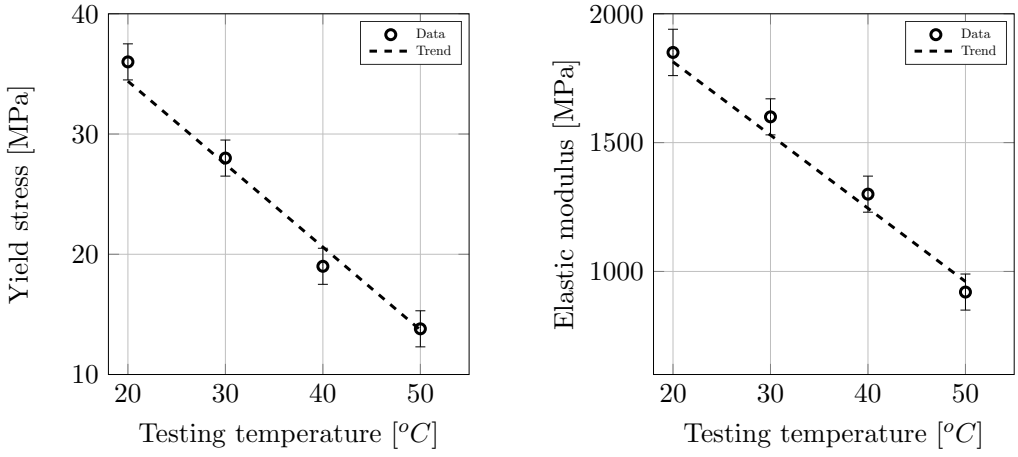

(a) Changes in yield stress

(b) Changes in elastic modulus

Figure 5.20: Evolution of the mechanical properties as function of testing temperature

again, a decrease in the yield stress and the elastic modulus is observed. These properties are plotted in *Fig.*5.20.

The values of the yield stress obtained for different testing temperatures were plotted in *Fig.*5.21 as a function of $(Tg - T_{test})$ together with the evolution of yield stress as a function of water content. As can be observed, they fit the prediction given by the Eyring relationship which allowed this approach to be validated once again.

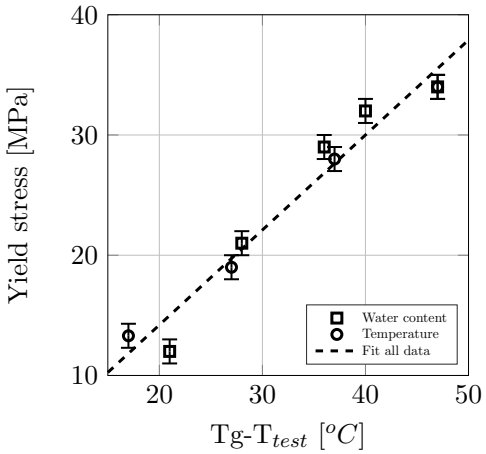

Figure 5.21: Relationship between yield stress and Tg-T$_{test}$ obtained from tensile tests with several water contents at 21^{o}C, and at several testing temperatures on dry specimens

5.4.2 Evolution of the yield function

The changes in yield function with water content is another important aspect to take into account when predicting the mechanical behaviour of a water-aged specimen. It should be remembered that the yield function is defined by the *von Mises stress* (σ_{VM}) and the *hydrostatic pressure* (σ_H). The form of the function is given by *Eq.*5.11:

$$f(\sigma_H, \sigma_{VM}) = \sigma_{VM} + a_1 \sigma_H \tag{5.11}$$

where a_1 is a coefficient determined as shown in *Section* 3.2.5. In the initial state (unaged), this coefficient (a_1=0.0023) was similar for the mechanical behaviour observed using both Arcan tests and bulk specimens.

Moreover, as shown (*Section* 5.3.5) the yield stress measured from the experimental tensile test performed on bulk specimens saturated in different ageing conditions can be expressed using physical considerations by defining it as a function of local Tg using the Eyring relationship. Similarly, it was defined as a function of water content using a linear equation (*Eq.*5.12) and represented in *Fig.*5.22a:

$$\sigma_y = 34 - 5.5 \times W_{H_20} \qquad \text{[MPa]} \tag{5.12}$$

where W_{H_2O} represents the water content in percent and σ_y the tensile yield stress.

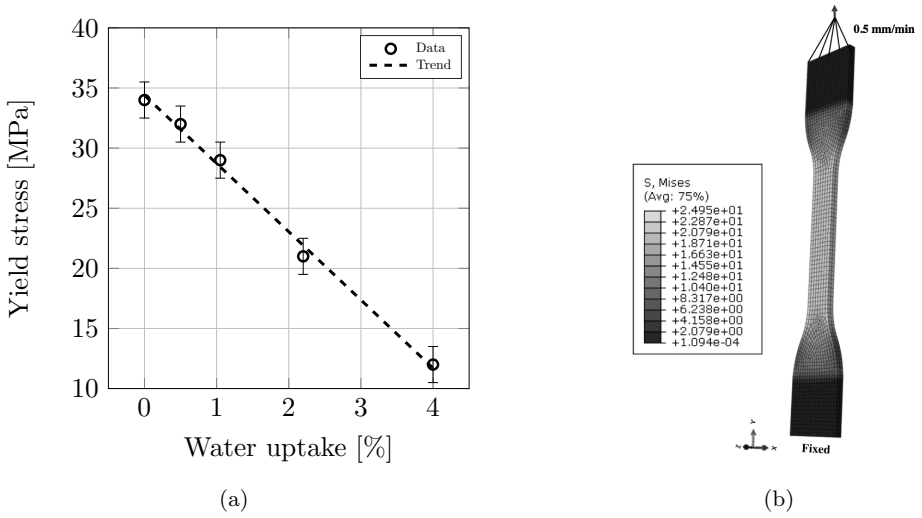

(a) (b)

Figure 5.22: (a) Evolution of the yield stress as a function of water uptake (b) Finite element model used for the identification procedure

In order to identify the evolution of the yield surface as a function of water content, the inverse identification method was used. For each yield stress determined experimentally, on specimens saturated with different water contents (0%, 0.5%, 1.05%, 2.25% and 4%), a coupled (σ_H, σ_{VM}) was associated via the FEM model presented in *Fig.*5.22b. Furthermore, the evolution of the yield function with water content (*Fig.*5.23) is described analytically using the equation (*Eq.*5.13) :

$$f(\sigma_H, \sigma_{VM}) = (32 - 4.75 W_{H_2O}) + 0.0023 \times \sigma_H^2 \quad \text{[MPa]} \tag{5.13}$$

5.4.3 Evolution of hardening parameters

To simplify the identification procedure, the hardening parameters were supposed to be not dependent on the water content, and the value identified using the Arcan tests (Chapter 3),

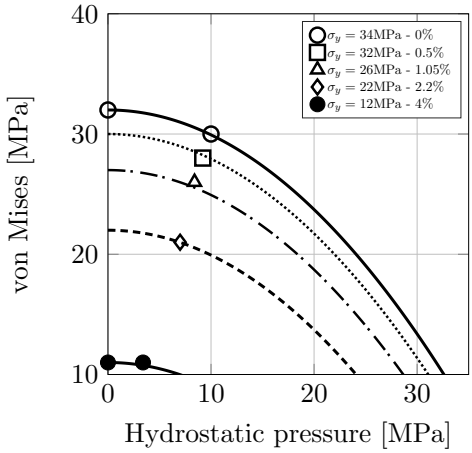

Figure 5.23: Changes in yield function for different water contents

which are equivalent to those used determined on bulk specimens were used in the next phase of this work.

5.5 Mechanical behaviour of an aged bulk specimen before saturation

5.5.1 Coupling the diffusion model with the constitutive law

Using the parameters identified in the previous section, it appears that a prediction of the tensile behaviour at 21^{o}C can be made during humid ageing: it may be possible to predict the water content through the thickness using the diffusion model. Knowing the local water content, it is then possible to define values for Young's modulus and Poisson's ratio using the empirical equations determined in *Section* 5.2. In parallel, it was possible to relate the water content to the Tg of the polymer and hence to define local yield stress using the physically based relationship (*Section* 5.4.1). The description of the other parameters of the model as a function of water content was made as shown in the previous sections.

The FEM model used in this simulation is represented in *Fig.*5.24. The H3 specimen was meshed with the same 8-node convection/diffusion type elements DCC3D8 as those used for validation of the diffusion model. One hundred elements were defined in the thickness. A water flow has been considered throughout the sample. Hence the water profiles were determined after different periods of time before complete saturation. Once the profiles were determined, the mechanical simulation was performed using the constitutive law together with the parameters depending on water uptake. The boundary conditions are the same as those presented in *Fig.*5.22b.

5.5.2 Validation tensile tests during ageing in seawater

The tensile behaviour of the bulk specimens was investigated after several immersion durations in sea water at 40^{o}C before saturation of the sample, meaning that in this case there was a

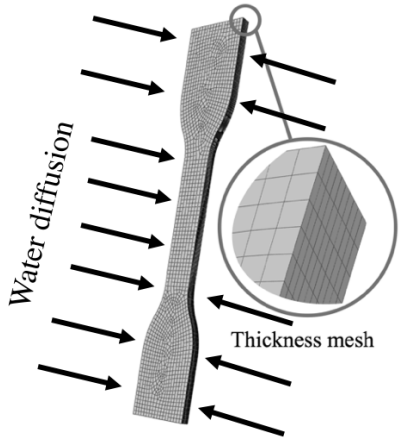

Figure 5.24: Water diffusion in a tensile sample

water-profile gradient through the specimen thickness. A summary of the samples tested is presented in *Tab.*5.2 and tensile behaviour is plotted in *Fig.*5.25. Here again the presence of water, even if there is a profile through the sample thickness, leads to a large decrease in elastic modulus and yield stress. An increase of strain at break and Poisson's ratio is also observed; all these values are plotted as a function of immersion time in *Fig.*5.26, *Fig.*5.27.

Table 5.2: Tests during ageing in seawater

Duration in sea water (40^{o}C)	**Amount of absorbed water (%)**
6 hours	1.0
24 hours	1.8
55 hours	2.8
336 hours	4.0

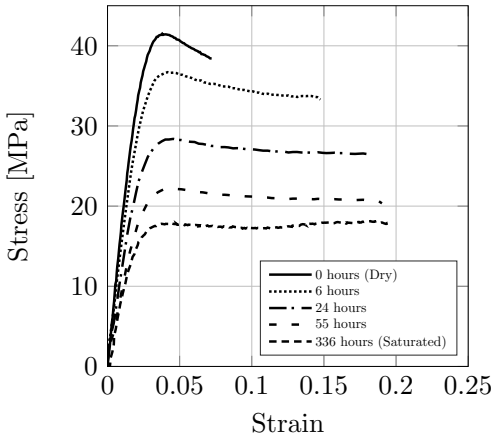

Figure 5.25: Tensile curves obtained for samples immersed in seawater at 40^{o}C for several durations

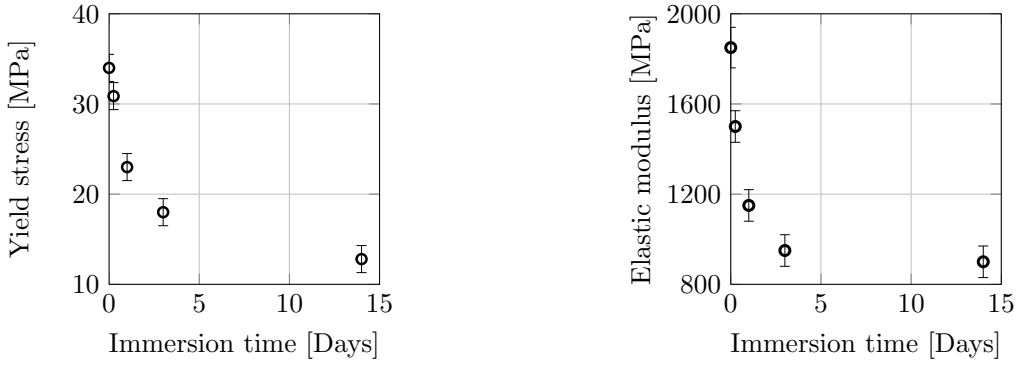

(a) Changes in yield stress

(b) Changes in the elastic modulus

Figure 5.26: Evolution of the mechanical properties as a function of immersion time

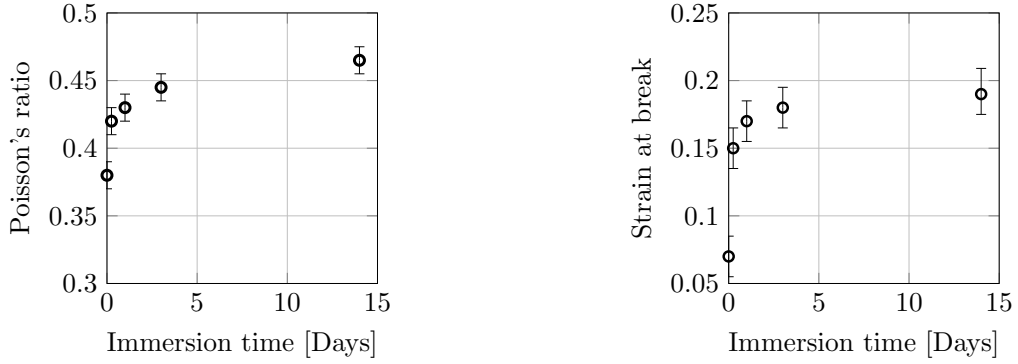

(a) Changes in Poisson's ration

(b) Changes of the strain at break

Figure 5.27: Evolution of the mechanical properties as a function of immersion time

5.5.3 Validation of the approach

The validity of this approach can now be considered by comparing experimental results obtained for different immersion durations in sea water (with water profile gradients) with predictions obtained by the model proposed here.

Results are plotted in *Fig*5.28. A good agreement is observed between the predicted tensile behaviour and experimental data.

5.5.4 Limits of prediction

As for all predictions of mechanical changes during ageing, the one that is proposed here has some limitations. First, this prediction is limited to a mechanical behaviour at room temperature because the temperature effect on Young's modulus and Poisson's ratio have not been considered here. Moreover, the model used here is not able to predict the strain at break, which is strongly affected by the presence of water. And finally, the relationships identified in this study depend on the nature of the polymer, meaning the approach developed here can be applied to other adhesives but it is not possible to directly use the values identified from this study.

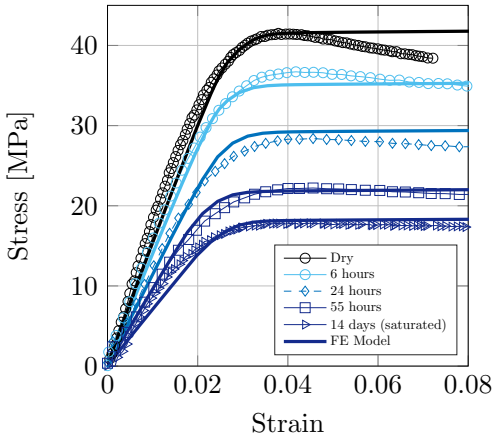

Figure 5.28: Comparison of predicted tensile behaviour (continuous lines) with experimental data (symbols) for different immersion times in seawater

5.6 Modelling the water diffusion in a bonded joint

The different tensile and shear tests (monotonic and creep) performed on bulk samples, as well as the study of the kinematics of diffusion, DSC and DMA tests, have led to a better understanding of the effects of water on the mechanical behaviour of the adhesive. Moreover, the identification of the model parameters as a function of water content allowed to predict and validate the mechanical behaviour of an aged bulk sample with a water profile, before complete saturation.

In this final section, the diffusion model developed previously will be coupled with the constitutive law in order to predict the mechanical behaviour of an aged bonded specimens (water-aged Arcan sample).

Two different scenarios have been considered here. In a first step, the model will be used to predict the mechanical behaviour of an aged bonded joint saturated in different humid conditions (32%RH, 50%RH and 75%RH) as well as in complete immersion state. In a second step the model will be used to predict the mechanical behaviour of an aged Arcan sample before complete saturation. In both cases, the numerical prediction will be compared with experimental results.

One the diffusion law had been identified and validated on bulk samples of adhesive (*Section* 5.1), it was possible to predict the moisture diffusion in an adhesively bonded assembly exposed to humid ageing or completely immersed in seawater. The *Abaqus* finite-element software was used for this simulation.

Two important assumptions were made when the diffusion of water in an Arcan sample was simulated. First, no water flow has been considered between the adhesive layer and the aluminium substrates. Moreover, the interface was not supposed to play any role in the kinetics of water diffusion. Hence, a normalised water concentration was applied on the free edges of the adhesive layer as shown in *Fig.*5.29a.

A qualitative representation of the water profile in an eighth part of an Arcan sample is represented in *Fig.*5.29b. In the adhesive layer, the dark shaded colour is equivalent to a complete saturation state of the adhesive (4% of water).

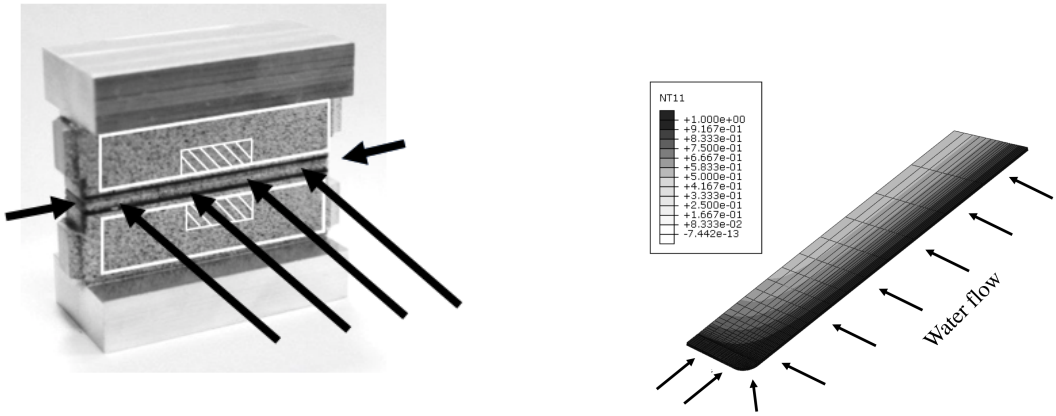

(a) Boundary conditions applied for the water diffusion

(b) Water profile through an eighth of an Arcan sample before saturation

Figure 5.29: Water diffusion in an Arcan sample

The model presented above was used to calculate the time needed to saturate an Arcan sample for different water temperatures. The results are represented in *Tab.*5.3. Because the final objective of this work was to validate the prediction of the model using experimental tests performed on aged samples, due to the time constraints, the temperature of 40^{o}C was used for this study. More specifically, Arcan samples were put in controlled conditioning chambers (32%RH, 50%RH and 75%RH) and immersed in seawater at 40^{o}C at the beginning of this thesis in order to saturate them with different water contents and compare their mechanical behaviour with the prediction of the developed model.

Table 5.3: Saturation times for an Arcan sample

Water temperature	**Time for saturation**
4^{o}C	12000 days
15^{o}C	7350 days
25^{o}C	2600 days
40^{o}C	520 days
60^{o}C	100 days

Unfortunately, the samples immersed in seawater at 40^{o}C were compromised due to an experimental problem. In order to still be able to have some experimental data of the adhesive behaviour in a bonded joint saturated in immersion (4% of water content), a second set of Arcan samples was immersed in seawater, but this time at 60^{o}C. It has been shown using the bulk samples, that for a water temperature of 60^{o}C, the quantity of diffused water at saturation is equivalent with that at 40^{o}C. However, this particular condition should be kept in mind for the experimental results that will be shown in the next sections.

5.7 Aged bonded joints with a constant water profile

5.7.1 Prediction of the mechanical behaviour

This was one of the final stages of this work. The diffusion model was coupled with the constitutive law and its water-dependent parameters in order to predict the mechanical behaviour of unaged bonded specimens saturated with different water quantities.

Five conditions were considered here: 0%, 0.5%, 1.05%, 2.25% and 4% of water uptake and constant profile. These conditions correspond to the mechanical behaviour of dry samples and samples saturated at (32%RH, 50%RH and 75%RH)s and immersed in seawater.

Simulations were performed for tensile, shear, and combined tensile shear behaviour. The results are represented in the *Fig.*5.30 and *Fig.*5.31. It is clear that the model is able to predict a loss in the mechanical properties of a bonded joint which is proportional to the water uptake in the adhesive. For the three studied loading conditions (tensile, shear and combined tensile/shear) the changes in the yield stress and in the Young's modulus can naturally be observed.

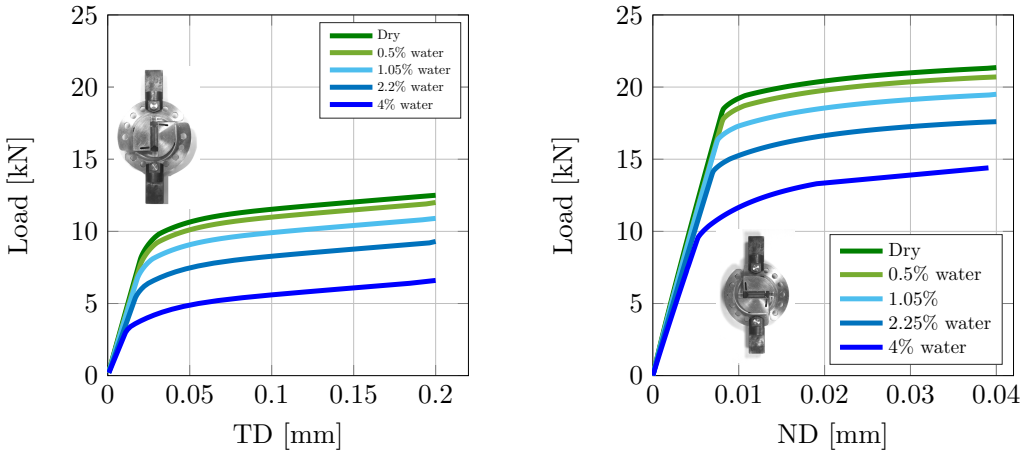

(a) Shear behaviour

(b) Tensile behaviour

Figure 5.30: Prediction of the mechanical behaviour with the moisture dependent model

5.7.2 Experimental tests used for validation

Due to time limitations and some constraints concerning the number of specimens used in this work (3 samples per condition), experimental tests, on saturated Arcan samples, were performed only under tensile and shear loading. The results can be observed in *Fig.*5.32.

In shear, the yield stress and the Young's modulus are decreasing with the amount of water at saturation (*Fig.*5.32a). The same trend is observed for the tensile behaviour (*Fig.*5.32b). However, the non-linear behaviour above the yield stress is considerably reduced by the humid ageing (0.5% and 2.25%) contrary to the immersion ageing (4%).

An unexpected result has been observed when these experimental curves were compared with the results obtained on dry samples (0% water). In both cases, the humid ageing (almost

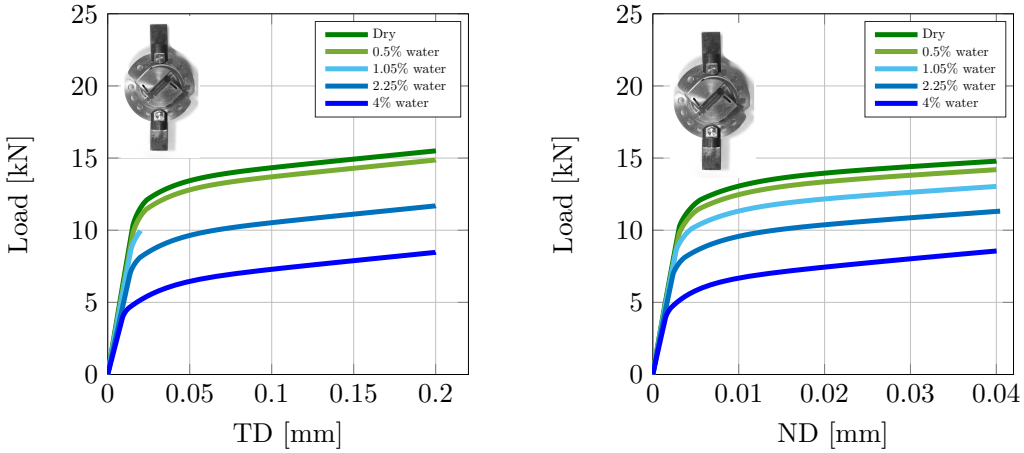

(a) Combined tensile/shear behaviour - tangential displacements

(b) Combined tensile/shear behaviour - normal displacements

Figure 5.31: Prediction of the mechanical behaviour with the moisture dependent model

two years at 40^{o}C in controlled relative humidity) seems to have improved the mechanical properties, especially in shear behaviour. For the tensile behaviour, these phenomena were less clear but still present.

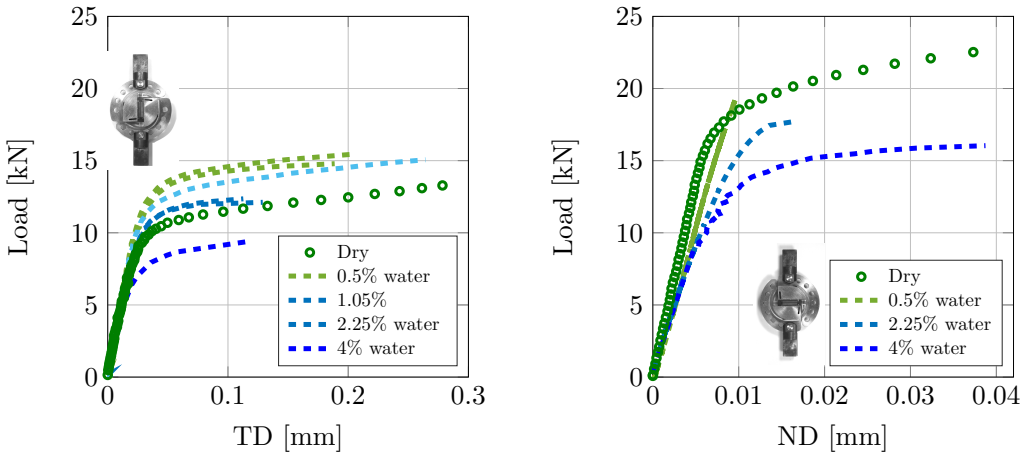

(a) Shear behaviour

(b) Tensile behaviour

Figure 5.32: Arcan samples saturated with different water contents - experimental results

5.7.3 Discussion of the results

The possible factors that might have caused this behaviour are still being investigated in the present time:

5.7.3.1 Residual stress in the specimens

A first proposal was to investigate the initial state of the Arcan specimens and to verify the existence of any residual stress in the adhesive layer due to the curing cycle. The stress release

during the humid ageing (almost two years at 40^{o}C and controlled relative humidity) might have improved the mechanical behaviour of the bonded assembly.

It is important to remember that the Arcan specimens are cured at 115^{o}C for 1h10 and they were prepared as shown in *Chapter* 2. The screws that are used to keep in place the two substrates and also to control the thickness of the adhesive layer are preventing the adhesive from moving freely during the curing cycle (boundary conditions of a confined environment) which may involve the introduction of a compressive state in the adhesive layer.

This idea was verified by analysing the mechanical behaviour of some Arcan specimens (at initial state) that have been tested after a three hours stress-relaxing treatment, performed at 80^{o}C without any constraints applied on the two substrates (exactly as the humid ageing conditions). The results showed no differences in the mechanical behaviour (tensile and shear) between the untreated specimens and the post-treated specimens.

After this investigation, two conclusions could be proposed: either there is no residual stress in the Arcan specimens due to the curing cycle; or the three hours stress-relaxing treatment was not sufficient to release the residual stress. It is important to note that the aged specimens were kept at 40^{o}C for almost two years before they were tested. This period is a lot more important than the three hours relaxation time. Investigations are still being made at the present time.

5.7.3.2 Swelling

The swelling could be another factor that can play an important role in the mechanical behaviour of the humid aged bonded specimens. The increase in volume due to the water uptake and ageing temperature may reduce the residual stress caused by the curing cycle which may lead to an increase in the mechanical behaviour of the bonded joint, contrary to what would have been expected.

5.7.3.3 Physical ageing

A study performed by *Cook et al*[177] characterised the changes in the mechanical properties of epoxy resins due to physical ageing. The authors concluded that an increase of the yield stress is observed when the material is aged below the glass transition temperature and this could be reversible if the samples are aged above the *Tg*. In the present case, the Arcan specimens used for validation have been exposed to 40^{o}C (in controlled humidity chambers) for almost 2 years. So they might have suffered a physical ageing (modification in the polymer chain mobility when exposed for a long time below Tg).

The bulk specimens have been exposed to the same environmental conditions but due to the short times of saturation (14 days), the effect of physical ageing was not present. This is an interesting hypothesis that needs further investigation.

5.7.3.4 The interface role

It is obvious that the interfaces and interphases are topics that were not touched in the present work. Moreover, the role of the interface can play an important role in the mechanical behaviour of an aged bonded joint.

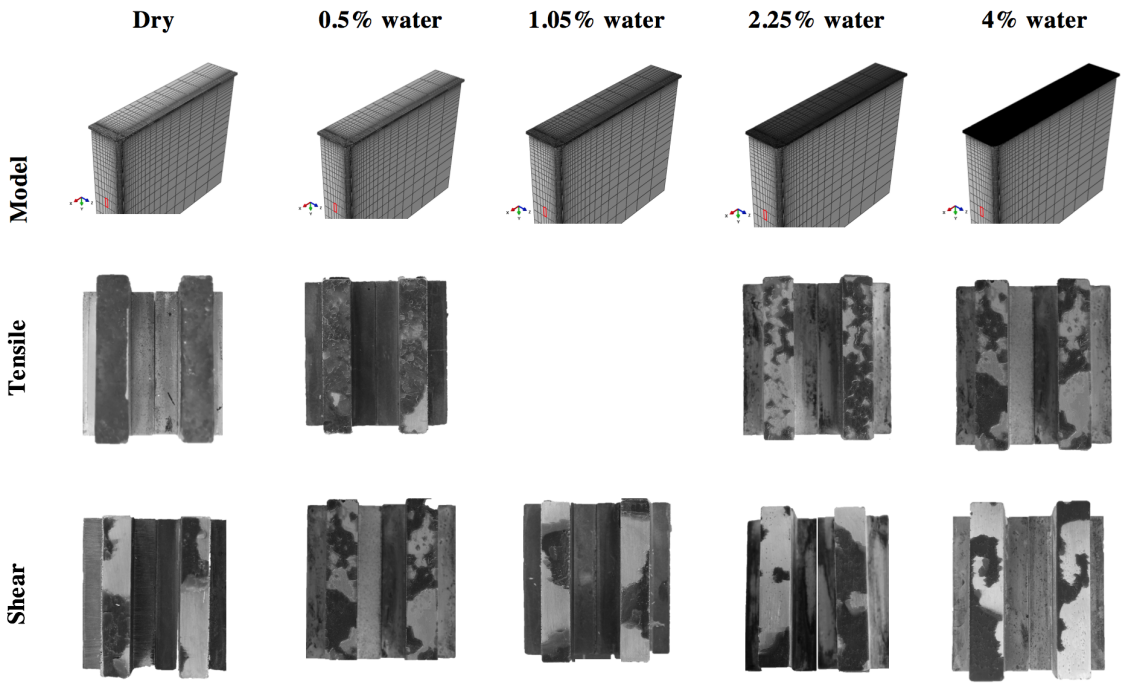

Figure 5.33: Fracture surfaces for different water contents and loading conditions

By analysing the fracture surfaces (*Fig.*5.33) of the tested samples, some conclusions could also be made. In tension, the failure is fully cohesive in the unaged state and it becomes a mixed failure with the water uptake. This can explain the premature failure of the specimens (just after the elastic threshold) and the quasi-absence of the non-linear behaviour (*Fig.*5.32b).

In the other direction (shear loading), the failure is mainly mixed in all the cases and does not seem to evolve with the water uptake. This may suggest that the increase in the mechanical properties might not be linked to the interface.

5.7.4 Comparison between model prediction and experimental results

It is not really surprising that the model prediction is not corresponding with the experimental results. But is important to note that both, the experimental results and the model prediction, present a decrease in the mechanical properties (yield stress and Young's modulus) when the amount of water increases in the adhesive.

Hence, it was possible to conclude that the model was partially validated. Further investigations are ongoing in order to determine the cause of the shift in the yield stress induced by the ageing conditions.

5.8 Aged bonded joints with a profile of water in the adhesive layer

A final investigation has been carried out on aged bonded joints, immersed in seawater, before complete saturation. As mentioned earlier, due to an experimental problem and time

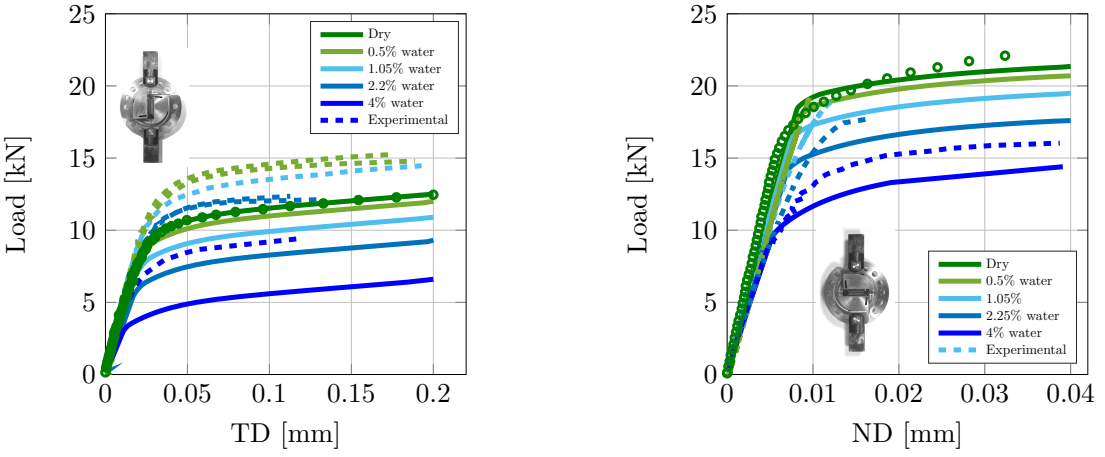

(a) Shear behaviour

(b) Tensile behaviour

Figure 5.34: Comparison between model prediction and the experimental results obtained on saturated samples with different water contents

constraints these tests were performed on samples immersed in seawater at 60^{o}C. This approach allowed a reduction in the saturation time to 3 months (*Tab.*5.3). Thus, these experimental conditions should be kept in mind when analysing the results.

5.8.1 Modelling the mechanical behaviour

Using the approach presented in *Section* 5.6.1 and the diffusion coefficient determined on bulk samples at 60^{o}C, it was possible to estimate the time needed to saturate a bonded specimen. During the immersion aging, the water uptake absorbed in an adhesive is time and space dependent. It evolves during ageing, giving different concentration gradients (*Fig.*5.35a). Thus, it was possible to describe the water profile through the adhesive layer for different ageing times. As can be observed in *Fig.*5.35b, after 100 days in immersion the Arcan specimen is completely saturated.

For validation, experimental tests have been performed on samples immersed for 30 days in seawater. The numerical prediction was performed using the diffusion model, which was able to describe the water uptake after this period of time (*Fig.*5.35b) and the identified constitutive law and its parameters dependency on the water concentration in the adhesive. As for the previous study (*Section 5.6.2*), two loading conditions were considered (tensile and shear behaviour).

5.8.2 Comparison between model prediction and experimental results

The *Fig.*5.36 shows the comparison between the numerical prediction and the experimental results. For this particular case the model predicts a decrease in the mechanical properties which is closer to the experimental results. However, some model predictions are still below the experimental results.

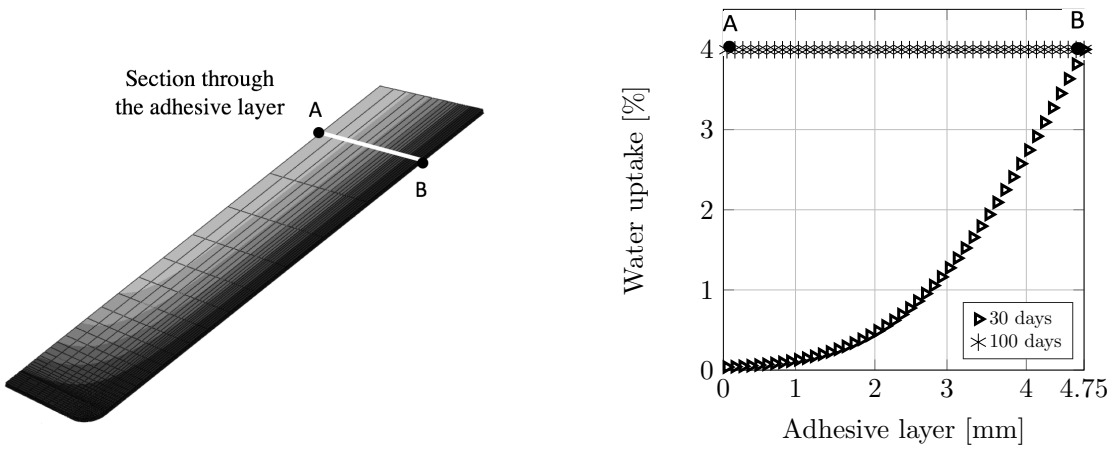

(a) Water profile through an eighth of the adhesive layer before saturation

(b) Water uptake

Figure 5.35: Water diffusion in an Arcan sample

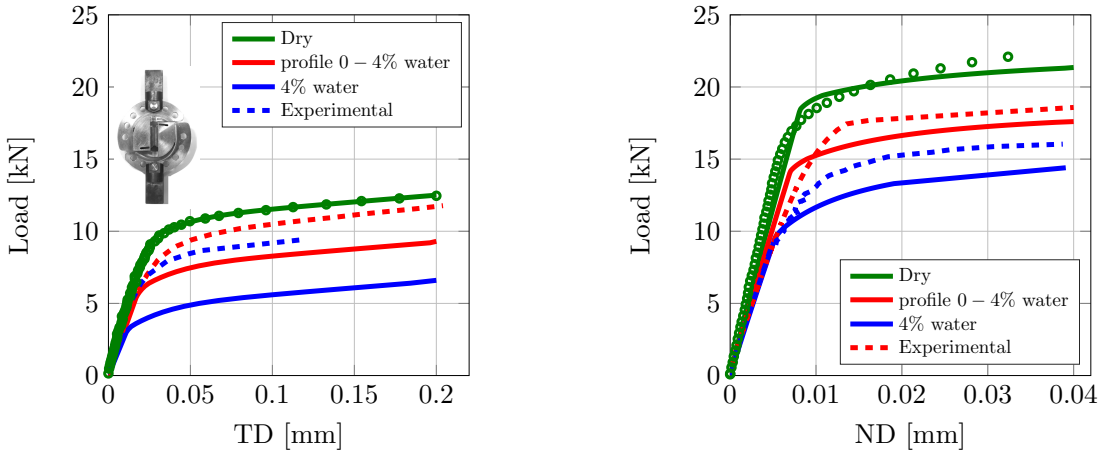

(a) Shear behaviour

(b) Tensile behaviour

Figure 5.36: Comparison between model predictions and experimental results obtained on saturated samples with different water contents

5.8.3 Overview

This chapter describes an approach to predict the influence of water on the tensile properties of the adhesive. It has been shown that for yield stress there is an equivalence between moisture content and testing temperature, when these are expressed in terms of (Tg-T_{test}), while Young's modulus and Poisson's ratio can be expressed as a function of moisture content. Using these relationships and the FE model that has been developed to combine the water diffusion and its mechanical properties, a prediction of the tensile behaviour have been made for different ageing periods before saturation. Results were in good agreement with experimental tests.

In the final part, the constitutive law together with the water concentration dependent parameters were used to predict the mechanical behaviour of un aged bonded joint. Important differences have been obtained between the numerical prediction and the experimental results.

Hence, some assumptions have been proposed to determine the causes and the nature of these observations.

Chapter 6

General conclusions and perspectives

This final chapter will provide the main conclusions. Since short conclusions have been presented at the end of each chapter, here, the entire work will be analysed with a critical eye and the main results will be given, together with some perspectives for future work.

This study was initiated in order to contribute to improving the knowledge on adhesives behaviour and adhesive bonding techniques.

An epoxy adhesive *Araldite 420A/B*, widely used for marine applications, has been studied with the aim of proposing a rapid method to characterise the effects of water ageing on its mechanical properties. The industrial challenges, such as time and cost reductions, are central to the objectives of this method, which should be able to reduce the number of experimental tests needed to assess long term mechanical behaviour.

Moreover, in the present work, an alternative to the complex laboratory tests used to characterise the properties of the adhesives in bonded joints has been proposed (tests on bulk samples) together with a technique to take advantage of the equivalence between time and temperature effects in order to reduce the time needed to quantify the water ageing effects.

From the assembly behaviour to the bulk behaviour of the adhesive

In most industrial applications a good adhesively bonded assembly requires a cohesive failure of the joint. Supposing that this requirement is accomplished by applying advanced surface treatments, is it possible to compare the mechanical behaviour of the adhesive in a bonded joint with its mechanical behaviour as a bulk specimen (*Fig.*6.1)?

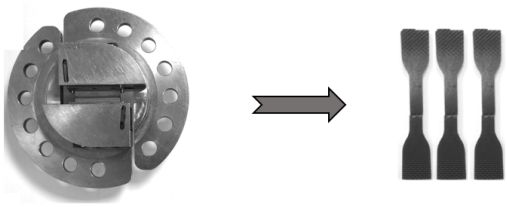

Figure 6.1: From assembly behaviour to the mechanical behaviour of a bonded specimen

To answer this question, bonded specimens were tested using the Arcan device. In parallel, experimental tests have been conducted on bulk specimens. These two preliminary campaigns were performed on dry samples and no water effect was considered in this stage (unaged stage).

The Arcan tests were performed using aluminium substrates and a surface treatment resulting in a cohesive failure in tensile loading and a cohesive/mixed failure in shear loading. In both cases, the results were considered as representative for the adhesive behaviour and no influence of the interface was considered.

Since the stress state is not uniform in the adhesive layer during an Arcan test, a constitutive law has been developed, and by using the inverse identification method and finite element models, it is now possible to determine the adhesive behaviour.

The constitutive law

The first main objective of this work was to propose the constitutive law able to describe the mechanical behaviour of a bonded joint. Research in the literature revealed that bonded joints have complex behaviours that depend on the loading conditions. While various models of

adhesive behaviour have been proposed, the originality of the present one is that the viscoelastic response is treated in two separate parts, hydrostatic and deviatoric. This has allowed different viscoelastic behaviours to be attributed to shear and tensile loading components. In addition, an original identification method for the viscoelastic parameters is presented. A viscoplastic contribution is also modelled in order to increase the capacity of the model. Moreover, experimental tests that have not been used in the identification procedure were used to validate it.

The main characteristics of the proposed constitutive law can be listed as follows:

Few experimental tests used in the identification procedure: It has been shown that only one multi-level creep recovery test is needed in two directions (tensile and shear). The loading of each level should be below the elastic threshold. For a better understanding of the time-dependent behaviour, long creep levels are recommended. The creep levels are used to identify the parameters that characterise the viscoelastic part.

Once the viscoelastic part of the model is defined, the viscoplastic part of the model can be identified. The yield surface is determined using monotonic tests in two directions (tensile and shear). For the identification of the loading rate dependent parameters, a second monotonic shear test is performed at another loading rate.

Only five different tests were sufficient to identify the total number of 22 parameters.

A step-by-step parameter identification method: Each model parameter is identified progressively. The elastic parameters are identified first, followed by the ones that characterise the viscoelastic part and finishing by the viscoplastic part. The global response of the model evolves as each parameter is identified. This allows the model to be adapted for different mechanical behaviour such as pure elastic, viscoelastic or, if completely identified, viscoelastic-viscoplastic behaviours.

Perspectives that may improve the use of the model

For further investigations, the sensibility of each parameter of the model can be studied. In order to quantify it, first, the relevant tests should be defined for each type of parameters (viscoelastic or viscoplastic). In a second phase, an approach should be developed to calculate an error with respect to the global mechanical response after changing a specific parameter with a certain ratio.

As from a qualitative point of view, it can be confirmed that the viscoelastic parameters (a, d_{max}, y_0^i, y_C^i where $i = H, D$) have a great influence in creep behaviour but they do not seem to influence that much the global mechanical response in monotonic tests. The spectrum parameters (n0, nc) characterise the form of the creep behaviour but they will not impact the predicted strains. Viscoplastic parameters have a great influence in both shear and tensile monotonic behaviour but they will not influence the creep behaviour as long as the applied load is below the elastic limit.

Results show that a good agreement with the experimental curves is obtained. To test its capability, it would be interesting to test the prediction of the model for more common geometries such as single lap joints.

In further investigations, the model can be used to predict the cyclic mechanical behaviour, which is very important when considering fatigue lifetime prediction. For this, the model should be able to predict the mechanical behaviour et high-loading rates. In order to accomplish this goal, developing links between the spectrum parameters of the model and the mechanical behaviour observed in DMA tests would be an interesting avenue of research. This has been studied a little during this work, but unfortunately due to time constraints the first results obtained were not reliable.

The validation using bulk specimens and vice-versa

The constitutive law, identified and validated using Arcan tests, was then used to predict the mechanical behaviour of the adhesive in bulk form. Hence, the tensile behaviour of the bulk adhesive has been predicted and compared with the experimental tests performed on bulk specimens in the initial state. The results show that using the proposed method, it was possible to predict the tensile mechanical behaviour of the bulk adhesive after identification of the model using the Arcan tests.

The identification of the constitutive law was then carried out on bulk samples, using the same approach, and validated on Arcan tests (*Fig.*6.2). A good agreement has been observed between the model prediction and the experimental tests. This result allowed us to conclude that it may be possible to characterise the effects of water ageing on bulk samples and, using the constitutive law, to predict the mechanical behaviour of an aged bonded specimen. By using this technique it was possible to decrease the time need to identify the model parameters as a function of water ageing, from several years to a few weeks.

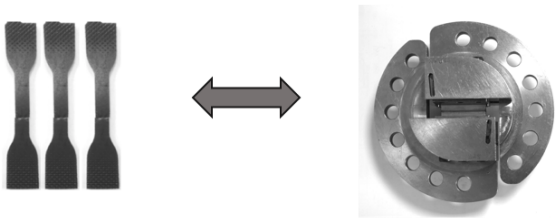

Figure 6.2: From bulk behaviour to Arcan behaviour and vice-versa

Indeed, even though the developed constitutive law is able to predict the creep behaviour and the influence of loading rate (viscous behaviour), only monotonic tests were used for validation of the correlation between bulk behaviour and that of the assembly.

Further investigations still have to be made in order to determine if the constitutive law identified on bulk specimens would be able to predict the creep behaviour of a bonded joint and to predict the mechanical response for different loading rates in the initial state. This would involve a great number of experimental tests but the results could be very interesting.

Limitations of this work

It is clear that this method can only be applied to predict the mechanical behaviour of bonded joints that present a cohesive failure. Moreover, it is important to verify from the very beginning that the adhesive presents the same characteristics (polymerisation state) in the bulk and in the bonded specimens. The sample manufacturing requires that the curing cycle and the boundary conditions should be the same in both cases (bulk and bonded specimens). Hence, it should be possible to characterise the same material.

Accelerated water ageing

An important part of the work was devoted to the study of the water effects on the mechanical behaviour of the adhesive. First, the results showed that the kinetics of water diffusion could be modelled using a Fick model. In addition, the diffusion coefficient seemed to follow an Arrhenius law for temperatures that are not close to the glass transition temperature. The water uptake for this epoxy adhesive represents 4% of the initial mass at saturation and does not evolve with the ageing temperature.

A temperature of 40^oC was chosen for rapid ageing and a thickness of 1 *mm* for bulk samples. Thus, the time for bulk sample saturation was reduced to 14 *days*, which was considered as a reasonable duration for this study.

Figure 6.3: Ageing tanks with continuously renewed natural seawater - IFREMER

Different environmental conditions have been used in this study: completely dry environments such as desiccators with 0%RH; conditioning chambers with controlled relative humidity (32%RH, 50%RH and 75%RH) and temperatures; tanks with renewable seawater (*Fig.*6.3) at different temperatures (4^oC, 15^oC, 25^oC, 40^oC and 60^oC).This environmental conditions enabled the bulk samples used in the identification of the constitutive law to be saturated with constant water profiles (or completely dry). Hence a dependence on the moisture concentration was proposed for different parameters of the models, which were then used to predict the 3D behaviour of a bonded joint exposed to humid environments.

Effects of water on the mechanical properties of the adhesive

The tensile tests performed on bulk specimens saturated under different environmental conditions allowed us to conclude that the mechanical properties of the adhesive such as Young's modulus or elastic threshold decrease with the amount of water in the adhesive. This is a classic result for this kind of epoxy material. Nevertheless, this is true for the complete polymerised state. Some anomalous phenomena could be encountered during humid ageing when the adhesive is not completely polymerised: the water decreases the mechanical properties of the adhesive but at the same time, in continues to polymerise which makes it very hard to differentiate between the mechanisms and understand the results. In the present case, the bulk samples were completely polymerised.

Other interesting results were observed after the short-term study of water ageing effects. The degradation of the mechanical properties observed in tensile tests seems to be fully reversible for the conditions used in the study and they do not evolve further after saturation.

Model prediction of the water-age effects

After the identification of the constitutive law and its water concentration dependent parameters, a first prediction has been made for bulk tensile behaviour of specimens with a water profile throughout their thickness (before saturation).

By comparing the model prediction with experimental results, it was possible to conclude that the developed constitutive law was able to predict the water ageing effects on tensile mechanical properties. Moreover, it has been shown that there is an equivalence between the moisture content and temperature effects on the yield stress, when they are expressed in terms of (Tg-T_{test}).

However, it is important to note that the model prediction is limited to the room temperature behaviour, since the temperature effects on Young's modulus and Poisson's ratio have not been considered here. This opens the way for other perspectives for this work.

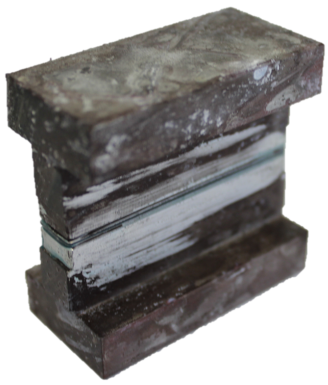

Figure 6.4: Aged Arcan specimen

The final validation of the approach has been performed on aged bonded specimens (*Fig.*6.4) for two ageing conditions. While one set of Arcan specimens has been tested in monotonic tensile and shear behaviour after saturation in different humid environments and full immersion

, another set of Arcan specimens was tested before complete saturation (with a water profile in the adhesive thickness).

Firstly, the constitutive law was used to determine the mechanical behaviour of the saturated samples. It was obvious that the model would predict a decrease in the mechanical properties of the adhesive as function of water content at saturation since it was identified on bulk sample that presented this kind of behaviour. However the prediction was not in agreement with the experimental results.

Some unexpected phenomena occurred during humid ageing, which increased the mechanical properties of the tested specimens. The degradation caused by the water ingress in the adhesive layer appears to have been balanced by other factors, this is discussed in Chapter 5.

One hypothesis is the existence of residual stress in the bonded specimens in the initial state, that might be released during the humid ageing. The swelling due to water ingress was also been examined and some further investigations are ongoing regarding this topic.

The most plausible phenomenon may be physical ageing of the adhesive. As has been shown in the literature, the mechanical properties of an epoxy material can increase, due to physical ageing, which occurs below the *Tg*. In order to reach saturation, the Arcan samples have stayed for almost two years at 40^oC in controlled humidity chambers. This long period might have been sufficient to activate the physical ageing mechanisms of the material, and this was not the case for bulk samples which were been subjected to two weeks in the same environment.

It might be possible that the water uptake decreases the mechanical properties of the bulk samples until complete saturation and then, the physical ageing may increase them back. This interesting hypothesis should be analysed by testing bulk samples that were exposed for long periods of time at humid ageing. An increase in their mechanical properties (above the initial ones) after such periods of time may answer this question.

Finally, the constitutive law was used to predict the mechanical behaviour of a bonded specimen before complete saturation in seawater. In this case the model prediction was closer to the experimental results but some further investigation is still needed in order to completely understand these differences.

Water effects and the role of the interface

Water effects on the interface behaviour (adhesive / adherents) have not been taken into account in this study. Nevertheless, the experimental results showed that in tensile behaviour, the failure was fully cohesive in the unaged state and it became a mixed failure with the water uptake.

By analysing the failure surface of a saturated Arcan specimen using a scanning electron microscope (SEM), it was possible to determine some spots on the adherent surfaces which have been identified as oxidation spots (*Fig.*6.5). It is clear that water diffusion can affect the mechanical behaviour of the interface, as shown by many studies, so this should also be taken into account in further studies.

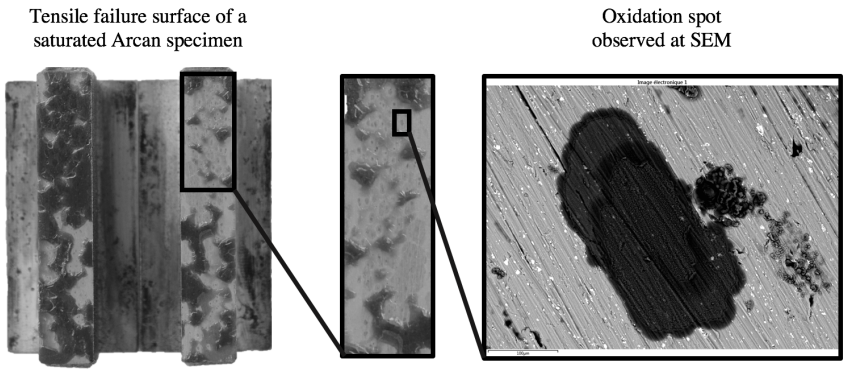

Figure 6.5: Failure surface SEM analysis on saturated Arcan specimen

Other perspectives

This study has raised many questions and other points can be cited for future work. Among those, the integration of the temperatures effects in the present model would be an important step in the model development. Moreover, the influence of water ageing on creep behaviour or as a function of loading rates are still topics that should be clarified. Finally, the effects of cyclic loading should be examined as these are critical in many marine applications.

Bibliography

[1] S.R. Hartshorn. *Structural adhesives: chemistry and technology*. Springer Science & Business Media, 2012.

[2] A.H. Landrock and S. Ebnesajjad. *Adhesives technology handbook*. William Andrew, 2008.

[3] Huntsman. Araldite adhesives core range - selector guide for industrial bonding, 2012. http://www.huntsman.com/advanced-materials: Marine Industry.

[4] D.A. Dillard. *Advances in structural adhesive bonding*. Elsevier, 2010.

[5] H. Wang, H. Shi, and Y. Wang. The wetting of leaf surfaces and its ecological significances. In *Wetting and Wettability*. InTech, 2015.

[6] Z. Chen, R.D. Adams, and L.F.M da Silva. Fracture toughness of bulk adhesives in mode i and mode iii and curing effect. *International Journal of Fracture*, 167(2):221–234, 2011.

[7] P. Davies, L. Sohier, J-Y. Cognard, A. Bourmaud, E. Choqueuse, D.and Rinnert, and R. Créac'hcadec. Influence of adhesive bond line thickness on joint strength. *International journal of adhesion and adhesives*, 29(7):724–736, 2009.

[8] N. Arnaud, J-Y. Cognard, and P. Davies. Analyse de l'effet du vieillissement en milieu humide sur le comportement mécanique d'adhésifs en assemblages sous sollicitations multi-axiales.

[9] J. Lemaitre, J-L. Chaboche, A. Benallal, and R. Desmorat. *Mécanique des matériaux solides-3eme édition*. Dunod, 2009.

[10] P. Majda and J. Skrodzewicz. A modified creep model of epoxy adhesive at ambient temperature. *International Journal of Adhesion and Adhesives*, 29(4):396–404.

[11] X. X Yu, A. D Crocombe, and G Richardson. Material modelling for rate-dependent adhesives. *International Journal of Adhesion and Adhesives*, 21(3):197–210.

[12] A. Schieffer, J-F. Maire, and D. Lévêque. A coupled analysis of mechanical behaviour and ageing for polymer-matrix composites. *Composites Science and Technology*, 62(4):543–549, 2002.

[13] J. Maurice, J-Y. Cognard, R. Creac'hcadec, P. Davies, L. Sohier, and S. Mahdi. Characterization and modelling of the 3d elastic–plastic behaviour of an adhesively bonded

joint under monotonic tension/compression-shear loads: influence of three cure cycles. *Journal of Adhesion Science and Technology*, 27(2):165–181, 2013.

[14] M. Bordes, P. Davies, J-Y. Cognard, L. Sohier, V. Sauvant-Moynot, and J. Galy. Prediction of long term strength of adhesively bonded steel/epoxy joints in sea water. *International Journal of Adhesion and Adhesives*, 29(6):595–608.

[15] M. Savvilotidou, A.P. Vassilopoulos, M. Frigione, and T. Keller. Development of physical and mechanical properties of a cold-curing structural adhesive in a wet bridge environment. *Construction and Building Materials*, 144:115–124, 2017.

[16] G.L. de Oliveira, A.J.A Gomez, M. Caire, Murilo A. Vaz, and M.F. da Costa. Characterization of seawater and weather aged polyurethane elastomer for bend stiffeners. *Polymer Testing*, 59:290–295, 2017.

[17] I.A. Ashcroft and J. Comyn. Effect of water and mechanical stress on durability. In *Handbook of adhesion technology*, pages 787–822. Springer, 2011.

[18] A. Mubashar, I..A Ashcroft, G.W. Critchlow, and A.D. Crocombe. Moisture absorption–desorption effects in adhesive joints. *International Journal of Adhesion and Adhesives*, 29(8):751–760, 2009.

[19] J.W. Wylde and J.K. Spelt. Measurement of adhesive joint fracture properties as a function of environmental degradation. *International Journal of Adhesion and Adhesives*, 18(4):237–246, 1998.

[20] A. Baldan. Adhesively-bonded joints and repairs in metallic alloys, polymers and composite materials: adhesives, adhesion theories and surface pretreatment. *Journal of materials science*, 39(1):1–49, 2004.

[21] N. Arnaud. *Analyse de l'effet du vieillissement en milieu humide sur le comportement mécanique d'adhésifs en assemblages sous sollicitations multiaxiales* . PhD thesis, Université de Bretagne Occidentale (UBO), Brest, 2014.

[22] A.D. Crocombe, Y.X. Hua, W.K. Loh, M.A. Wahab, and I.A. Ashcroft. Predicting the residual strength for environmentally degraded adhesive lap joints. *International journal of Adhesion and Adhesives*, 26(5):325–336, 2006.

[23] H.L. Alfonso Medina. *Characterization and modeling of multi-material assemblies under mixed quasi-static loadings for the design of automotive structures.* Theses, Université de Bretagne Occidentale (UBO), Brest, December 2016.

[24] R. D. Adams. *Adhesive bonding: science, technology and applications.* Elsevier, 2005.

[25] J. Koller, I. Baumer, and D. Mania. High-tech in the middle palaeolithic: Neandertal-manufactured pitch identified. *European Journal of Archaeology*, 4(3):385–397, 2001.

[26] M. Cârciumaru, R.M. Ion, E-C. Niţu, and R. Ştefănescu. New evidence of adhesive as hafting material on middle and upper palaeolithic artefacts from gura cheii-râşnov cave (romania). *Journal of Archaeological Science*, 39(7):1942–1950, 2012.

[27] B. Michel. Le collage: un moyen ancestral, moderne et durable d'assemblage, 2004. http://www.culturesciences.chimie.ens.fr/le-collage-un-moyen-ancestral-moderne-et-durable-dassemblage

[28] A. Lucas and J. Harris. *Ancient Egyptian materials and industries*. Courier Corporation, 2012.

[29] J.G. Landels. *Engineering in the ancient world*. Univ of California Press, 2000.

[30] Arthur W Judge. Aircraft and automobile materials of construction, vol. 2: Non-ferrous and organic materials: a treatise for aircraft, automobile, and mechanical engineers, manufacturers, constructors, designers, draughtsmen, students, and others, 1921.

[31] J. Cognard. *Science et technologie du collage*. PPUR presses polytechniques, 2000.

[32] J.W. McBain and D.G. Hopkins. On adhesives and adhesive action. *The Journal of Physical Chemistry*, 29(2):188–204, 1925.

[33] K.W. Allen. Some reflections on contemporary views of theories of adhesion. *International journal of adhesion and adhesives*, 13(2):67–72, 1993.

[34] T. Young. An essay on the cohesion of fluids. *Philosophical Transactions of the Royal Society of London*, 95:65–87, 1805.

[35] J.W. Gibbs. The collected work. *Vol. I*, pages 54–371, 1931.

[36] Y.P. Joshi. Shape of a liquid surface in contact with a solid. *European Journal of Physics*, 11(2):125, 1990.

[37] D.N. Staicopolus. The computation of surface tension and of contact angle by the sessile-drop method. *Journal of Colloid Science*, 17(5):439–447, 1962.

[38] C.L. Randow, C.A. Williams, T.C. Ward, D.A. Dillard, J.G. Dillard, and J.P. Wightman. An investigation of the cling of thin polymeric films. *The Journal of Adhesion*, 63(4):285–307, 1997.

[39] S.S. Voyutskii and V.L. Vakula. The role of diffusion phenomena in polymer-to-polymer adhesion. *Journal of Applied Polymer Science*, 7(2):475–491, 1963.

[40] J. Bikerman. Causes of poor adhesion: Boundary layers. *Industrial & Engineering Chemistry*, 1967.

[41] G.W. Critchlow, K.A. Yendall, D Bahrani, A Quinn, and F Andrews. Strategies for the replacement of chromic acid anodising for the structural bonding of aluminium alloys. *International Journal of Adhesion and Adhesives*, 26(6):419–453, 2006.

[42] L.F.M da Silva and C. Sato. *Design of adhesive joints under humid conditions*. Springer, 2013.

[43] J.D. Minford. Durability of structural adhesive bonded aluminum joints. *Adhesives Age*, 21(3):17–23, 1978.

[44] L.F.M. da Silva, A. Öchsner, and R.D. Adams. *Handbook of adhesion technology*. Springer Science & Business Media, 2011.

[45] NF T 76-142. Méthode de préparation de plaques d'adhésifs structuraux pour la réalisation d'éprouvettes d'essai de caractérisation. 1988.

[46] L.F.M. da Silva, R.D. Adams, and M Gibbs. Manufacture of adhesive joints and bulk specimens with high-temperature adhesives. *International journal of adhesion and adhesives*, 24(1):69–83, 2004.

[47] EN ISO 527. Plastics - determination of tensile properties - part 1: General principles. 2012.

[48] NF T 51-101. Plastiques - determination des caracteristiques en compression. 1981.

[49] S. Gali, G. Dolev, and O. Ishai. An effective stress/strain concept in the mechanical characterization of structural adhesive bonding. *International Journal of Adhesion and Adhesives*, 1(3):135–140, 1981.

[50] D ASTM. 5379. *Standard test method for shear properties of composite materials by the V-notched beam method*, 2005.

[51] L. Arcan, M. Arcan, and I.M. Daniel. Sem fractography of pure and mixed-mode interlaminar fractures in graphite/epoxy composites. In *Fractography of Modern Engineering Materials: Composites and Metals*. ASTM International, 1987.

[52] R. El-Hajjar and R. Haj-Ali. In-plane shear testing of thick-section pultruded frp composites using a modified arcan fixture. *Composites Part B: Engineering*, 35(5):421–428, 2004.

[53] ISO 6721. 5379. *Plastics: Determination of dynamic mechanical properties*, 2011.

[54] L.F.M. Da Silva and R.D. Adams. Measurement of the mechanical properties of structural adhesives in tension and shear over a wide range of temperatures. *Journal of Adhesion Science and Technology*, 19(2):109–141, 2005.

[55] L. Lilleheden. Mechanical properties of adhesives in situ and in bulk. *International journal of adhesion and adhesives*, 14(1):31–37, 1994.

[56] J.P. Jeandrau. Technologie du collage structural pour les applications en mécanique. *Publications CETIM, Etablissement de Saint-Etienne*, 1993.

[57] ISO 6721. Adhesives – determination of tensile lap-shear strength of rigid-to-rigid bonded assemblies. 2003.

[58] J-Y. Cognard, R. Créac'hcadec, L. Sohier, and D. Leguillon. Influence of adhesive thickness on the behaviour of bonded assemblies under shear loadings using a modified tast fixture. *International Journal of Adhesion and Adhesives*, 30(5):257–266, 2010.

[59] R.B. Krieger. Stress analysis concepts for adhesive bonding of aircraft primary structure. In *Adhesively bonded joints: Testing, analysis, and design*. ASTM International, 1988.

[60] R. Creac'hcadec. Analyse et modélisation du comportement non-linéaire d'assemblages collés pour application marine. 2008.

[61] ISO 6922. Adhesives – determination of tensile strength of butt joints. 1987.

[62] J-Y. Cognard, P. Davies, B. Gineste, and L. Sohier. Development of an improved adhesive test method for composite assembly design. *Composites Science and Technology*, 65(3):359–368, 2005.

[63] J-Y. Cognard, P. Davies, B. Gineste, and L. Sohier. Development of an improved adhesive test method for composite assembly design. *Composites Science and Technology*, 65(3):359–368, 2005.

[64] J-Y. Cognard. Numerical analysis of edge effects in adhesively-bonded assemblies application to the determination of the adhesive behaviour. *Computers & Structures*, 86(17):1704–1717, 2008.

[65] D. Thevenet, R. Créac'hcadec, L. Sohier, and J-Y. Cognard. Experimental analysis of the behavior of adhesively bonded joints under tensile/compression–shear cyclic loadings. *International Journal of Adhesion and Adhesives*, 44:15–25, 2013.

[66] P. Bidaud, R. Créac'Hcadec, D. Thevenet, J-Y. Cognard, and P. Jousset. A prediction method of the cyclic behavior of adhesively bonded structures under fatigue loading. In *10th European Adhesion Conference*, 2014.

[67] J-Y. Cognard, D. Leguillon, and N. Carrere. Analysis of the influence of geometric parameters on the stress distributions in adhesively bonded scarf joints using 2d models under elastic assumption. *The Journal of Adhesion*, 90(11):877–898, 2014.

[68] H. Nakano, Y. Omiya, Y. Sekiguchi, and T. Sawa. Three-dimensional fem stress analysis and strength prediction of scarf adhesive joints with similar adherends subjected to static tensile loadings. *International Journal of Adhesion and Adhesives*, 54:40–50, 2014.

[69] N. Carrere, C. Badulescu, J-Y. Cognard, and D. Leguillon. 3d models of specimens with a scarf joint to test the adhesive and cohesive multi-axial behavior of adhesives. *International Journal of Adhesion and Adhesives*, 62:154–164.

[70] L.F.M. da Silva, A. Ochsner, and R.D. Adams. *Handbook of adhesion technology, Ed. Springer, 2011.*

[71] G. C. Papanicolaou, P. Charitidis, D. E. Mouzakis, E. Karachalios, G. Jiga, and D. V. Portan. Experimental and numerical investigation of balanced boron/epoxy single lap joints subjected to salt spray aging. *International Journal of Adhesion and Adhesives*, 68:9–18, 2016.

[72] J-Y. Cognard, R. Créac'hcadec, L. Sohier, and P. Davies. Analysis of the nonlinear behavior of adhesives in bonded assemblies—comparison of TAST and arcan tests. *International Journal of Adhesion and Adhesives*, 28(8):393–404, 2008.

[73] L.F.M. da Silva and A. Ochsner. *Modeling of adhesively bonded joints, Ed. Springer, 2008.*

[74] T. Iwamoto, T. Nagai, and T. Sawa. Experimental and computational investigations on strain rate sensitivity and deformation behavior of bulk materials made of epoxy resin structural adhesive. *International Journal of Solids and Structures*, 47(2):175–185.

[75] J. A. Harris and R. D. Adams. An assessment of the impact performance of bonded joints for use in high energy absorbing structures. *Proceedings of the Institution of Mechanical Engineers, Part C: Journal of Mechanical Engineering Science*, 199(2):121–131, 1985.

[76] L.F.M. da Silva, R. D. Adams, and M. Gibbs. Manufacture of adhesive joints and bulk specimens with high-temperature adhesives. *International Journal of Adhesion and Adhesives*, 24(1):69–83, 2004.

[77] W. K. Chiu and R. Jones. Unified constitutive model for thermoset adhesive, FM73. *International Journal of Adhesion and Adhesives*, 15(3):131–136.

[78] A. D. Crocombe. Modelling and predicting the effects of test speed on the strength of joints made with FM73 adhesive. *International Journal of Adhesion and Adhesives*, 15(1):21–27.

[79] C. Badulescu, C. Germain, J-Y. Cognard, and N. Carrere. Characterization and modelling of the viscous behaviour of adhesives using the modified arcan device. *Journal of Adhesion Science and Technology*, 29(5):443–461, 2015.

[80] R. Mahnken and M. Schlimmer. Simulation of strength difference in elasto-plasticity for adhesive materials. *International Journal for Numerical Methods in Engineering*, 63(10):1461–1477, 2005.

[81] P. Jousset and M. Rachik. Implementation, identification and validation of an elasto-plastic-damage model for the finite element simulation of structural bonded joints. *International Journal of Adhesion and Adhesives*, 50:107–118, 2014.

[82] P. C. Pandey, H. Shankaragouda, and Arbind Kr. Singh. Nonlinear analysis of adhesively bonded lap joints considering viscoplasticity in adhesives. *Computers & Structures*, 70(4):387–413, 1999.

[83] M. Zgoul and A.D. Crocombe. Numerical modelling of lap joints bonded with a rate-dependent adhesive. *International Journal of Adhesion and Adhesives*, 24(4):355–366, 2004.

[84] R. Christensen. *Theory of viscoelasticity: an introduction*. Elsevier, 2012.

[85] E.C. Bingham. *Fluidity and plasticity*, volume 2. McGraw-Hill, 1922.

[86] D. Peretz and Y. Weitsman. Nonlinear viscoelastic characterization of fm-73 adhesive. *Journal of rheology*, 26(3):245–261, 1982.

[87] S.K. Ha and G. Springer. Time dependent behavior of laminated composites at elevated temperatures. *Journal of composite materials*, 23(11):1159–1197, 1989.

[88] E.P. Cernocky and E. Krempl. A non-linear uniaxial integral constitutive equation incorporating rate effects, creep and relaxation. *International Journal of Non-Linear Mechanics*, 14(3):183–203, 1979.

[89] S. Bodner and Y. Partom. Constitutive equations for elastic-viscoplastic strain-hardening materials. *Journal of Applied Mechanics*, 42(2):385–389, 1975.

[90] N. Carrere, C. Badulescu, J-Y. Cognard, and D. Leguillon. 3d models of specimens with a scarf joint to test the adhesive and cohesive multi-axial behavior of adhesives. *International Journal of Adhesion and Adhesives*, 62:154–164, 2015.

[91] N. Arnaud, R. Créac'Hcadec, and J-Y. Cognard. A tension/compression–torsion test suited to analyze the mechanical behaviour of adhesives under non-proportional loadings. *International Journal of Adhesion and Adhesives*, 53:3–14, 2014.

[92] J-F. Maire. *Etudes théorique et expérimentale du comportement de matériaux composites en contraintes planes*. PhD thesis, Besançon, 1992.

[93] R.A. Schapery. On the characterization of nonlinear viscoelastic materials. *Polymer Engineering & Science*, 9(4):295–310, 1969.

[94] D. Lévêque, A. Mavel, C Petipas, J-F. Maire, and A. Schieffer. Prévision de la durée de vie et performances résiduelles des composites carbone/résine. *Rapport technique Onera n RT*, 66(7086):12–20, 2000.

[95] H.L.A Medina. *Characterization and modeling of multi-material assemblies under mixed quasi-static loadings for the design of automotive structures.* PhD thesis, Université de Bretagne Occidentale (UBO), Brest, 2016.

[96] J-Y. Cognard, R. Créac'Hcadec, J. Maurice, P. Davies, M. Peleau, and L. F. M. Da Silva. Analysis of the influence of hydrostatic stress on the behaviour of an adhesive in a bonded assembly. *Journal of Adhesion Science and Technology*, 24(11):1977–1994, 2010.

[97] P Jousset and M Rachik. Pressure-dependent plasticity for structural adhesive constitutive modeling. *Journal of Adhesion Science and Technology*, 24(11-12):1995–2010, 2010.

[98] P. Bidaud. *Analysis of the cyclic behavior of an adhesive in an assembly for offshore windmills applications*. PhD thesis, Université Bretagne Occidentale, 2014.

[99] B. Duncan and G. Dean. Measurements and models for design with modern adhesives. *International journal of adhesion and adhesives*, 23(2):141–149, 2003.

[100] C.H. Wang and P. Chalkley. Plastic yielding of a film adhesive under multiaxial stresses. *International Journal of Adhesion and Adhesives*, 20(2):155–164, 2000.

[101] G.D. Dean, B.E. Read, and B.C. Duncan. Project paj2 report no 7 an evaluation of yield criteria for adhesives for finite element.

[102] M. Vogler, G. Ernst, and R. Rolfes. Invariant based transversely-isotropic material and failure model for fiber-reinforced polymers. *Computers, Materials, & Continua*, 16(1):25–50, 2010.

[103] J. Maurice. Characterization and modeling of the 3d elastic-plastic behavior of structural adhesive films for aeronautical applications. *Brest: Université de Bretagne Occidentale*, 2012.

[104] A. Griffith. The phenomena of rupture and flow in solids. *Philosophical transactions of the royal society of london. Series A, containing papers of a mathematical or physical character*, 221:163–198, 1921.

[105] D.S. Dugdale. Yielding of steel sheets containing slits. *Journal of the Mechanics and Physics of Solids*, 8(2):100–104, 1960.

[106] Ulf Stigh. Damage and crack growth analysis of the double cantilever beam specimen. *International Journal of Fracture*, 37(1):R13–R18, 1988.

[107] A Moradi, N. Carrère, D. Leguillon, E. Martin, and J-Y. Cognard. Strength prediction of bonded assemblies using a coupled criterion under elastic assumptions: Effect of material and geometrical parameters. *International Journal of Adhesion and Adhesives*, 47:73–82, 2013.

[108] N. Carrère, E. Martin, and D Leguillon. Comparison between models based on a coupled criterion for the prediction of the failure of adhesively bonded joints. *Engineering Fracture Mechanics*, 138:185–201, 2015.

[109] J. Comyn. *Design of adhesive joints under humid conditions - Diffusion of water in adhesives*. Springer, 2013.

[110] P. Fernandes, G Viana, RJC Carbas, M Costa, LFM da Silva, and MD Banea. The influence of water on the fracture envelope of an adhesive joint. *Theoretical and Applied Fracture Mechanics*, 89:1–15, 2017.

[111] L.P. Canal and V. Michaud. Micro-scale modeling of water diffusion in adhesive composite joints. *Composite Structures*, 111:340–348, 2014.

[112] A. Fick. On liquid diffusion. *Journal of Membrane Science*, 100(1):33–38, 1995.

[113] J. Crank and G.S Park. Diffusion in polymers. *London: Academic press Inc. Ltd*, 1968.

[114] H. Fujita. Diffusion in polymer-diluent systems. *Fortschritte Der Hochpolymeren - Forschung*, pages 1–47, 1961.

[115] M.D. Placette, X. Fan, J-H. Zhao, and D. Edwards. Dual stage modeling of moisture absorption and desorption in epoxy mold compounds. *Microelectronics Reliability*, 52(7):1401–1408, 2012.

[116] M. Heshmati, R. Haghani, and M. Al-Emrani. Effects of moisture on the long-term performance of adhesively bonded frp/steel joints used in bridges. *Composites Part B: Engineering*, 92:447–462, 2016.

[117] M. Bordes. *Etude du vieillissement de liaisons adhésives en milieu marin pour application offshore*. PhD thesis, Insa Lyon, 2009.

[118] H.G. Carter and K.G. Kibler. Langmuir-type model for anomalous moisture diffusion in composite resins. *Journal of Composite Materials*, 12(2):118–131, 1978.

[119] S. Popineau, C. Rondeau-Mouro, C. Sulpice-Gaillet, and M. Shanahan. Free/bound water absorption in an epoxy adhesive. *Polymer*, 46(24):10733–10740, 2005.

[120] J. Brettle, D.M. Brewis, J. Comyn, B.C. Cope, M.T. Goosey, and R.D. Hurditch. The interaction of water with an epoxide adhesive based on the diglycidylether of bisphenol-a and triethylene tetramine. *International journal of adhesion and adhesives*, 3(4):189–192, 1983.

[121] M. Fernández-García and M.Y.M. Chiang. Effect of hygrothermal aging history on sorption process, swelling, and glass transition temperature in a particle-filled epoxy-based adhesive. *Journal of Applied Polymer Science*, 84(8):1581–1591, 2002.

[122] D.M. Brewis, J. Comyn, A.K. Raval, and A.J. Kinloch. The effect of humidity on the durability of aluminium-epoxide joints. *International Journal of Adhesion and Adhesives*, 10(4):247–253, 1990.

[123] A. Toscano, G. Pitarresi, M. Scafidi, M. Di Filippo, G. Spadaro, and S. Alessi. Water diffusion and swelling stresses in highly crosslinked epoxy matrices. *Polymer Degradation and Stability*, 133:255–263, 2016.

[124] J. Verdu. *Action de l'eau sur les plastiques*. Ed. Techniques Ingénieur, 2000.

[125] F.N. Kelley and F. Bueche. Viscosity and glass temperature relations for polymer-diluent systems. *Journal of Polymer Science Part A: Polymer Chemistry*, 50(154):549–556, 1961.

[126] R. Simha and R.F. Boyer. On a general relation involving the glass temperature and coefficients of expansion of polymers. *The Journal of Chemical Physics*, 37(5):1003–1007, 1962.

[127] H.H. Shih, L.E. Hornberger, R.L. Siemens, and A.E. Zachariades. The reversible plasticization of the aromatic copolyester of poly (ethylene terephthalate) and 60 mol%

p-acetoxybenzoic acid with 1, 1, 1, 3, 3, 3-hexafluoro-2-propanol. *Journal of applied polymer science*, 32(5):4897–4908, 1986.

[128] W.K. Loh, A.D. Crocombe, M. Abdel Wahab, and I.A. Ashcroft. Modelling anomalous moisture uptake, swelling and thermal characteristics of a rubber toughened epoxy adhesive. *International journal of adhesion and adhesives*, 25(1):1–12, 2005.

[129] M.J. Adamson. Thermal expansion and swelling of cured epoxy resin used in graphite/epoxy composite materials. *Journal of materials science*, 15(7):1736–1745, 1980.

[130] L. El-Sa'ad, M.I. Darby, and B. Yates. Moisture absorption characteristics of rubber particulate filled epoxy adhesives. *Journal of materials science*, 24(5):1653–1659, 1989.

[131] S. Chiaki. *Design of adhesive joints under humid conditions - Influences of Water on the Adhesive Properties*. Springer, 2013.

[132] M Savvilotidou, AP Vassilopoulos, M Frigione, and T Keller. Effects of aging in dry environment on physical and mechanical properties of a cold-curing structural epoxy adhesive for bridge construction. *Construction and Building Materials*, 140:552–561, 2017.

[133] S. Sugiman, A.D. Crocombe, and I.A. Aschroft. Experimental and numerical investigation of the static response of environmentally aged adhesively bonded joints. *International Journal of Adhesion and Adhesives*, 40:224–237, 2013.

[134] R. Leger, A. Roy, and J-C. Grandidier. A study of the impact of humid aging on the strength of industrial adhesive joints. *International Journal of Adhesion and Adhesives*, 44:66–77, 2013.

[135] I.A. Ashcroft, R.P. Digby, and S.J. Shaw. A comparison of laboratory-conditioned and naturally-weathered bonded joints. *The Journal of Adhesion*, 75(2):175–201, 2001.

[136] A.J. Kinloch. Durability of structural adhesives. introduction., aj kinloch, 1983.

[137] B.E. Gontcharova. *Vieillissement d'assemblages collés acier/composite dans l'eau et sous charge*. PhD thesis, 1997.

[138] M.R. Bowditch. The durability of adhesive joints in the presence of water. *International Journal of Adhesion and Adhesives*, 16(2):73–79, 1996.

[139] K Vine, P Cawley, and AJ Kinloch. The correlation of non-destructive measurements and toughness changes in adhesive joints during environmental attack. *The Journal of Adhesion*, 77(2):125–161, 2001.

[140] M.M.A Wahab, A.D. Crocombe, A. Beevers, and K. Ebtehaj. Coupled stress-diffusion analysis for durability study in adhesively bonded joints. *International Journal of Adhesion and Adhesives*, 22(1):61–73, 2002.

[141] M-A. Bruneaux. *Durabilité des assemblages collés: Développement d'un modèle mécanique prédictif avec prise en compte des caractéristiques physico-chimiques de l'adhésif*. PhD thesis, École nationale des ponts et chaussées (France), 2004.

[142] RA Gledhill and AJ Kinloch. Environmental failure of structural adhesive joints. *The journal of adhesion*, 6(4):315–330, 1974.

[143] S. Popineau. *Durabilité en milieu humide d'assemblages structuraux collés type aluminium/composite*. PhD thesis, École Nationale Supérieure des Mines de Paris, 2005.

[144] A.D. Crocombe. Durability modelling concepts and tools for the cohesive environmental degradation of bonded structures. *International Journal of Adhesion and Adhesives*, 17(3):229–238, 1997.

[145] Y. Hua, A.D. Crocombe, M.A. Wahab, and I.A. Ashcroft. Continuum damage modelling of environmental degradation in joints bonded with ea9321 epoxy adhesive. *International Journal of Adhesion and Adhesives*, 28(6):302–313, 2008.

[146] R. Créac'Hcadec and T. Cognard, J-Y.and Heuzé. On modelling the non-linear behaviour of thin adhesive films in bonded assemblies with interface elements. *Journal of Adhesion Science and Technology*, 22(13):1541–1563, 2008.

[147] ISO 6721. Plastics - determination of dynamic mechanical properties – part 6: Shear vibration – non-resonance method. 1996.

[148] ASTM D4065. Standard practice for plastics: Dynamic mechanical properties: Determination and report of procedures, 2012.

[149] J-Y. Cognard, L. Sohier, and P. Davies. A modified arcan test to analyze the behavior of composites and their assemblies under out-of-plane loadings. *Composites Part A: Applied Science and Manufacturing*, 42(1):111–121, 2011.

[150] J-Y. Cognard. Numerical analysis of edge effects in adhesively-bonded assemblies application to the determination of the adhesive behaviour. *Computers & Structures*, 86(17):1704–1717, 2008.

[151] ISO 11357. Differential scanning calorimetry (dsc) – part 1: General principles. 2016.

[152] J.C. Lagarias, J.A. Reeds, M.H. Wright, and P.E. Wright. Convergence properties of the nelder–mead simplex method in low dimensions. *SIAM Journal on optimization*, 9(1):112–147, 1998.

[153] N. Carrere, F. Laurin, and J-F. Maire. Micromechanical-based hybrid mesoscopic 3d approach for non-linear progressive failure analysis of composite structures. *Journal of Composite Materials*, 46(19-20):2389–2415, September 2012.

[154] P. Davies. Marin industry. In *Handbook of adhesion technology*, pages 1237–1262. Springer, 2011.

[155] L. Silva, S. Tognana, and W. Salgueiro. Study of the water absorption and its influence on the young's modulus in a commercial polyamide. *Polymer Testing*, 32(1):158–164, 2013.

[156] J. Zhou and J.P. Lucas. Hygrothermal effects of epoxy resin. part i: the nature of water in epoxy. *Polymer*, 40(20):5505–5512, 1999.

[157] J. Zhou and J.P. Lucas. Hygrothermal effects of epoxy resin. part ii: variations of glass transition temperature. *Polymer*, 40(20):5513–5522, 1999.

[158] B. De Nève and M.E.R. Shanahan. Effects of humidity on an epoxy adhesive. *International Journal of Adhesion and Adhesives*, 12(3):191–196, 1992.

[159] M.J. Cowling. *A Review of Adhesive Bonding for Offshore Structures*. Health and Safety Executive, 1997.

[160] M. Bordes, P. Davies, J-Y. Cognard, L. Sohier, V. Sauvant-Moynot, and J. Galy. Prediction of long term strength of adhesively bonded steel/epoxy joints in sea water. *International journal of adhesion and adhesives*, 29(6):595–608, 2009.

[161] D.M. Brewis, J. Comyn, and J.L. Tegg. The durability of some epoxide adhesive-bonded joints on exposure to moist warm air. *International Journal of Adhesion and Adhesives*, 1(1):35–39, 1980.

[162] M.P. Zanni-Deffarges and M.E.R. Shanahan. Diffusion of water into an epoxy adhesive: comparison between bulk behaviour and adhesive joints. *International Journal of Adhesion and Adhesives*, 15(3):137–142, 1995.

[163] R.A. Gledhill, A.J. Kinloch, and S.J. Shaw. A model for predicting joint durability. *The journal of Adhesion*, 11(1):3–15, 1980.

[164] C.D.M. Liljedahl, A.D. Crocombe, M.A. Wahab, and I.A. Ashcroft. Modelling the environmental degradation of adhesively bonded aluminium and composite joints using a czm approach. *International Journal of Adhesion and Adhesives*, 27(6):505–518, 2007.

[165] J. Comyn. Kinetics and mechanism of environmental attak. In *Durability of structural adhesives*, pages 85–131. Applied science publishers, 1983.

[166] K.B. Katnam, J.P. Sargent, A.D. Crocombe, H. Khoramishad, and I.A. Ashcroft. Characterisation of moisture-dependent cohesive zone properties for adhesively bonded joints. *Engineering Fracture Mechanics*, 77(16):3105–3119, 2010.

[167] R. Mahnken and M. Schlimmer. Simulation of strength difference in elasto-plasticity for adhesive materials. *International journal for numerical methods in engineering*, 63(10):1461–1477, 2005.

[168] G Viana, M Costa, MD Banea, and LFM da Silva. A review on the temperature and moisture degradation of adhesive joints. *Proceedings of the Institution of Mechanical Engineers, Part L: Journal of Materials: Design and Applications*, 231(5):488–501, 2017.

[169] G. Viana, M. Costa, M.D. Banea, and L.F.M. Da Silva. Behaviour of environmentally degraded epoxy adhesives as a function of temperature. *The Journal of Adhesion*, 93(1-2):95–112, 2017.

[170] P-Y. Le Gac, D. Choqueuse, and D. Melot. Description and modeling of polyurethane hydrolysis used as thermal insulation in oil offshore conditions. *Polymer Testing*, 32(8):1588–1593, 2013.

[171] M. Broudin, V. Le Saux, P-Y. Le Gac, C. Champy, G. Robert, P. Charrier, and Y. Marco. Moisture sorption in polyamide 6.6: Experimental investigation and comparison to four physical-based models. *Polymer Testing*, 43:10–20, 2015.

[172] E. Gaudichet-Maurin, F. Thominette, and J. Verdu. Water sorption characteristics in moderately hydrophilic polymers, part 1: Effect of polar groups concentration and temperature in water sorption in aromatic polysulfones. *Journal of applied polymer science*, 109(5):3279–3285, 2008.

[173] P-Y. Le Gac, G. Roux, P. Davies, B. Fayolle, and J. Verdu. Water clustering in polychloroprene. *Polymer*, 55(12):2861–2866, 2014.

[174] R.F. Fedors. Osmotic effects in water absorption by polymers. *Polymer*, 21(2):207–212, 1980.

[175] B. Fayolle and J. Verdu. *Vieillissement physique des matériaux polymères*. Ed. Techniques Ingénieur, 2005.

[176] N. Tual. *Durability of carbon/epoxy composites for tidal turbine blade applications*. Theses, Université de Bretagne Occidentale, November 2015.

[177] W.D. Cook, M. Mehrabi, and G. Edward. Ageing and yielding in model epoxy thermosets. *Polymer*, 40(5):1209–1218, 1999.

Influence of water ageing on the behaviour of adhesives - a rapid characterization of the evolution of mechanical properties of bonded joints

Most of the adhesives used in the marine industry are polymers with a mechanical behaviour which is strongly influenced by environmental conditions (water activity or temperature). Therefore, it is important for engineers and designers to be able to consider these effects during the different stages of development and manufacturing of a bonded structure.

The present work presents a method for analysing the influence of water ageing on the behaviour of an epoxy adhesive in an adhesively bonded assembly. First, a viscoelastic-viscoplastic model is developed to characterise the mechanical response of the adhesive at initial state in a bonded joint using the modified Arcan device. The model is identified using the inverse identification method and the considered samples are tested at an unaged stage (no water activity). The results obtained after the identification process are used to predict the bulk behaviour of the adhesive. A comparison between numerical results and experimental tests realised on bulk specimens is then made in order to validate this first approach.

In a second phase, in order to decrease the times for samples saturation, the evolution of the mechanical properties of the adhesive in bulk form is tested under different water ageing conditions (immersion in seawater and different relative humidity). The obtained results allowed to identify the evolution of the model parameters as a function of water content. In parallel, a diffusion model was developed to characterise the water ingress in the bonded joint. These two approaches are then combined to model the water profiles and to consider the evolution of mechanical properties of a water aged adhesively bonded assembly, for different immersion times. Finally, to validate the framework, the prediction is compared with experimental tests performed on aged specimens.

Keywords: Epoxides; Mechanical properties of adhesives; Creep / mechanical relaxation; Spectral viscoelasticity; Viscoplasticity; Arcan device; Water ageing; Glass transition temperature, Plasticization; Finite element analysis.

Développement d'une méthode rapide pour caractériser le comportement mécanique d'adhésifs dans un assemblage intégrant la prise en compte de l'effet du vieillissement hydrique

La majorité des adhésifs utilisés dans l'industrie marine sont des polymères avec un comportement mécanique qui est fortement influencé par les conditions environnementales (vieillissement hydrique ou température). Par conséquent, il est très important pour les ingénieurs travaillant dans des bureaux d'études d'être capable de prendre en compte ces effets lors des différentes étapes de développement et conception des assemblages collés.

Le présent travail propose une méthode d'analyse de l'influence du vieillissement hydrique sur le comportement mécanique d'un adhésif structural époxy dans un assemblage collé. Tout d'abord, un modèle viscoélastique-viscoplastique a été développé pour caractériser la réponse mécanique de l'adhésif dans un joint de colle. Pour cela, le dispositif expérimental Arcan a été utilisé. Le modèle est identifié en utilisant la méthode d'identification inverse et les échantillons sont testés à l'état non-vieilli (pas de vieillissement hydrique). Les résultats obtenus après la démarche d'identification sont utilisés pour prédire le comportement mécanique d'éprouvettes massiques.

Dans un deuxième temps, afin de diminuer les temps de saturation d'échantillons, l'évolution des propriétés mécaniques de l'adhésif est analysée sous différentes conditions de vieillissement hydrique (immersion dans l'eau de mer et en humidité relative contrôlée) grâce à des essais sur éprouvettes massiques. Les résultats obtenus seront utilisés pour identifier l'évolution de chaque paramètre du modèle proposé, en fonction de la quantité d'eau absorbée. En parallèle, un modèle de diffusion a été développé pour caractériser le gradient de teneur en eau des joints de colle. Les deux approches sont ensuite combinées pour modéliser les profils d'eau pour différents temps de vieillissement et prédire l'évolution des propriétés mécaniques du joint de colle après le vieillissement. Finalement, pour valider la méthode proposée, la prédiction du modèle est comparée avec des essais réalisés sur assemblages collés vieillis.

Mots clés: Époxy; Propriétés mécaniques d'adhésifs; Fluage/Relaxation; Viscoélasticité; Viscoplasticité; Montage Arcan; Vieillissement hydrique; Température de transition vitreuse; Plastification